“Ss. Cyril and Methodius” University in Skopje

FACULTY OF MECHANICAL ENGINEERING SKOPJE

Filip V. Stojkovski

INTERACTION OF THE GUIDE VANE BLADES SHAPE WITH THE HYDRODYNAMIC PARAMETERS AND THE EFFICIENCY OF VARIABLE-SPEED FRANCIS TURBINE

- Doctoral Thesis -

SKOPJE, 2022

Supervisor: Prof. Zoran Markov, Ph.D.
Faculty of Mechanical Engineering Skopje
“Ss. Cyril and Methodius” University in Skopje

Committee members:

Prof. Zoran Markov, Ph.D.
Faculty of Mechanical Engineering Skopje
“Ss. Cyril and Methodius” University in Skopje

Prof. Predrag Popovski, Ph.D.
Faculty of Mechanical Engineering Skopje
“Ss. Cyril and Methodius” University in Skopje

Assoc. Prof. Viktor Iliev, Ph.D.
Faculty of Mechanical Engineering Skopje
“Ss. Cyril and Methodius” University in Skopje

Prof. Ole Gunnar Dahlhaug, Ph.D.
Norwegian University of Science and Technology (NTNU)
Trondheim, Norway

Assoc. Prof. Andrej Lipej, Ph.D.
University in Novo Mesto
Faculty of Mechanical Engineering, Slovenia

Date of public defence: 19.04.2022

TECHNICAL SCIENCE – MECHANICAL ENGINEERING

FILIP V. STOJKOVSKI, M.Sc. Mech. Eng.

INTERACTION OF THE GUIDE VANE BLADES SHAPE WITH THE HYDRODYNAMIC PARAMETERS AND THE EFFICIENCY OF VARIABLE-SPEED FRANCIS TURBINE

ABSTRACT:

Despite the unstable nature of the unconventional renewable energy sources, the trend of increasing usage of them in Europe and all the scenarios and forecasts made in that direction, lead to the need of balancing energy in the grid and increasing flexibility in electricity production. To address these needs, hydropower plants as hydropower facilities are most suitable to cover these fluctuations.

This brought the idea of applying variable speed operation to hydraulic turbines, where adjusting their rotational speed results in more efficient water to energy usage ratio, and increases their operating range at the same time.

In this doctoral dissertation the emphasis is on the guide vanes, which are the main stationary distribution element of the turbines and serve to regulate the flow, as well as the power of the machine. The analyses are based mainly at defining the main kinematic flow parameters that are dominant in the vaneless space between the turbine runner and the guide vanes. According to that, a new type non-uniform blades were developed, in order to see their impact on the flow parameters and efficiency at variable speed operated turbine.

The analyses were performed with CFD numerical flow simulation on various developed models of guide vanes, from where positive conclusions and directions for further development of this technique for guide vane design are obtained.

KEY WORDS:

Guide vanes, Francis turbine, Variable-speed operation, CFD, Non-uniform blades

This dissertation is dedicated to my father, who is my endless inspiration and motivation, my mother, for her encouragement and selfless support, and my brother for believing in me.

I would like to express gratitude to my supervisor, for guiding me through the studies and for involving me in the challenging project HydroFlex, where I tested and upgraded my knowledge in the field of hydraulic turbomachinery and their design. Also, special thanks to all project members for their openness for communication to exchange ideas. My deepest gratitude to the friends and colleagues, where without their companionship, understanding, motivation and words of encouragement I could not go all this way.

This doctoral dissertation is realized within the project HydroFlex which is funded by the research and innovation programme of the European Union Horizon 2020 according to the grant agreement no. 764011.

This project has received funding from the European Union's Horizon 2020 research and innovation programme under grant agreement No 764011

“Learn the rules like a pro, so you can break them like an artist”

— Pablo Picasso

List of Symbols

Symbol	Unit	Description
g	[m/s^2]	Gravitational acceleration
ρ	[kg/m^3]	Fluid density
μ	[Pa s]	Fluid dynamic viscosity
π	[-]	Mathematical constant
ns	[-]	Turbine specific speed
n_{ed}	[-]	Speed factor
Q_{ed}	[-]	Discharge factor
Ted	[-]	Torque factor
ψ	[-]	Energy coefficient
φ	[-]	Discharge coefficient
ω	[rad/s]	Angular velocity
n	[min^{-1}]	Rotational speed
Q	[m^3/s] ; [l/s]	Flow rate
H	[m]	Head
x, y, z	[-]	Cartesian coordinate system
r, φ, z	[-]	Cylindrical coordinate system
t	[s]	Time
v	[m/s]	Fluid velocity
p	[Pa]	Pressure
Ω	[1/s]	Fluid vorticity
Γ	[m^2/s]	Circulation
R	[m]	Radius
D	[m]	Diameter
B	[m]	Height
A	[m^2]	Area, Surface
c	[m/s]	Absolute fluid velocity
u	[m/s]	Transport velocity
w	[m/s]	Relative fluid velocity
F	[N]	Force
T	[Nm]	Torque
P	[W]	Power
η	[-]	Efficiency
α	[°]	Angle of fluid streamlines
β	[°]	Angle of relative velocity ; Angle of guide vane blade leading/trailing edge
δ	[°]	Runner blade leading/trailing edge angle ; Guide vane blade leaning angle

φ	[°]	Guide vanes enclosure angle
L, l	[m]	Length
Z_{gv}	[-]	Number of guide vane blades
t_o	[m]	Guide vane blades cascade pitch
a_o	[m]	Guide vane opening clearance
A, B, C	[-]	Constants
P	[-]	Parameter
τ	[Pa]	Fluid flow shear stress
y+	[-]	Nondimensional height
m	[-]	Module
ε	[-]	Turbulence dissipation ; Relative error
k	[-]	Turbulence kinetic energy

Contents

Introduction

Hydropower counts as a renewable energy source because of its inexhaustibility, i.e. because the water mass participates in the hydro cycle of the Earth. Before commercial electricity became widely available, water energy was used to irrigate and power various machinery, such as mills, textile machinery, sawmills, hoists, etc. Since the beginning of the 20th century, the term hydropower has been used most often in conjunction with the modern development of hydropower plants for electricity production.

Hydropower is contained in river streams, rapid watersheds, as well as the coastal sea level change through the effects of tides and sea waves. The total potential of water flows in the world is estimated at 4.5 [TW]. About a quarter of this potential can be used to generate electricity. In 1975, only 15% of this potential was used to generate electricity. Three-quarters of the usable hydropower potential is found in the underdeveloped or developing countries, such as Africa and Latin America, where only 6% of them is used. The other quarter of this energy is found in the developed countries where it is 35% used.

Water flow energy is converted in hydropower plants. There are several types of hydropower plants:

- Run-of-river hydropower plants,
- Conventional (Dam storage) hydropower plants,
- Pumped-Storage hydropower plants, and
- Small hydropower plants.

Utilisation of water potential for electricity production is economically competitive with the production of electricity from fossil and nuclear fuels, so hydropower is the most important renewable energy source on the planet.

Hydropower, or watercourse energy, is the largest renewable energy source in the world, covering about 62% of the world's renewable electricity generation, compared to 21% for wind energy and 7% for solar photovoltaic energy. The remaining 10% are from other unconventional energy sources. Hydropower is a cheap and sustainable source of energy. It is well known that hydropower provides great opportunities in terms of the electricity grid, such as energy storage in storage hydropower plants, monitoring of variable network loads, and system inertia. When there is a need of increased flexibility of electricity production, for example a relatively fast connection to the grid, hydropower is characterised by a very short period of time to achieve it. It also facilitates the integration into the network of alternating production of wind and solar energy, through the ability of balancing. The key feature of hydropower is its longevity. Hydropower plants can operate for a period of 100 years or even longer, compared to other renewable energy conversion techniques that are estimated to operate for 20 to 30 years.

Renewable electricity generation in Europe is expected to fluctuate. Renewable energy sources that are currently a trend in Europe are the solar and the wind energy, which are unstable by nature and depend mainly on the weather conditions [1]. Because of this, the need to balance production increases. Production balancing means flexibility, which can be easily achieved from the hydropower plants, so, by following this trend, they will gain a lot of importance in the electricity production.

The term flexibility describes the potential for balancing between electricity production and demand by adjusting production or demand for electricity whenever there is a deviation from the normal quantity in the system. These imbalances originate from different elements of the power system and set different requirements for the source of flexibility.

In Europe, the hydropower sector has an increasing need for flexibility in electricity generation, and thus flexibility in its operation. Practice shows that hydraulic turbines in hydropower plants are increasingly operated at off-design operational conditions, more and more during the year [2]. According to the hydrology and field conditions where the hydropower plants are built, the most commonly used turbine is the Francis turbine. Conventional practice defines that the design of these machines is suitable for operation at constant synchronous speed, for the needs of generating electricity in the generator. In this case, operating conditions are defined by the available head and flow rate through the turbine, leading to inefficient operation, hydraulic losses, etc. So, the conventional Francis turbines are single-synchronous controlled machines with constant speed, unique geometry with constant number and type of blades, where the power is regulated by the guide vanes through their opening and closing, which change the flow rate through the turbine at different head.

Everything that defines today's Francis turbine is, in fact, a limitation of the turbine character as an energy machine, especially the constant synchronous speed. This led to the idea that these machines need to be operated at variable rotational speeds, which will represent a dual-regulation turbine - by flow rate and by rotational speed. It turns out that a change i.e. rotational speed correction can improve the efficiency of the hydrodynamic processes of energy transformation in the turbines, and thus the efficiency of the turbine itself, leading to more efficient electricity production. Increased use of wind turbines has led to the development of variable speed generators using static inverters. The potential application of this technique to hydraulic turbines has received increased attention of power engineers at various symposia and is being explored in universities around the world.

For variable speed operation of turbines at larger head denivelations, it is possible to install a smaller generator. The turbine will give less output power due to the variable speed, and increased flexibility in production can be achieved for decreasing the head [3]. Transient modes, as well as adverse effects of hydraulic shock are expected to be avoided or reduced, which may result in a reduction in the overall size of all hydraulic equipment, thus obtaining more cost-effective equipment, regarding both performance and maintenance.

The benefit of the variable speed turbines depends on the operating conditions of the plant, where feasibility analyses should be made for the use of this technique and operating scenarios should be defined. In general, technical improvements to variable speed turbines are expected in the direction of:

- Improved performance at off-design heads when head changes, and
- Improving performance at off-design flow rates, thereby increasing the usable range of flow rates for energy production.

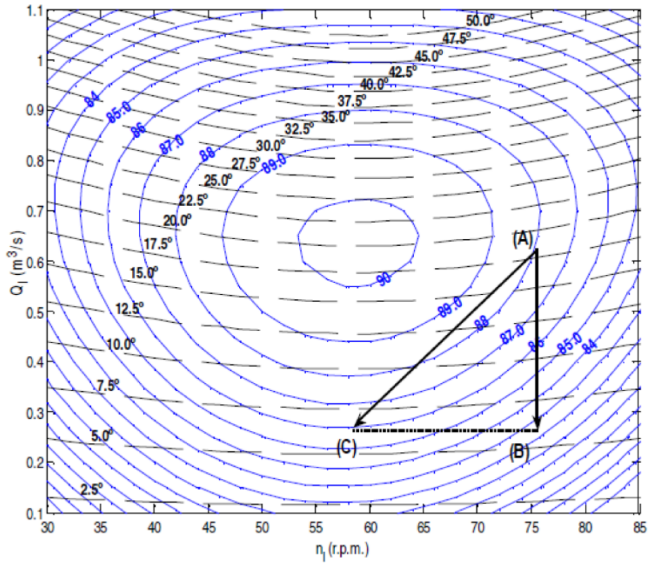

Fig.1 Operation example to improve efficiency with variable speed [4]

1. Concept of variable speed and review of relevant research in the field

Defining the potential efficiency of variable speed operation depends on quantitative analysis of turbine improvements [3]. In the analysis of Sheldon [3] for 3 Francis turbines with different specific speeds $n_s = 24.5 - 44.7 - 56.1$ he gets an increase in the produced energy relative to the used water, with the main goal to maximise the efficiency of the operation. These results are related to the type of Francis turbine tested, and it is expected that another type of runner might not result with the same output. In the analysis of Alexander [3], contrary to the previously mentioned analyses, the focus is on how to obtain an expansion of the operating characteristic with a variable speed, as opposed to achieving maximum efficiency. From this analysis it is concluded that the types of turbines that are characterised by narrower operating characteristics can be expected to expand their operating range by using the variable speed technique.

In the analysis of C. Farell [3], where the two previously mentioned analyses are sublimated, simple mathematical relations related to the variable speed are developed. Using the Euler equation of turbomachines, a simplified mathematical model is developed to predict the dependencies between the variable speed and the flow rate through the turbine for a constant opening of the guide vanes, expressed by the equation:

$$Q = An + \frac{B\eta}{n} \; [m^3/s] \tag{1}$$

where A and B are coefficients - constants for the given turbine at constant opening of the guide vanes for constant head, and η is the turbine efficiency. Mainly, the resulting characteristics obtained from his analysis are presented in Fig.1.1. for one specific turbine type.

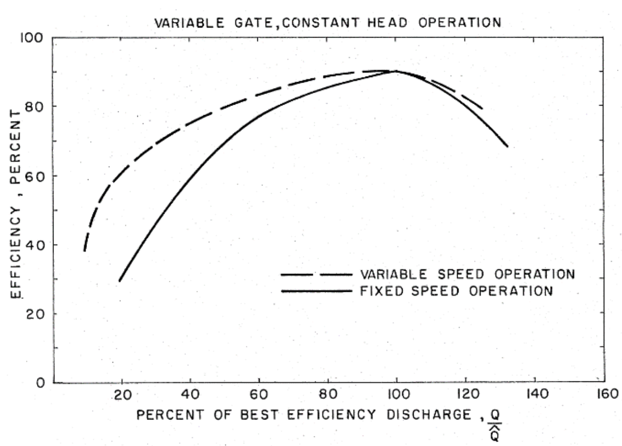

Fig.1.1 Extension of the operating range with variable speed [3]

The authors claim that different runner geometries and turbine characteristics can affect performance when it comes to variable speeds. They also claim that the turbines with higher specific speeds (low head turbines) had the greatest performance improvement and showed the best utilisation of the flow rate by increasing the rotational speed.

The author G. I. Topazh [5] derives the same dependence, calling it the ability to regulate the flow rate in radial-axial (Francis) turbines, giving values of the coefficients A and B from which runner geometric parameters they come from, reducing them to the flow and speed reduced parameters Q_{11} and n_{11}. The author also deals with the shape of the flow in the vaneless space between the guide vanes and the runner, which he defines as potential or helical flow, depending on the meridian cross section of the turbine.

G. I. Krivchenko [6] has presented the mean values of the velocity vectors and their relations in a simpler was - as velocity triangles at the runners inlet and outlet. He also defined the shock free inflow conditions at constant flow rate and variable rotational speed.

V. V. Barlit [7] in his book gives a simplified expression of the Euler equation, where he proposes that there is no return vortex behind the runner (operating in the zone of maximum efficiency); From there, he derives the required guide vane outflow angle, depending on the head, flow rate, and rotational speed. It also gives an overview of how to design (profile) the guide vane blades for the defined angles of the velocity triangles.

V. B. Andreev [8] and N. N. Kovalev [9] give an overview of the construction of the guide vanes from a mechanical point of view, as well as regarding their energetic features, defining the effects of the shape of the blades on the flow rate, but also on the efficiency of the turbine. The recommended geometric constructive coefficients for the design of the guide vanes are also defined here.

Wilhelmi J. R. [10] performs laboratory research on a pump turbine and its characteristic with variable speed, in the direction of optimal control. G. P. Heckelsmueller [11] analyses the application of Francis turbines with variable speed, using data from model tests and analysing the ratio of the benefit obtained from the required flow rate and power, with variable speed. A. Borghetti [12], on the other hand, deals with the variable speed of turbines in small hydropower plants, developing control block models for tracking the point of highest efficiency according to the turbine hill chart. E. Bortoni [13] deals with the general benefit of variable speed turbines by examining them in the laboratory for variable heads. He also gives an overview of the runner inlet velocity triangles that appear at variable rotational speeds, deriving an analytical calculation approach. Sh. Abubakirov [14] analyzes turbine operating charts changes from synchronous to variable speed operation, and proposes a turbine control algorithm.

Recent research related to this issue mainly moves towards the analysis of the turbine runner and the overall characteristics of the turbine, not looking at the flow effects caused by the guide vanes on the runner itself and their impact on the general characteristic. On the other hand, efforts are being made to integrate and automate state-of-the-art software tools for numerical simulations and computer manipulations for effective and efficient modelling and optimisation of turbine flow elements, in order to improve their performance, to estimate the increase of their service life, to design turbines for variable speed as well as for a large number of start/stop dynamic loads on the machines themselves All of this is required by the energy sector today, in direction of increasing the flexibility in energy generation. The aim is to obtain state-of-the-art equipment, where the next step would be performing model testing of the computer-optimised equipment, for obtaining the characteristics and performance that the equipment provides. In that direction, a so-called parametric definition of the flow element geometry is performed, which will be used for rapid manipulation and creation of various designs in the computer space and their evaluation through numerical simulations, both fluid flow and structural.

In his thesis, Sundfor [15] deals with a test design of a high-pressure Francis turbine runner that would operate at a variable speed. A. Nordvik [16] in his thesis deals with numerical simulations of an existing Francis turbine runner and defines the variable speed operational path, obtained by simulations and compared with model tests. I. Iliev [17] in his doctoral dissertation deals with the optimisation of a geometrically parameterised high-pressure Francis turbine runner variable speed capability, using the so-called Surrogate modelling – a technique where the outcome of the result cannot be directly quantified, but vice versa, solution is derived from the obtained results (outcome). E. Tengs [18] contributes to the creation of a computer design tool for obtaining a Francis turbine with variable speed, both from fluid flow and structural point of view (FSI – Fluid Structure Interactions).

From the current research in the field, with a review of the guide vanes and their impact on how to improve the turbine characteristics at off-design points, a significant contribution has been made by B. J. Lewis [19]. In his research, he analyses the discharge of water jets additional from the guide vanes blades trailing edges in order to correct the inlet swirl and its intensity created by the cascade. Swirl intensity correction in front of the turbine runner improves turbine performance at off-design operations.

S. Chitrakar [20] has made an important contribution. In a narrower sense, he analyses the impact of present gaps between the guide vane blades and the regulating rings, which occur due to sediments in the water, how they affect on the general velocity profile and on efficiency. He performs the analyses with the help of numerical simulations, as well as with a laboratory experiment. B. Thapa [21] deals with the optimisation of the performance of a segment of a radial cascade - guide vanes for laboratory research, by analysing and correcting the inlet flow conditions in the cascade, as well as the velocity distributions that are achieved by it. In a similar area of these two authors, Y. Chen [22] has also contributed with regard to the mechanism of sedimentation and the formation of gaps, as well as the imbalance of the blade pressures, and G. Kumar [23] regarding the effects of gaps on guide vanes on the occurrence of eddy currents. K. Çelebioğlu [25] deals with the general design procedure of a conducting apparatus, testing different blades numerically and how they generally affect the mechanical properties of the guide vanes. W.W. Zhang [26] has analysed the effects of a double-row cascade (tandem vanes) - double-row guide vanes - on reducing the eddy currents in the turbine draft tube. C. Devals [27] deals with the general optimisation of the entire distributor – spiral casing, stay vanes and guide vanes of the turbine, with a very little reference to the guide vanes.

From the above relevant research, it can be summarised that the analysis mainly goes in the direction towards the general effect of the turbine that operates with variable speed, the behaviour of the turbine runner and its improvements if variable speed operation is considered, as well as the general turbine control designed to operate with this technique. Regarding the guide vanes in hydraulic turbines, the current research is more focused on the possible impacts and caused anomalies in them and how they affect the general characteristics of the turbine, as well as some general rules for their design.

In this doctoral dissertation, a step has been made towards analysing several parameters of the guide vanes. Cohesion of the blade design is made, directly dependent on the flow parameters required for the runner at a certain operating point. At the same time, certain geometric parameters of the guide vanes were analysed and how they influence on the turbine characteristics. Also, the meaning of variable speed operation is derived, from fluid flow kinematics point of view at the runner inlet and how directly affect the shape of the blades of the guide vanes, with an aim to extend the operating characteristics.

Starting from the mathematical definition of the flow conditions prevailing in the vaneless space between the guide vanes and the runner, Chapter 2 outlines the necessary physical laws that will be used to further define the geometry of the guide vanes. There is also a brief overview of the physical laws that apply to variable speed turbines, as well as what is expected to be obtained from it.

Chapter 3 deals with the geometry of the guide vanes, which is parametrically defined. The whole process of obtaining different blades of a conducting apparatus, depending on the turbine rotating axis, implemented in the MATLAB programming language, in order to obtain various shapes of blades that have been examined.

Chapter 4 briefly describes the conditions of the analysis that will be conducted in the further presentations, which quantities are of interest for this research, as well as a review of the standards for evaluation of the turbine parameters.

Chapter 5 sets out the basics of numerical modelling and simulation. It explains which mathematical models are used to describe turbulent flows, and defines the reference zero model, the Francis 99 turbine, its numerical evaluation of the performance and definition of the numerical error given by the model set. This analysis is needed to verify the model that will be used in further analysis of various guide vane blades.

Chapter 6 presents the effects of certain geometric parameters on turbine efficiency. A total of 37 models of conductive blades with different configurations were examined in order to examine the differences they give on the efficiency, and to define a hydraulically favourable blade.

Chapter 7 represents the main analysis of this dissertation, i.e. the influence of non-uniformly profiled blades on the turbine operating rage at variable rotational speed. Since the turbine at a changed speed has a new operating point, i.e. new operating conditions, blades with different angles (variable trailing edge angle) are defined through the blade height for directing the outflow to the runner. The analyses shows that certain segments of the blade that have different angles on the trailing edge direct the flow favourably when the runner has changed the rotational speed.

The conclusion evaluates all the steps taken, what is defined, what can be improved, and which steps for further work can be taken. Special attention is paid to the main idea for the design of non-uniform blades, where it is concluded that the physical kinematic conditions prevailing in the vaneless space for variable rotational speed can be achieved with additional optimisation. The effects they give are visible in more analysed models, not in the direction of efficiency maximisation, but more in the direction of operating zone extension and improving the inflow patterns to the runner.

2. Mathematical models of the fluid flow in the guide vanes and the turbine runner

2.1. Flow created from stationary radial cascade (guide vanes)

The conclusion drawn from the previous analyses is that the fluid flow is permanently “deformed”, i.e. changes the direction of its movement when it flows through radial cascade, creating a radial vortex movement. When the turbine operates, the turbine flow rate, as well as the very form of the inflow in the turbine runner, is controlled by the guide vanes, where the runner torque varies depending on the position of the blades in the guide vanes. The flow in the vaneless space can be described with the equation of ideal fluid flow in Lamb-Gromeko vector form [5][7]:

$$\frac{\partial \vec{V}}{\partial t} + \vec{\Omega} \times \vec{V} = -\nabla(gH) \tag{2.1}$$

where H is the fluid specific energy, $\vec{V} = \left(\vec{V_z}, \vec{V_r}, \vec{V_u}\right)$ is the absolute velocity vector with its projections in a cylindrical coordinate system, and $\vec{\Omega} = rot\vec{V}$ is a vector of the vorticity that has its projections in a cylindrical coordinate system and is expressed as:

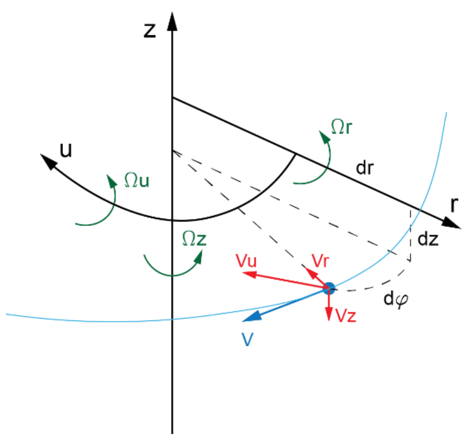

Fig.2.1 Absolute vector of flow in a cylindrical coordinate system in the vaneless space

$$\begin{aligned} \Omega_r &= \frac{\partial v_z}{\partial \varphi} - \frac{\partial v_u}{\partial z} \\ \Omega_z &= -\frac{\partial v_u}{\partial r} + \frac{\partial v_r}{\partial \varphi} \\ \Omega_u &= -\frac{\partial v_r}{\partial z} + \frac{\partial v_z}{\partial r} \end{aligned} \tag{2.2}$$

Experimental studies have shown that in the vaneless space between the guide vanes and the runner, the flow can be analysed as a stationary axisymmetric. Taking into account that in stationary axisymmetric flow the energy of the flow at the runner inlet can be considered constant, it is obtained that:

$$\frac{\partial \vec{V}}{\partial t} = 0\,; \; \frac{\partial (v, H)}{\partial \varphi} = 0 \tag{2.3}$$

From here, two forms of flow can be derived, i.e. potential (non-rotating) or rotational (helical) flow. At the potential flow, it can be written that there is no change in the velocity vector in the radial direction:

$$\frac{\partial(v_u r)}{\partial z}dz + \frac{\partial(v_u r)}{\partial r}dr + \frac{\partial v_u}{r\partial\varphi}rd\varphi = d(v_u r) = 0 \tag{2.4}$$

For helical flow, the vector of rotation and the vector of velocity are parallel to each other:

$$\frac{\partial v_u}{\partial r}dr + \frac{\partial v_u}{\partial z}dz = d(v_u r) = 0 \tag{2.5}$$

From both cases, we get the product of the tangential component and the radius, where the first derivative of this product is zero, thus obtaining the "Free Vortex Law" where the velocity is inversely proportional to the distance:

$$v_u r = const. \tag{2.6}$$

Assuming that the tangential component of the velocity vector about the axis of rotation lies on the contour of a circle, it can be written as:

$$\Gamma = \oint v_u\, dl = 2r\pi v_u = const. \tag{2.7}$$

which shows that the circulation at a certain distance from the axis of rotation of the flow is kept constant. Therefore, it can be concluded that the guide vanes form a stationary axisymmetric flow in the vaneless space, which can be potential or rotational flow. In the event of a potential flow, the swirling is constant at all points of the fluid in the vaneless space. In the case of a rotational flow, the swirl is constant along the streamline and changes from one streamline to another. The question that arises is in which cases it occurs potentially, and in which cases there is a helical flow in the vaneless space between the guide vanes and the runner. The shape of the meridian cross section behind the guide vanes towards the runner is defined, schematically presented in the following Figures.

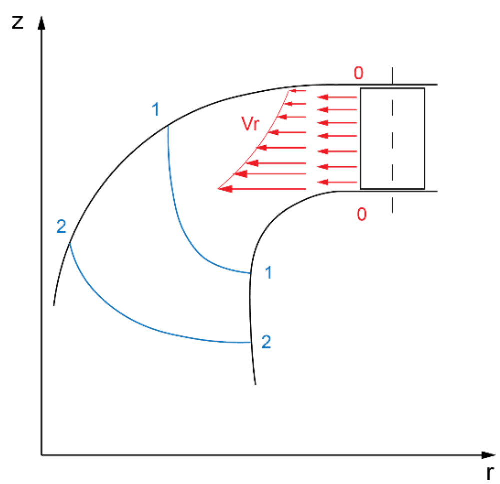

Fig.2.2 Schematic view of the meridian section of a high-speed Francis turbine [5]

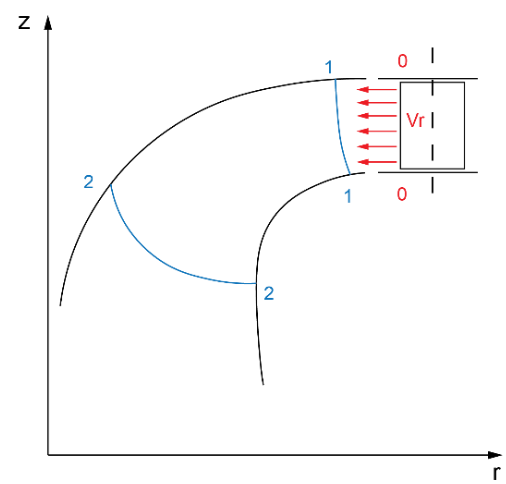

Fig.2.3 Schematic view of the meridian section of a low-speed Francis turbine [5]

On the meridian section scheme of a high-speed Francis turbine, the leading edges of the runner blades are indented towards the axis of turbine rotation, which leads to unevenness of the radial velocity profile. The flow is following the section contours where the lower contour declines, and that leads to changes in the radial velocity by height of the blades. A uniform velocity profile is obtained at the outlet of the guide vanes, where the runner blades leading edges are not in contact. Therefore, the current cannot be considered as potential, but as helical:

$$\frac{\partial(v_u r)}{\partial z} dz \neq 0\ ;\ \Omega_r = \frac{\partial(v_u r)}{\partial z} dz \neq 0 \tag{2.8}$$

On the other hand, at a low-speed Francis turbine, it can be noticed that the leading edges of the runner blades are positioned where the radial velocity does not change by height, so in these turbines the flow in the vaneless space can be analysed as potential.

The flow velocity at the guide vanes outlet is a vector sum of its projections in a cylindrical coordinate system [6]

$$\overrightarrow{v_o} = \overrightarrow{v_{or}} + \overrightarrow{v_{ou}} \tag{2.9}$$

where v_{or} represents the projection of the velocity of flow in a radial direction, which directly depends on the flow rate and height of the guide vanes and is expressed as:

$$v_{or} = \frac{Q_d}{2R_o \pi B_o} \tag{2.10}$$

and v_{ou} represents the projection of the velocity on the guide vane outlet circumference:

$$v_{ou} = v_o cos\alpha_o\ ;\ v_{ou} R_o = const. \tag{2.11}$$

The flow rate through the turbine mainly depends on the opening clearance, as well as on the shape of the blades in the guide vanes. In Fig. 2.4, three characteristic blade shapes are presented. According to the theory, at the same openings, and a different blades shape, resulting in a different outflow angle, differences in turbine flow rates are obtained. Concave blades form a smaller outflow angle, and by that a reduced flow rate; and, vice versa, convex blades form a larger outflow angle, and thus increased flow rate. The angle actually expresses the projection degree of the outlet velocity in the radial (flow) and peripheral (circulation) direction.

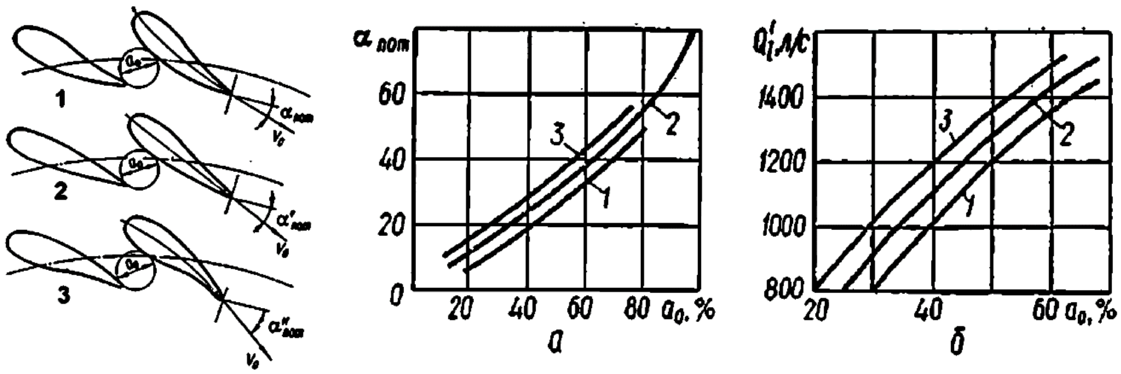

Fig.2.4 Influence of the blades shape on turbine flow rate
at constant opening clearance [7][9]

2.2. Flow in the runner

Based on the "Classical Turbine Theory", a midline is drawn along the meridian section, which will represent a streamline in that section, starting from the leading edge to the trailing edge of the runner blades [6]. The flow in turbines is always rotational, so the theory of Fluid Mechanics defines it as a flow through a rotating blade channels. Fluid particles moving along the streamline (Fig. 2.5 streamline marked as pk) with relative velocity $\vec{w}$, simultaneously rotate about the axis of rotation with the streamline.

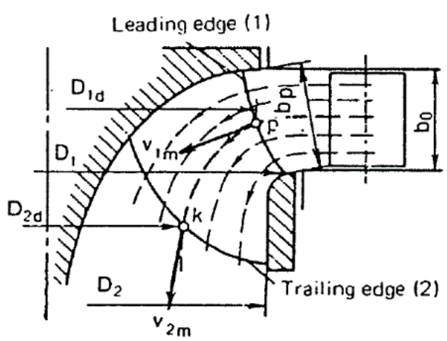

Fig.2.5 Meridian section of Francis turbine [6]

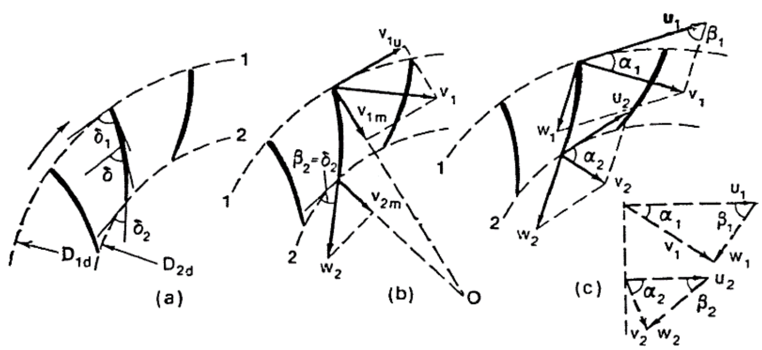

Fig.2.6 Orthogonal projection of the streamline [6]

The transportation velocity component that directly depends on the rotational speed of the runner is expressed as pure kinematic magnitude. If $\vec{\omega}$ represents the angular velocity at which the fluid rotates about the axis of rotation, then the transport (peripheral) velocity of any fluid particle at a given distance R which lies on the streamline will be:

$$u = R\omega \tag{2.12}$$

In the case of a stationary coordinate system and in the case where the angular velocity is constant, the flow is non-stationary, and the absolute velocity $\vec{v}$ is a vector sum of relative and transport velocities:

$$\vec{v} = \vec{w} + \vec{u} \tag{2.13}$$

Turbine operating conditions are defined through 2 parameters: the flow rate Q and the runner rotational speed n. For a given runner size, the vector components of the velocity triangle can be derived. So, at the runner inlet on the blades leading edges, the transport component will be:

$$u_1 = \frac{2R_1\pi n}{60} \tag{2.14}$$

The projection of the absolute velocity vector in the meridian section gives the meridian component of the velocity which is derived as:

$$c_{1m} = \frac{Q_d}{2R_1\pi B_1} \tag{2.15}$$

The tangential component of the absolute velocity vector, according to the free vortex law, will depend on the flow conditions created by the guide vanes:

$$c_{1u} = v_{ou}\frac{R_o}{R_1} \tag{2.16}$$

The ratio of these two velocity components gives the angle of the absolute velocity vector in the velocity triangle:

$$tg\alpha_1 = \frac{c_{1m}}{c_{1u}} \tag{2.17}$$

The absolute velocity vector is the vector sum of these two components:

$$\overrightarrow{c_1} = \overrightarrow{c_{1u}} + \overrightarrow{c_{1m}} \tag{2.18}$$

The derived vector relations also apply to the runner outlet, presented on blades trailing edges on radius R_2. The equations of axisymmetric flow in the inter-blade channel of a turbine runner and the blade forces are derived from G. Lorenz [7] in the form of:

$$F_r - \frac{1}{\rho}\frac{\partial p}{\partial r} = \frac{dv_r}{dt} - \frac{v_u^2}{r} \tag{2.19}$$

$$F_u = \frac{dv_u}{dt} + \frac{v_u v_r}{r} \tag{2.19.1}$$

$$F_z - g - \frac{1}{\rho}\frac{\partial p}{\partial z} = \frac{dv_z}{dt} \tag{2.19.2}$$

which are projections of the resultant force F_L that acts on the runner blades, represented in a cylindrical coordinate system. For $\omega = const.$, the torque transmitted to the turbine shaft (around the axis of rotation) is derived from the second Lorentz equation for the peripheral component of the force:

$$F_u = \frac{dv_u}{dt} + \frac{v_u v_r}{r} = \frac{dv_u}{dt} + \frac{v_u}{r}\frac{dr}{dt} = \frac{1}{r}\left(\frac{rdv_u}{dt} + \frac{v_u dr}{dt}\right) = \frac{1}{r}\frac{d(v_u r)}{dt} \tag{2.20}$$

The elementary torque acting on the side of the runner with an elementary mass is:

$$dT = F_u r dm = d(v_u r)\frac{dm}{dt} = \rho dQ d(v_u r) \tag{2.21}$$

The sum of torque is equal to the change in torque from runners inlet to outlet:

$$T = \rho \int_1^2 d(v_u r) dQ = \rho Q[(v_{1u} r)_1 - (v_{2u} r)_2] \tag{2.22}$$

From the equation for the hydraulic available power of the turbine:

$$P_H = \rho g H_n Q_d \tag{2.23}$$

the mechanical power of the turbine shaft:

$$P_M = T\omega = T\frac{2\pi n}{60} \tag{2.24}$$

and their relationship that defines turbine efficiency:

$$\eta = \frac{P_M}{P_H} = \frac{T\omega}{\rho g H_n Q_d} = \frac{[(v_{1u} r)_1 - (v_{2u} r)_2]\omega}{g H_n} \tag{2.25}$$

where the individual products of $r\omega = u$, it is obtained that:

$$g H_n \eta = u_1 v_{1u} - u_2 v_{2u} \tag{2.26}$$

i.e. translated into turbomachine manner as:

$$g H_n \eta = u_1 c_{1u} - u_2 c_{2u} \tag{2.26.1}$$

This represents the main equation of the turbines, i.e. the so-called Euler equation for turbomachines, where H_n represents the net head of the turbine runner, i.e. the energy. On the other hand, if the relationship $(v_{iu} r)_i = \Gamma_i$ it is obtained that:

$$g H_n \eta = \frac{\omega}{2\pi}(\Gamma_1 - \Gamma_2) \tag{2.27}$$

from where it is concluded that the torque and head of the turbine depend on the differences in the circulations created at the runner inlet and outlet. The equation shows that maximum energy efficiency (best efficiency point) is obtained when:

$$u_2 c_{2u} = 0 \; ; \; \Gamma_2 = 0 \tag{2.28}$$

while adopting $\eta = 1$, thus giving Euler's equation the form of:

$$gH_n = u_1 c_{1u} = \frac{n}{60}\Gamma_1 = \frac{2\pi n}{60} R_1 c_{1u} \; ; n \; [min^{-1}] \tag{2.29}$$

2.2.1. Conditions for optimal runner inflow (shock-free conditions)

The construction of the velocity triangle of known runner dimensions and the opening position of the guide vanes depends on the runner rotational speed and the flow rate. The following conclusions are based on these parameters. An example is shown when the turbine is running at a constant flow rate Q and variable rotational speed n [6].

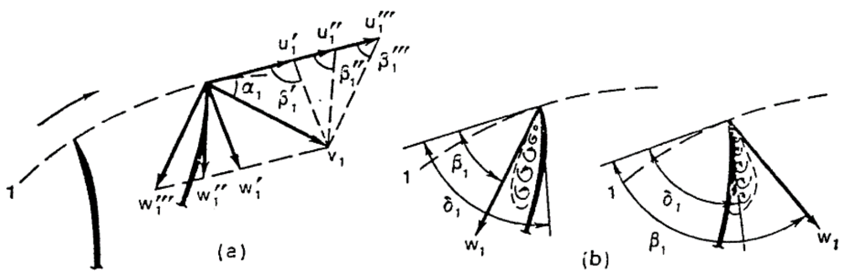

Fig.2.7 Velocity triangle at runner inlet [6]

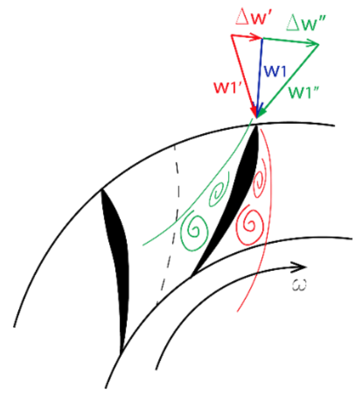

Fig.2.8 Inflow shock losses

The vector of absolute velocity under such operating conditions remains constant because it does not depend on the rotational speed, while the transport and relative velocity components change. Due to change of the rotational speed, the relative velocity does not maintain the angle at the blades leading edges, which leads to flow separations at the runner inlet and causes additional energy losses:

$$\beta_1 < \delta_1 \ for \ n'; \ \beta_1 > \delta_1 \ for \ n''' \tag{2.30}$$

A conclusion is drawn that the optimal inflow condition is obtained at $\beta_1 = \delta_1$, the so-called "Shock Free" flow. This condition is a purely geometric condition which is taken in the further analyses as a reference in the design of guide vane blades, to be designed and positioned in the cascade to provide this type of flow, independent from the rotational speed, which is the purpose of this research. Losses at runner inlet due to Shock flow conditions can be expressed simplified as [28]:

$$\Delta\eta_{inc} = \frac{\overrightarrow{\Delta w}}{\sqrt{2gH_n}} \ ; \ \overrightarrow{\Delta w} = \overrightarrow{w_1'} - \overrightarrow{w_1} \ ; \ \overrightarrow{\Delta w} = \overrightarrow{w_1''} - \overrightarrow{w_1} \tag{2.31}$$

2.2.2. Conditions for optimal runner outflow (non-swirling conditions)

On the other hand, maximum energy is transformed in the turbine at $\Gamma_2 = 0$ at the runner outlet. At the runner outlet, the blades trailing edges in Francis turbines form a cascade which is rather dense, so the angle of relative velocity can be assumed to be equal to the trailing edges angle $\beta_2 \approx \delta_2$. Also, the intensity of the relative velocity remains constant with the change of the rotational speed and mainly depends on the flow rate through the turbine.

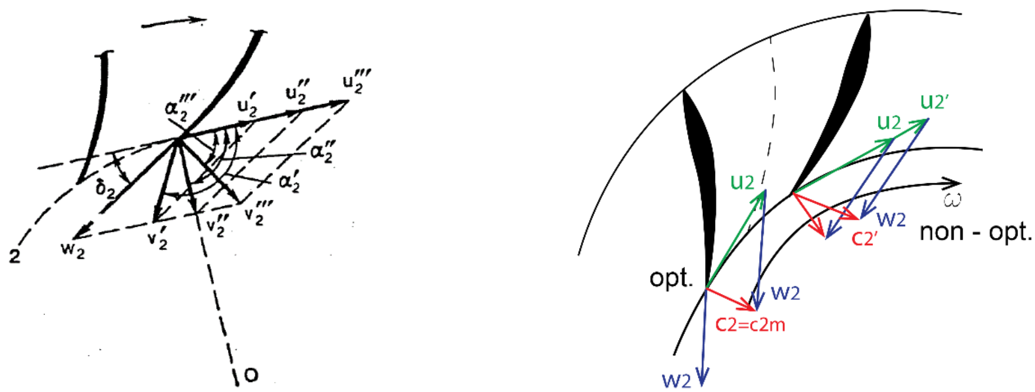

Fig.2.9 Velocity triangles at runner outlet [6]

Fig. 2.9 shows the influence of the rotational speed on the absolute velocity projection at the runner outlet towards the transport component, which causes circulation at the runner outlet. The losses that result from this phenomenon can be written as [28]:

$$\Delta\eta_{sw} = \frac{c_{2u}}{\sqrt{2gH_n}} \quad (2.32)$$

The influence of the outlet velocity triangle on the energy exchange degree is presented in the following analysis as a consequence which arises from the established kinematic conditions between the guide vanes and the runner inlet, and from the operation of the turbine itself.

2.3. Interrelationships of flow parameters in the guide vanes and the runner and their derivation

If the peripheral component of the absolute velocity vector is replaced by the relation:

$$c_{1u} = \frac{c_{1m}}{tg\alpha_1} = \frac{Q_d}{2R_1\pi B_1 tg\alpha_1} \tag{2.33}$$

then Euler's equation takes a form of [29][30]:

$$gH_n = \frac{n}{60}\frac{Q_d}{B_1 tg\alpha_1} \tag{2.34}$$

from which the angle of the absolute velocity vector required at the runner inlet is directly derived as:

$$tg\alpha_1 = \frac{n}{60}\frac{Q_d}{B_1 gH_n} \tag{2.34.1}$$

According to the law of free vortex, the angle that the guide vanes should provide at the runner inlet is expressed through the equations:

$$\frac{c_{1u}R_1}{R_o} = v_{ou} \tag{2.35}$$

$$v_{or} = \frac{Q_d}{2R_o\pi B_o} \; ; R_o > R_1 \; ; B_o \approx B_1 \tag{2.35.1}$$

where the flow angle will be:

$$tg\alpha_o = \frac{v_{or}}{v_{ou}} > \; tg\alpha_1 \tag{2.36}$$

The derived relations are crucial in the following chapter, where the profiling of the blades is performed in relation to the required flow angle from the guide vanes to the runner.

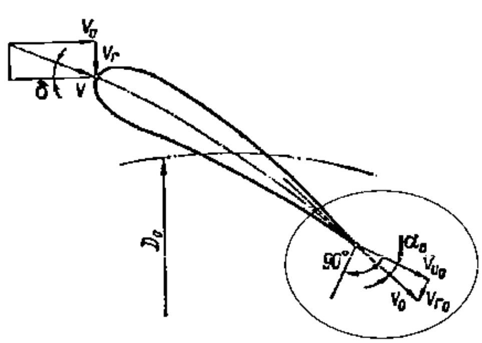

Fig.2.10 Profiling a blade in the guide vanes [7]

2.4. Flow modelling at variable speed (kinematic analysis)

From the previous derived relations for the flow in the vaneless space, it is evident that with a change of rotational speed (from kinematic point of view), the flow angle from the guide vanes changes, which directly influences the designing of the guide vane blades. At the same time, for maintaining a constant head and constant opening clearance of the blades, when turbine speed changes, the flow rate changes too. A simplified expression of this phenomenon is given by the expression [31]:

$$A \cdot \frac{dQ}{d\omega} = \frac{u_2^2 - gH_n\eta}{\omega^2} + \frac{gH_n}{\omega}\frac{d\eta}{d\omega} \tag{2.37}$$

where A represents a certain coefficient with a positive value depending on the turbine, and u_2 represents the transport velocity component of the rotation at the runner outlet. From here, the change in efficiency with the rotational speed can be neglected, in order to reduce it to a general expression as:

$$A\frac{dQ}{d\omega} = \frac{u_2^2 - gH_n\eta}{\omega^2} \tag{2.37.1}$$

from where the following kinematic relations are obtained:

- For $u_2 = \sqrt{gH_n\eta}$, at constant opening of the guide vanes, the flow rate through the turbine does not depend on the increase of rotational speed;

- For $u_2 > \sqrt{gH_n\eta}$, at constant opening of the guide vanes, the flow rate through the turbine increases with the increase of rotational speed;

- For $u_2 < \sqrt{gH_n\eta}$, at constant opening of the guide vanes, the flow rate through the turbine decreases with the increase of rotational speed.

The first condition is characteristic of Francis turbines with medium specific speed, the second condition of high-speed, and the third condition of low-speed Francis turbines [31]. In this research, the reference turbine is a high-head (low specific speed) Francis turbine, where the results demonstrate that increase of rotational speed decreases the flow, and vice versa. Theoretically, the inlet velocity triangles obtained in this case are represented in Fig. 2.11. It can be observed in the Figure, that there is a change in the flow angle from the guide vanes to the turbine runner, which affects the profiling of the blades in the guide vanes. The intensities of the angles that change depend on the type of turbine and are not unambiguous, just like the intensity of the flow rate change. The condition for obtaining shock free flow is transferred onto all velocity triangles, as previously stated, to obtain optimal flow conditions at the runner inlet, where the ratio of the transport velocity component and the relative velocity component are observed through the angle of the blade leading edge.

It is practically impossible to maintain the theoretically optimal velocity triangle at the runner outlet when changing the rotational speed, and, on the other hand, it is theoretically shown that it can be achieved by correcting the flow rate through the turbine. On the other hand, this contradicts the physicality of the variable speed of a low-speed Francis turbine, where it is obtained that the flow rate through the turbine decreases at increased speeds, and that an increase in flow rate (Fig.2.11 $+\Delta Q$) is required to obtain the optimal outlet velocity triangle, and vice versa. In other words, the optimal outlet velocity triangle of the runner is inversely proportional to the optimal inlet velocity triangle, so at a constant head and variable turbine speed, the process is expected to be always accompanied by losses at the runner outlet.

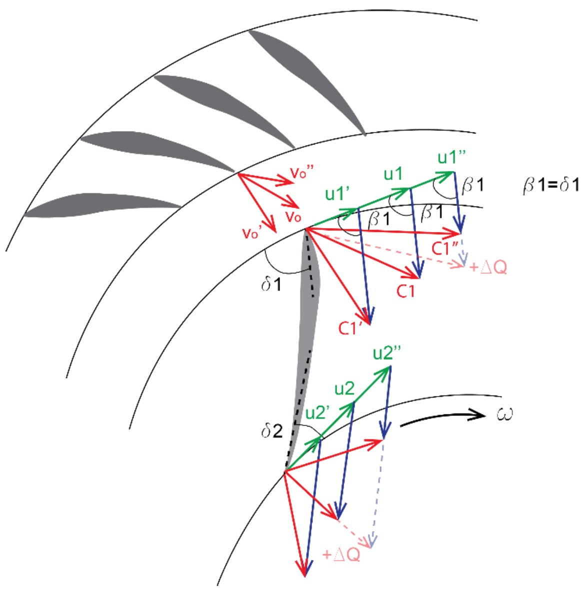

Fig.2.11 Changing the velocity triangles at variable speed

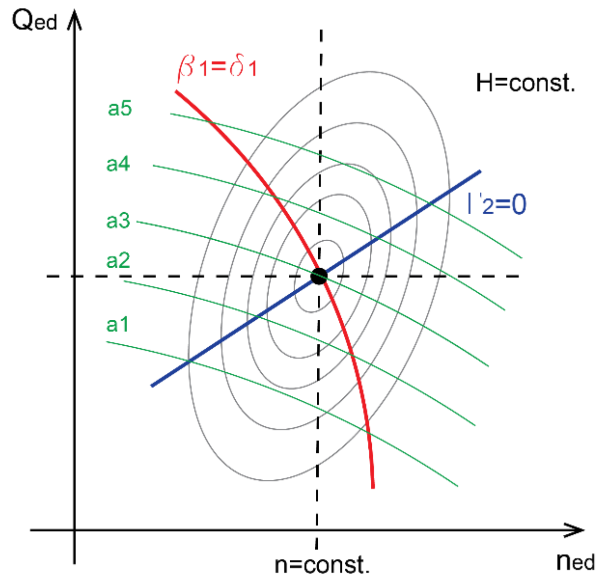

Fig.2.12 Reverse proportionality of the optimal inflow and outflow conditions of the runner [28]

From Fig. 2.11, the change of the velocity triangle at an increased rotational speed for a certain increase in flow rate ($+\Delta Q$) corresponds to the requirements of the law of similarity of operation of turbines, where the velocity triangle scales for $\eta = const.$, which leads to head change due to the need to increase the flow rate (Affinity law curve):

$$\frac{Q_d}{Q'} = \frac{n_d}{n'} ; \frac{H_n}{H'} = \left(\frac{n_d}{n'}\right)^2 = \left(\frac{Q_d}{Q'}\right)^2 \tag{2.38}$$

In Fig. 2.12 a schematic representation of the universal hill characteristic of a Francis turbine is given, with the inverse proportionality of the optimal runner flow conditions, derived at a constant head, for several positions of the guide vanes.

For such a configuration, it can be observed that at a constant synchronous rotational speed, with guide vanes opening, the efficiency of the turbine decreases. If there is a change in the rotational speed of the runner, those points can be shifted locally in the direction of increased efficiency (Fig. 2.13) and by that obtaining a scheme of the optimal path when operating a turbine with variable rotational speed.

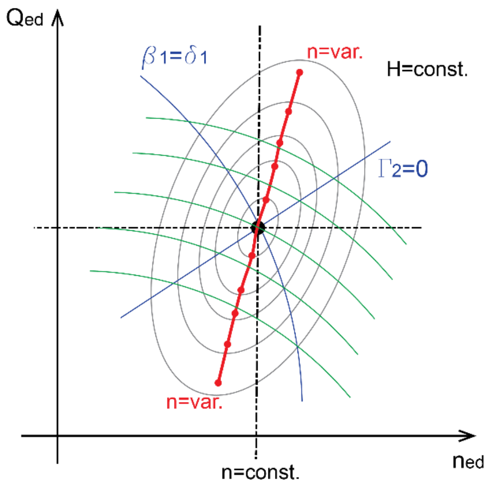

Fig.2.13 Optimal operation path with variable speed (without changing the geometric configuration of the guide vanes) [28]

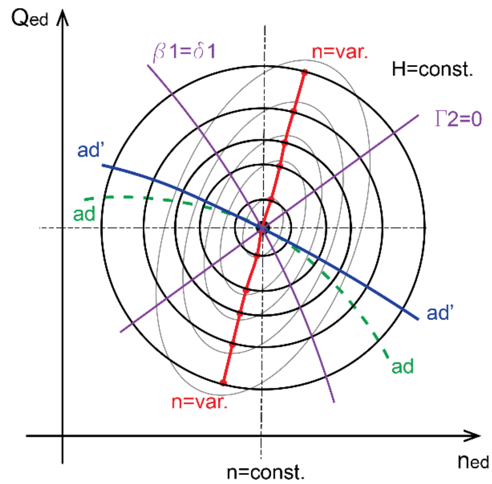

Fig.2.14 Operation with variable speed (by changing the geometric configuration of the guide vanes)

In Fig. 2.13, where the optimal path scheme is defined at a variable speed, there is no change in the characteristic of the guide vanes. The role of the guide vanes, in addition to the flow rate regulation, directly affects the shape of the operating characteristics of the turbine. Following the obtained path points and aiming to achieve a wider operating characteristic (schematically represented as concentric circles of iso-efficiencies), correction of the guide vane geometry is required (Fig.2.14), which, placed in its design position a_d, would lead to extension of the field of iso-efficiencies.

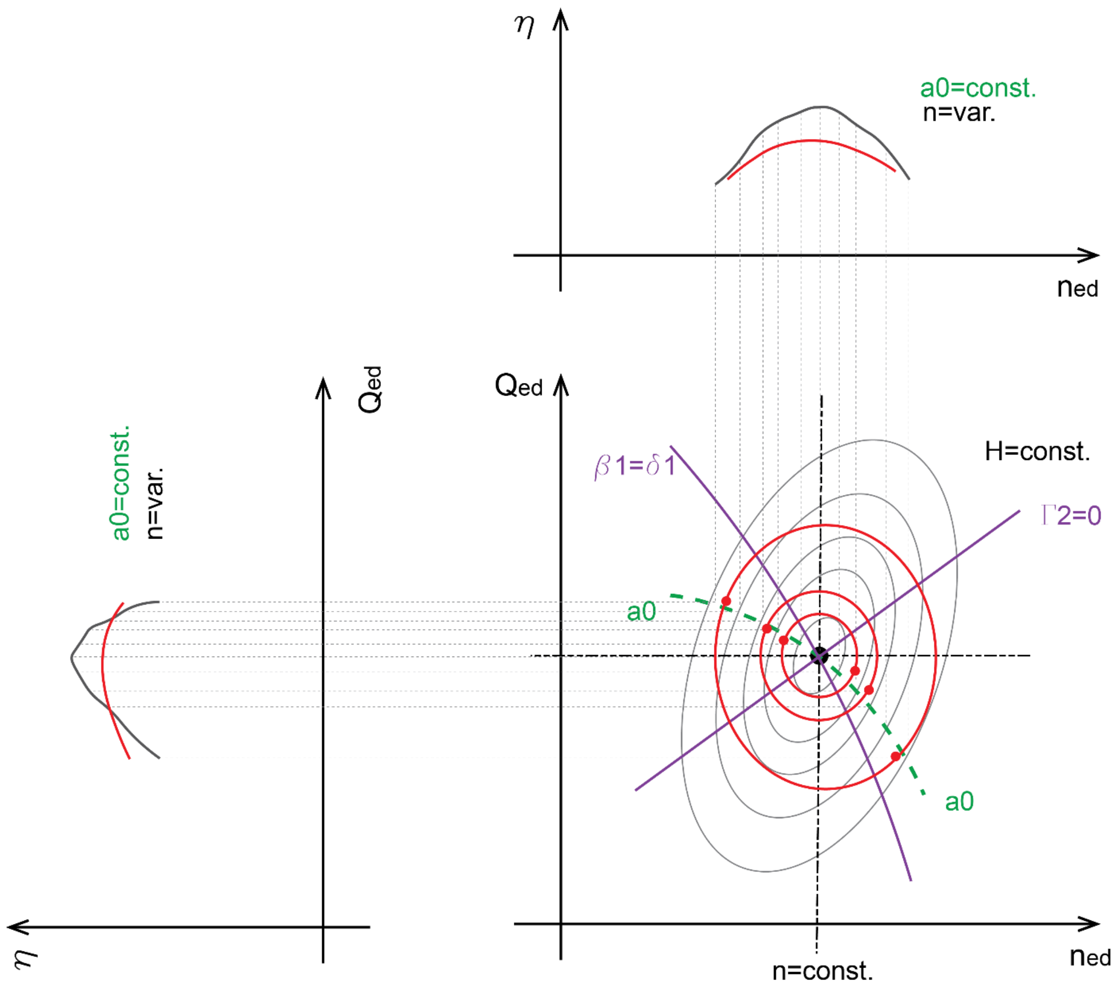

Fig.2.15 Schematic representation of expected behavior for corrected guide vane geometry in order to extend the operating range

In the scheme in Fig. 2.14 it can be noticed that in their design position at reduced speeds, the guide vanes should allow increased flow rate through the turbine and vice versa. For the given design position of the guide vanes, the change of the efficiency caused by the change of rotational speed is analysed in the following presentations through a direct analysis of the influence of the geometry of the guide vane blades on the extension of the turbine characteristics.

3. Derivation of the shape of the guide vane blades based on the initial calculation of flow parameters

3.1. Strategies and approach approach to guide vane design

In this chapter, the process of obtaining the shape of the blades of the guide vanes, as well as the complete radial cascade of profiles is elaborated. In the previous chapter, the mathematical dependencies of certain kinematic flow quantities of interest to the analysed problem were derived, on the basis of which a methodology for their correlation with the geometric shape of the blades and the cascade itself is performed in this chapter.

For the design of the guide vanes, the following strategies can be derived, depending on the goal that the radial cascade should meet:

- Design of a radial cascade of profiles in order to meet certain hydraulic performance (hydraulically favourable cascade)
- Design of a radial cascade of profiles for the purpose of turbine regulation (energy-efficient cascade)

At first glance, the two approaches are relatively similar, yet they differ in terms of the goal to be achieved, i.e. not every hydraulically favourable cascade meets the energy needs for turbine regulation, and vice versa. These conclusions are presented in the following chapters. What is common to both approaches is that the cascade, not dependent on the goal to be fulfilled, is shaped geometrically with respect to previously calculated or given kinematic flow quantities.

3.2. Geometric parameters of the radial cascade of the guide vanes

A radial cascade is defined with its geometric parameters and the interdependencies are derived in the following section.

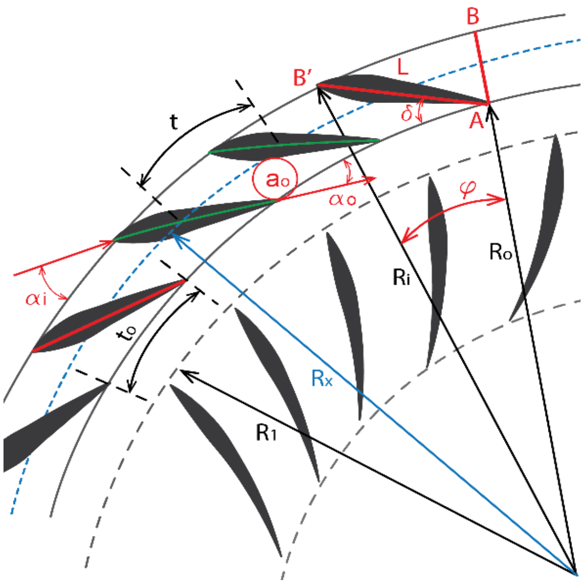

Fig.3.1 Geometric scheme of radial cascade

Tab.1 Description of geometric parameters

Symbol	Unit	Description
R_i [m]	[m]	Cascade inlet design radius
R_o [m]	[m]	Cascade outlet design radius
R_x [m]	[m]	Cascade axis circumference radius
B_{gv} [m]	[m]	Cascade height
R_1 [m]	[m]	Runner blades inlet radius
φ [deg]	[deg]	Blade chord wrap angle
point A	[-]	Starting point for chord placement
point B	[-]	Starting point for the end of chord
point B'	[-]	Rotated point B about the blade chord wrap angle
L [m]	[m]	Blade chord length
t [m]	[m]	Cascade pitch measured at axis circumference
t_o [m]	[m]	Cascade pitch measured at blades outlet
L / t [-]	[-]	Cascade density at axis circumference
α_i [deg]	[deg]	Cascade inlet flow angle
α_o [deg]	[deg]	Cascade outlet flow angle
δ [deg]	[deg]	Blade chord angle enclosed with outlet radius
a_o [m]	[m]	Blades opening
a_o / L [-]	[-]	Relative blade opening

All geometric sizes of the cascade are derived from the axis of rotation of the turbine. All individual listed geometric parameters in the further context are combined in order to obtain dimensionless quantities, i.e. a non-dimensional (normalized) cascade.

The first major parameter of the cascade is the outlet radius R_o which is related to the runner blades leading edge radius, which is represented as the difference in distance between the trailing edges of the cascade blades and the leading edges of the runner blades over the ratio:

$$C_{Ro} = \frac{R_o}{R_1} \tag{3.1}$$

Cascade inlet radius R_i where the leading edge of the cascade blades is located is represented as a percentage with the difference in distance between the two radii of the cascade through the ratio:

$$C_{Ri} = \frac{R_i}{R_o} \tag{3.2}$$

Starting point defined at the outlet radius R_o for positioning the trailing edge of the blades, i.e. the blade chord line is noted with the point *A*. The chord line end is defined with the point *B*. A schematic representation is provided in the following figures.

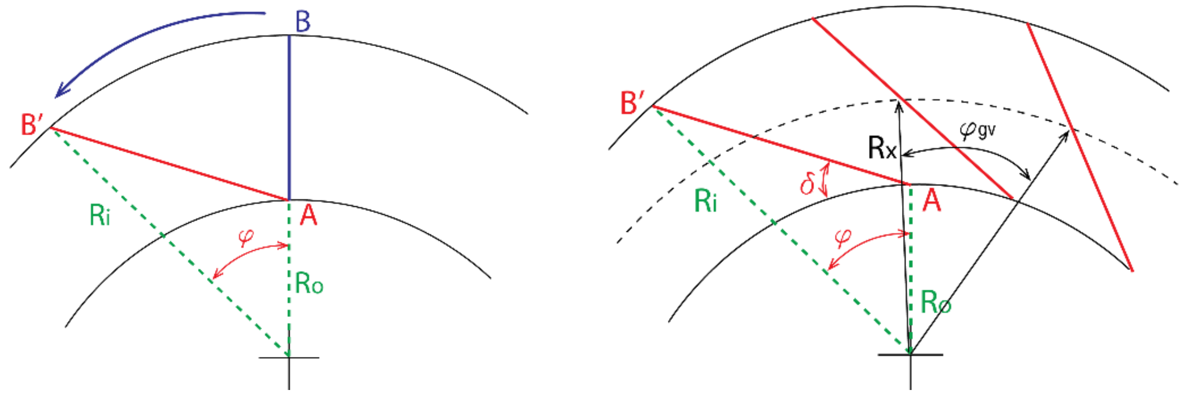

Fig.3.2 Scheme of blade chord line construction [32]

Rotating the point *B* around the turbine rotational axis, for a certain angle φ or the so-called blade enclosure angle, point *B'* which represents the beginning i.e. the leading edge of the blade is obtained, and the segment *AB'* represents the blade profile chord line. For a certain number of chord lines (blades) in the cascade, the angular pitch of the blades will be:

$$\varphi_{gv} = \frac{360}{Z_{gv}} \tag{3.3}$$

which differs from the blade enclosure angle. The chord line of the blade forms an angle δ with the outlet circle, which will be noted as the chord line inclination angle. This angle, together with the enclosure angle and the flow angle from the cascade are analysed in the chapter 6, where it is concluded that collinearity should be provided between the chord line inclination angle and the flow angle needed for the runner. If this criterion is introduced as:

$$\delta_{rel} = \frac{\delta}{\alpha_o} \approx 1 \tag{3.4}$$

then, the enclosure angle of the blade in the cascade is the result of all the above conditions and is expressed as:

$$\varphi = \text{atan}\left(\frac{\frac{1}{2Y_B'}\left(R_o - \sqrt{R_o^2 + 4X_B'Y_B'tan\delta}\right)}{tan\delta}\right) \tag{3.5}$$

where X_B' и Y_B' represent coordinates of the point B' (Fig. 3.2) arising as a result of the adopted number of blades and the length, i.e. the cascade density.

Chord line length *L* represents the blade length and depending on the adopted number of blades in the cascade Z_{gv}, the parameter of cascade density is derived [34]:

$$\frac{L}{t_o} = \frac{L}{\frac{2R_o\pi}{Z_{gv}}} \tag{3.6}$$

where the pitch t_o it is usually expressed by the dividing circle of the cascade on which the axes of rotation (pivot points) of the blades in the cascade lie, but for the reason that this geometric parameter is not of interest to the research, the pitch is calculated at the cascade outlet circle, as relevant for the analysis.

The inlet circle of the guide vanes is calculated using the Pythagorean Theorem from the projections of the length of the chord line along the *x* and *y*-axes and the outlet radius:

$$R_i = \left(L_x^2 + \left(L_y + R_o\right)^2\right)^{0,5} \tag{3.7}$$

Parameterisation of the opening clearance a_o between the blades shows particular difficulty, whether it is analysed between 2 profiles or theoretically 2 chord lines, where its interpretation on a relative basis is analytically represented through the relation:

$$a_{on} = \frac{a_o}{L} \tag{3.8}$$

3.3. Criteria for blade profile design

3.3.1. Calculation of flow kinematic parameters in the vaneless space

Guide vane blade profile design is represented as a consequence of the flow kinematic quantities present at the very entrance to the turbine runner, for certain design (operating) turbine conditions. As shown in Chapter 2, from the Euler equation, the simplified relation remains in the analysis for the optimal operating point of the turbine (Eq.2.29 and 2.34.1).

By calculating the inlet velocity triangle in the runner, for the design parameters of the turbine, the peripheral component of the absolute flow velocity at the runner inlet gives the inlet circulation to the runner:

$$\Gamma_1 = 2R_1\pi c_{u1} \tag{3.9}$$

According to the law of free vortex, the circulation in the vaneless space is maintained, so the ratio of the peripheral (tangential) components to the absolute velocity in that space is obtained as:

$$\Gamma_o = \Gamma_1\ ;\ v_{ou} = c_{1u}\frac{R_1}{R_o} \tag{3.10}$$

where v_{ou} is a projection of the outlet velocity of the guide vanes along the circumference of the cascades outlet circle.

The radial component of the absolute velocity, i.e. the runners meridional inlet velocity is calculated through the geometric boundaries of the runner inlet and the designed flow rate as:

$$c_{1m} = \frac{Q_d}{2R_1 \pi B_1} \tag{3.11}$$

The kinematic relation needs to be preserved as:

$$tg\alpha_1 = \frac{c_{1m}}{c_{1u}} \tag{3.12}$$

in order to obtain a constant meridional velocity (reduction of flow losses) and to be scaled to the guide vanes outlet radius for:

$$R_o > R_1 \tag{3.13}$$

a solution would be to reduce the height of the guide vane blade in the cascade in relation to the height of the runner:

$$B_o < B_1 \tag{3.13.1}$$

Due to constructive reasons, in the case of low-speed Francis turbines which have a proximity of the runner and the guide vanes, the height of the guide vanes is performed almost equal to the inlet height of the runner:

$$B_o \approx B_1 \tag{3.13.2}$$

resulting in a reduction of the radial velocity component, and thus a reduction in the flow angle they provide:

$$v_{or} = \frac{Q_d}{2R_o \pi B_o} \tag{3.14}$$

$$tg\alpha_o = \frac{v_{or}}{v_{ou}} < \ tg\alpha_1 = \frac{c_{1m}}{c_{1u}} \tag{3.15}$$

These relations show the flow laws in the vaneless space between the guide vanes and the runner. The flow velocity at the guide vanes outlet is:

$$v_o = (v_{0r}^2 + v_{ou}^2)^{0.5} \tag{3.16}$$

from which the required opening clearance between two blades can be roughly defined as:

$$a_{0p} = \frac{Q_d}{Z_{gv} B_o v_o} \tag{3.17}$$

3.3.2. Blade profile camber line definition

There are several recommendations and standards for performing the camber line equations of hydro profiles (airfoils), where some of them give many limitations in terms of the shape (brakes and slopes) of the profile. For this reason, a 3rd order polynomial function is derived from the theory of wing development in tailless aircrafts:

$$y_c = Ax^3 - Bx^2 + Cx = (ab - a)x^3 - abx^2 + ax \quad (3.18)$$

where x is a dimensionless length of the blade (profile). The coefficients of the polynomial are solved and defined in strictly defined limits of dimensionless chord length from 0 to 1, where the boundary conditions are defined for those two positions. That is, the first derivative of the polynomial will be:

$$\frac{dy_c}{dx} = 3Ax^2 - 2Bx + C = 3(ab - a)x^2 - 2abx + a \quad (3.18.1)$$

where for $x = 0$, the derivative of the function at the starting point gives the tangent to the angle of inclination of the line, i.e.:

$$a = C = tg(\beta_i) \quad (3.18.2)$$

and for $x = 1$, the derivative of the function gives the tangent of the angle of inclination of the line, i.e.:

$$tg(\beta_o) = 3\big(B - tg(\beta_i)\big) - 2B + tg(\beta_i) = 3B - 3tg(\beta_i) - 2B + tg(\beta_i) \quad (3.18.3)$$

$$tg(\beta_o) = B - 2tg(\beta_i) \quad (3.18.4)$$

$$B = tg(\beta_o) + 2tg(\beta_i) \quad (3.18.5)$$

The polynomial coefficients defined in this way, through the angles of the tangents at the beginning and the end of the chord line, give the camber line function:

$$y_c = Ax^3 - Bx^2 + Cx \quad (3.19)$$

with the coefficients:

$$B = tg(\beta_o) + 2tg(\beta_i) \quad (3.19.1)$$

$$A = B - tg(\beta_i) \quad (3.19.2)$$

$$C = tg(\beta_i) \quad (3.19.3)$$

where β_i represents the inlet angle of the blade chord line enclosed with the inlet angle of the flow in the cascade, and β_o represents the outlet angle of the blade chord line enclosed with the outlet flow angle of the cascade.

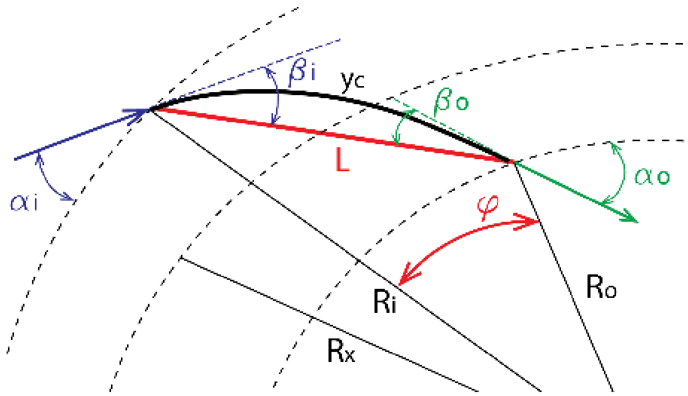

Fig.3.3 Schematic representation of the camber line derived between the flow angles and the chord line [33]

This shows that the camber line coefficients are strongly dependent on the flow angles through the blade chord line. This equation was developed to obtain profiles with the so-called reflective camber line, which is presented in the following figures.

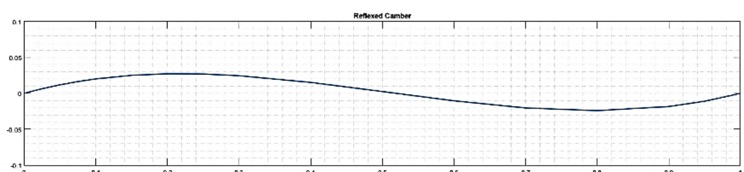

Fig.3.4 Example of a camber line for a negative angle at the chord line ending

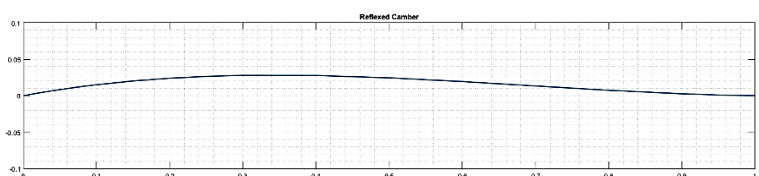

Fig.3.5 Example of a camber line for a positive angle at the chord line ending

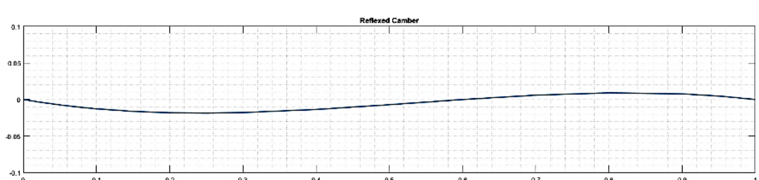

Fig.3.6 Example of a camber line for a negative angle at the chord line beginning

3.3.3. Blade profile thickness distribution with weighted parameters

The general expression for describing the thickness distribution of a profile is [35]:

$$y_T = x^m (1-x)^n f(x) \tag{3.20}$$

and represents a change in the relative thickness of the profile, where m, and n are parametric quantities, and $f(x)$ is a function that has no real roots in the interval from 0 to 1. This expression can be written in many different forms as needed. Also, for obtaining other standardised profiles, the laws of distribution from the leading edge to the location of the maximum thickness are applied through a parabolic, hyperbolic, or elliptical law, which gives the equation various forms. Instead of this approach, the so-called "Bezier Spline" function is used, which requires several weight parameters to which the function asymptotically tends.

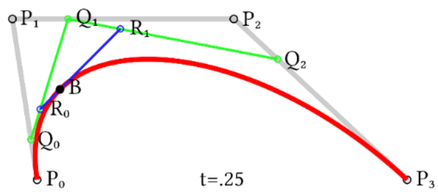

Fig.3.7 Bezier curve example with n=4 weight parameters

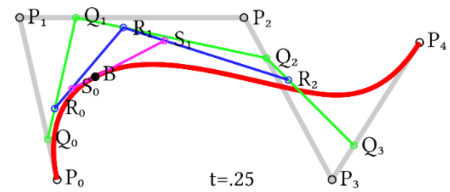

Fig.3.8 Bezier curve example with n=5 weight parameters

The weight parameters of the curve are given through some natural and geometric laws, such as:

- The weight parameters that describe the leading edge of the profile are derived according to a simple law of single parabola (NACA standards);
- The weight parameters that describe the location and intensity of the maximum thickness are free for manipulation in the zone of 20-45% of the chord length;
- The weight parameters that describe the tail of the profile (trailing edge distribution) have a downward trend with a mutual angle of inclination in the range of 4 to 8 degrees to avoid possible flow separations.

Practically, more weight parameters give a more accurate asymptotic curve for the distribution function. For this case, 9 weight parameters are performed to which the profile distribution curve is described.

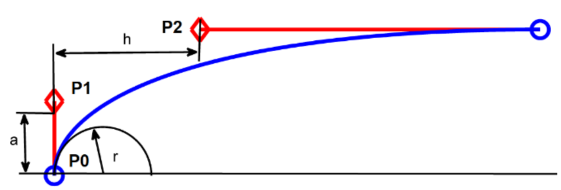

Fig.3.9 Bezier asymptotic curve example for leading edge thickness distribution [36]

The leading edge is defined by three weights: P_0, P_1 and P_2 which actually represent points on xy plane with coordinates $P_0(P_{0x}\ P_{0y})$, $P_1(P_{1x}\ P_{1y})$ and $P_2(P_{2x}\ P_{2y})$. The coordinate values of the initial (zero) parameter are:

$$P_0 = (0{,}0) \tag{3.21}$$

which defines the starting point of the curve at the coordinate origin, which must be preserved. Weight parameters P_1 and P_2 are directly dependent on the adopted maximum thickness that the profile should have, expressed as a percentage of the unit length:

$$t_y = \frac{1}{2}\frac{T_y}{100}x\,; x = 1 \tag{3.21.1}$$

where T_y represents the actual maximum profile thickness as a percentage of the length, and t_y is half the actual thickness which should be given equally on both sides (pressure and suction profile contours) related with the camber line. The thickness parameter is related to $P_4(P_{4x}\ P_{4y})$ where $P_{4y} = t_y$ represents the magnitude of the maximum thickness, and $P_{4x} = dx$ which represents the location of the maximum profile thickness along the x axis, expressed as a percentage of the unit length of the chord. The weight parameters P_3 and P_5 have equal magnitudes along the y coordinate, and along the chord line they are located on $\pm 10 \div 20\%$ from the adopted location of maximum thickness dx, in order to concentrate those points in the zone of maximum thickness, and to increase tendency of the asymptotic curve in that zone. The weight parameter P_3 is adopted to represent the smaller radius of the ellipse that describes the leading edge of the profile. The weight parameters P_1 and P_2 are represented as tangent coordinates that describe the elliptical law of the leading edge, occupying the radius of the initial inscribed circle in the profile (parameter P_1 according to NACA standards):

$$r = 0.204T_y\,; P_{1x} = 0\,; P_{1y} = 2r \tag{3.21.2}$$

The weight parameter P_2 is derived towards the beginning of the profile curvature according to the location of the maximum thickness, taken from the Russian standards [8] for construction of hydro profiles in terms of the location of the maximum thickness and magnitude as $P_{2x} = 0.11dx$ and $P_{2y} = 0.8t_y$.

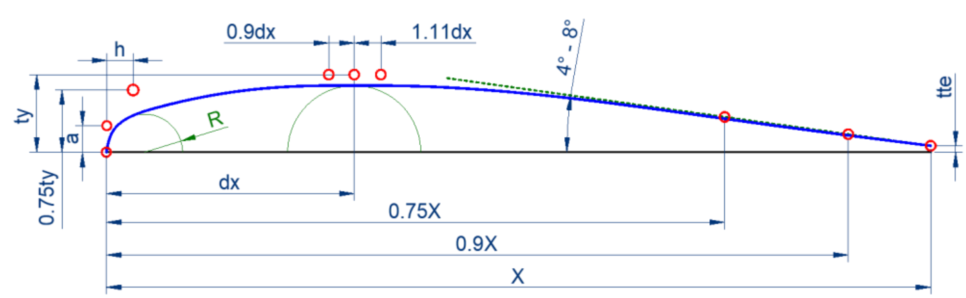

Fig.3.10 Weight parameters that define the thickness distribution of the profile

The weight parameters P_6 and P_7 are at 75% and 90% of the chord length of the profile where their magnitude along the y coordinate is directly dependent on the adopted thickness at the end of the profile. The weight parameter P_8 represents the minimum thickness of the profile at its very end, where according to the Russian recommendations [8] for making guide vane blades is $P_{8y} = 0.01x$ at length of $P_{8x} = x$. P_{6y} and P_{7y} have a downward trend with respect to a defined angle of $4 - 8$ $[deg]$ to prevent eventual flow separations. The Bezier Spline curve [37] can be written as:

$$B(t) = \sum_{i=0}^{n} \binom{n}{i} (1-t)^{n-i} t^i P_i \ ; \ \binom{n}{i} = \frac{n!}{i!\,(n-i)!} \tag{3.22}$$

where n is the number of weight parameters, i the very parameter number, t-variable and P_i is the weight parameter. The following figures show several derived standard profiles compared to profiles obtained with this technique.

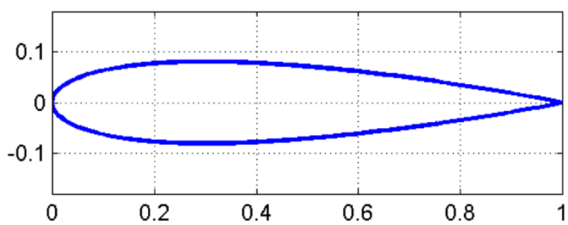

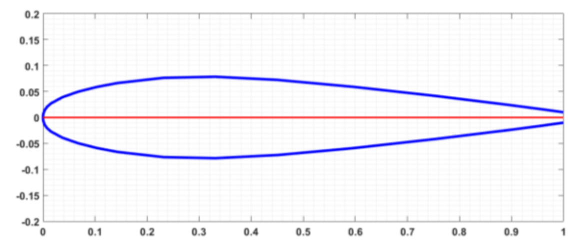

$NACA\ 0016\ (dx = 0.3\ ; T_y = 0.16)$

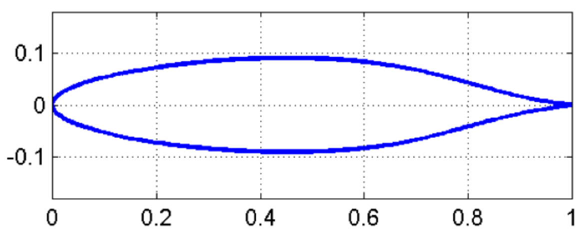

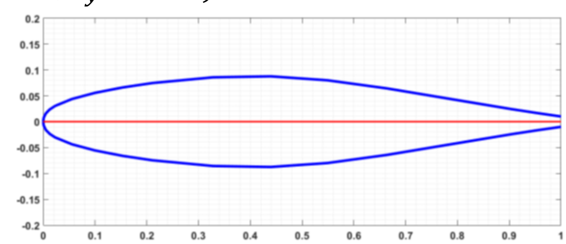

$NACA\ 66 - 018\ (dx = 0.45\ ; T_y = 0.18)$

Fig.3.11 Standard derived profiles

Fig.3.12 Bezier created profiles

3.4. Geometric dimensionless (normalised) radial cascade

The entire calculation procedure and the criteria for profiling the blades of the guide vanes are implemented in a calculation code in MATLAB. For initial design parameters of a turbine, such as flow rate, head, runner inlet diameter, and rotational speed, the calculation procedure is performed by defining the required flow velocities and angles that are present at the runner inlet, as well as the required velocities and angles at the guide vanes outlet. In that sense, in the following presentations, the geometric specification of the cascades will be given in dimensionless form, representing the percentage of the outlet diameter versus the inlet diameter of the runner, the cascades inlet and outlet diameters ratio, the density, the number of blades, angle relative to the pitch angle of the cascade, and the location and maximum thickness of the blades.

3.4.1. Example 1 - HPP St. Petka in Macedonia

Tab.3.1 Turbine input parameters

Qd [m3/s]	Hn [m]	n [rpm]	D1 [m]	B1 [m]
50	40	214,29	2,484	0,97

Tab.3.2 Obtained cascade parameters

L/t [-]	Cro [-]	Cri [-]	Zgv [-]	fi_n [-]	dx [-]	ty [-]
1,15	1,075	1,16	24	1,2184	0,275	0,17

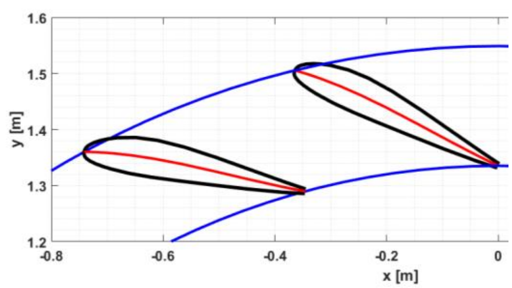

Fig.3.13 Geometry of calculated guide vane configuration (ex.1.)

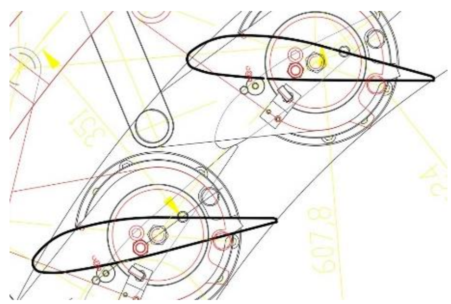

Fig.3.14 Existing geometry technical drawing

3.4.2. Example 2 - HPP Tokke in Norway

Tab.3.3 Turbine input parameters

Qd [m3/s]	Hn [m]	n [rpm]	D1 [m]	D2 [m]	B1 [m]
31	377	375	3,1875	1,7799	0,306

Tab.3.4 Obtained cascade parameters

L/t [-]	Cro [-]	Cri [-]	Zgv [-]	fi_n [-]	dx [-]	ty [-]
1,333	1,06	1,093	28	1,3665	0,2	0,2

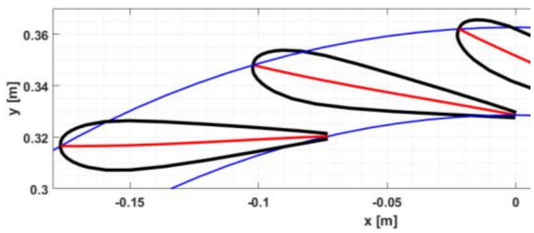

Fig.3.15 Geometry of calculated guide vane configuration (ex.2.)

Fig.3.16 Existing geometry technical drawing

4. Criteria for analysis

As mentioned in Chapter 2, the analysis generally goes in several directions, considering the interaction between the shape of the blades, the hydrodynamic conditions, and the variable speed. According to this, the main criteria on which the conclusions will be made are derived. It will be considered in what way different types of guide vane geometries affect turbine efficiency and velocity profiles created in the vaneless space. In other words, if the analysis starts from the turbine's needs to operate with variable speed, what is the guide vane configuration that arises and by that, what kind of velocity profiles are obtained in the vaneless space.

This analysis is complicated by the introduction of new parameters, whether they are geometric, hydraulic, or energy parameters. The narrowing of the analysis moves towards the definition of several parameters:

a) Geometric parameters of the guide vanes: number of blades, cascade density, enclosed blade angle, and, additionally, blade opening clearance;

b) Hydraulic parameters: flow pattern, velocity profiles, and additional pressure losses and energy losses;

c) Energy parameters: efficiency of the turbine and operating range expansion.

4.1. Flow field criterion, velocity profiles, and dominant hydrodynamic quantities

The flow field and the velocity profiles obtained in the vaneless space between the guide vanes and the runner are drastically different from the analytical methods of calculating average velocities, which were derived in the previous chapters. The velocity profile is viewed three-dimensionally, along the outlet circle of the guide vanes, and by height. The results obtained for the different cases, when analysing the influence of the variable speed on the velocity profile, will be considered in the sections of uniformed flow along with the height of the blade (blade midspan surface). For the cases of non-uniform blades at three heights of the blade, where a criterion for uniformity of the velocity profile according to BS 1042: Section 2.4. (1989) – Measurement of fluid flow in closed conduits (Part 2. Velocity-area method) [38], which gives:

$$Y = \frac{\sigma_{Ui}}{U} = \frac{1}{U}\sqrt{\left[\frac{\sum_{i=1}^{n}(U_i - U)^2}{n-1}\right]} \tag{4}$$

and represents the standard deviation of the individual velocity values obtained along the measuring zone. Thus, the index of uniformity of the profile is calculated, and it is related to the type of the cascade, which gives a complete hydraulic-geometric parameterisation of the conducting apparatus.

Other hydraulic quantities in the vaneless space, such as pressure distribution, circulation, etc. are calculated as averaged values on the surface of the guide vanes outlet and are analysed in relation to the required adopted values that the cascade should achieve.

4.2. Criterion for extending the operating characteristic of a turbine with variable speed

This criterion, as mentioned in Chapter 2, is defined in relation to the design position of the openness of the guide vanes $a_o = const.$ where the deviation of the turbine efficiency around its optimum will be analysed, for different rotational speeds. As mentioned, the cascade which gives smaller efficiency deviations at variable speeds results in an extension of the turbine operating range.

Therefore, conclusions were drawn for profiling the blades by height, instead of using single-profile blades; it is expected that a certain zone of the blade is a dominant carrier when directing the flow towards the guide vane outlet, about the required rotational speed of the runner.

4.3. Methods for comparing results

The calculations of the turbine coefficients for defining the characteristic are made on the basis of the standard IEC60193 [39] for performance evaluation, using dimensionless parameters n_{ed} $[-]$, Q_{ed} $[-]$ and T_{ed} $[-]$.

Due to the existence of several parameters in the analysis, some of the results are presented in 3D charts, where the *x* and *y*-axes represent certain geometric parameters of the guide vanes, versus the design parameters of the guide vanes (design flow rate), in order to define the geometries of the guide vanes that are closely or precisely defined for the given input parameters of the turbine. The turbine efficiency is presented as an outcome on the vertical *z*-axis.

The points obtained in space are interconnected by a statistically trending approximate surface according to the method of least squares (Response Surface Methodology) which provides a view of the dependencies of the variables with the responsive variable, in this case, the turbine efficiency. The approximate surface introduces an error in the approximation through the points obtained from the analyses, but it globally gives a view of the mutual influences of the individual parameters, from where the conclusions will be drawn and the following models will be derived.

5. Numerical modelling

The performed analyses and the obtained results in this dissertation are based on numerical flow modelling, with special review to the approach to flow simulation in hydraulic turbines, using the commercial software package ANSYS FLUENT 20. The numerical models are firstly based on defining the individual fluid domains, which practically represent the individual subsets of the hydraulic turbine, such as the spiral casing, stay vanes and guide vanes, turbine runner, and the draft tube. Their presentation for the purposes of the simulations is done through the discretisation of the fluid flow volumes and defining the initial and boundary conditions in which the numerical solution is expected.

5.1. Fluid flow governing equations and turbulence modelling

If a three-dimensional flow of an incompressible fluid is considered where the density is constant $\rho = const.$, then the basic principles are known [40]:

- Law of mass conservation (Continuity equation)

$$\nabla\vec{v} = \frac{\partial v_x}{\partial x} + \frac{\partial v_y}{\partial y} + \frac{\partial v_z}{\partial z} = 0 \tag{5.1}$$

- Law of momentum conservation (Navier-Stokes equations)

$$\frac{\partial\vec{v}}{\partial t} + \nabla\cdot(\vec{v}\otimes\vec{v}) = -\nabla p + \nabla\cdot\tau + \vec{F} \tag{5.2}$$

$$\tau = \mu(\nabla\vec{v} + \nabla\vec{v}^T) - \frac{2}{3}\nabla\cdot\vec{v}I \tag{5.3}$$

The turbulent flow is characterised by velocity fluctuations over time about one constant value of the velocity, the so-called average velocity. Considering one of the components of the velocity, it can be written that:

$$\overline{v_x(t)} = v_x = \frac{1}{\Delta t}\int_t^{t+\Delta t} v_x(t)dt \tag{5.4}$$

where at any given moment the instantaneous velocity is the sum of the mean and fluctuating components (pulsation):

$$v_x(t) = v_x + v_x'(t) \tag{5.5}$$

Other fluctuating hydromechanical, vector or scalar quantities are written as:

$$f(t) = f + f'(t) \tag{5.6}$$

Substituting these expressions into the Navier-Stokes equation gives the so-called Reynolds equation for turbulent flow of incompressible viscous fluid (RANS):

$$\frac{\partial \vec{v}}{\partial t} + \overline{(\vec{v'}, \nabla)\vec{v}} = -\nabla p + \nabla \cdot \left(\tau - \overline{v'}\right) + \vec{F} \tag{5.7}$$

To solve the Reynolds equation, it is always necessary to go along with the continuity equation. To obtain the turbulence, the member in the equation $\overline{v'}$ represents the Reynolds flow stresses, which need to be mathematically modelled in order to complete the solution. The Reynolds stresses are in relation to the gradients of the mean velocity and the turbulent viscosity, where for a two-dimensional flow, they are written as:

$$\overline{v'} = \overline{v_x v_y} = \mu_t \left(\frac{\partial v_x}{\partial x} + \frac{\partial v_y}{\partial y}\right) - \frac{2}{3}\delta_{xy} \cdot \left(k + \mu_t \frac{\partial v_z}{\partial z}\right) \tag{5.8}$$

the so-called Boussinesq hypothesis, so the Reynolds transport equation can be written as:

$$\frac{\partial v_x}{\partial t} + \frac{\partial}{\partial y}\left(v_x v_y\right) = -\frac{\partial p'}{\partial x} + \frac{\partial}{\partial y}\left[\mu_{eff}\left(\frac{\partial v_x}{\partial y} + \frac{\partial v_y}{\partial x}\right)\right] + F \tag{5.9}$$

where $\mu_{eff} = \mu + \mu_t$ is the effective viscosity and the pressure is:

$$p' = p + \frac{2}{3}k + \frac{2}{3}\mu_{eff}\frac{\partial v_z}{\partial z} \tag{5.10}$$

where for incompressible flows the last member is neglected. If it is assumed that the turbulent viscosity is dependent on the kinetic energy of turbulence:

$$\mu_t = C_\mu \rho \frac{k^2}{\varepsilon} \tag{5.11}$$

where C_μ is a constant, and k and ε are alternately the kinetic and dissipative energies of turbulence, and they are the result of two transport equations:

$$\frac{\partial}{\partial t}(\rho k) + \nabla(\rho V k) = \nabla \cdot [(\mu + \frac{\mu t}{\sigma k})\nabla k] + P_k - \rho\varepsilon \tag{5.12}$$

$$\frac{\partial(\rho\varepsilon)}{\partial t} + \nabla \cdot (\rho V \varepsilon) = \nabla \cdot \left[\left(\mu + \frac{\mu t}{\sigma\varepsilon}\right)\nabla\varepsilon\right] + \frac{\varepsilon}{k}(C_{\varepsilon 1}P_k - C_{\varepsilon 2}\rho\varepsilon) \tag{5.13}$$

These two equations are known as $k - \varepsilon$ standard turbulence model. In case of rotational frames in the numerical model, as an example of rotational frame movement of a turbine runner, the turbulent viscosity is calculated in the same way, where the coefficient $C_\mu \neq const.$ and is expressed as:

$$C_{\mu} = \frac{1}{A_0 + A_s \frac{kV}{\varepsilon}} \tag{5.14}$$

where A_0 and A_s are constants, $V = f(\overline{\Omega})$ is depending on the mean value of the fluid flow rotation seen in the rotating domain, which is dependent on the angular velocity of the domain $\overline{\Omega} = f(\omega_k)$. The transport equations for k and ε will then be:

$$\frac{\partial}{\partial t}(\rho k) + \nabla(\rho V k) = \nabla \cdot [(\mu + \frac{\mu t}{\sigma k})\nabla k] + P_k - \rho\varepsilon \tag{5.15}$$

$$\frac{\partial(\rho\varepsilon)}{\partial t} + \nabla \cdot (\rho V \varepsilon) = \nabla \cdot \left[\left(\mu + \frac{\mu t}{\sigma \varepsilon}\right)\nabla\varepsilon\right] + \rho C_1 S \varepsilon - \rho C_2 \frac{\varepsilon^2}{k + \sqrt{\mu\varepsilon}} + \frac{\varepsilon}{k} C_{\varepsilon 1} C_{\varepsilon 3} G_b + S_{\varepsilon} \tag{5.16}$$

These two equations are also $k - \varepsilon$ turbulence model, known as “Realizable” model that exceeds certain limits in the equation of kinetic energy dissipation of the turbulence in the standard description, where parameters of rotating flow domains in the numerical model are inserted and performs better prediction in case of flow separations along the walls. This model has been adopted and will be used in further numerical simulations.

5.2. Modelling of Boundary Layer Flow

Turbulent flows depend on the presence of walls. In the flow field where the average velocity is obtained, the non-slip condition of the walls has an impact. Modelling close to the walls significantly affects the reliability of the numerical solution, if the walls are the main source of turbulence or eddy current. Therefore, accurate representations of flow near walls allow predictions of turbulent flows in those areas.

Numerous experiments show that the zone near the wall (boundary layer) can generally be divided into three smaller zones. In the internal layer, called the "viscous sublayer", the flow is almost laminar, and molecular viscosity plays a dominant role in maintaining fluid motion. In the outer layer, called the completely turbulent layer, turbulence plays a major role. There is a zone between the viscous sublayer and the completely turbulent layer where the effects of molecular viscosity and turbulence are equally influential.

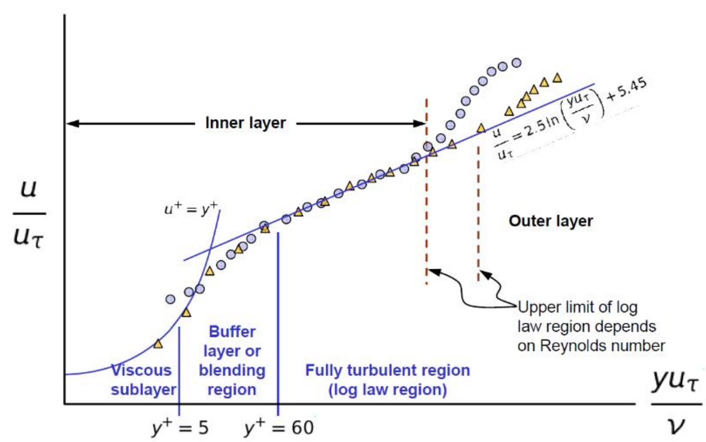

Fig.5.1 Zones in the boundary layer of the flow

Common practice shows that engineering analyses do not require flow modelling in the viscous sublayer and that the numerical modelling of the boundary layer flow along the walls is satisfied with a great accuracy, by using the above turbulence models and defining a dimensionless distance from the wall to the core of the flow within $30 < y^+ < 300$, i.e. in the zone of logarithmic law of distribution. The stated dimensionless distance is nothing more than a calculation of the height and growth of the cells in the numerical mesh from the walls to the flow core. Thus, the dimensionless value of the height of the first cell next to the wall is calculated as:

$$y^+ = \frac{\rho v_\tau y}{\mu} \tag{5.17}$$

where v_τ represents the friction velocity of the fluid in the wall zone, where the tangential stress τ_w is calculated depending on the coefficient of frictional resistance of the wall.

$$v_\tau = \sqrt{\frac{\tau_w}{\rho}} \tag{5.18}$$

Flow around aerodynamic bodies is adopted, an approximate value of the frictional resistance is given in the theory as a dependence of the ratio of the maximum thickness of the profile and the length of its chord line $C_{wt} = f(t_y/L) = 0.08 \div 0.04$ [41]. For simplification, an average coefficient of resistance of the profiles $C_{wt} = 0.06$ is adopted. From here, the tangential stress is calculated as:

$$\tau_w = \frac{1}{2} C_{wt} \rho v_\infty^2 \tag{5.19}$$

where v_∞ represents the average velocity of the flow in the profile zone. If the initial value for the dimensionless height of the first cell is set, the actual height of the first cell in the boundary layer can be calculated as:

$$y = \frac{y^+ \mu}{v_\tau \rho} \tag{5.20}$$

According to the chart in Fig. 5.1, for solving the boundary layer in the purely logarithmic area where the completely turbulent layer is dominant, the dimensionless value of the cell height is $y^+ > 60$, so that in the further simulations the value is adopted as $y^+ = 100$. It is recommended that the number of cells in the boundary layer is not less than three, and the mutual growth of cells is within the range of 1.1 to 1.3, thus adopting an increase in the further simulations of 1.2.

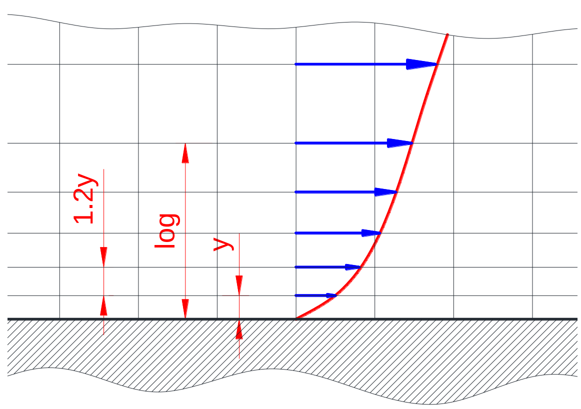

Fig.5.2 View the development of the cells for solving the boundary layer in the logarithmic zone

5.3. Description of the reference model from the analysis - The Francis 99 turbine

The Francis 99 turbine represents a scaled model (1:5.1) of a prototype turbine at the Tokke hydropower plant in Norway [42]. The turbine is consisted of a spiral casing with inserted 14 stay vane blades, 28 guide vane blades, and a runner with 15 full and 15 splitter blades which form 30 front (leading) edges at the runner inlet, as well as an elbow type draft tube with variable cross-section. The runner inlet and outlet diameters are $D_1 = 0.63\ [m]$ and $D_2 = 0.349\ [m]$, respectively. The turbine model is situated at the Water Power Laboratory at the Norwegian University of Science and Technology in Trondheim. The cross-section of the turbine model is given in Fig. 5.3.

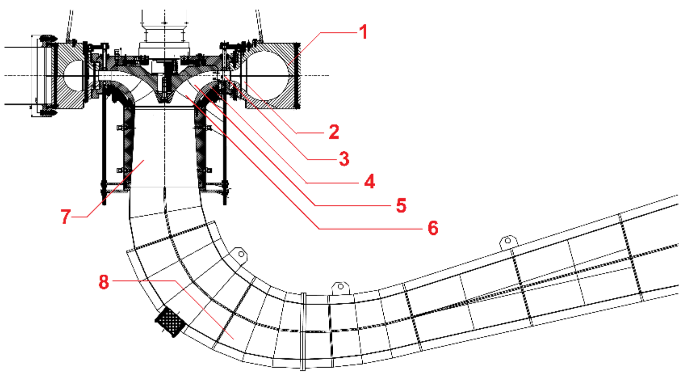

Fig.5.3 Cross-section through the Francis 99 turbine model [42]

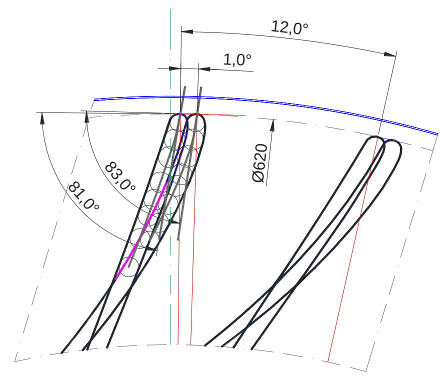

Fig.5.4 Geometric details at the runner inlet

The turbine model is composed of (1) spiral casing, (2) stay vanes, (3) guide vanes, (4) turbine runner, (5) main blades of the runner, (6) splitter blades, (7) draft tube cone section and (8) draft tube elbow section. The turbine runner represents a low-speed (high-head) Francis turbine with 15 full and 15 splitter blades. From the performed model tests, the following data is available for the turbine in the partial (low) operating mode (PL – Part load), in the zone of maximum efficiency (BEP – best efficiency point) and in the high operating mode (HL – High load):

Tab.5.1 Derived characteristics of the model Francis 99 [42]

	ρ [kg/m3]	g [m/s2]	ned [-]	Qed [-]	η [-]	Hn [m]	Q [m3/s]	n [rpm]	T [Nm]
PL	999.23	9.821	0.215	0.07	0.7169	12.29	0.071	406.2	144.06
BEP	999.19	9.821	0.18	0.15	0.9303	11.91	0.203	335.4	628.41
HL	999.2	9.821	0.195	0.19	0.9066	11.24	0.221	369.6	605.62

5.4. Definition of a numerical model, verification and determination of numerical error and deviations from laboratory measurements

According to the previously mentioned methods of numerical modelling, an analysis was performed with CFD simulation of the model of the Francis 99 turbine, which is a taken as a reference in this dissertation and the further analyses, and it will be referred to as "zero model" or Model 0.

In the previous analyses and published results in papers [29], [30], [43], [44], [45], the simulations are conducted without the participation of the spiral casing and the stay vanes, because analyses have been conducted on the inflow effects in the guide vanes, the inflow directions and its effects, as well as on a range of different models of guide vane blades that deviate from the conventional geometry available, to obtain more results and data on the behaviour of the guide vane geometry on the turbine characteristics.

With this simplification, a reduction of the required computational time is obtained at the same time; the numerical model under examination has a reduced number of elements, thus the model is composed of the guide vanes, the runner, and the draft tube cone section. The spiral casing and the stay vanes of the turbine model have been previously analysed through numerical simulations, where energy losses are obtained and later included in the calculation model to determine the net head (Fig. 5.5).

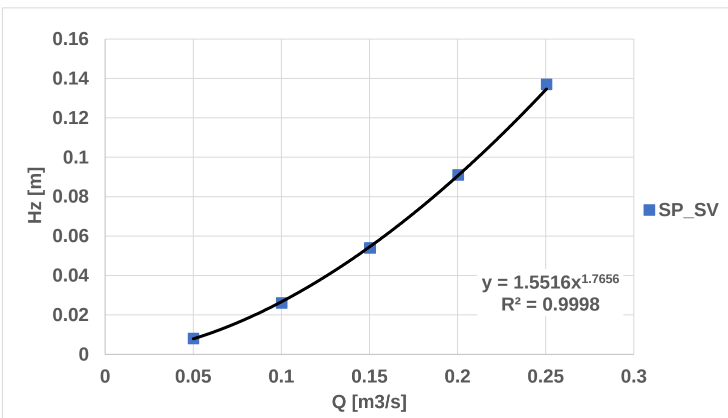

$$\Delta H_z = m_{sp} Q^n$$
$$m_{sp} = 1.5516$$
$$n = 1.7656$$

Fig.5.5 Hydraulic losses curve of spiral casing and stay vanes and module and exponent of hydraulic loss curve

For the performance of the numerical model, the starting data are the energy parameters of the turbine model, where for the best efficiency point the data is as follows:

Tab.5.2 Derived data for best efficiency point of the turbine

BEP	ρ [kg/m3]	g [m/s2]	ned [-]	Qed [-]	D1 [m]	D2 [m]	n [rpm]	Hn [m]	Qd [m3/s]	T [Nm]
	998.2	9.81	0.18	0.15	0.62	0.349	333.33	11.76	0.2017	624.44

5.4.1. Runner meshing

The runner with its characteristic dimensions is presented in Fig. 5.6. The runner mesh is performed according to analytical calculations for the growth of cells along the walls, for the given flow rate, i.e. calculation of the relative flow velocity at the inlet. For $D_1 \approx 0.62\ [m]$, $n = 333.33\ [min^{-1}]$, $B_1 \approx 0.06\ [m]$,$Q_d = 0.2017\ [m^3/s]$ and runner blades leading edge angle of $\delta_1 \approx 82\ [°]$, the velocity triangle is analytically determined at the inlet, where the relative velocity is

$$w_1 \approx 1.75\ [m/s]$$

The calculated value for the relative velocity is assumed to be 2[m/s], for the reason that the thickness of the blades is not taken into account. Therefore, the height of the first cell is calculated as 0.05 [mm], and 5 cells are provided for the description of the boundary layer with mutual growth of 1.2 (20% growth). The runner is consisted of $6 \cdot 10^5$ cells.

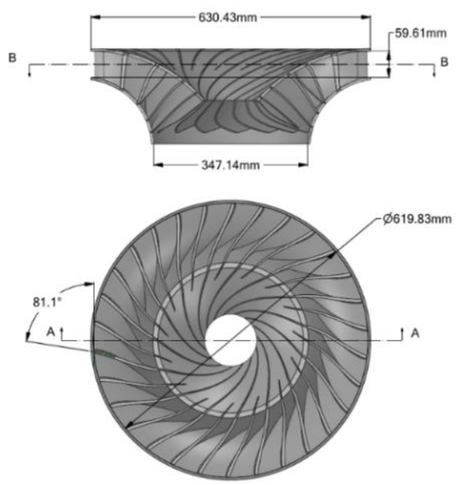

Fig.5.6 Cross-section of the Francis 99 model runner

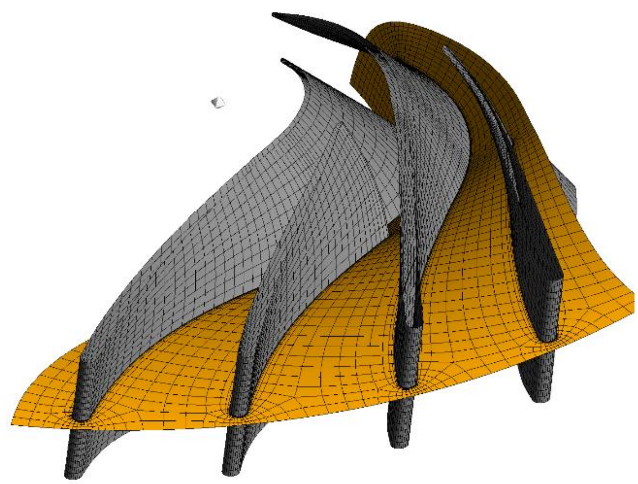

Fig.5.7 Runner mesh

5.4.2. Guide vane meshing

The guide vanes with their characteristic dimensions are presented in Fig.5.8. The analytical calculation of the velocities in the vaneless space obtained that the maximum velocity between two blades is

$$v_o \approx 10\ [m/s]$$

thus the height of the first cell on the walls of the blades of the guide vanes is 0.025[mm]. The developed mesh is consisted of $5 \cdot 10^5$ до $6 \cdot 10^5$ cells.

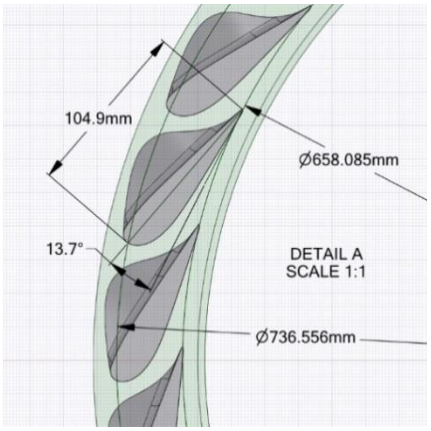

Fig.5.8 Guide vanes dimension of model Francis 99

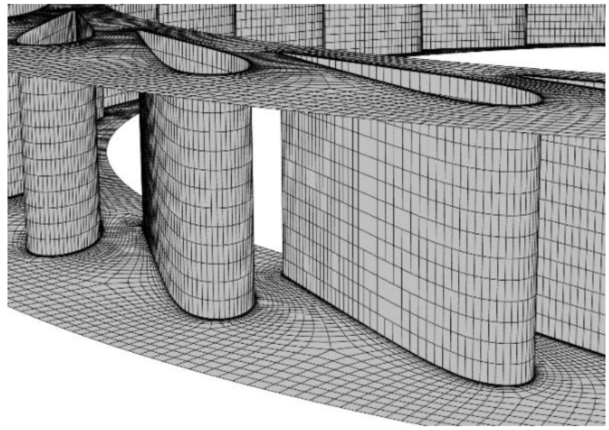
Fig.5.9 Guide vanes mesh

5.4.3. Draft tube mesh

As previously mentioned, only the conical part of the draft tube is taken into account in order to reduce the time required for the simulations. At the design flow rate at the runner outlet diameter, the velocity is calculated as

$$v_{diff} \approx 2\ [m/s]$$

from where the height of the first cell of the draft tube wall is calculated as $y = 0.4\ [mm]$. The boundary layer is described by 5 cells with mutual growth of 1.2. The draft tube is consisted of $9 \cdot 10^4$ cells.

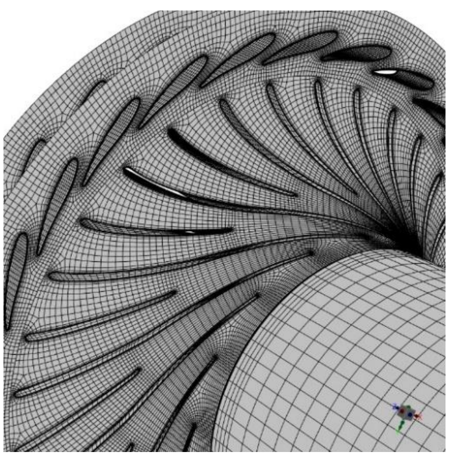
Fig.5.10 Example of mesh – Bottom view

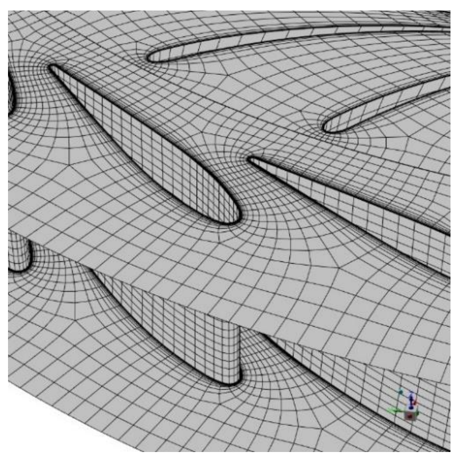
Fig.5.11 Example of mesh at guide vanes and turbine runner

5.4.4. Boundary conditions of the numerical model

Because the emphasis of the analysis itself is on the guide vanes and their effects on the flow that is created at the runner inlet, as well as their influence on the operating characteristics, the spiral casing and the stay vanes are not included in the simulation analyses. Because previous research [43] has been done, these 2 elements of the turbine are excluded from the analysis, where analyses were made to define the enclosure angle of the blades, the manner and influence of the inflow in the guide vanes by comparing convex and concave blades in the cascade, as well as to analyse different blade lengths and cascade densities.

At the guide vanes inlet, the constant flow rate is given as a boundary condition, for the reason that the solution convergence is better, with percentual components at the circumference on the inlet circle giving radial and tangential component of the vectors (streamlines inclination) constant at full circle. The boundary condition at the draft tube is defined as outlet static pressure. The runner is a separate volume in the numeric domain with given angular velocity around the vertical rotational axis, which numerically assigns to the volume cells a rotational component, i.e. the flow in that volume in terms of relative velocity is solved, and the overall flow pattern of the solution is a "frozen rotor" – quasi-stationary flow pattern. The surfaces of the volume used to describe the turbine runner (the blades, the hub, and the shroud) are numerically free to rotate fictitiously in the direction of rotation of the runner, but without a set value (rotating vector) on the walls themselves, in order to accept the impulse from the rotation of the volume and transfer the velocities and pressures of the fluid towards the walls (turbine operating principle). The boundary conditions are schematically presented in Fig. 5.12.

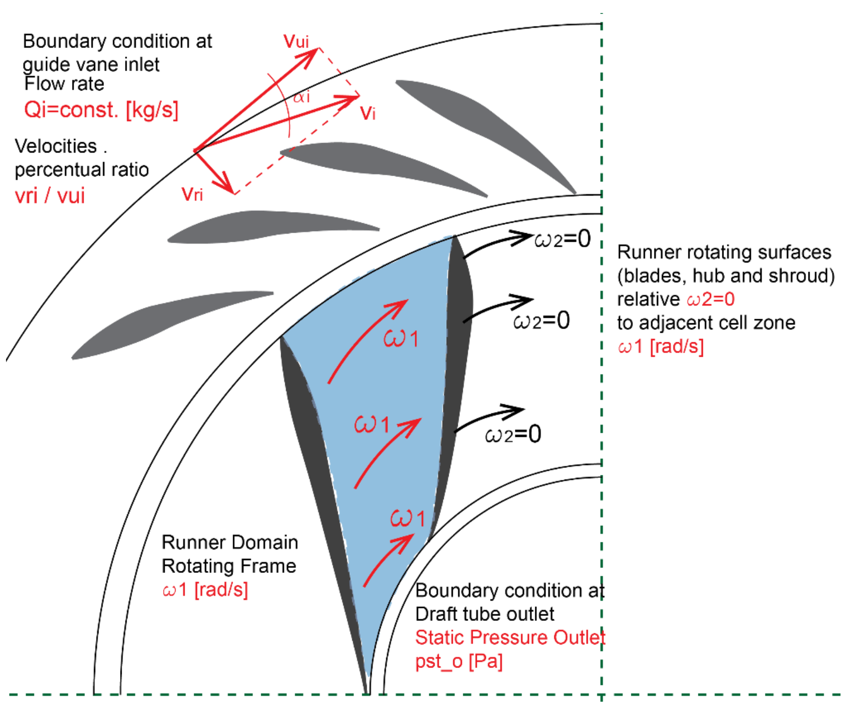

Fig.5.12 Schematic representation of the boundary conditions

5.5. Results and numerical error estimation

Numerical simulations have been successfully converged by achieving the accuracy of the solution up to 10^{-6}. Analogously, an arbitrary point is set in the flow domain, at which the velocity convergence is monitored (observed); it represents an additional criterion for of flow field solving and defining the required number of iterations to obtain it.

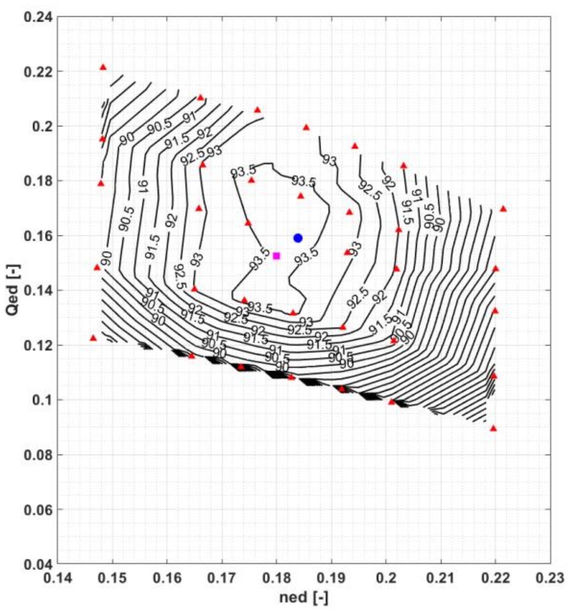

Fig.5.13 Numerically obtained hill chart

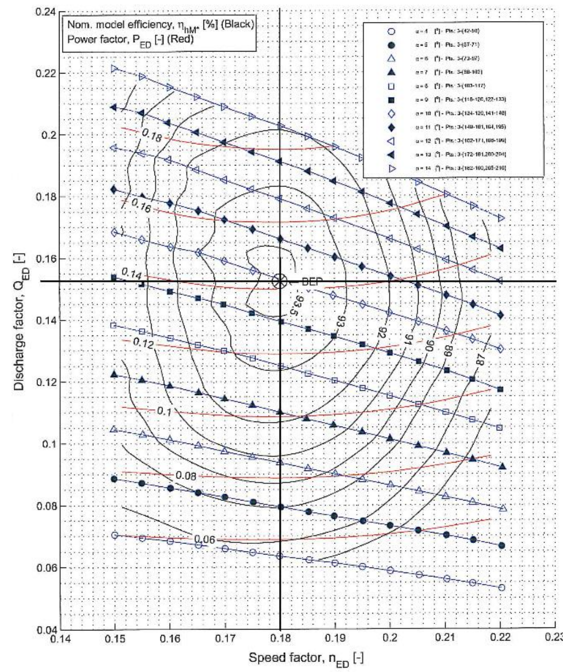

Fig.5.14 Model test hill chart [46]

The relative error of the numerical simulations in the zone of obtained maximum efficiency can be calculated according to the location of the point through the reduced turbine parameters

$$\varepsilon_{n_{ed}} = \left|\frac{n_{ed_m} - n_{ed_{cfd}}}{n_{ed_m}}\right| \cdot 100 \approx 1.67\ [\%]$$

$$\varepsilon_{Q_{ed}} = \left|\frac{Q_{ed_m} - Q_{ed_{cfd}}}{Q_{ed_m}}\right| \cdot 100 \approx 3.92[\%]$$

$$\varepsilon_{\eta} = \left|\frac{\eta_m - \eta_{cfd}}{\eta_m}\right| \cdot 100 \approx 0.107\ [\%]$$

To check the solution and define the numerical error, a comparison was made by intersecting the two diagrams for reduced speeds $n_{ed} = 0.165 \div 0.18 \div 0.195\ [-]$ for the same openings of the guide vanes.

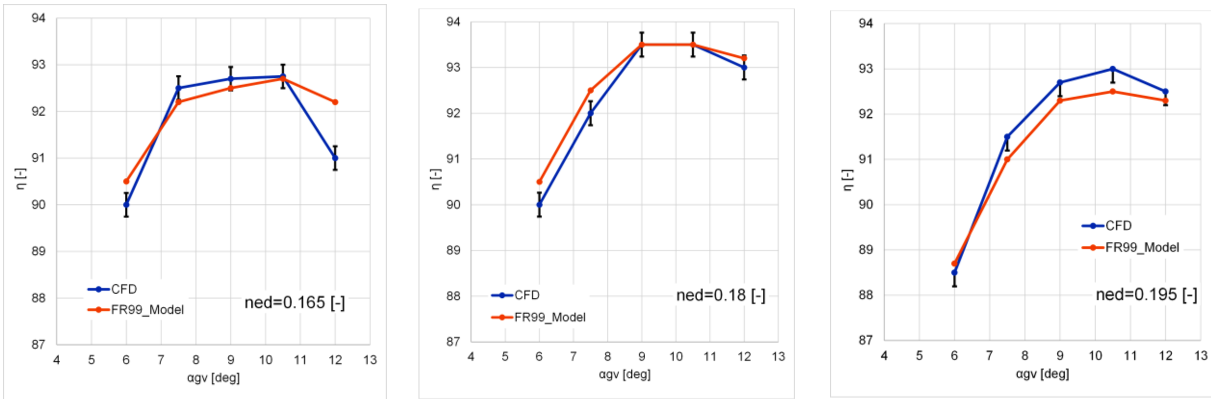

Fig.5.15 Cross-section through the hill charts

A) $n_{ed} = 0.165\ [-]$ Average error 0.252 [%] | B) $n_{ed} = 0.18\ [-]$ Average error 0.262 [%] | B) $n_{ed} = 0.195\ [-]$ Average error -0.303 [%]

It can be seen that the numerical solution of Model 0 does not deviate drastically from the laboratory model tests of the Francis 99 turbine. The point of maximum efficiency which is obtained by numerical simulations is shifted by rotational speed and by flow rate, where the deviation errors from the model are 1.67 [%] and 3.92 [%], respectively. The intensity of the maximum efficiency numerically obtained is 93.7 [%] compared to the model of 93.6 [%], i.e. with an error of 0.107 [%]. For another comparison, three intersections of the two hill charts were made at constant speed factors. For the first cross-section, the efficiency errors obtained numerically versus the model measurements range from +1.302 to -0.325 [%], i.e. an average cross-sectional error of 0.252 [%]. For the second section, the errors are in the range from 0 to +0.552 [%], i.e. the average section error is from 0.262 [%], and in the third section, the errors are in the range from +0.225 [%] to -0.55 [%], i.e. average cross-sectional error of -0.303 [%].

With this comparison and evaluation, it can be concluded that the simplification of the numerical domain for the turbine description, in order to simplify the flow domain and reduce the solution time of the solver, gave accurate prediction of the turbine characteristic. All the steps taken to define it, numerical modelling and approach, meshing of the elements, the adopted boundary conditions, turbulence modelling, as well as they way to guide the numerical simulations, proves to be correct and quite precise and accurate, with negligible deviations from the available measured data.

6. Influence of individual geometrical parameters of the guide vanes on the hydrodynamic conditions and the efficiency of the turbine

In this chapter, the results of partial analyses are derived where the effects between the geometry, flow conditions, and turbine efficiency at constant and variable speeds are treated [43][44]. The initial analyses are aimed at defining some general mutual influences, as well as at defining the boundaries in which the analyses will be conducted.

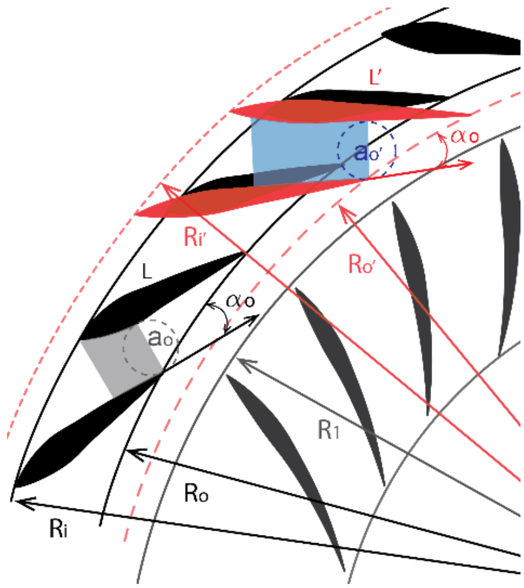

Fig.6.1 Schematic view of the change of geometric parameters [43]

6.1. Analysis of the influence of the geometric parameters on efficiency at constant rotational speed

Based on the design parameters of the turbine, i.e. the best efficiency zone, 37 models of guide vanes were developed in the vaneless space between the runner and the stay vanes. The developed models are consisted of 24, 26, 28, and 32 blades, which form cascades with different density, clearance, radii ratios, and blade chord line closure angle. The criteria to profile the trailing edge of the blades for all the models is equal $\alpha_o = const.$ and directly depends of the calculated outflow angle of the blades for the given turbine design point. The developed models are presented in Table 6.1.

Tab.6.1 – Developed guide vane model configurations

Komb. [-]	Zgv [-]	fi_n [-]	Cro [-]	Cri [-]	L/t [-]	ao/L [-]	ao/t [-]	δ_rel [-]	dx [-]	ty [-]
1	32	1.42	1.025	1.1	1.571	0.179	0.28	1.021	0.3	0.16
2	32	1.42	1.05	1.1	1.534	0.186	0.285	1.044	0.3	0.16
3	32	1.42	1.075	1.1	1.498	0.192	0.287	1.061	0.3	0.16
4	32	1.42	1.1	1.1	1.463	0.199	0.291	1.083	0.3	0.16
5	32	1.42	1.075	1.1	1.572	0.179	0.281	1.021	0.3	0.16
6	32	1.42	1.075	1.125	1.633	0.213	0.347	1.401	0.3	0.16
7	32	1.42	1.075	1.15	1.702	0.239	0.407	1.752	0.3	0.16
8	32	1.24	1.075	1.08	1.353	0.203	0.275	0.99	0.3	0.16
9	28	1.24	1.025	1.1	1.374	0.214	0.295	1.021	0.3	0.16
10	28	1.24	1.05	1.1	1.342	0.222	0.299	1.044	0.3	0.16
11	28	1.24	1.075	1.1	1.31	0.23	0.301	1.061	0.3	0.16
12	28	1.24	1.1	1.1	1.281	0.239	0.306	1.083	0.3	0.16
13	28	1.24	1.075	1.1	1.374	0.214	0.294	1.021	0.3	0.16
14	28	1.24	1.075	1.125	1.428	0.252	0.36	1.401	0.3	0.16
15	28	1.24	1.075	1.15	1.488	0.281	0.418	1.752	0.3	0.16
16	28	1.4	1.075	1.1	1.528	0.16	0.245	0.737	0.3	0.16
17	28	1.32	1.075	1.1	1.452	0.203	0.294	1.021	0.3	0.16
18	28	1.09	1.075	1.08	1.183	0.244	0.289	0.99	0.3	0.16
19	26	1.16	1.025	1.1	1.276	0.237	0.302	1.021	0.3	0.16
20	26	1.16	1.05	1.1	1.245	0.246	0.306	1.044	0.3	0.16
21	26	1.16	1.075	1.1	1.217	0.254	0.309	1.061	0.3	0.16
22	26	1.16	1.1	1.1	1.189	0.263	0.313	1.083	0.3	0.16
23	26	1.16	1.075	1.1	1.277	0.236	0.302	1.021	0.3	0.16
24	26	1.16	1.075	1.125	1.327	0.277	0.368	1.401	0.3	0.16
25	26	1.16	1.075	1.15	1.383	0.308	0.426	1.752	0.3	0.16
26	26	1.3	1.075	1.1	1.42	0.178	0.252	0.737	0.3	0.16
27	26	1.23	1.075	1.1	1.349	0.224	0.302	1.021	0.3	0.16
28	26	1.01	1.075	1.08	1.099	0.27	0.297	0.99	0.3	0.16
29	24	1.07	1.025	1.1	1.178	0.264	0.311	1.021	0.3	0.16
30	24	1.07	1.05	1.1	1.15	0.274	0.316	1.044	0.3	0.16
31	24	1.07	1.075	1.1	1.124	0.284	0.319	1.061	0.3	0.16
32	24	1.07	1.1	1.1	1.097	0.294	0.323	1.083	0.3	0.16
33	24	1.07	1.075	1.1	1.179	0.265	0.312	1.021	0.3	0.16
34	24	1.07	1.075	1.125	1.225	0.308	0.377	1.401	0.3	0.16
35	24	1.07	1.075	1.15	1.276	0.341	0.436	1.752	0.3	0.16
36	24	1.2	1.075	1.1	1.311	0.2	0.263	0.737	0.3	0.16
37	24	1.13	1.075	1.1	1.245	0.25	0.312	1.021	0.3	0.16

Numerical simulations of the models are performed under the constant head and rotational speed conditions, according to the adopted best efficiency point of the turbine. The results obtained for the efficiency of the turbine are presented on a relative basis, correlated with each other and later compared with the reference zero model from the previous simulations presented in Chapter 5. The mutual comparison is performed depending on the number of blades in the guide vanes, to obtain a global and local image of the influences of individual geometric parameters.

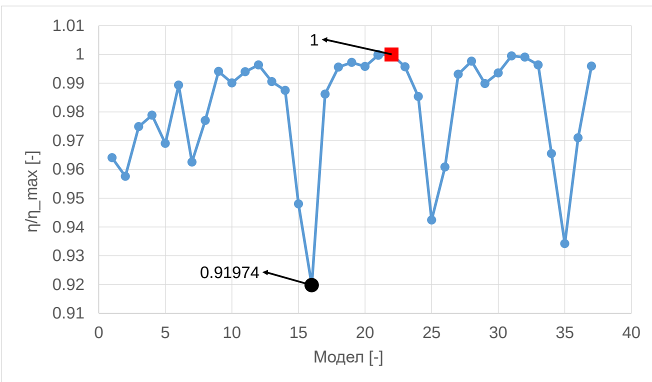

Fig.6.2 Individual efficiencies by developed configuration [43]

6.1.1. Influence of the guide vanes density and clearance

The global image of the influence of the cascade density and the relative clearance of the blades in the cascade is presented in terms of the maximum efficiency obtained from the simulations, regardless of the number of blades in the cascade.

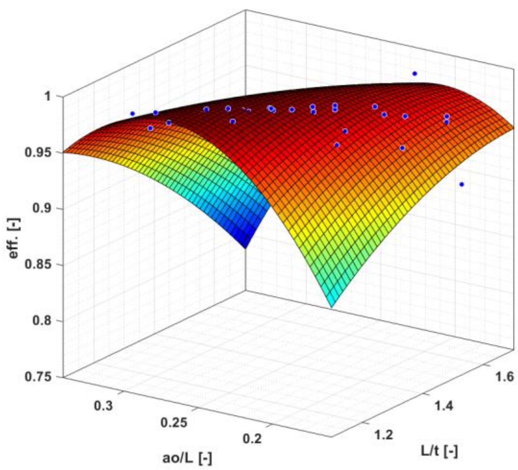

Fig.6.3 Cascade density and clearance influence on turbine efficiency

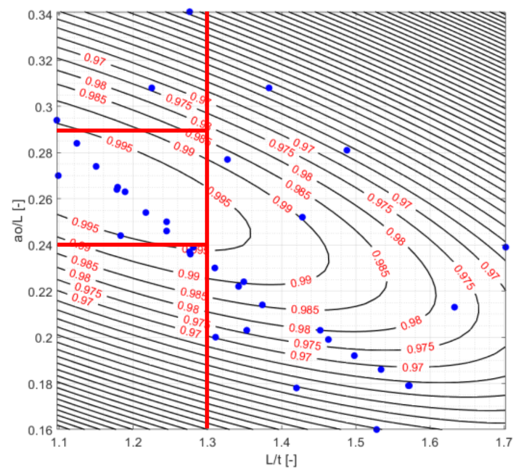

Fig.6.4 Cascade density and clearance influence on turbine efficiency

From Figures 6.3 and 6.4., it can be seen that the zone of maximal efficiency is satisfied for cascade densities in the range of 1.1 to 1.3, and relative clearance in the range from 0.24 to 0.29, regardless of the number of blades. The maximal efficiency zone corresponds with the turbine design flow rate, so the global image of the relative clearance is derived on basis of the design flow rate.

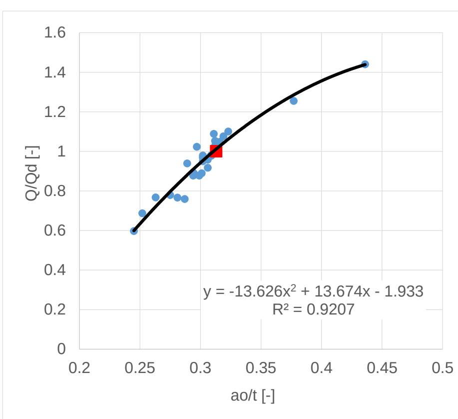

Fig.6.5 Cascade relative clearance influence on design flow rate on basis of cascades pitch

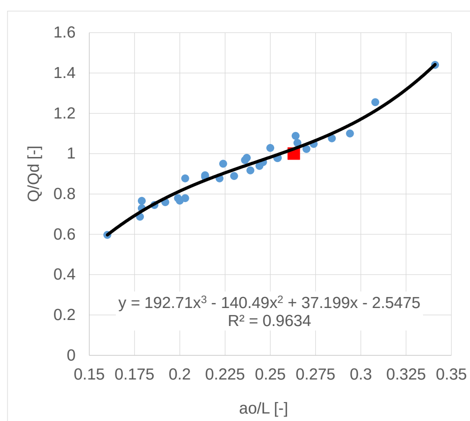

Fig.6.6 Cascade relative clearance influence on design flow rate on basis of blade length

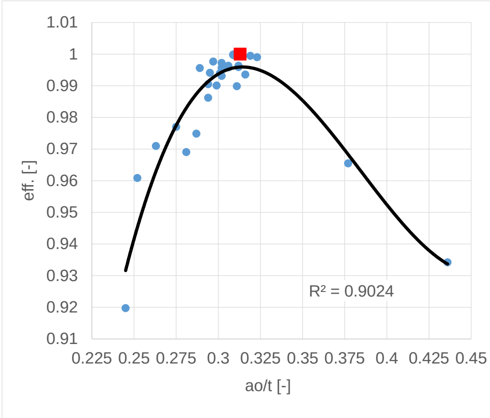

Fig.6.7 Cascade relative clearance influence on efficiency on basis of cascades pitch

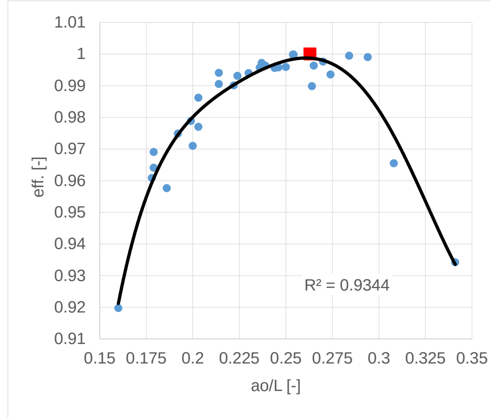

Fig.6.8 Cascade relative clearance influence on efficiency on basis of blade length

From the charts, it can be seen that the values corresponding to the clearance where the design flow rate is obtained are identical to the values for maximum efficiency. The clearance between the blades is represented in relation to the cascade pitch and in relation to the blade length, where the constraints are obtained, and these relations are adopted for further analysis, for developing cascades with these setups. The cascade pitch is analysed globally and individually by the number of blades in the guide vanes, from where its constraints were obtained. Optimization curves are obtained for the values of the cascade pitch, are included in the further analysis.

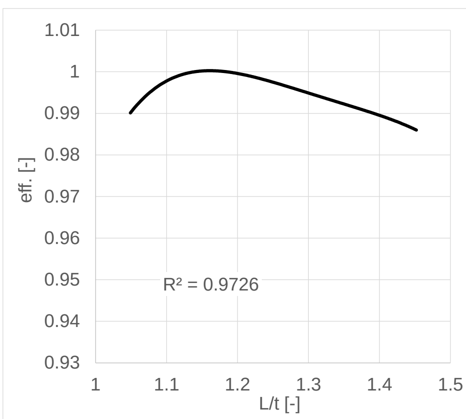

Fig.6.9 Global cascade density influence on efficiency

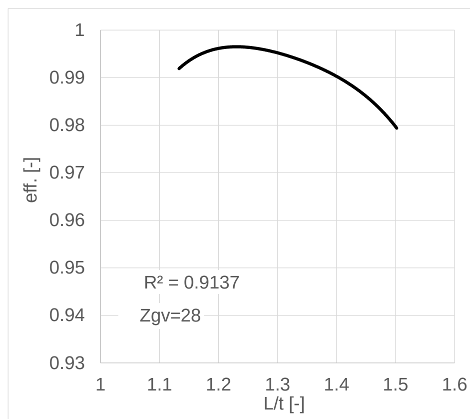

Fig.6.10 Cascade density influence on efficiency for 28 blades

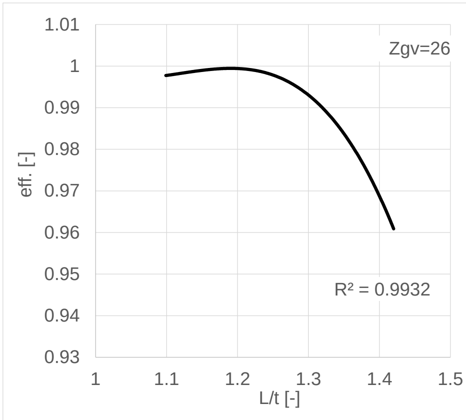

Fig.6.11 Cascade density influence on efficiency for 26 blades

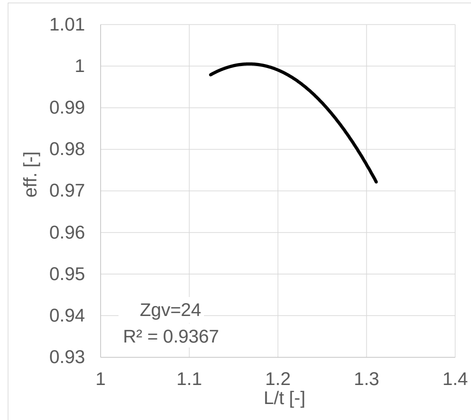

Fig.6.12 Cascade density influence on efficiency for 24 blades

6.1.2. Influence of the blade enclosure angle and chord line leaning angle

In its design position, the enclosure angle of the guide vane blades directly influences the turbine efficiency, and by that its constraints are defined, to reduce deviations from the maximum efficiency zone when it comes to defining the initial guide vane configuration for the given turbine design point. On the other hand, compared with the guide vanes outflow angle, the blade chord line leaning angle shows that the deviation of the best efficiency zone is minimized when they are collinear.

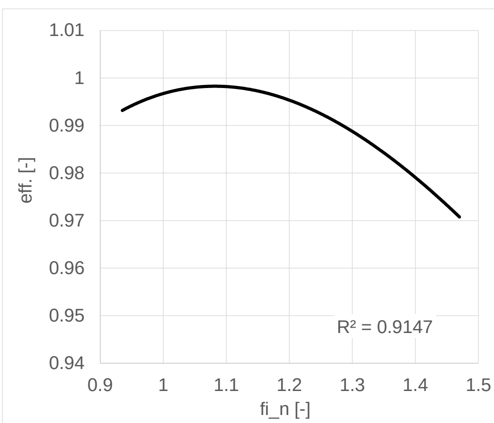

Fig.6.13 Blades enclosure angle influence on efficiency

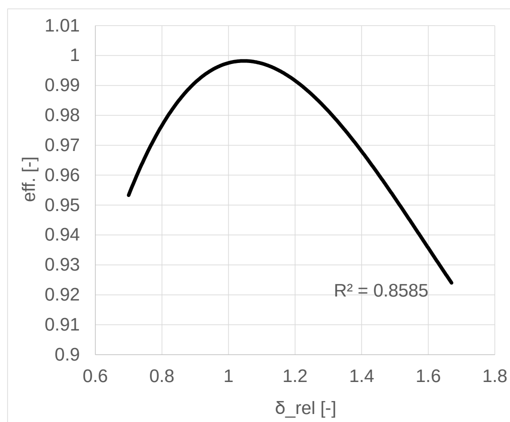

Fig.6.14 Blades chord length leaning angle influence on efficiency

6.1.3. Development of a favourable guide vane configuration from the obtained results

From the above obtained results for the particular geometric parameters and their influence on the turbine efficiency at the turbine design point, a favourable configuration which lies between the mentioned constraints is developed, and it is used in the following analysis.

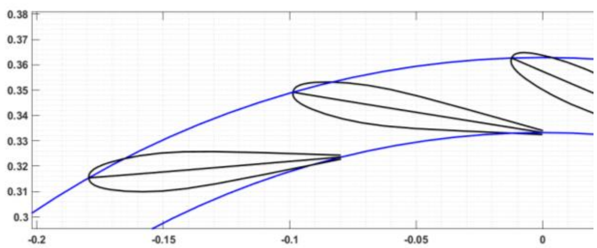

Fig.6.15 Developed configuration geometry in MATLAB

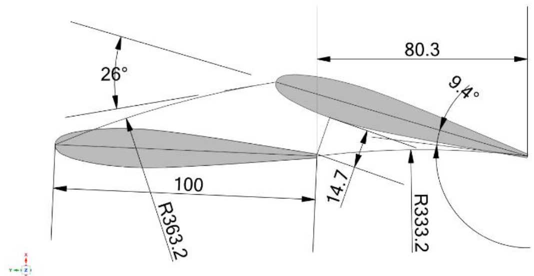

Fig.6.16 Dimensions of the developed configuration

The developed configuration has $Z_{gv} = 26$ blades, forming a cascade with density of $L/t = 1.242$, has a relative opening clearance in ratio with the blade length of $a_0/L = 0.147$. The inlet/outlet radii ratios to the runner respectfully are $C_{Ri} = 1.172$ and $C_{Ro} = 1.075$. The blades chord length leaning angle towards the needed outflow angle is $\delta_{rel} = 1$. Maximal thickness location on the blade is at $dx = 0.3$ and the relative maximal thickness is $t_y = 0.17$.

For simplifying the following analysis of non-uniform blades, it was convenient for the geometry to be adopted as symmetrical profile blades, where based on it, the degrees of blade curvature are more simply defined and presented.

7. Modelling and analysis of the effects caused from non-uniform blades shape of the guide vanes

7.1. Development of the idea

Starting from the previously executed analyses, mathematical relations and conclusions, an idea came up to use the variable-speed operation for achieving extended operational range. As previously mentioned, when the turbine runs with a variable speed, with constant head, a change of the flow rate - inversely proportional of the rotational speed - is inevitable. Thereby, taking into account the condition of optimal inflow at runner inlet (shock free entry), a conclusion is derived that a guide vane blade consisted of 1 profile, whose angle and chord line correspond with one operational point of the turbine, cannot satisfy the needed flow kinematic parameters against the change of the rotational speed.

According to the theory, Fig.7.1 presents a comparison between three geometries of guide vane blades. The blades are positioned to equal opening clearance (a=const.), and they form different outflow angles towards the turbine runner (different trailing edge angles). In these conditions, the three different configurations give different flow rates, depending of the trailing edge configuration.

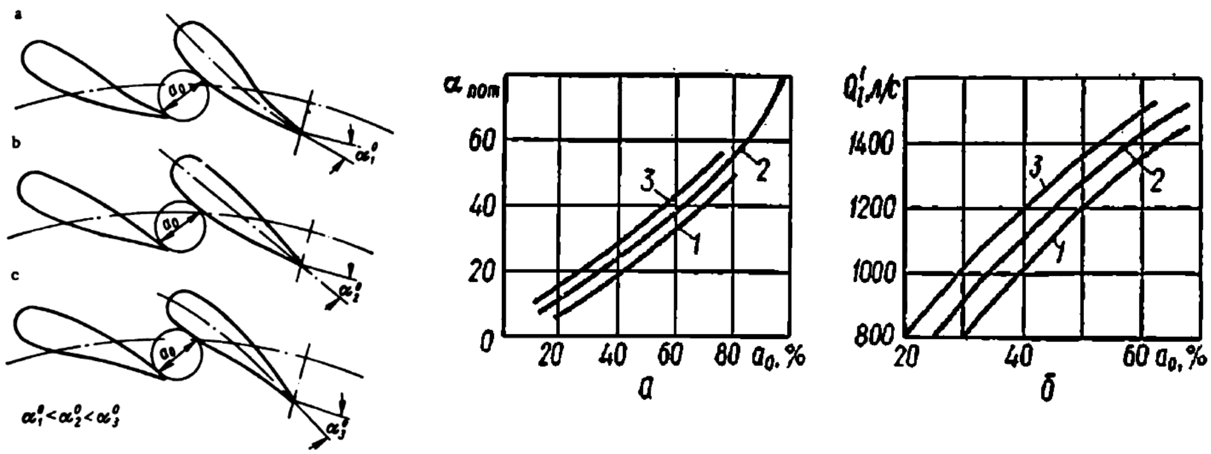

Fig.7.1 Influence of the blade shape on the flow rate through the turbine for constant clearance [7][9]

The following hypothesis comes up: what if the blades of the guide vanes were designed as a combination of these profiles?

The starting assumption is that partial segments of the blade, through the blades' height, will guide the fluid flow towards the runner, depending on the flow kinematic conditions needed for variable speeds. For example, the blade segment where the trailing edge angle is suitable for reduced rotational speed will influence the fluid flow to follow that angle towards the runner. Conversely defined, the blade segment where the trailing edge angle is suitable for flows of increased rotational speed will influence the fluid flow to follow that angle towards the runner.

The main study is based on several geometries of guide vanes, which were developed and numerically tested for one operating point of the turbine, and in the manner of how they behave when variable speed is applied, while they maintain the exact position. For the most promising configurations, a wider analysis was made, taking several opening positions of the blades, to observe the zones where the characteristics extends.

Despite the fact that the possibilities to develop non-uniform (twisted) blades are theoretically almost unlimited, still, two neighbouring blades shall be designed so that they can form a total closure (overlap and saddling contact) between them, to stop the flow and shut down the turbine. As the axis of blade rotation has not got a geometrical or kinematical role in the blade rotation and its positioning, it is obtained that two neighbouring blades which are non-uniformly designed have to maintain a constant opening clearance throughout their height. Only in that case, the needed full closure and overlap contact saddling of the blades can be achieved.

7.2. Development of test models

The way of developing test models depends directly on the kinematic flow state that is obtained for changed rotational speed and the head and flow rate through the turbine. Testing of this dependence was made on several guide vane models, kept for constant clearance, to get insight into the change of the flow rate caused by a change of rotational speed, for constant head operation, and change of head for constant flow rate operation. Independent of the guide vane design, the turbine runner shows the following characteristics (Fig. 7.2 and 7.3.).

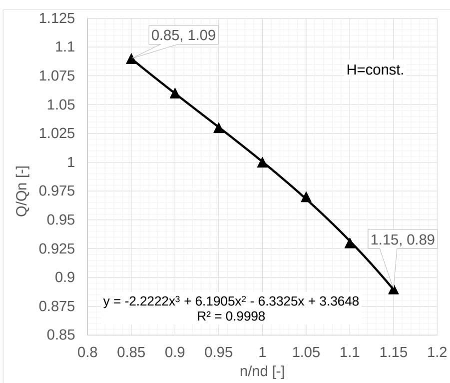

Fig.7.2 Relative flow rate change with change of rotational speed for $H = const.$

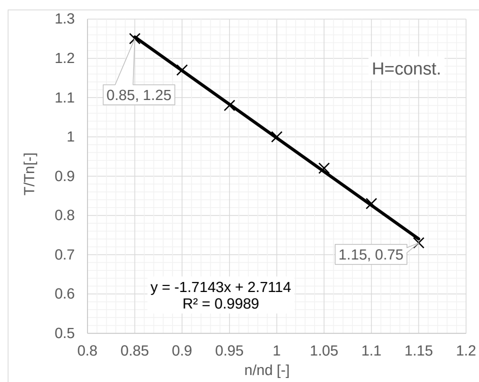

Fig.7.2.1 Relative torque change with change of rotational speed for $H = const.$

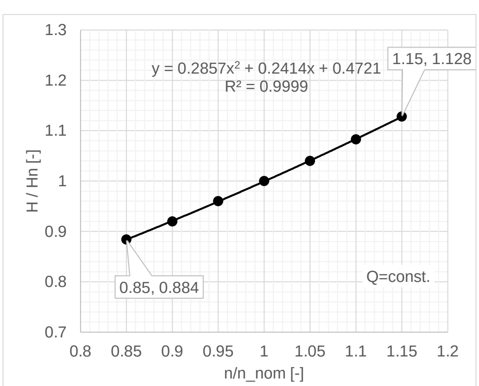

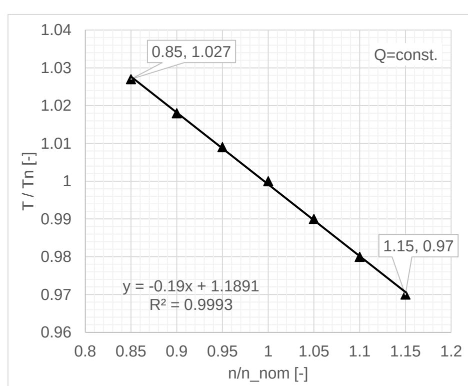

Fig.7.3 Relative head change with change of rotational speed for $Q = const.$

Fig.7.3.1 Relative torque change with change of rotational speed for $Q = const.$

It can be seen in Fig.7.2 that for the turbine test model (Francis 99), independently of the type of the guide vanes in front of the runner, the characteristics of the flow rate change through the turbine lies in the range between ±10 [%] for change of rotational speed from the nominal for the range of ±15[%]. The torque in the range of ±15[%] of the nominal rotational speed changes for ±25[%].

On Fig.7.3. for the turbine test model independently of the type of the guide vanes in front of the runner, the characteristics of the head change for ±12 [%] for change of rotational speed from the nominal for the range of ±15[%]. The torque in the range of ±15[%] of the nominal rotational speed changes for ±3[%].

Through these percentual ratios, the velocity triangles are derived with an aim to obtain the changes of the angle of attack and the intensity of the absolute velocity from the guide vanes to the runner inlet.

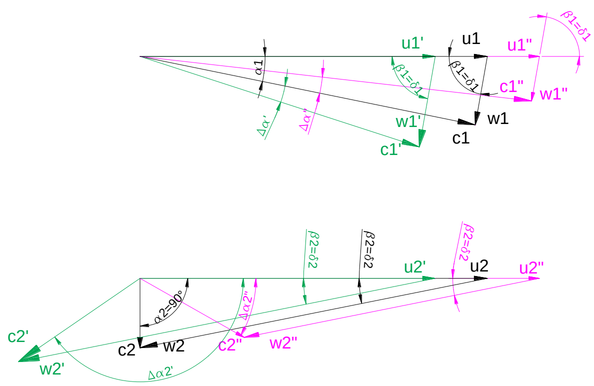

Fig.7.4 Velocity triangles at variable speed for $H = const.$

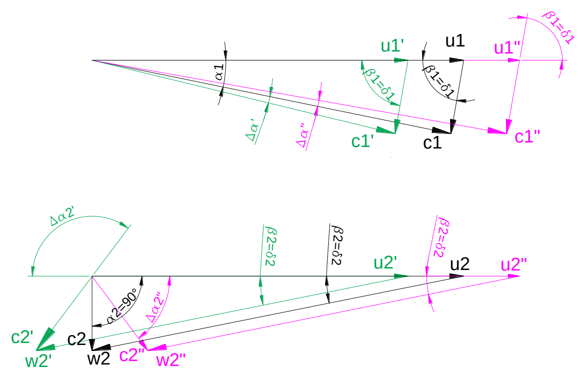

Fig.7.5 Velocity triangles at variable speed for $Q = const.$

The velocity triangles at the runner inlet are derived according to the changes of rotational speed and for keeping shock-free inflow conditions to the runner. The velocity triangles at the outlet are obtained as a consequence of the changed rotational speed and the change of flow rate, following the runner blades trailing edge angle. For the turbine parameters (geometric and flow) the following results are obtained (Tab.7.1 and 7.1.1).

Tab.7.1 Calculated velocity triangles at runner inlet for $H = const.$

D1 [m]	*D2 [m]*	*B1 [m]*	*δ1 [deg]*	*δ2 [deg]*	*n [-]*	*n [min-1]*	*H [m]*	*Q [m3/s]*	*u1 [m/s]*	*c1m [m/s]*	*w1 [m/s]*	*u1-c1u [m/s]*	*c1u [m/s]*	*c1 [m/s]*	*α1 [deg]*	*Δα [deg]*
0.62	0.35	0.06	82.9	18.2	1	333.33	11.5	0.2	10.82	1.71	1.72	0.21	10.61	10.75	9.26	-
					1.15	383.33	11.5	0.178	12.44	1.52	1.53	0.19	12.25	12.34	6.92	-2.34
					0.85	283.33	11.5	0.194	9.2	1.87	1.88	0.23	8.97	9.16	11.69	2.43

Tab.7.1.1 Calculated velocity triangles at runner inlet for $Q = const.$

D1 [m]	*D2 [m]*	*B1 [m]*	*δ1 [deg]*	*δ2 [deg]*	*n [-]*	*n [min-1]*	*H [m]*	*Q [m3/s]*	*u1 [m/s]*	*c1m [m/s]*	*w1 [m/s]*	*u1-c1u [m/s]*	*c1u [m/s]*	*c1 [m/s]*	*α1 [deg]*	*Δα1 [deg]*
0.62	0.35	0.06	82.9	18.2	0.85	283.33	8.92	0.2	9.2	1.71	1.72	0.21	8.99	9.15	10.73	1.47
					1	333.33	11.7	0.2	10.82	1.71	1.72	0.21	10.61	10.75	9.26	0
					1.15	383.33	14.86	0.2	12.44	1.71	1.72	0.21	12.23	12.35	7.99	-1.27

According to the calculated values in tab.7.1, for $H = const.$ it can be seen that small changes of the absolute velocity angle are obtained, in the range of -2.34 [°] for +15 [%] increased rotational speed of the runner and decreased flow rate for 11[%] of Q_{nom}, to +2.43 [°] for -15 [%] reduced rotational speed and increased flow rate for 9 [%] of Q_{nom}. For $Q = const.$, the changes are in the range of +1.47 [°] for -15 [%] reduced rotational speed and -1.27 [°] for +15 [%] increased rotational speed of the runner.

These values represent a starting point for designing non-uniform blades, where the range is increased for the analysis needs, dependent on how the trailing edge angles intensities influence the turbine characteristics. For flow evaluation and visualisation, besides the radial outlet, three sections through the blade height are taken into account, which represent three zones: zone Z1 – root of the blade, zone Z0 – middle of the blade, and zone Z2 – top of the blade; they are mentioned several times in the following sections.

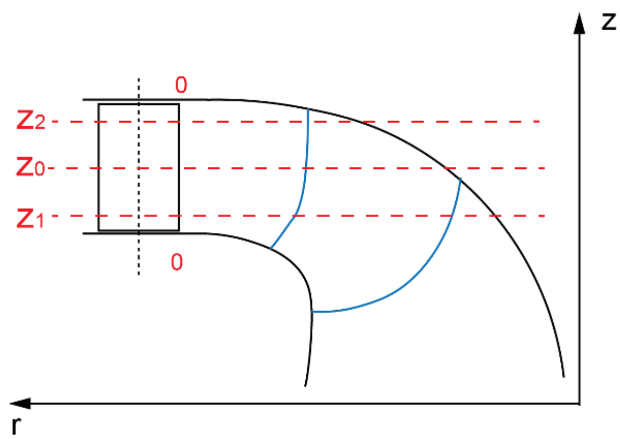

Fig.7.6 Cut zones for flow analysis through the height of the vaneless space

7.2.1. Starting geometry (Model SYM – Symmetrical profile)

The developed geometry described in the previous chapter is numerically tested for the given range of rotational speed change. The geometry given in Fig. 7.7 is formed from symmetrical profile of the blade, positioned for the best efficiency operating point of the turbine.

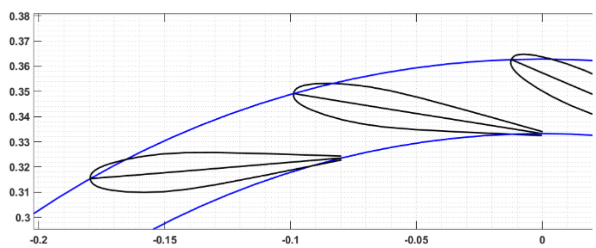

Fig.7.7 Developed geometry in MATLAB

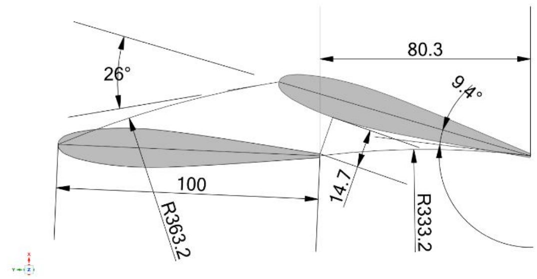

Fig.7.8 Model SYM Dimensions

The model is tested for constant flow rate of $Q = 200\ [l/s]$ in its design position, with changes in the runners' rotational speed in the range of ±20[%] from the nominal speed.

Tab.7.2 Constants in the numerical model

ρ [kg/m3]	g [m/s2]	μ [kg/ms]	D1 [m]	D2 [m]	B1 [m]	Ak1 [m2]	Ak2 [m2]
998.2	9.81	0.001003	0.62	0.35	0.06	0.117	0.096

The results are presented on normalised basis and nondimensional numbers, except for the efficiency, which is presented as numerically obtained absolute value and serves to evaluate the developed models. The results are presented in the Table 7.3.

Tab.7.3 Model SYM - Results

n [min-1]	Q [m3/s]	Hn [m]	T [Nm]	Ph [kW]	Pm [kW]	η [-]	ned [-]	Qed [-]	ψ [-]	φ [-]
266.66	0.20036	9.48	618.5585	18.6	17.27	0.9285	0.161	0.17	38.435	1.051
283.33	0.20036	9.87	612.9505	19.36	18.19	0.9396	0.168	0.166	35.446	0.99
300	0.20036	10.28	607.4283	20.17	19.09	0.9465	0.174	0.163	32.93	0.935
316.66	0.20036	10.72	602.1851	21.03	19.97	0.9496	0.18	0.159	30.821	0.885
333.33	0.20036	11.17	596.6872	21.92	20.83	0.9503	0.186	0.156	28.983	0.841
350	0.20036	11.62	590.7491	22.8	21.65	0.9496	0.191	0.153	27.347	0.801
366.66	0.20036	12.1	584.702	23.74	22.45	0.9457	0.196	0.15	25.947	0.765
383.33	0.20036	12.6	578.8613	24.72	23.24	0.9401	0.201	0.147	24.721	0.731
400	0.20036	13.11	572.8662	25.72	24	0.9331	0.206	0.144	23.622	0.701

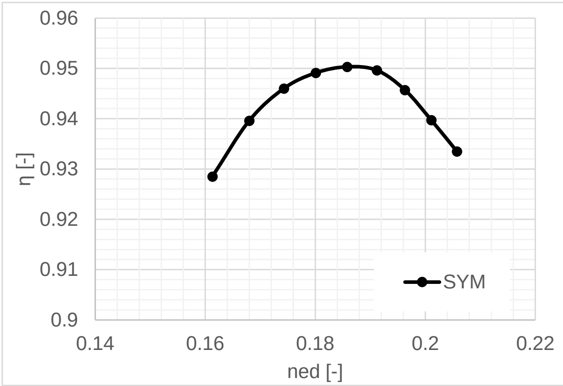

Fig.7.9 Turbine efficiency against speed factor

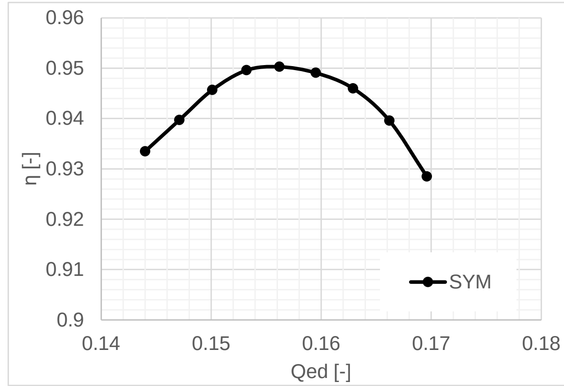

Fig.7.10 Turbine efficiency against discharge factor

It can be seen from the results that the symmetrical profile literally gives an almost symmetrical distribution of the characteristic in both ways of the optimum, with a slighter decrease in efficiency towards the decreased rotational speeds. With the change of the rotational speed, the pressure changes, i.e. increase of the rotational speed increases the pressure, because of the need to pass the same amount of flow rate (Fig. 7.11).

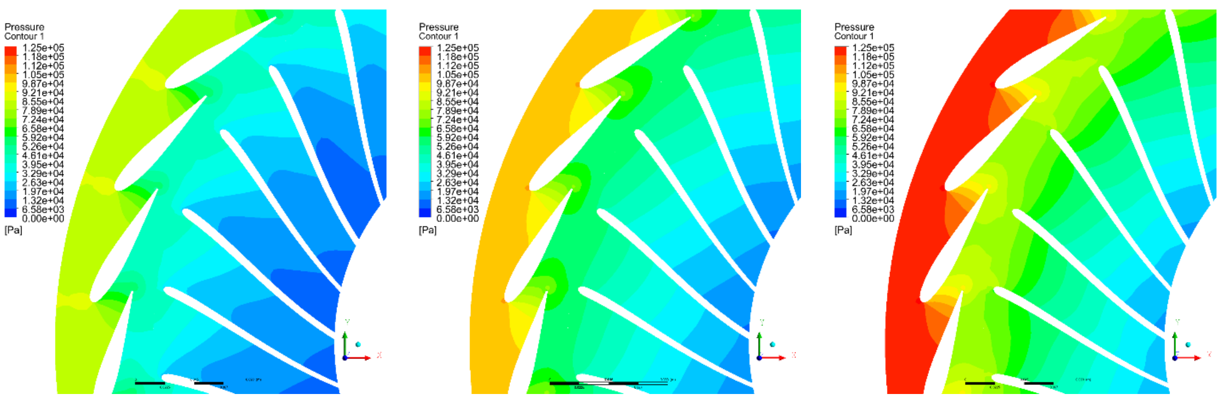

Fig.7.11 Static pressure contours (Model SYM)

A) $n = 0.8n_{nom}$ B) $n = n_{nom}$ C) $n = 1.2n_{nom}$

From the static pressure contours, the difference in the pressure intensities is evident, as the stagnation point of the pressure at the runner blades leading edges. At decreased rotational speed, the stagnation point is on the pressure side of the runner blades. As the rotational speed increases, this point location changes until the relative flow between the runner blades starts to interact with the blades from the suction side. These effects are presented in the following Figures, with the vectors of relative velocity between the runner blades.

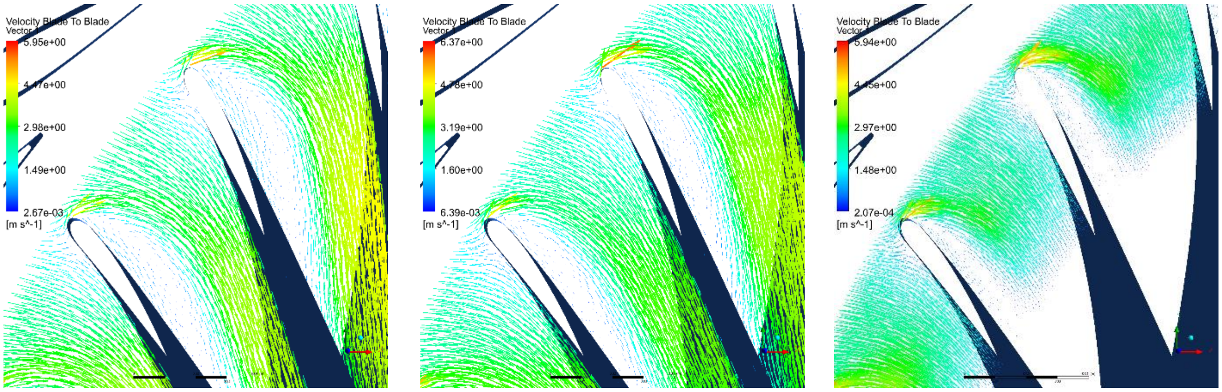

Fig.7.12 Relative velocity vectors for $n = 0.8n_{nom}$ (Model SYM)

Z1 – Blade root Z0 – Middle of blade Z2 – Blade top

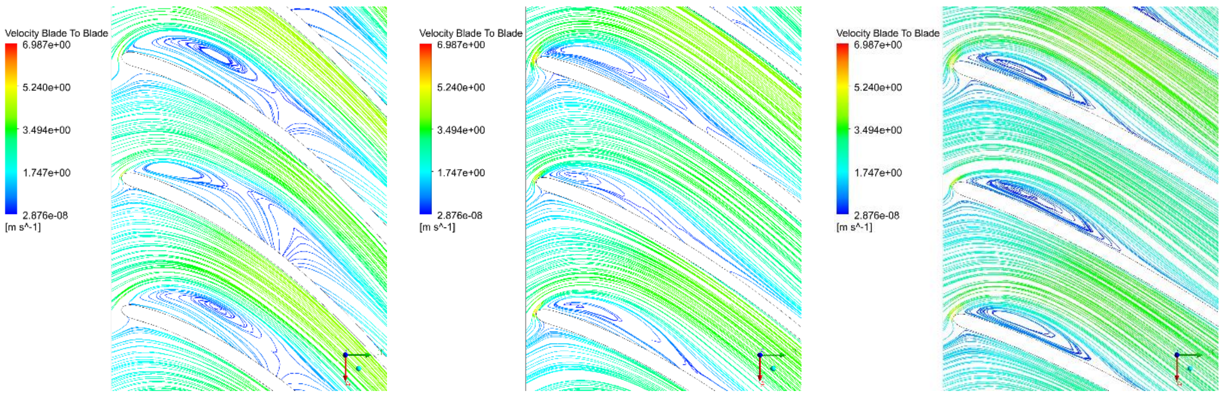

Fig.7.13 Relative streamlines in runner for $n = 0.8n_{nom}$ – Conformal mapped (Model SYM)

Z1 – Blade root Z0 – Middle of blade Z2 – Blade top

In Fig.7.12, the relative velocity vectors are presented in the runner, which are relevant for flow description inside the runner. At decreased rotational speed, a shock flow entry is noticed at the blades pressure side, which leads to flow separations. Observing the three sections by the blade height, it can be noticed that the flow separation intensities are not equal. Increased flow separation is obtained at the blade top, which shows that the difference of the runner blades leading edges between the crown and band, influence the flow separation intensities, and it needs to be taken into account for defining the trailing edge of the guide vane blades.

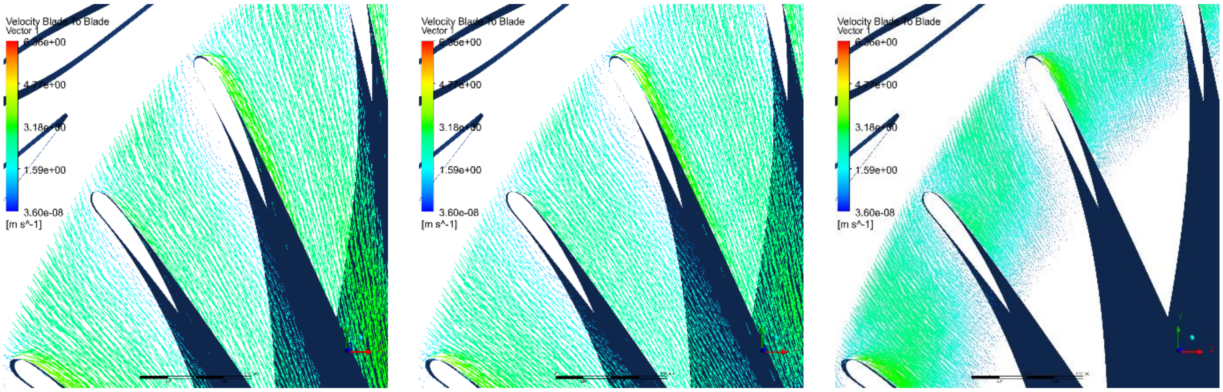

Fig.7.14 Relative velocity vectors for $n = n_{nom}$ (Model SYM)

Z1 – Blade root Z0 – Middle of blade Z2 – Blade top

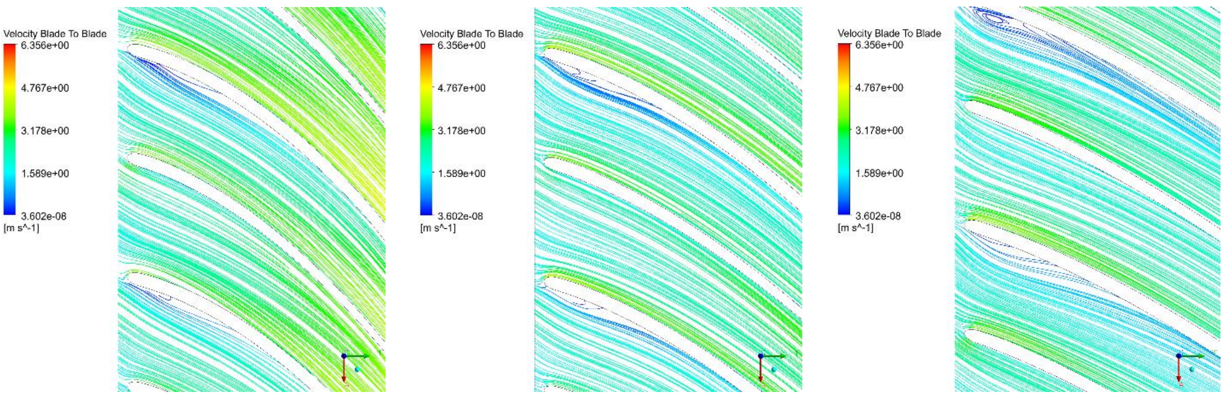

Fig.7.15 Relative streamlines in runner for $n = n_{nom}$ – Conformal mapped

Z1 – Blade root Z0 – Middle of blade Z2 – Blade top

For nominal rotational speed, it can be seen that there are almost no flow separations, in all three sections through the blade height. More intensified flow separations are still present at the blades top, which shows the influence of the runner blade leading edge span angle difference.

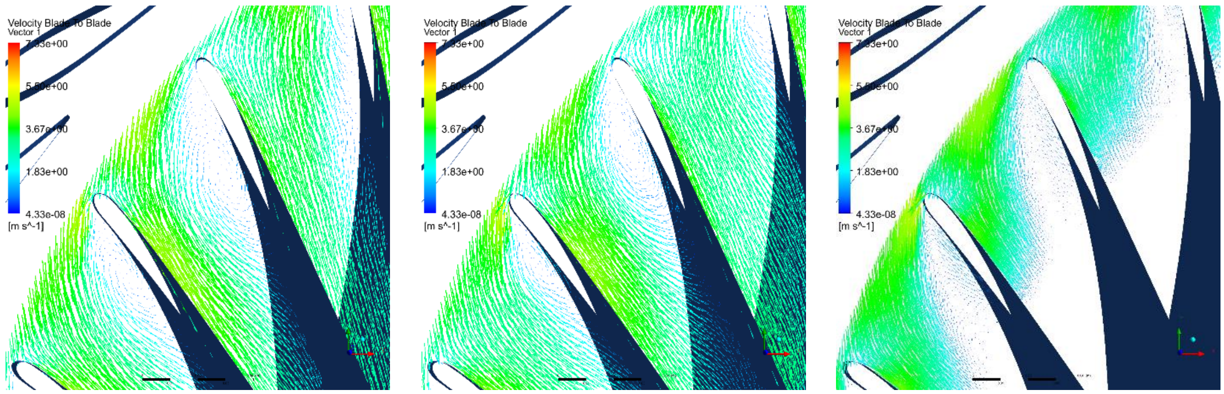

Fig.7.16 Relative velocity vectors for $n = 1.2n_{nom}$

Z1 – Blade root Z0 – Middle of blade Z2 – Blade top

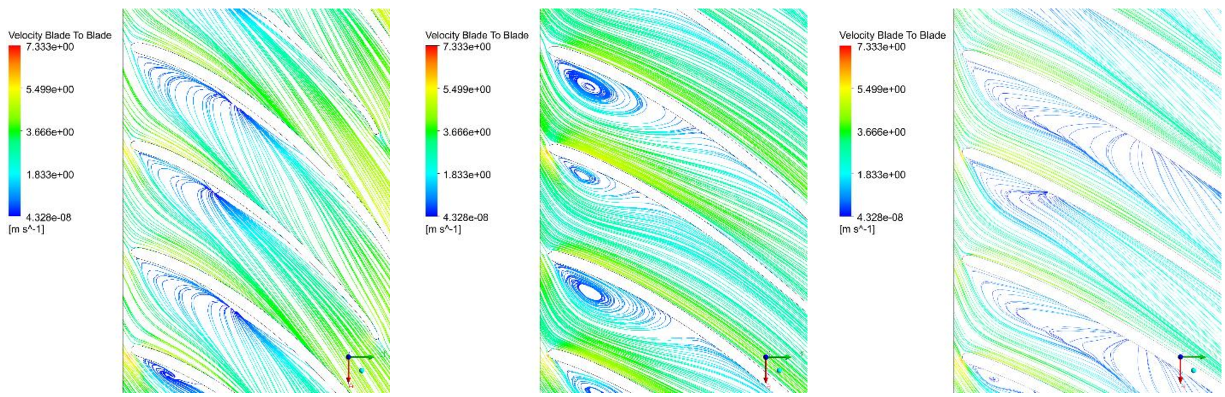

Fig.7.17 Relative streamlines in runner for $n = 1.2n_{nom}$ – Conformal mapped

Z1 – Blade root Z0 – Middle of blade Z2 – Blade top

For increased rotational speed, the flow separations in the runners' changes throughout the blades' height. At the blade root, it is intensified, but in the middle it is slightly decreased, which seams like the flow is centralized in this state. This intuitively shows how the distribution of the profiles at the non-uniform blades shall be, i.e. it demonstrates that there is a need of a change in the trailing edge geometry at the guide vane blades' root and top.

Analysing the flow separations, it can be concluded that the blade top of the guide vanes shall have a trailing edge correction towards increased rotational speeds (angular decrease of the trailing edge), and in the zone of the blade root, a correction towards decreased rotational speeds (angular increase of the trailing edge). With this, it is expected that the separations will decrease in the partial zones, which will lead to a more fluent flow and decrease of the shock entries at the runner inlet.

7.2.2. Influence of the trailing edge angle deformation

Aside from the calculated values for the absolute velocity vector angles for various rotational speeds, larger portions of trailing edge angles deformations are analysed here in order to see the influence of the trailing edge angle on the turbine characteristics. Four configurations are developed with trailing edge deformation, where the blade is fully developed from one type of profile, keeping the opening clearance as constant.

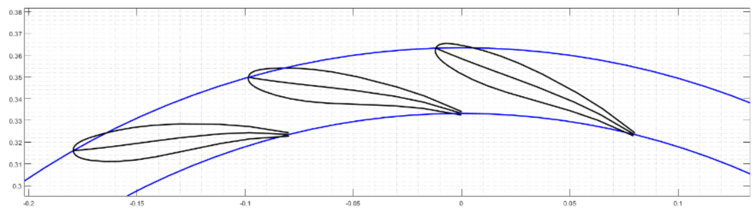

Fig.7.18 Model (+)10

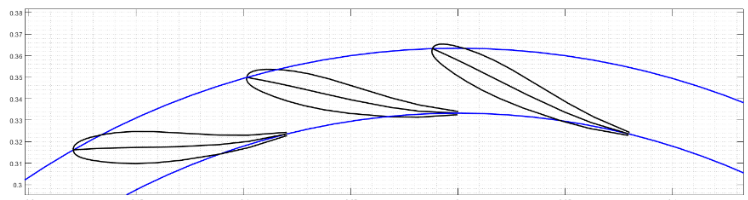

Fig.7.19 Model (-)10

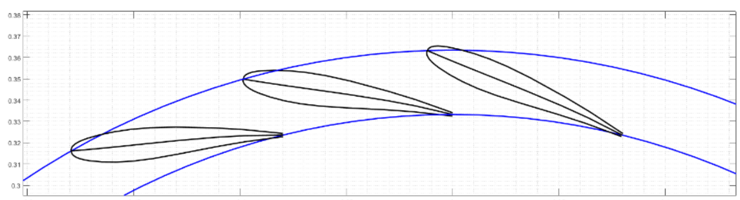

Fig.7.20 Model (+)5

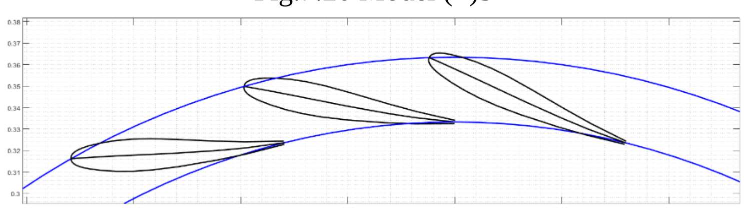

Fig.7.21 Model (-)5

The models generated in MATLAB are numerically tested for conditions equal to those of the starting Model SYM and are then compared to it on the same basis, with the goal to define the mutual differences and effects that the blades have on the turbine characteristics.

7.2.2.1. Model (+)10

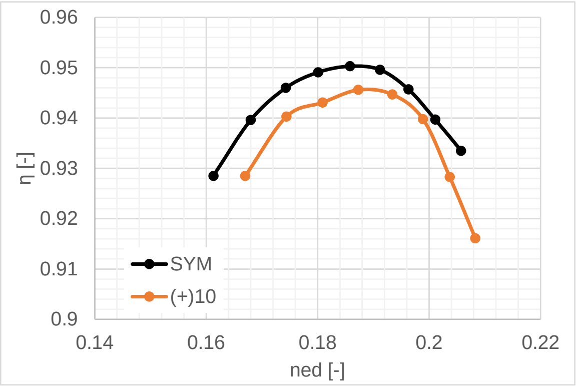

Fig.7.22 Comparison [SYM and (+)10]

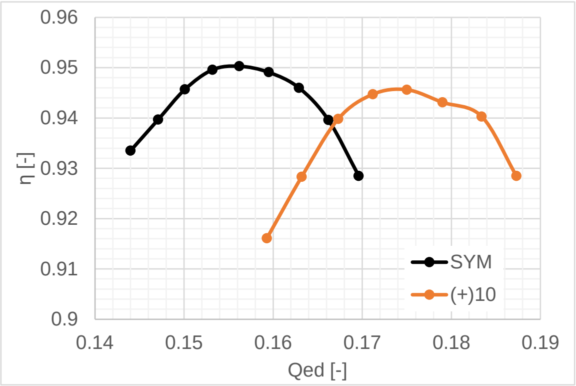

Fig.7.23 Comparison [SYM and (+)10]

According to the obtained results, it can be noticed that there is decrease in efficiency of the turbine, which is expected, because the change of the trailing edge angle does not correspond to the best efficiency operating point of the turbine. At the same time, this model shifts the characteristics in direction of increased flow rates, where local optimum is achieved.

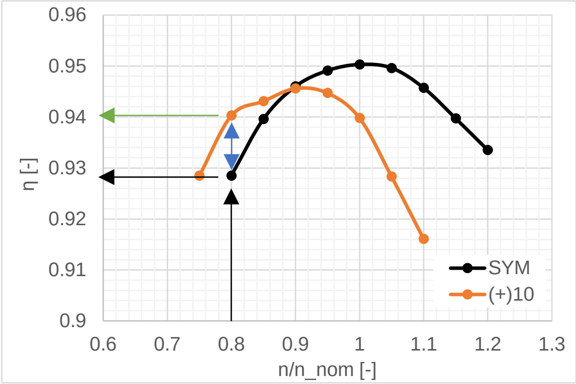

Fig.7.24 Comparison [SYM and (+)10)]
for $Q = const., H \neq const.$

The trailing edge angular deformation of (+)10 degrees compared with the symmetrical profile gives the local optimum in the zone of $0.9n_{nom}$, i.e. decreased rotational speed for 10 [%]. It is noticeable that for $n = 0.8n_{nom}$ it comes to efficiency increase, where a comparison of the flow patterns was made compared with the symmetrical profile from Fig.7.12, where it can be seen that this zone is covered up and no flow separations are present in the runner.

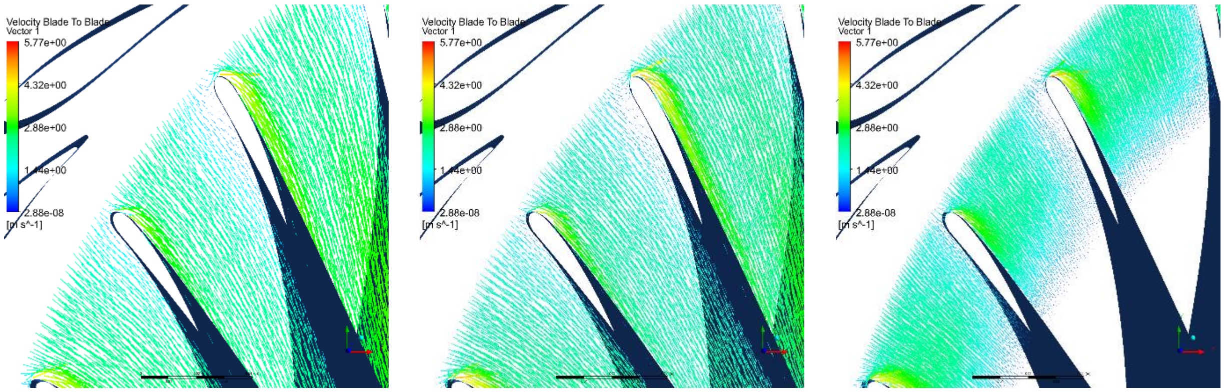

Fig.7.25 Relative velocity vectors for $n = 0.8n_{nom}$ (Model (+)10)

Z1 – Blade root Z0 – Middle of blade Z2 – Blade top

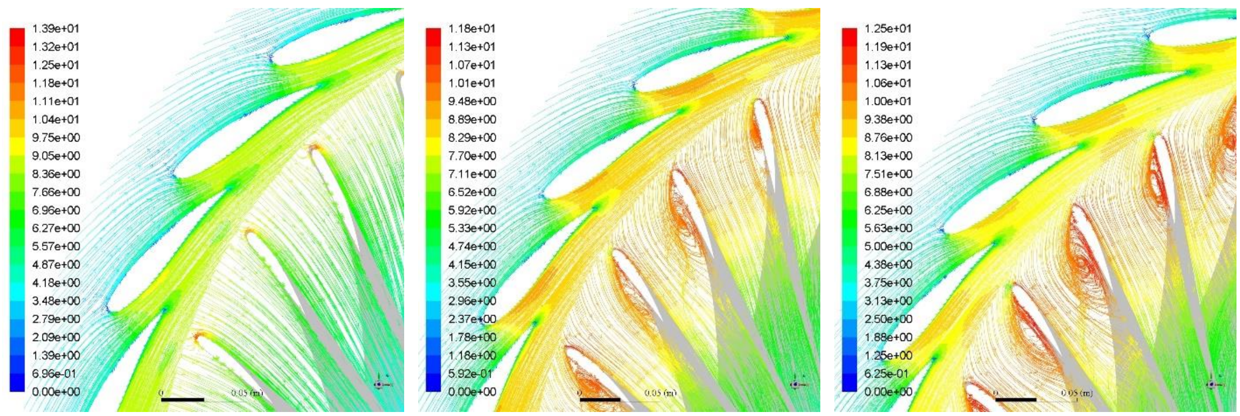

Fig.7.26 Relative stremlines in runner (Model (+)10)

A) $n = 0.8n_{nom}$ B) $n = n_{nom}$ C) $n = 1.1n_{nom}$

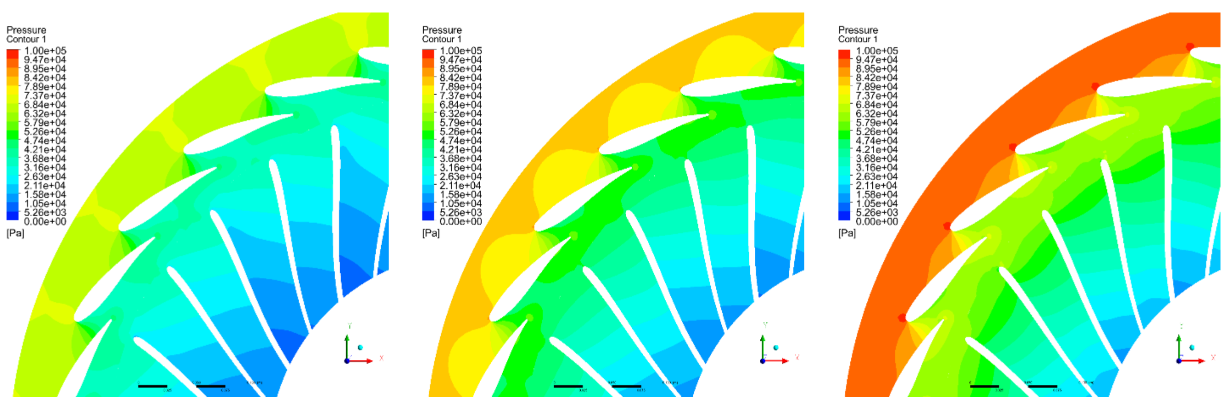

Fig.7.27 Static pressure contours (Model (+)10)

A) $n = 0.75n_{nom}$ B) $n = 0.9n_{nom}$ Local optimum C) $n = 1.05n_{nom}$

7.2.2.2. Model (-)10

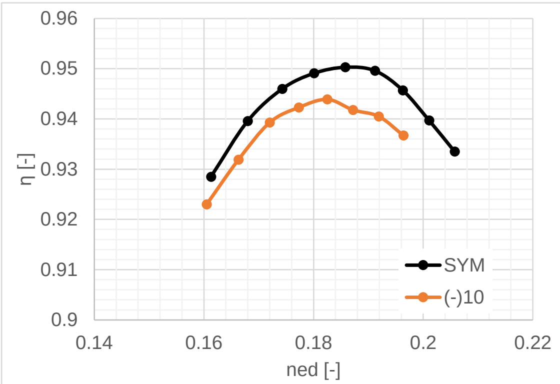

Fig.7.28 Comparison [SYM and (-)10]

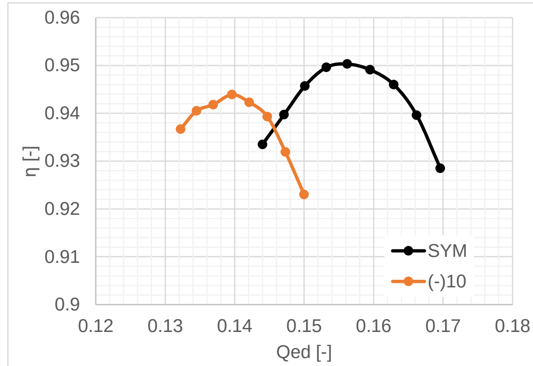

Fig.7.29 Comparison [SYM and (-)10]

According to the charts in Fig. 7.29, in this case, there is also a decrease in efficiency and a shift of the characteristics in direction of decreased flow rates, where a local optimum is achieved. The local optimum is obtained in the zone of $1.1n_{nom}$, i.e. for increased rotational speed of 10 [%].

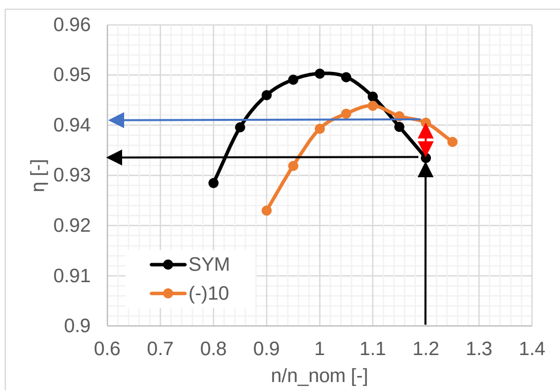

Fig.7.30 Comparison [SYM and (-)10)]
for $Q = const., H \neq const.$

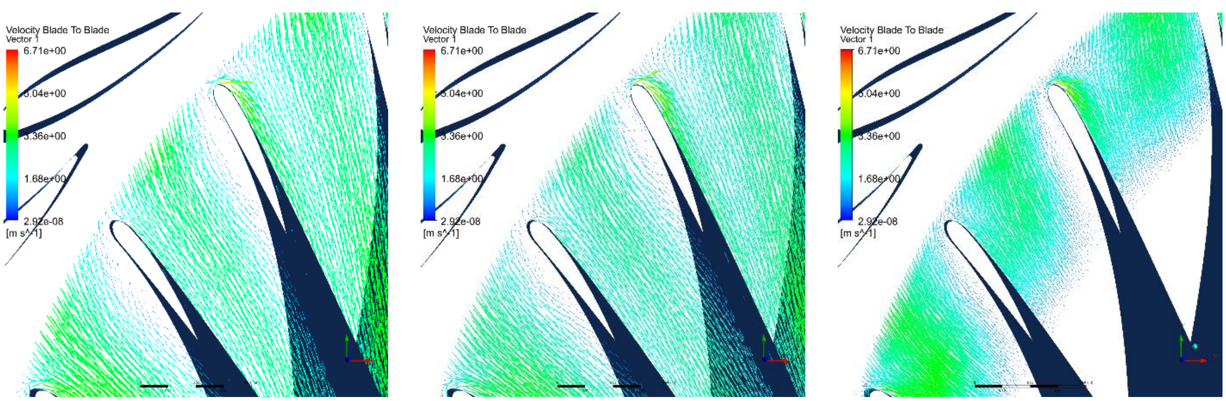

Fig.7.31 Relative velocity vectors for $n = 1.2n_{nom}$ (Model (-)10)
Z1 – Blade root Z0 – Middle of blade Z2 – Blade top

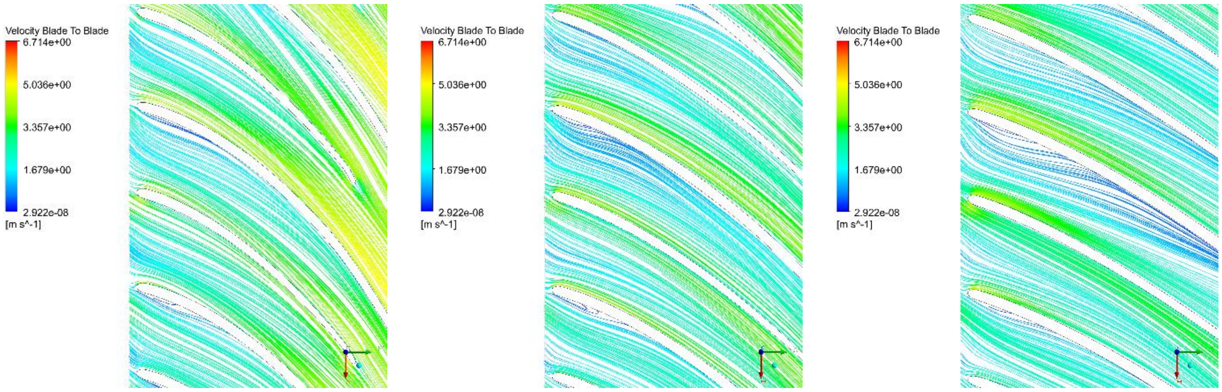

Fig.7.32 Relative sstreamlines in runner for $n = 1.2n_{nom}$ – Conformal mapped (Model (-)10)
Z1 – Blade root Z0 – Middle of blade Z2 – Blade top

Compared with the vectors of the symmetrical profile for $n = 1.2n_{nom}$, an evident improvement is obtained for this rotational speed value, using a blade with negative angular change of the trailing edge of (-)10 degrees. The relative streamlines show that there are no flow separations between the runner blades, which leads to increased efficiency for this rotational speed. Same as in the previous model, pressure increase is obtained as the rotational speed also increases, for the same amount of discharge needs to pass.

7.2.2.3. Model (+)5

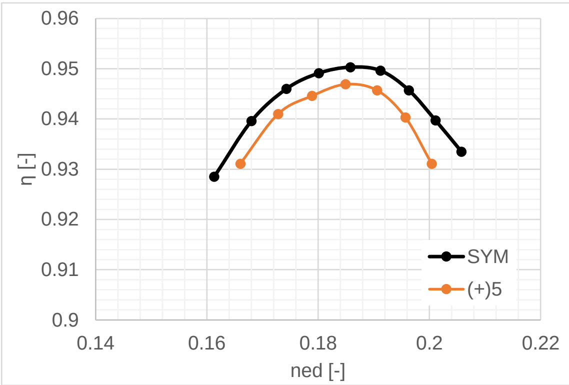

Fig.7.33 Comparison [SYM and (+)5]

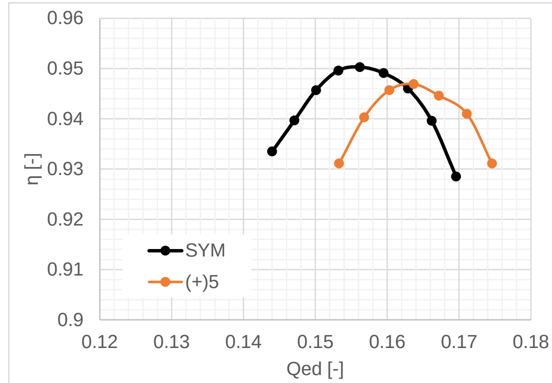

Fig.7.34 Comparison [SYM and (+)5]

The trailing edge deformation of (+)5 degrees compared with the symmetrical profile contributes to characteristics shift towards increased flow rates, where a local optimum is obtained in the zone of $0.95n_{nom}$, i.e. for decreased rotational speed of 5%.

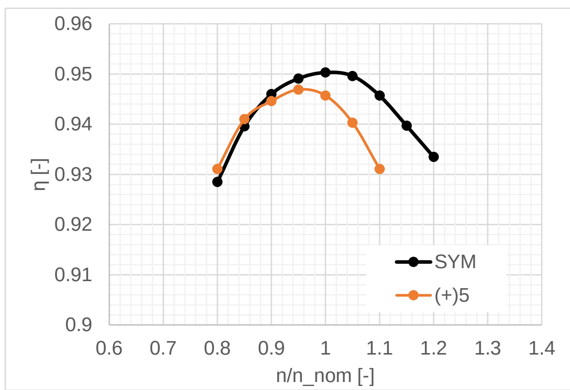

Fig.7.35 Comparison [SYM and (+)5)]
for $Q = const., H \neq const.$

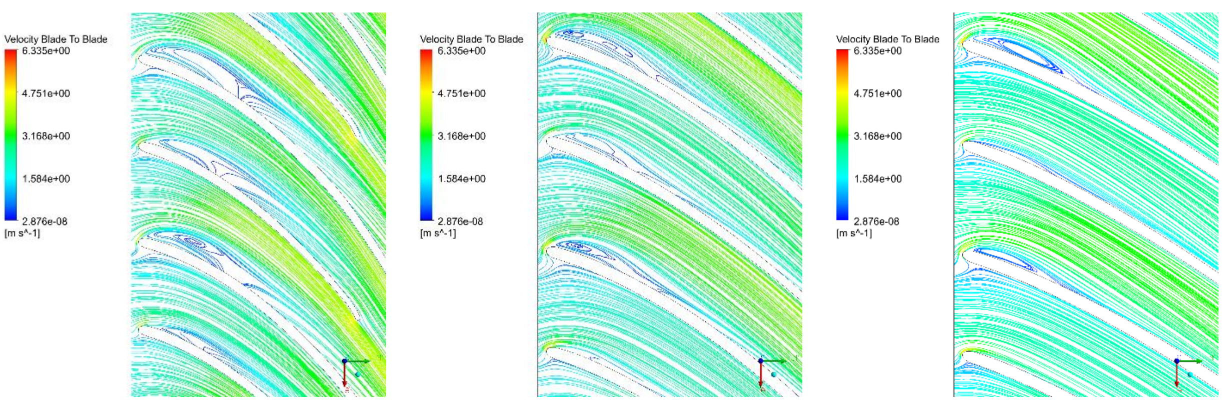

Fig.7.36 Reative streamlines in runner for $n = 0.8n_{nom}$ – Conformal mapped (Model (+)5)
Z1 – Blade root Z0 – Middle of blade Z2 – Blade top

For $n = 0.8n_{nom}$ the Chart in Fig. 7.35 shows insignificant increase in efficiency; by observing the streamlines, it can be concluded that this blade does not cover this operating zone efficiently, and it is followed by flow separations, compared with Model (+)10. According to that, this model is not included in the following analysis because it does not provide any qualitative improvement of the flow pattern and the efficiency.

7.2.2.4. Model (-)5

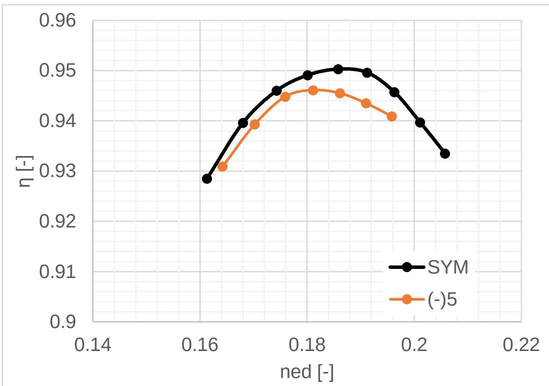

Fig.7.37 Comparison [SYM and (-)5]

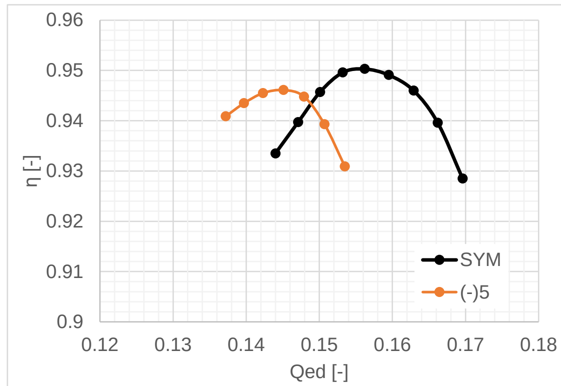

Fig.7.38 Comparison [SYM and (-)5]

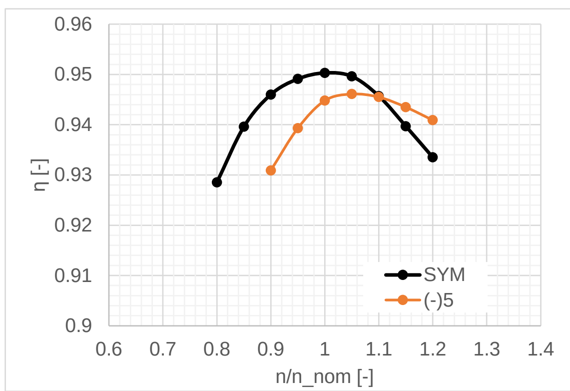

Fig.7.38.1 Comparison [SYM and (-)5)]
for $Q = const., H \neq const.$

According to the results, the effects obtained with trailing edge deformation of the blades are evident. Analysing the relative streamlines in the runner (Fig. 7.39) compared with the symmetrical blade, the flow separation is evident, even though with decreased intensity, which causes the efficiency to increase for $n = 1.2n_{nom}$. Compared with Model (-)10, for this rotational speed the efficiencies become equal, and, compared on the basis of flow rate, it comes to increased efficiency. This model will be analysed in a combination with other profiles to see its participation in the operating range extension.

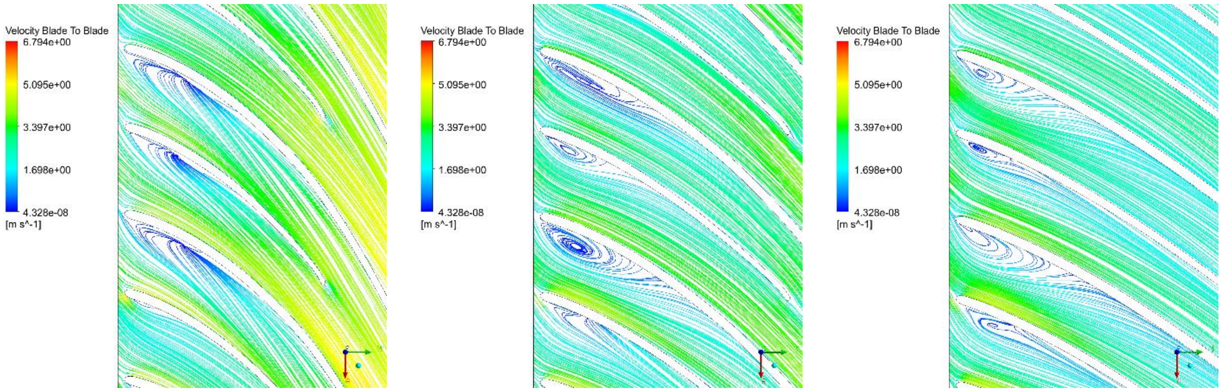

Fig.7.39 Relative streamlines in runner for $n = 1.2n_{nom}$ – Conformal mapped (Model (-)5)
Z1 – Blade root Z0 – Middle of blade Z2 – Blade top

7.2.2.5. Comparison of the models with trailing edge angle deformation

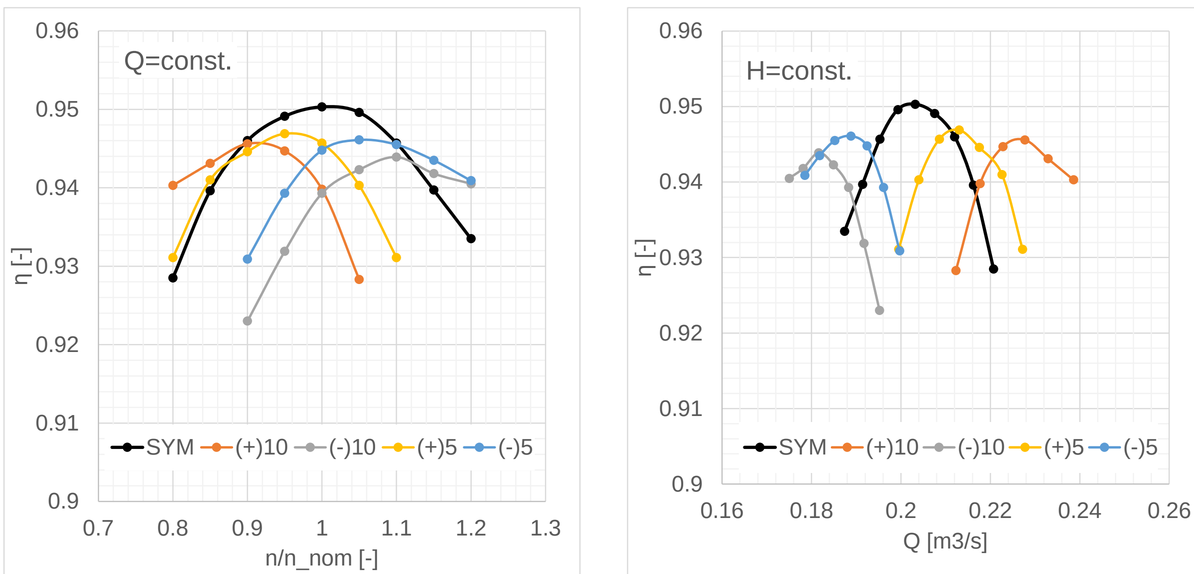

Fig.7.40 Comparison of the models

According to the obtained results, it can be concluded that with a change of rotational speed, certain blades lead to improvement in the flow pattern and the efficiency at off-design operating points. Observing the relative flow in the runner, for $n = 0.8n_{nom}$, the blades with a positive trailing edge angle of (+)10 degrees give most favourable flow pattern, and also increase the efficiency. For nominal rotational speed, the symmetrical blades give the best efficiency and most favourable flow pattern. For $n = 1.2n_{nom}$, from rotational speed point of view, both models with negative trailing edge angle of (-)5 and (-)10 give same efficiency, but from discharge point of view, model (-)5 gives better efficiency, but worse flow pattern compared with model (-)10.

The velocity profiles are analysed at the blades' outlet, on a radial coordinate defined with the blades pitch (Fig. 7.41). Because the pitch of the blades is equal for the developed models, it is represented with a relative value of $t_o = 1\ [-]$. Despite the constant flow rate in the models, a change in the velocity intensities is obtained, which results from the different angles of the trailing edges.

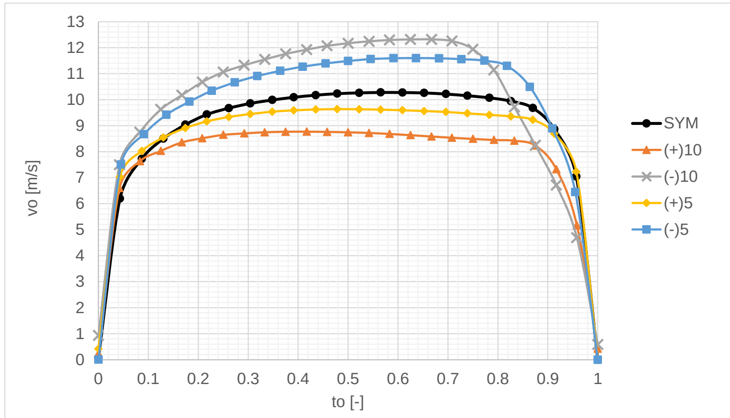

Fig.7.41 Comparison of the velocity profiles

Comparing the velocity profiles, the influence of each of the configurations on the velocity profile distribution can be identified. The uniformity of the velocity profile gives increased inflow efficiency. The models with a negative trailing edge angle of (-)10 and (-)5 degrees have intensified non-uniformity of the velocity and leaning the flow towards the neighbouring blade.

7.2.3. Influence of a blade with collinear chord line and trailing edge angle

On the basis of the results presented in Chapter 6, where the dependence between the blade chord leaning angle and the guide vane outflow angle when they meet collinearly was derived, the most favourable results in terms of efficiency are obtained. Accordingly, two models are defined here. Due to structural and energy reasons related to the turbine runner which is a reference in the analysis, the formation of a maximum fully rotated blade is possible only in the range of (±)4 degrees of rotation, and at the same time, the closure criteria to be met, which means the blades to form equal opening clearances.

The development of these 2 models is nothing more than taking the symmetrical profile once rotated for (+)4 degrees and once for (-)4 degrees. As it rotates, the clearance shrinks and expands, so both models are characterised with different blade length, with the aim of achieving the exact opening clearance as the starting model SYM (Fig.7.42 and Fig.7.43).

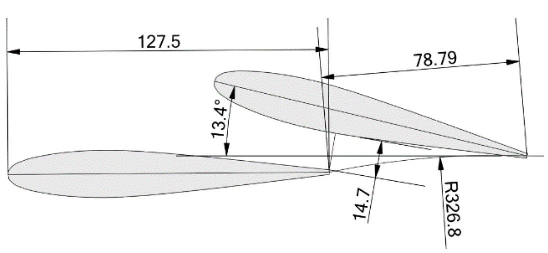

Fig.7.42 Model (+)4 ROT

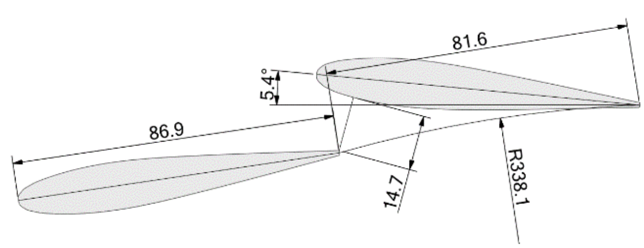

Fig.7.43 Model (-)4 ROT

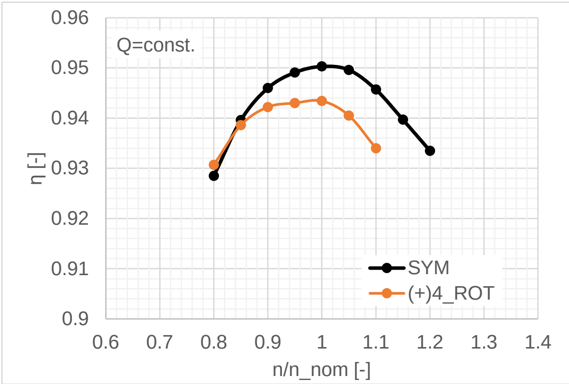

Fig.7.44 Comparison [SYM and (+)4 ROT]

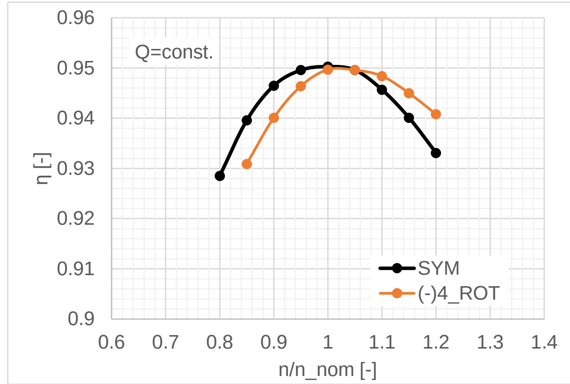

Fig.7.45 Comparison [SYM and (-)4 ROT]

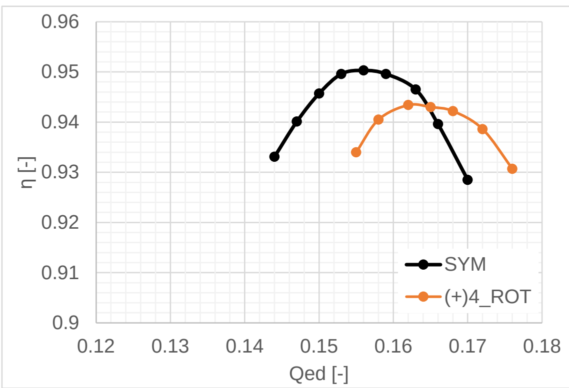

Fig.7.46 Comparison [SYM and (+)4 ROT]

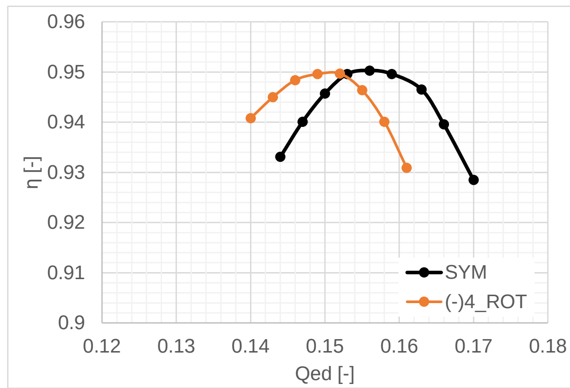

Fig.7.47 Comparison [SYM and (-)4 ROT]

According to the results, the efficiency drops when the blades are rotated in direction of opening (Model (+)4 ROT), there is a local optimum achieved and the characteristic is shifted towards increased flow rates, i.e. decreased rotational speed of $0.95n_{nom}$. On the other hand, the negative rotated blades (Model (-)4 ROT) give slight efficiency drop for increased speed, the characteristic shifts and has a local optimum towards decreased flow rates at $n = 1.05n_{nom}$.

The relative streamlines are derived in the runner, for the limit operational points of ±20% of the nominal speed. Both models show flow separations in the runner blade for these conditions.

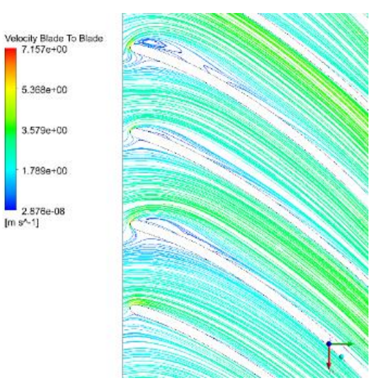

Fig.7.48 Model (+)4 ROT
$n = 0.8n_{nom}$

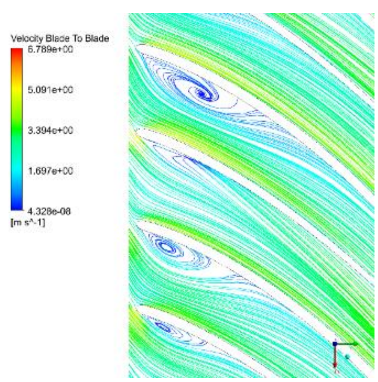

Fig.7.49 Model (-)4 ROT
$n = 1.2n_{nom}$

7.2.4. Comparison of the results for the blades with trailing edge angle change and the blades with collinear chord line with the outflow angle

With an aim to determine which blade type gives increased contribution towards the efficiency and off-design operating zones coverage, a primary comparison between the models is made, plotted against nondimensional factors.

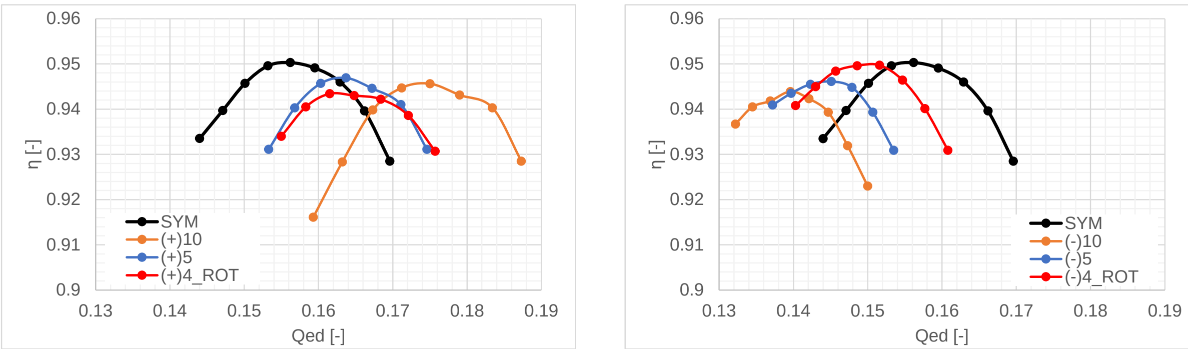

Fig.7.50 Comparison of the Models and the influences presented on the basis of discharge factor

From the charts it can be seen that the blades with positive trailing edge angle (Models (+)5 and (+)10) give extension of the characteristics towards increased flow rates with better efficiency than the positively rotated model (+)4ROT. On the other hand, the model with negative rotation (-)4 ROT gives better performance towards decreased flow rates, compared with the models with negative trailing edge angle.

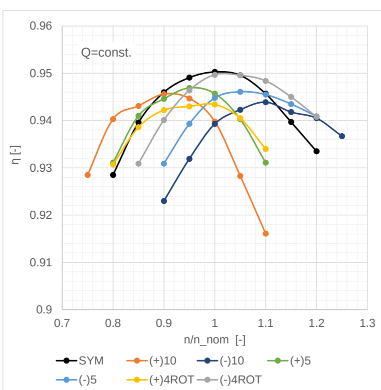

Fig.7.51 Comparison of efficiencies for $n \neq const.$ and $Q = const.$

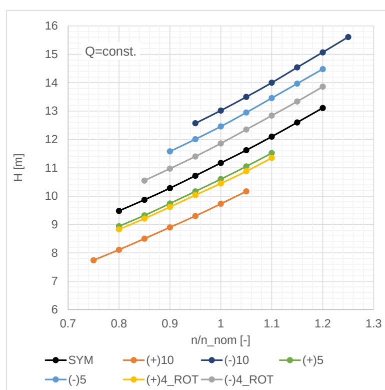

Fig.7.52 Comparison of the head for $n \neq const.$ and $Q = const.$

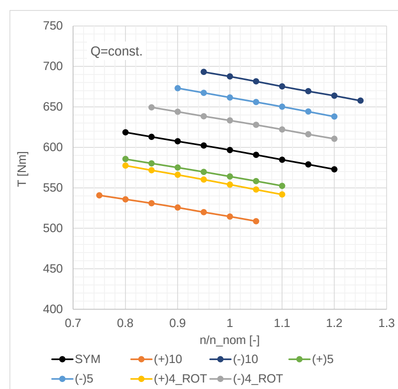

Fig.7.53 Comparison of the torques for $n \neq const.$ and $Q = const.$

It can be noticed from the comparison charts that for constant flow rate and variable speed, it comes to changes in the head and the developed torques. These characteristics are presented in terms of speed, discharge, and torque factors.

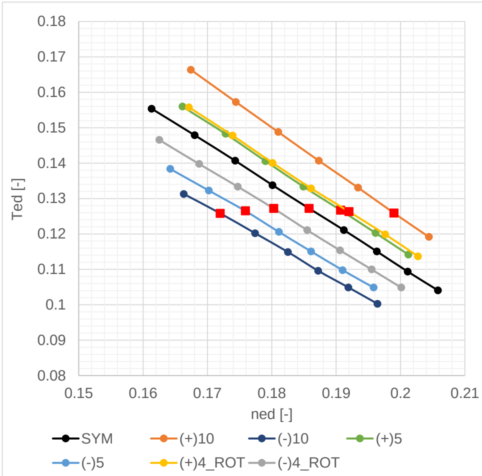

Fig.7.54 Comparison of torque factors for $n \neq const.$ and $Q = const.$

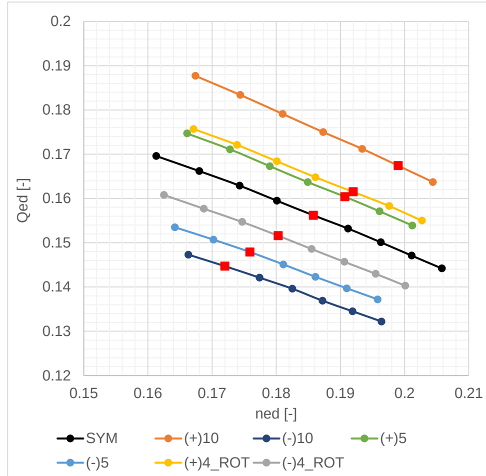

Fig.7.55 Reduced characteristics $n \neq const.$ и $Q = const.$

The charts illustrate the torque, the speed and the discharge factors. With square red dots are presented the points where the rotational speed is at nominal value. In that way it can be noticed how each configuration influences the operating zone, i.e. tends towards increased or decreased rotational speed, respectively towards decreased or increased flow rates. In the following context, based on the reduced characteristics, the analysed models will be compared against the symmetrical blades, at the same rate of change of rotational speed, which will show eventual extensions or shrinks of the operational range of the turbine, analysed as pure geometric shape (area under the curve), for the reason that each of these reduced characteristics represents certain state of the total turbine characteristic and are not comparable to each other. Further, for up to 2-3 rotational positions of the blades, the hill charts are generated for the developed configurations, and plotted for $H = const.$ and $Q = const.$ and compared with the symmetrical blades to obtain the operating zone extension and efficiency increase for off-design rotational speeds, presented as in Chapter 2 in Fig.2.15.

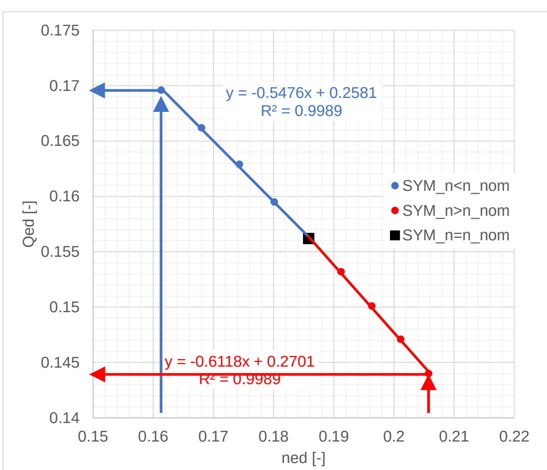

Fig.7.56 Reduced characteristics obtained for symmetrical blades

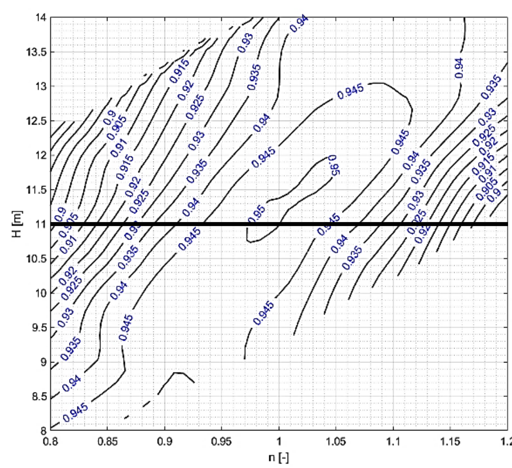

Fig.7.56.1 Hill chart for symmetrical blades

For the symmetrical profile (Fig.7.56) by using the trapezoidal integral rule for calculating the area under the curve, an area towards the speed factor is obtained of

$$A_{n_{ed_{sym}}} = 0.007\ [-]$$

and towards the discharge factor of

$$A_{Q_{ed_{sym}}} = 0.0047\ [-]$$

From the obtained hill chart on Fig.7.56.1, as the peak efficiency is obtained for $H = 11[m]$ and $Q = 0.2\ [m^3/s]$, for these conditions, a slice in the hill chart is presented for these two values, to obtain the characteristic operational curve (Fig.7.56.2).

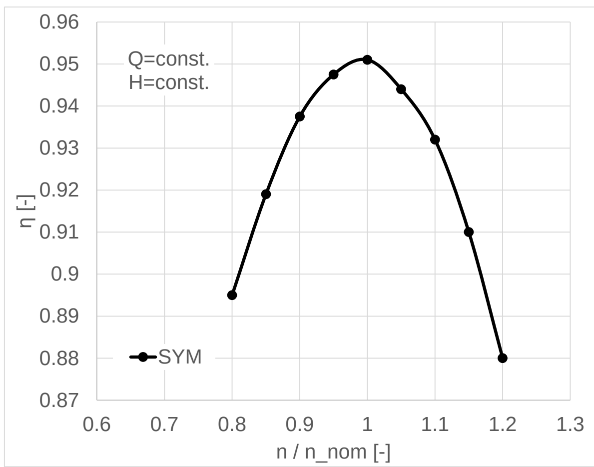

Fig.7.56.2 Slice of the hill chart for symmetrical blades for
$n \neq const.;\ Q = const.; H = const.$

The idea that is elaborated further is to develop non-uniform blades, formed as a combination of different profiles through the blades height, according to the obtained results. The purpose is to direct the flow towards the needed outflow angle suitable for the given rotational speed with an aim to cover efficiently the range and to expand it. According to the results, the tested models are formed as a combination of blade profiles with a different participation in the blade, depending on the characteristics that needs to be achieved.

7.3. Analysis of non-uniform blades

7.3.1. Configuration 1

This configuration is derived with an aim of primary recognition of the effects and the flow parameters induced by the non-uniform blade. The expectations are that the characteristic's results will fall averagely between the partial characteristics of the symmetrical profile and the trailing edge deformed profile. The geometry is shown in Fig. 7.57.

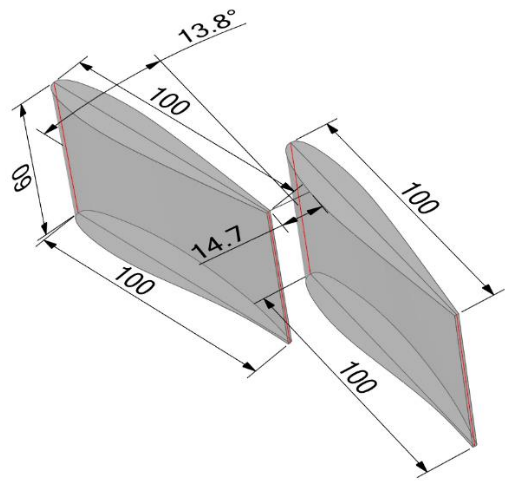

Fig.7.57 Configuration 1 (+)10-SYM

It can be noticed in Figure 7.57 that the blade is formed of 2 profiles, a symmetrical profile and a profile with trailing edge angle in positive direction of (+)10 degrees, directly lofted, without defining partial portions of profile participation in the blade. The opening clearance between the blades is kept constant.

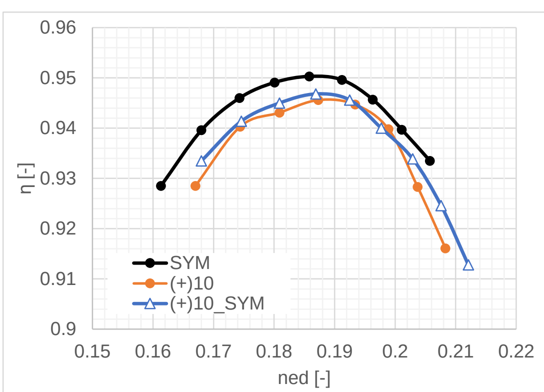

Fig.7.58 (+)10-SYM characteristics

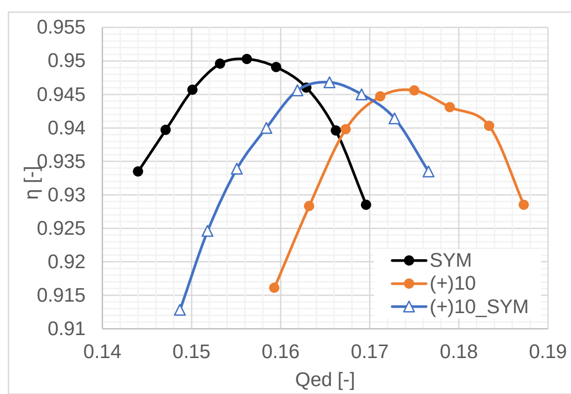

Fig.7.59 (+)10-SYM characteristics

According to the obtained results, the characteristics fall between the partial characteristics of the symmetrical profile and the profile with a positive angle on the trailing edge. In the zone of reduced rotational speeds, the presence of the profile section with a trailing edge angle curvature of +10 degrees can be noticed. A local optimum is achieved in the zone of $0.95n_{nom}$, which shows that the weighting outflow blade angle is with cca. +5 degrees. It was expected that the curve would follow the trend of the symmetrical profile, but drop in efficiency occurred and the zone was not fully covered.

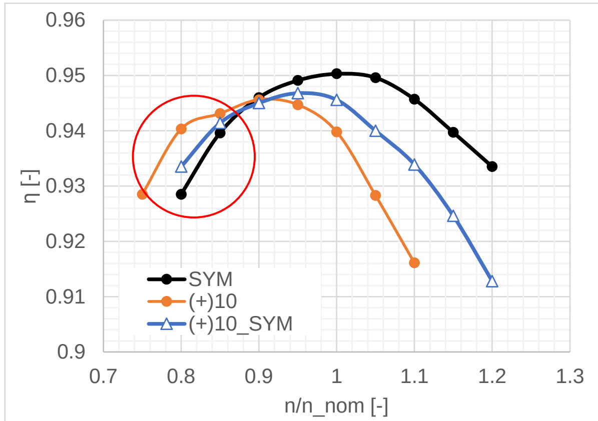

Fig.7.60 Comparison [SYM and (+)10-SYM]
for $n \neq const.$ and $Q = const.$

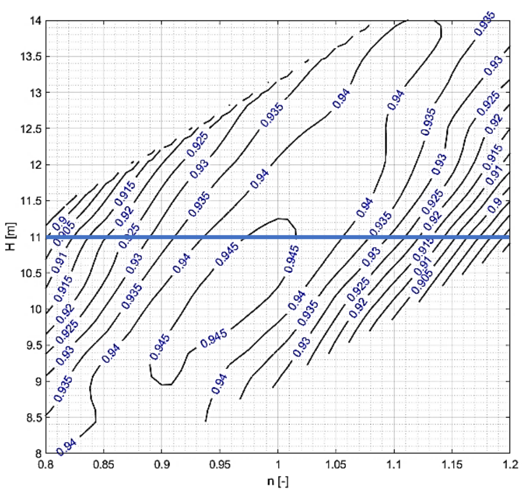

Fig.7.60.1 (+)10-SYM Hill Chart

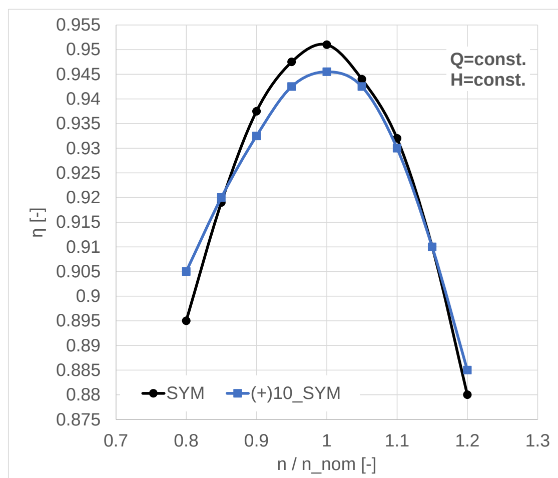

Fig.7.60.2 Comparison [SYM and (+)10-SYM]
$n \neq const.;\ Q = const.; H = const.$

From the obtained results it can be seen that the non-uniform blade of configuration (+)10-SYM compared to Model SYM gives slightly better performance at off design operation. The operating characteristic of Model SYM is narrower and shows a peak at the optimum, compared to model (+)10-SYM, where the characteristics is wider and has flatten optimal zone. For off-design rotational speed of $n = 0.8n_{nom}$, the model (+)10-SYM shows increased efficiency of cca. 1 [%] and for $n = 1.2n_{nom}$ for cca. 0.5 [%]. The optimal zone of model (+)10-SYM decreases for cca. 0.6 [%], leading to flatten (wider) zone of operation. Overall, this shows that non-uniform blade design can lead to off-design improvements.

According to relative streamlies of the flow in the runner, observing the three sections by the blade height, the difference is evident in the inflow patterns, especially at reduced rotational speed. The blade root where the trailing edge angle is curved for +10 degrees contributes to more favourable inflow conditions and fulfilment of the runner blade channels, decreasing the rate of flow separations. In the middle section of the blade, where the influence of the curved trailing edge is lost, a change in the direction of the relative flow vectors is noticed, which results in gaining an increased shock inflow conditions and flow separations at the suction side of the runner blades. The same effect intensifies at the blade top section, where the influence of the trailing edge curvature is almost gone.

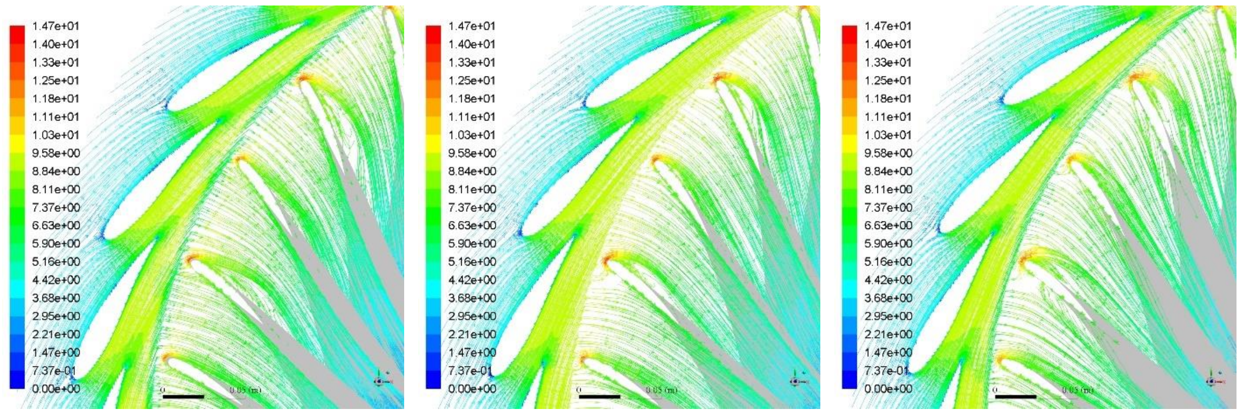

Fig.7.61 Relative streamlines at runner inlet for $n = 0.8n_{nom}$ (Model (+)10-SYM)
Z1 – Blade root Z0 – Middle of blade Z2 – Blade top

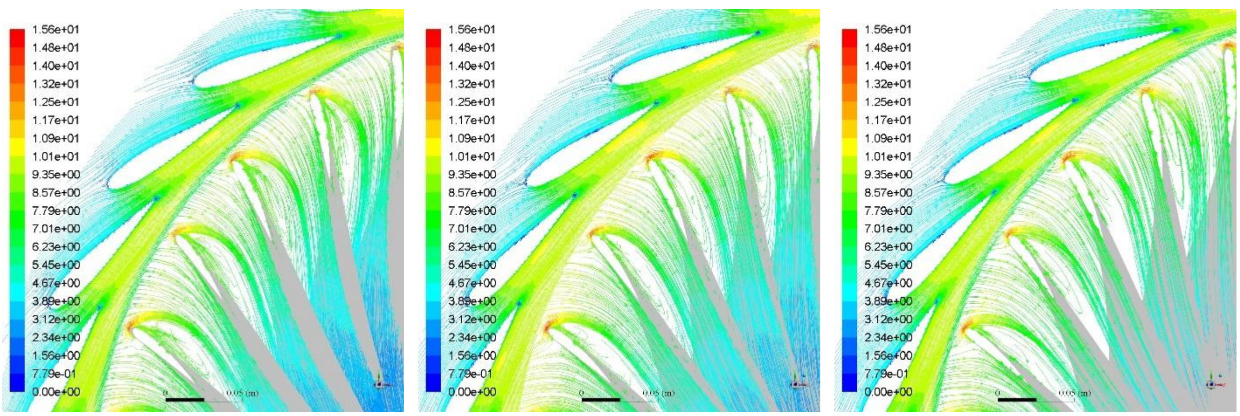

Fig.7.62 Relative streamlines at runner inlet for $n = 0.8n_{nom}$ (Model SYM)
Z1 – Blade root Z0 – Middle of blade Z2 – Blade top

Fig. 7.61 presents the relative streamlines at runner inlet for the Model (+)10-SYM, and Fig.7.62 for the Model SYM. The difference is evident compared with the fully symmetrical blade, for $n = 0.8n_{nom}$, where it can be seen on all sections where the trailing edge angle is curved for +10 degrees influences the flow direction and it makes more favourable inflow conditions.

For increased rotational speed, the filament of the runner blades channels is followed by flow separations. For the analysis of the flow phenomena, the velocity profiles are derived for the three height sections of the blade, as ±9.2% from the blade's height, top, and bottom. The profiles are compared with the singular blade's velocity profiles.

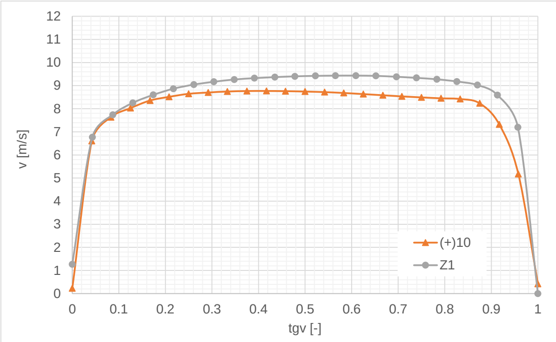

Fig.7.63 Comparison of velocity profiles for Model (+)10 and zone Z1 where it is dominant

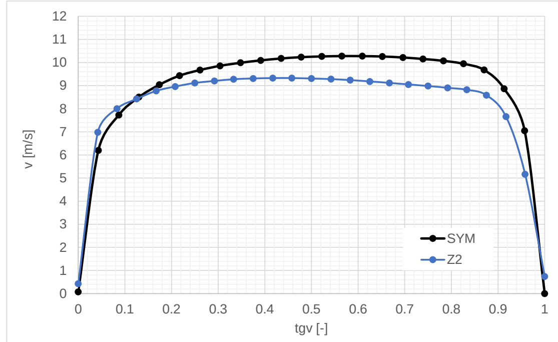

Fig.7.64 Comparison of velocity profiles for Model SYM and zone Z2 where it is dominant

From this comparison, it can be seen that the combination of these two profiles interferes each other. In the zone where the profile is with trailing edge curved angle of +10 degrees compared with the blade created of this type of profile only, it comes to a change in the shape and velocity intensity increase. Vice versa, in the zone where the symmetrical profile in the blade is dominant, a a change in velocity profile as well as decrease of the velocity intensity occurs.

This comparison shows that the lofted type of blade (direct connection of two profile types), without particular percentual participation inside the blade, leads to mutual interference of the geometries in the forming of the velocity profile and their particular influence on the velocity profile creation cannot be seen. In addition, it can be seen that the characteristic curve that is obtained fits up between the two partial characteristic curves from the two types of blades, so in future, the characteristics of the non-uniform blade can be estimated between the two partial characteristic curves.

The comparison of the reduced characteristics shows that there is extension of the areas under the curve, towards the speed factor of cca. 2.9 [%] and towards discharge factor of cca. 12.8 [%].

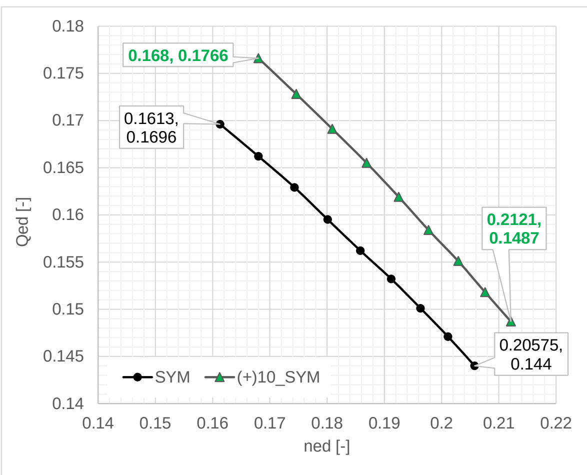

Fig.7.65 Comparison of the reduced characteristics

$$A_{n_{ed_1}} = 0.0072\ [-] > A_{n_{ed_{sym}}} = 0.007\ [-]$$

$$A_{Q_{ed_1}} = 0.0053\ [-] > A_{Q_{ed_{sym}}} = 0.0047\ [-]$$

7.3.2. Configuration 2

This configuration is developed as an assembly of two profiles with angular curvature of trailing edge and a symmetrical profile, where all the profiles are represented with 25% in the blades' height, and the rest 25% are geometrical transition zones between the segments.

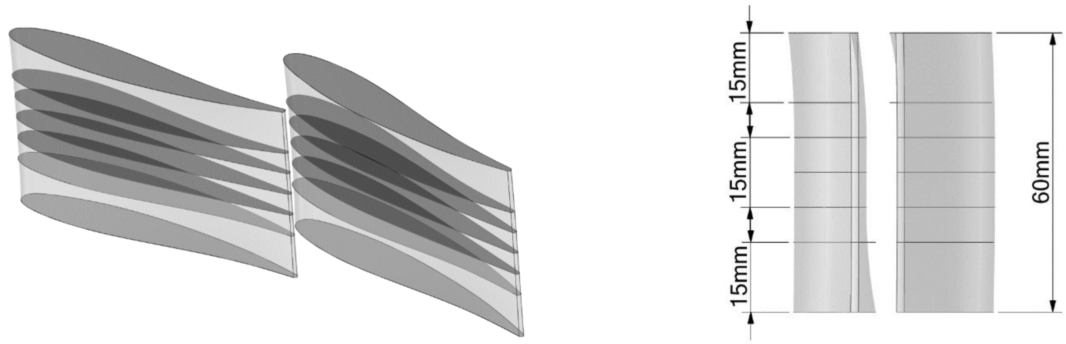

Fig.7.66 Configuration 2 geometry (+)10-SYM-(-)10-3x25%

Given that the profile with a positive angular curvature of the trailing edge of (+)10 degrees shows better performance for reduced rotational speed, at 10% reduced speed from the nominal, for achieving this flow, less energy is needed. Vice versa, the profile with a negative angular curvature of the trailing edge which shows better performance for increased rotational speed, at 10% increased speed from the nominal, more energy is needed to achieve this flow. The fluid flow always follows the direction of less effort, and so, the expansion inclination in this configuration is in the direction of reduced speed (Fig.7.67).

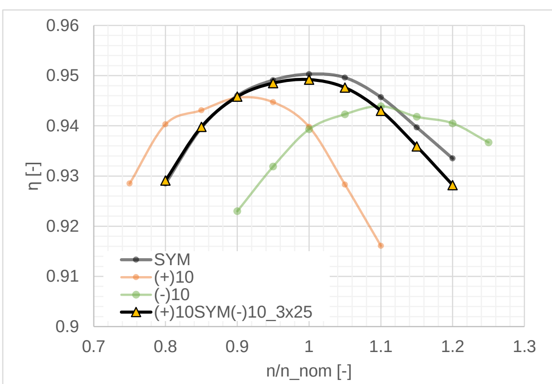

Fig.7.67 Comparison for $Q = const., H \neq const.$

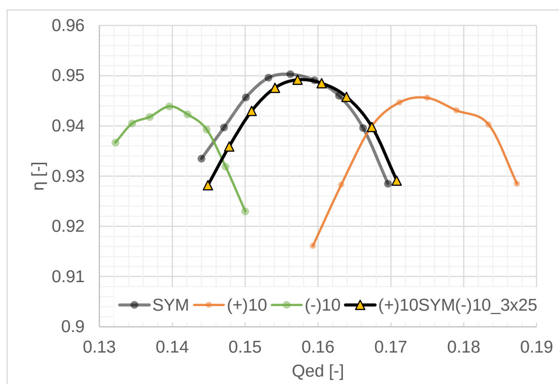

Fig.7.68 Comparison on basis of discharge factor

Compared on the basis of rotational speed, the characteristics show no extensions and the efficiency is bit lower. Compared on the basis of flow rate, a shift of the characteristics is obtained in a way of increased flow rates, i.e. reduced rotational speeds.

7.3.3. Configuration 3

Configuration 3 is configuration 2, but mirrored, to check if the reversed profile schedule has an influence on the characteristics. The results are shown in Fig.7.69.

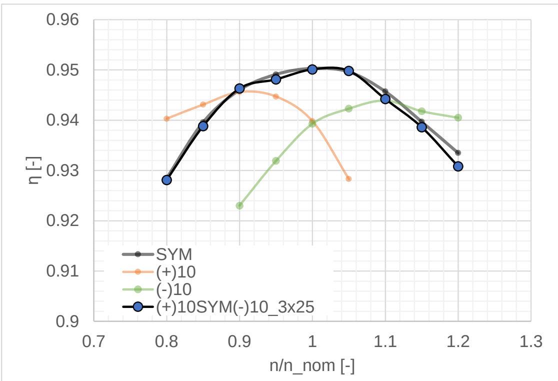

Fig.7.69 Comparison on basis of rotational speed

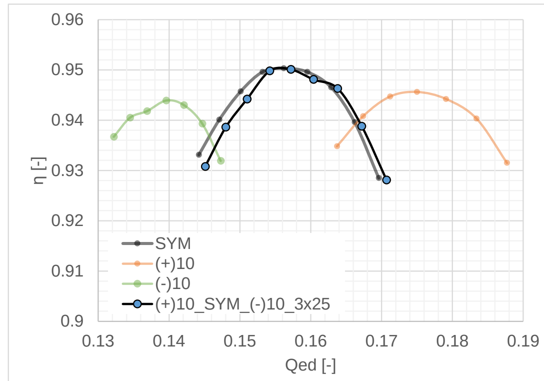

Fig.7.70 Comparison on basis of discharge factor

It can be noticed that in the narrow zone around the optimum, it comes to a slight alignment of the characteristics, which can point out that there is a slight expansion in that zone. The efficiency drops for reduced rotational speed show slight violation, a tendency that the operating range expands. The comparison with the symmetrical profile is given in Fig. 7.71.

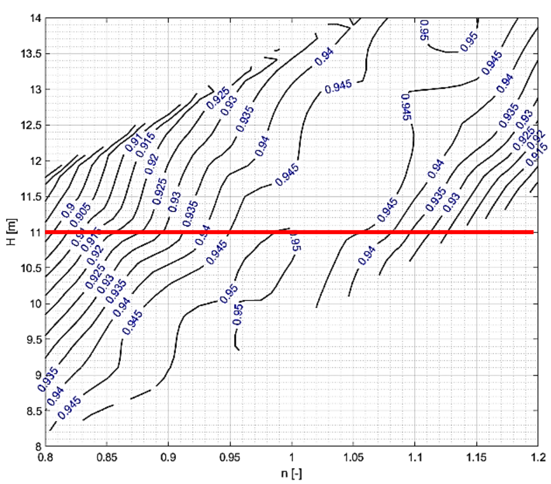

Fig.7.70.1 Configuration 3 - Hill Chart

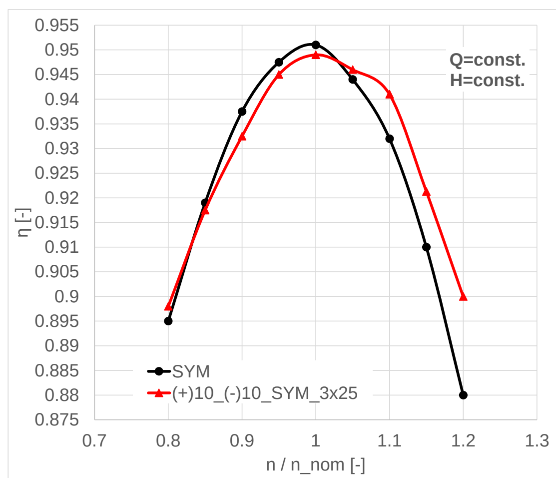

Fig.7.70.2 Comparison with Model SYM
$n \neq const.;\ Q = const.;H = const.$

From the obtained results it can be seen that the non-uniform blade of Configuration 3 compared to Model SYM gives better performance at off-design operation for increased rotational speed. For off-design rotational speed of $n = 0.8n_{nom}$, configuration 3 shows insignificant increased efficiency of cca. 0.3 [%] and for $n = 1.2n_{nom}$ for cca. 2 [%]. The optimal zone of Configuration 3 decreases for cca. 0.2 [%].

The comparison of the reduced characteristics shows that there is extension of the areas under the curve, towards the speed factor of cca. 1.4 [%] and towards discharge factor of cca. 2.1 [%].

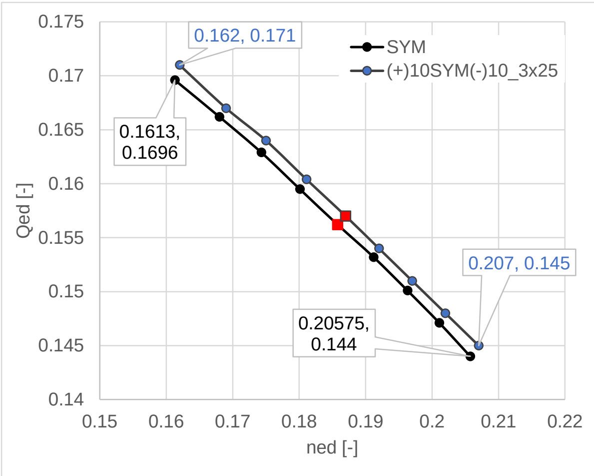

Fig.7.71 Comparison of the reduced characteristics (configuration 3 and symmetrical profiled blade)

$$A_{n_{ed_3}} = 0.0071\ [-] > A_{n_{ed_{sym}}} = 0.007\ [-]$$

$$A_{Q_{ed_3}} = 0.0048\ [-] > A_{Q_{ed_{sym}}} = 0.0047\ [-]$$

According to the flow pattern, it can be noticed that particular profile segments of the blade, with angular curvature of the trailing edge, placed at the blades' root and top, do not participate in flow improvements. The blade section with profile with positive angular curvature of the trailing edge of +10 degrees for reduced rotational speed of $n = 0.8n_{nom}$ shows flow separations at the runner blades suction side. For nominal rotational speed $n = n_{nom}$ the midsection of the guide vane blades directs the flow efficiently, and, in the blade root section where the blade section has a profile with a negative angular curvature of the trailing edge of -10 degrees, it shows flow separations for increased rotational speeds.

It can be concluded from this that the equal trailing edge curvatures of the blade trailing edge with same curvature angles form an angle similar to the symmetrical blade and cannot achieve the effect of flow direction for the given rotational speed, when they are compared to uniform profiled blades. Also, the comparison shows that the different guide vane configurations have different hydraulic losses. Increased pressure drops occur in blades with a negative angular curvature of the trailing edge. The reason for this is that the vector of velocity has increased projection in circumferential direction. And vice versa, the blades with a positive angular curvature of the trailing edge have a velocity vector projection increased in the radial direction. The cascades and the whole turbine configuration are tested for constant flow rates and equal opening clearances of the blade. Because the trailing edge curvatures, it comes to acceleration or deceleration flow behind the guide vanes, and so the difference in the losses occurs. The following analysis are made for blades consisted of profiles with similar energy losses, like, for example, the profile with a positive angular curvature of the trailing edge of +10 degrees and negatively rotated blade od (-)4ROT.

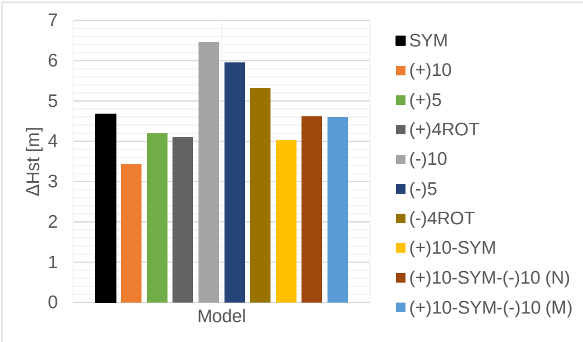

Fig.7.72 Static pressure drop comparison between the developed models

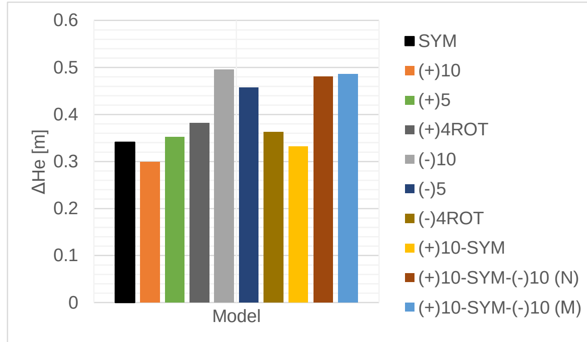

Fig.7.73 Total pressure drop comparison between the developed models

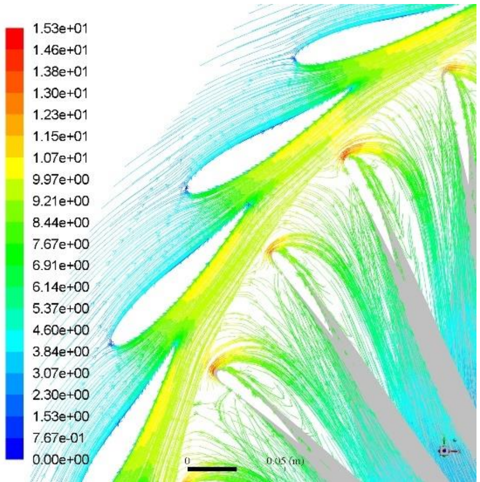

A) Model (+)10-SYM-(-)10-3x25%
Z1 – Blade root

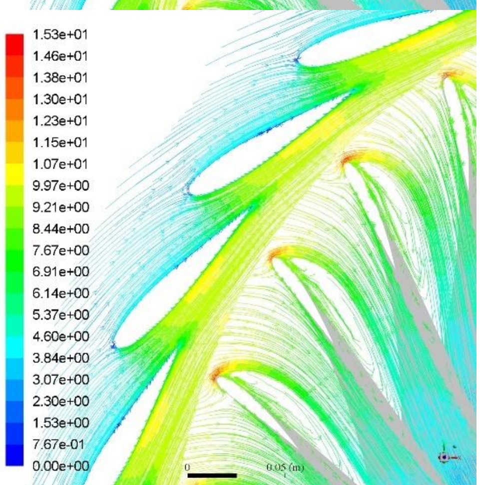

B) Model (+)10-SYM-(-)10-3x25%
Z0 – Middle of blade

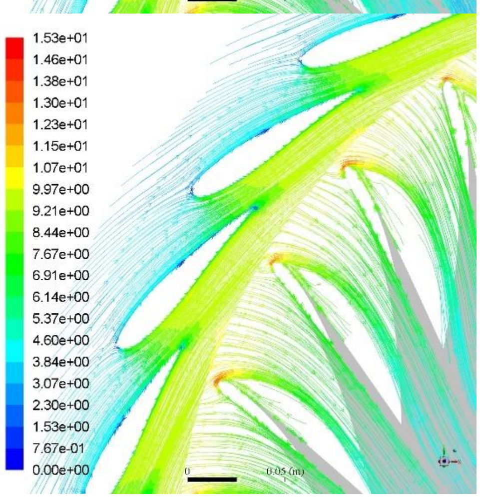

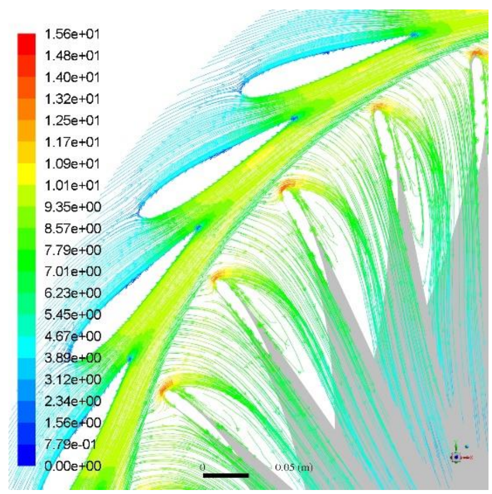

C) Model (+)10-SYM-(-)10-3x25%
Z2 – Blade top

C.1) Model SYM for Comparison

Fig.7.74 Relative streamlines at runner inlet for $n = 0.8n_{nom}$

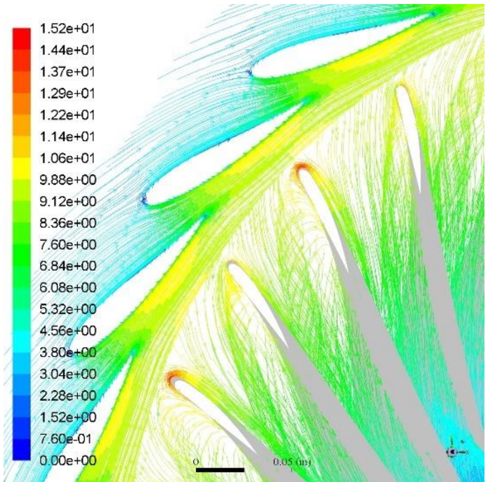

A) Model (+)10-SYM-(-)10-3x25%
Z1 – Blade root

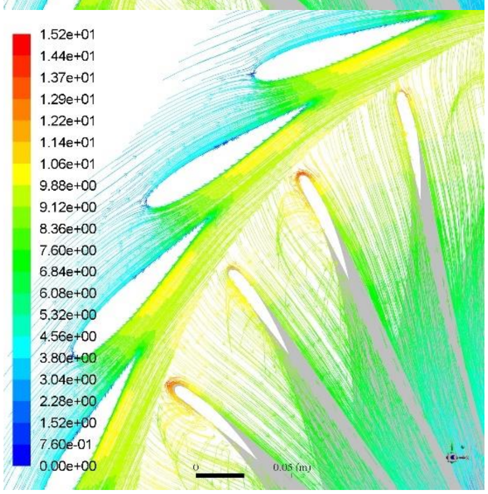

B) Model (+)10-SYM-(-)10-3x25%
Z0 – Middle of blade

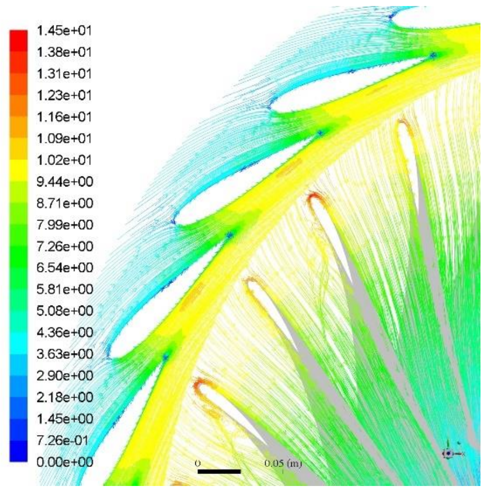

B.1) Model SYM for Comparison

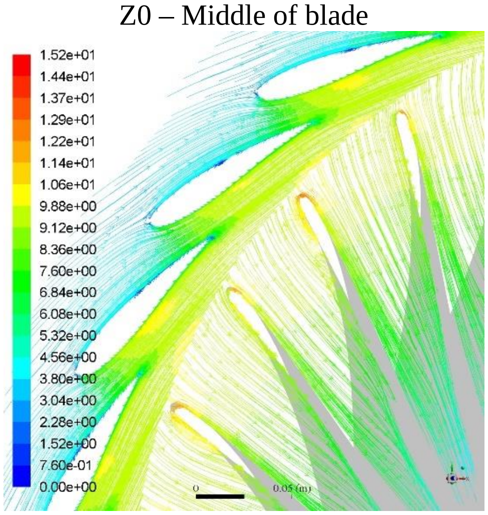

C) Model (+)10-SYM-(-)10-3x25%
Z2 – Blade top

Fig.7.75 Relative streamlines at runner inlet for $n = n_{nom}$

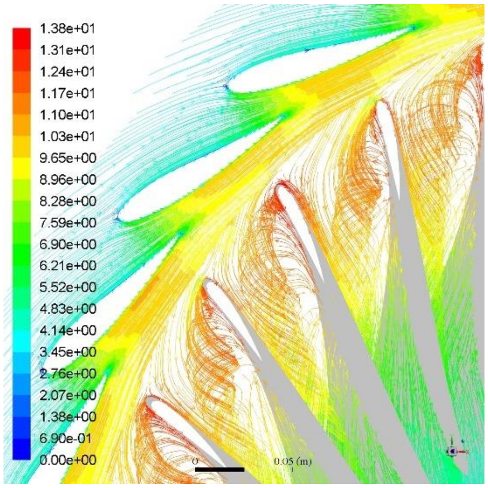

A) Model (+)10-SYM-(-)10-3x25%
Z1 – Blade root

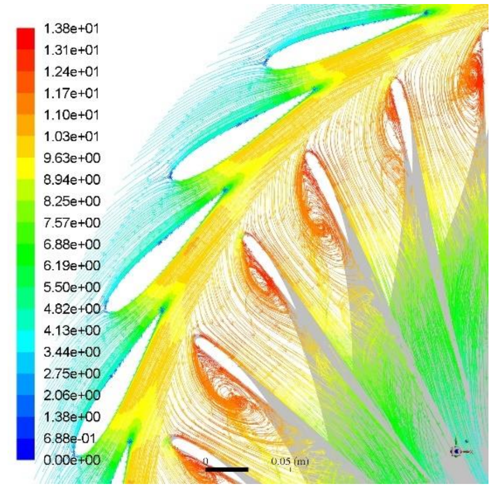

A.1.) Model SYM for comparison

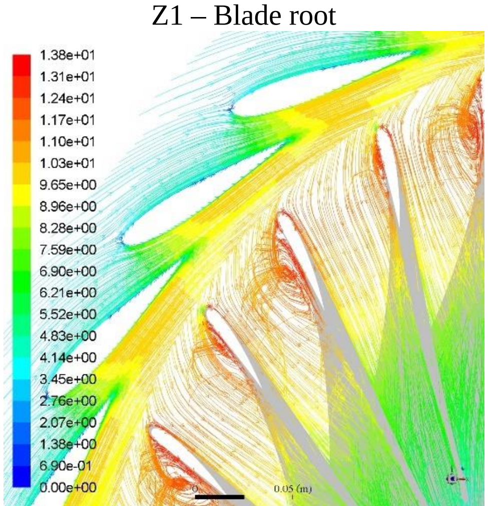

B) Model (+)10-SYM-(-)10-3x25%
Z0 – Middle of blade

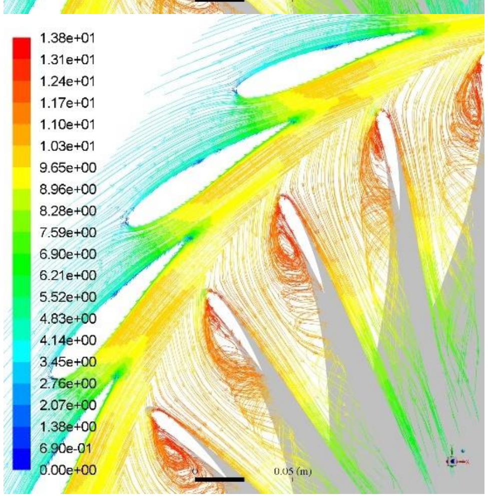

C) Model (+)10-SYM-(-)10-3x25%
Z2 – Blade top

Fig.7.76 Relative streamlines at runner inlet for $n = 1.2n_{nom}$

7.3.4. Configuration 4

The previous results show that the derived configurations of non-uniform blades do not lead to a significant extension of the operating characteristics. The effect of improving the flow pattern in partial operating modes is evident, especially for Model (+)10-SYM which has unilaterally positive angular curvature of the trailing edge. The following considered configuration is an assembly of a symmetrical profile with a negatively rotated profile from Model (-)4ROT. The distribution of the two profiles by height depends on the range covered by each of them.

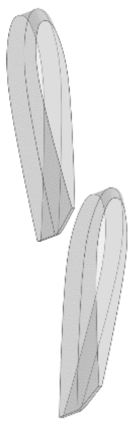

Fig.7.77 Sketch of the blades

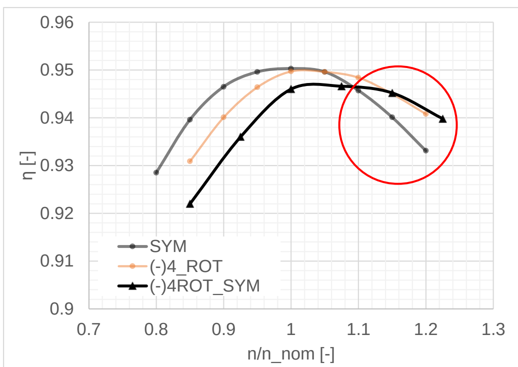

Fig.7.77.1 Comparison of the models and improvement zone for $n = 1.15n_{nom}$

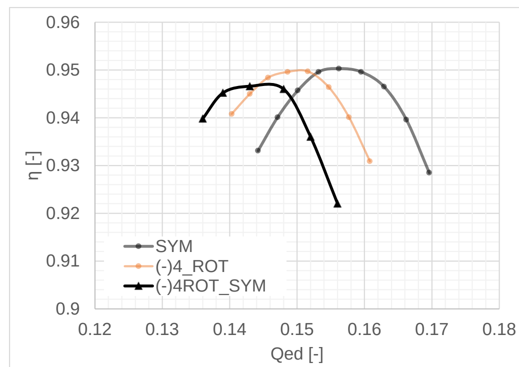

Fig.7.78 Comparison of the models on basis of reduced flow rate

According to the results, this configuration did not fall between the two partial characteristics; a shifted characteristic is obtained with a tendency to operate in the zone of increased rotational speed, where there is also an increase in efficiency. The flow pattern is analysed in three sections of the blade by height, for rotational speed of $n = 1.15n_{nom}$, where the difference in efficiencies is noticed and compared with the flow patterns with the symmetrical profile. This configuration shows consistency and efficiency maintenance more predominantly in the zone of increased rotational speed from $n = (1.05 \div 1.2)n_{nom}$, which is assumed to be able to sustain this trend in combination with other blade profiles.

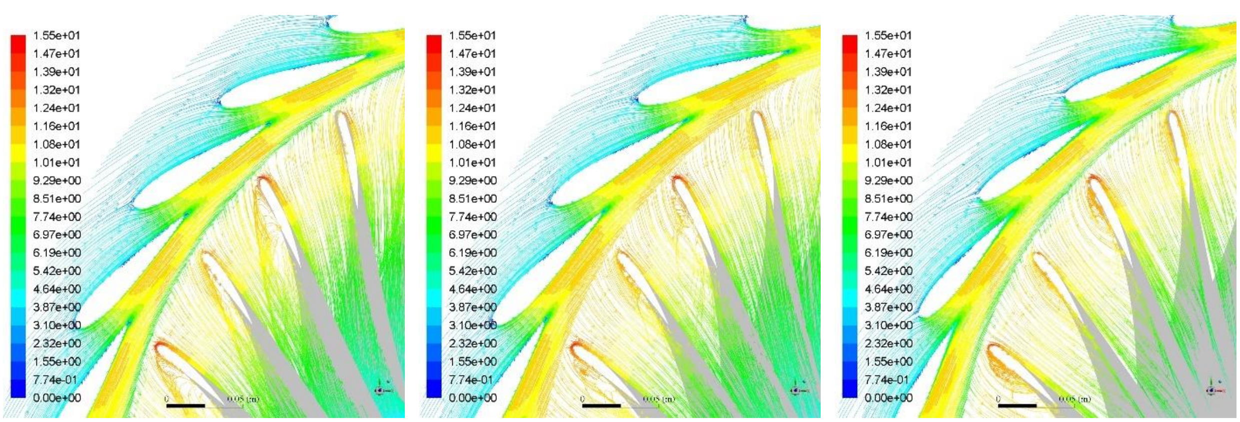

Fig.7.79 Relative streamlines at runner inlet for $n = 1.15n_{nom}$ (Model (-)4ROT-SYM)
A) Zone Z1 – Blade root B) Zone Z0 – Middle of blade C) Zone Z2 – Blade top

According to the flow patterns, the presence of the rotated blade that corrects the flow at the runner inlet is evident, affecting from the middle of the blade to the top, where it is dominant. In the blade root zone, the symmetrical profile is dominant, and it is noticed that there are partial flow separations on the pressure side of the runner blades.

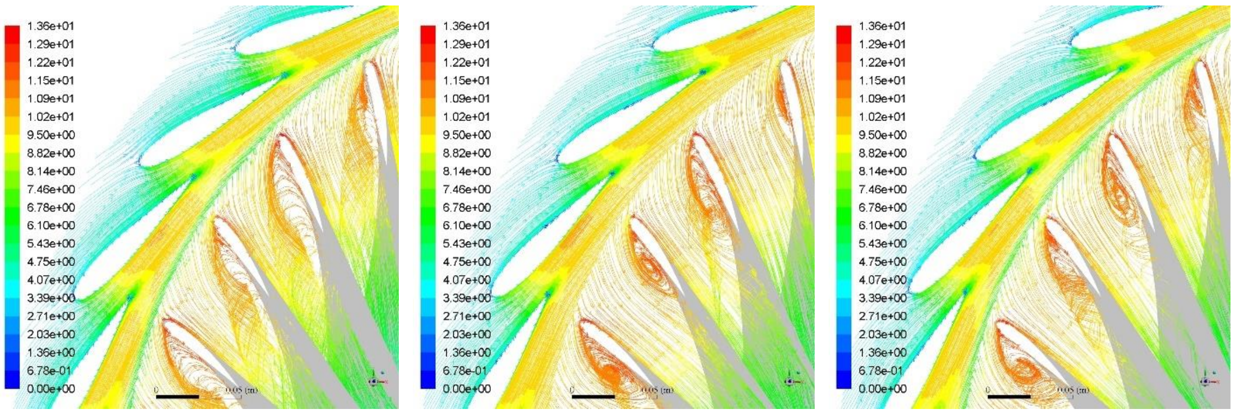

Fig.7.80 Relative streamlines at runner inlet for $n = 1.15n_{nom}$ (Model SYM)

A) Zone Z1 – Blade root B) Zone Z0 – Middle of blade C) Zone Z2 – Blade top

In Fig. 7.80, the relative streamlines for symmetrical blade profile for $n = 1.15n_{nom}$, are shown to compare the flow patterns with the developed Model (-)4ROT-SYM. The differences are obvious in all of the three zones of the blade. In the blade root zone, where the two models have the symmetrical profile shape, due to the partial impact of the rotated profile which induces less flow separations, compared with the flow pattern of Model SYM.

7.3.5. Configuration 5

This configuration is a combination of profiles with a positive curvature of the trailing edge of +10 degrees, symmetrical profile, and negatively rotated profile with collinear chord line (-)4ROT. The outcome of the previous results from individual uniform blades composed of these profiles is to develop this configuration, which show the best performance in terms of increased and decreased rotational speed and similar energy losses in the cascades.

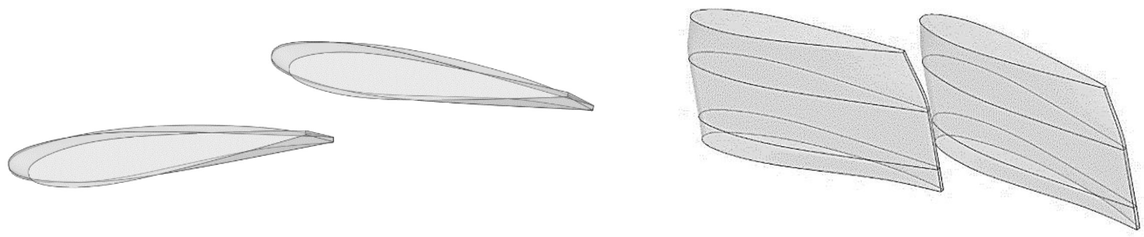

Fig.7.81 3D configuration view

The profile height layout is adopted according to the points in the characteristics obtained for the individual blades. The range of ± 20 [%] of the rotational speed is taken as a representative by height of the blade, and which profile how much contributes in it (Fig.7.82).

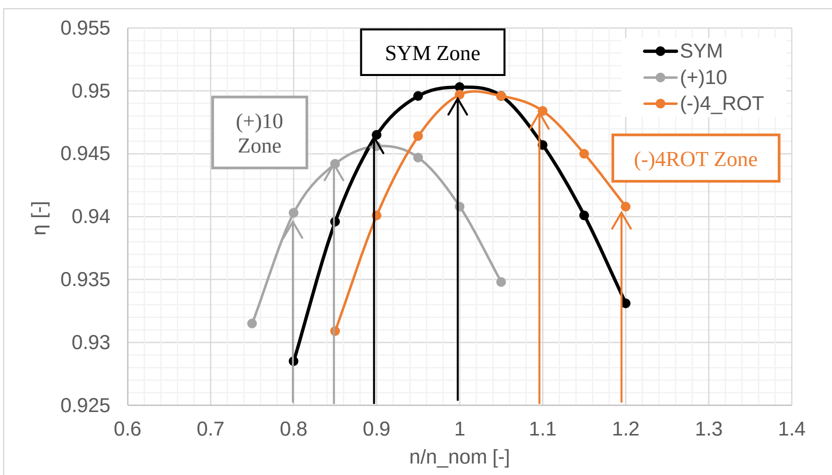

Fig.7.82 Division of the participation of the profiles in the blade according to the performance of the expanding zones

The chart shows the participation zones of the individual uniform blades. From here, it is started with dividing the blade by height, according to the performance of the profile expected to be obtained. Eight points of division are obtained, which give the maximum efficiency for the given rotational speed, according to the order of the rotational speeds that are examined. Two operating points belong to the blade with a curved trailing edge of (+)10, three points to the symmetrical blade and three points to the blade with a rotated profile with collinear chord line (-)4ROT. The height of the guide vanes is $B_o = 60[mm]$, so as a percentage of the height, the profile with a trailing edge curvature of +10 degrees is participating with 25% in the blade (15 mm), and the symmetrical profile and the rotated profile with 37.5% (22.5 mm) each.

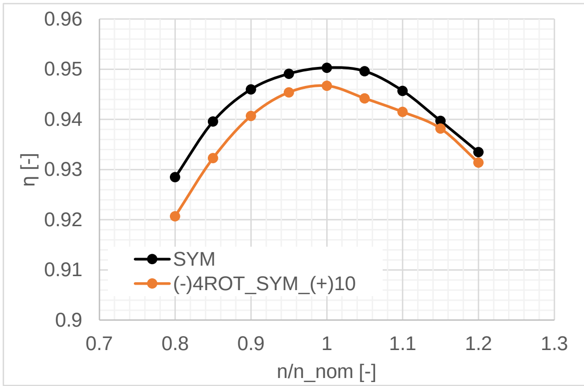

Fig.7.83 Comparison on basis on rotational speed

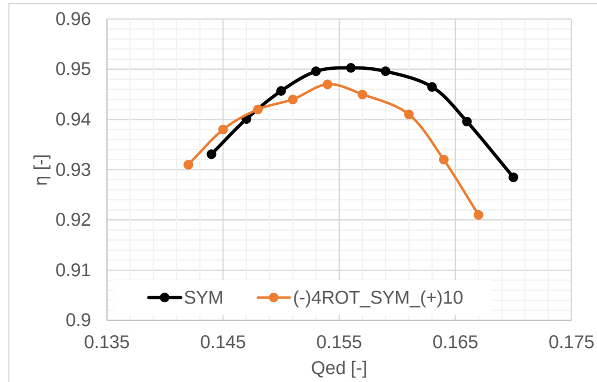

Fig.7.84 Comparison on basis on discharge factor

According to the results, there is a decrease in efficiency, and a milder slope of the characteristic in the direction of increased speed, indicating that the rotated blade (-)4ROT in that zone manages to affect the characteristic. There is a gradual change of the characteristic before the local optimum, which shows a small dose of consistency of the operating range in that zone. In the direction of reduced speed, the characteristic decreases, which indicates that the profile (+)10 at the blade root does not cover sufficiently the reduced speed zone. For 3 positions, the hill chart is obtained in a narrow zone, to see how influences the characteristics in general.

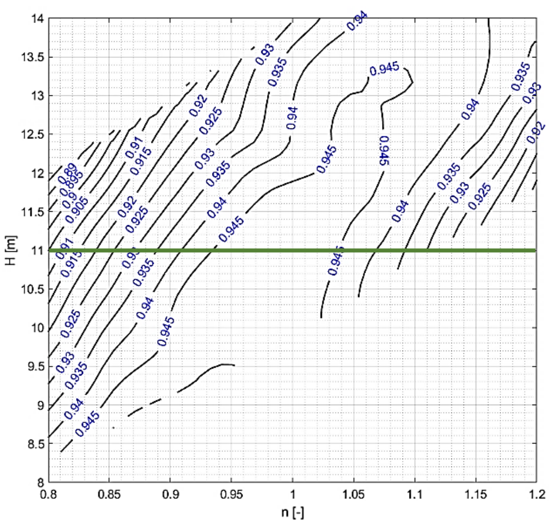

Fig.7.84.1 Configuration 5 - Hill Chart

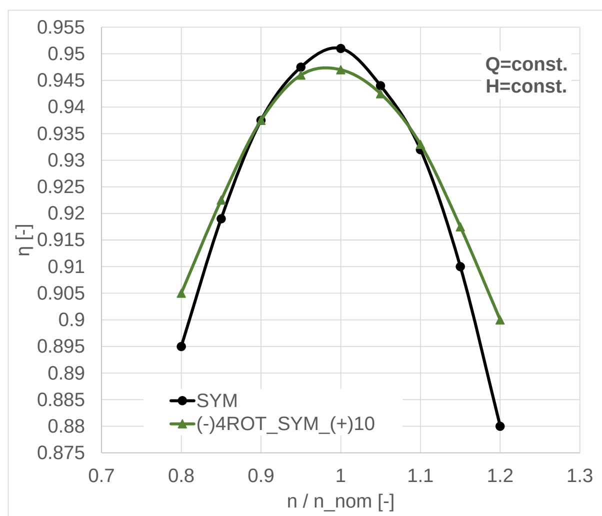

Fig.7.84.2 Comparison with Model SYM
$n \neq const.;\ Q = const.; H = const.$

From the obtained results it can be seen that the non-uniform blade of Configuration 5 compared to Model SYM gives better performance at off-design operating rotational speed. For off-design rotational speed of $n = 0.8n_{nom}$, configuration 5 shows increased efficiency of cca. 1 [%] and for $n = 1.2n_{nom}$ for cca. 2 [%]. The optimal zone of Configuration 5 decreases for cca. 0.4 [%].

The comparison of the reduced characteristics shows that there is shrinkage of the areas under the curve, towards the speed factor of cca. -2.9 [%] and towards discharge factor of cca. -4.3 [%].

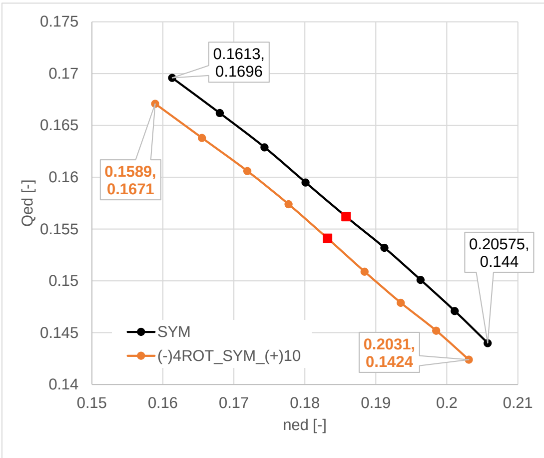

Fig.7.85 Comparison of the reduced characteristics

$$A_{n_{ed_5}} = 0.0068\ [-] < A_{n_{ed_{sym}}} = 0.007\ [-]$$

$$A_{Q_{ed_5}} = 0.0045\ [-] < A_{Q_{ed_{sym}}} = 0.0047\ [-]$$

A comparison of the flow pattern of this configuration with the fully symmetrical blade was made. In Fig.7.86, it can be seen that the flow separates at the pressure side of the runner blades for $n = 1.15n_{nom}$ which does not give an increase in efficiency (Fig.7.83) in that zone and is identical compared with the symmetric profile.

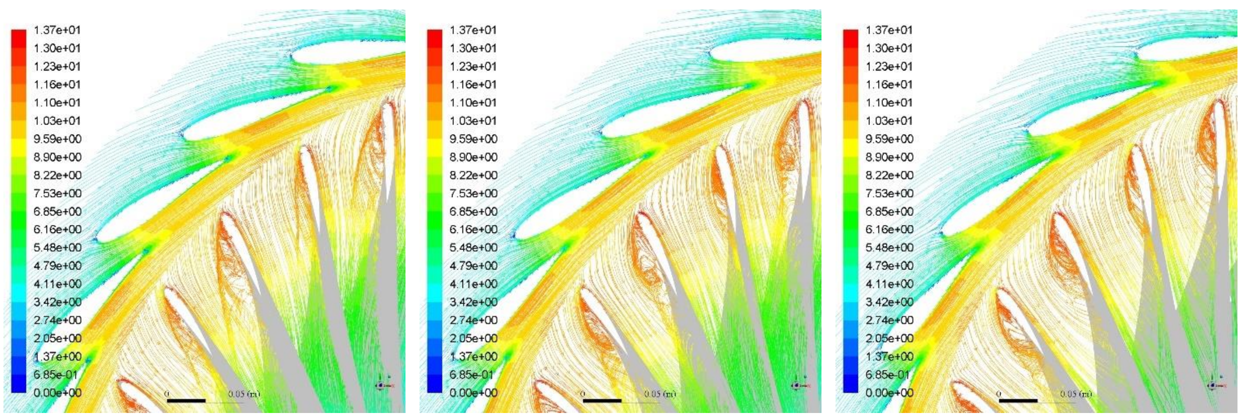

Fig.7.86 Relative streamlines at runner inlet for $n = 1.15n_{nom}$ (Model (-)4ROT-SYM-(+)10)
A) Zone Z1 – Blade root B) Zone Z0 – Middle of blade C) Zone Z2 – Blade top

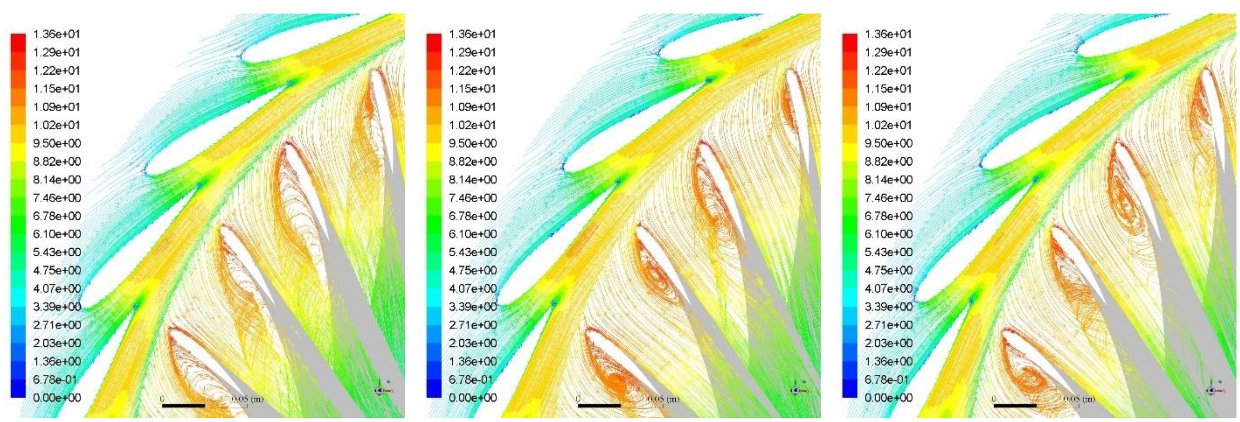

Fig.7.87 Relative streamlines at runner inlet for $n = 1.15n_{nom}$ (Model SYM)
A) Zone Z1 – Blade root B) Zone Z0 – Middle of blade C) Zone Z2 – Blade top

7.3.6. Configuration 6

This configuration is a modification of configuration 5, done by replacing the profile with a curved trailing edge of (+) 10 degrees to (+) 15 degrees in order to obtain coverage of the zone at reduced rotational speeds.

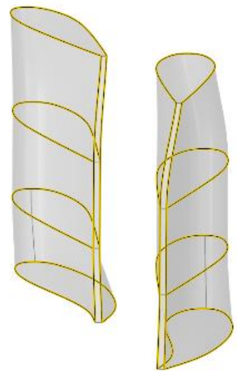

Fig.7.88 Blades sketch

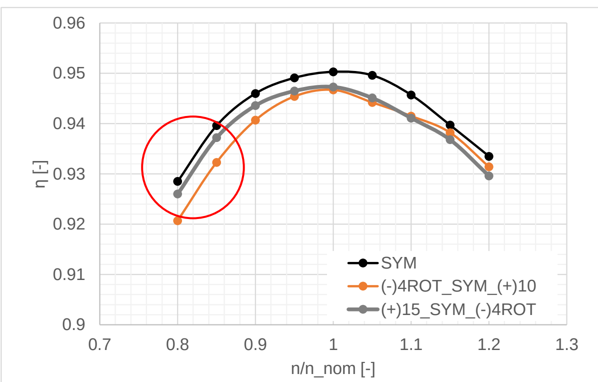

Fig.7.88.1 Comparison on basis on rotational speed

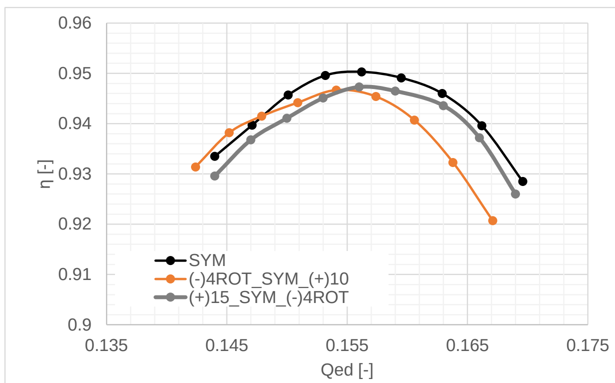

Fig.7.89 Comparison on basis on discharge factor

According to the results, the additional deformation of the trailing edge contributes to the correction of the efficiency and change of the characteristic for reduced speed. On the other hand, a slightly smaller decrease in efficiency is obtained at increased speeds. The following figures of the flow patterns show that the flow is affected by the additional curvature of the output edge, compared with the previous model, get reduced flow separations, so there is an increase in efficiency in that area compared with the previous Model.

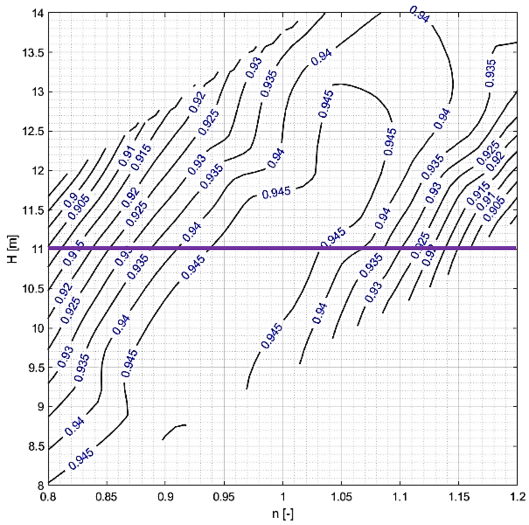

Fig.7.90.1 Configuration 6 - Hill Chart

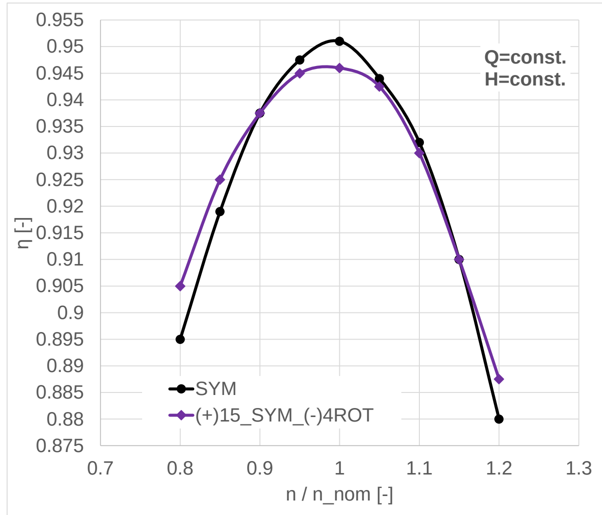

Fig.7.90.2 Comparison with Model SYM
$n \neq const.;\ Q = const.; H = const.$

From the obtained results it can be seen that the non-uniform blade of Configuration 6 compared to Model SYM gives better performance at off-design operating rotational speed. For off-design rotational speed of $n = 0.8n_{nom}$, configuration 6 shows increased efficiency of cca. 1 [%], for $n = 0.85n_{nom}$ shows increased efficiency of cca. 0.6 [%] and for $n = 1.2n_{nom}$ for cca. 0.75 [%]. The optimal zone at $n = n_{nom}$ of Configuration 6 decreases for cca. 0.5 [%].

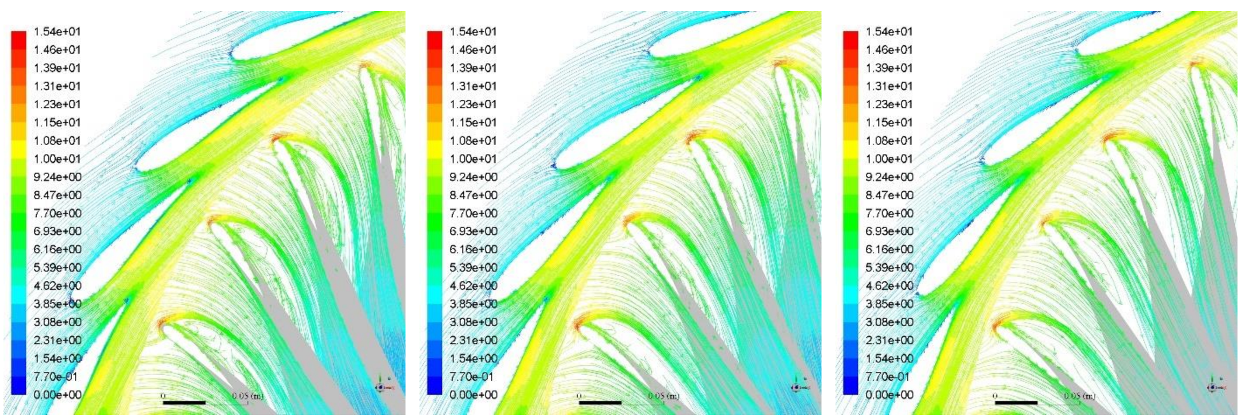

Fig.7.91 Relative streamlines at runner inlet for $n = 0.8n_{nom}$ (Model (+)15-SYM-(-)4ROT)
A) Z1 – Blade root (+)15 B) Z0 – Middle of blade (+)10 C) Z2 – Top of blade (-)4

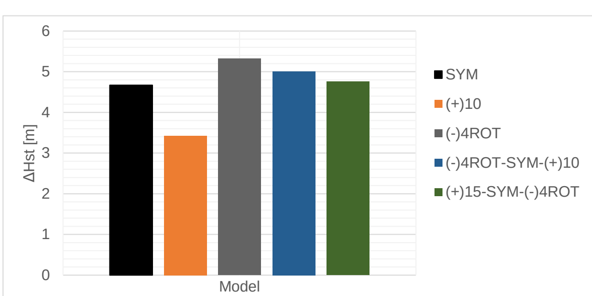

Fig.7.92 Comparison of the static pressure drop of the Models

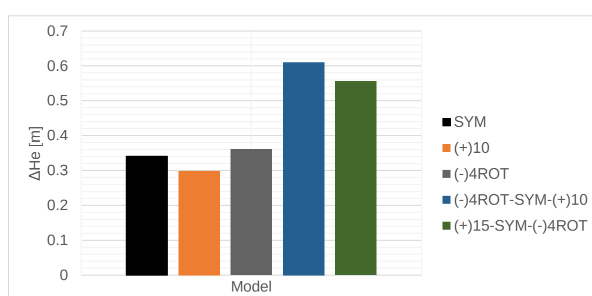

Fig.7.93 Comparison of the total pressure drop of the Models

According to the static pressure drop chart, the last two Models compared with the symmetrical reference blade have almost identical static pressure drop and increased total pressure drop, which shows that they inefficiently distribute the energy through them. On the other hand, the charts of the change of the total pressure at the inlet and outlet of the runner under identical operating modes are performed, where it can be seen that there is almost no difference in the degree of energy exchange.

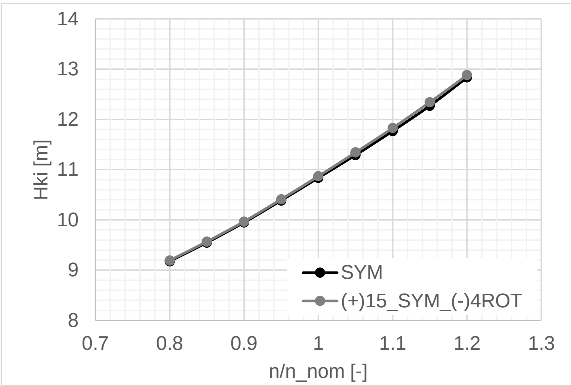

Fig.7.94 Runner inlet head comparison

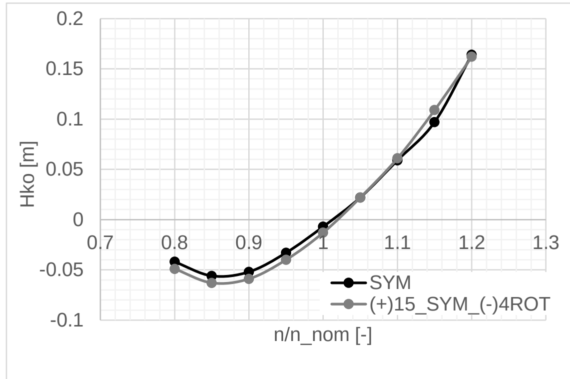

Fig.7.95 Runner outlet head comparison

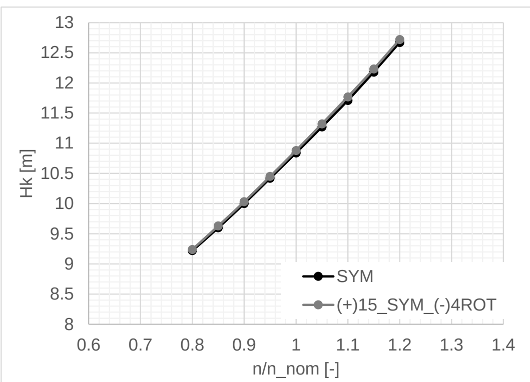

Fig.7.96 Runner head comparison

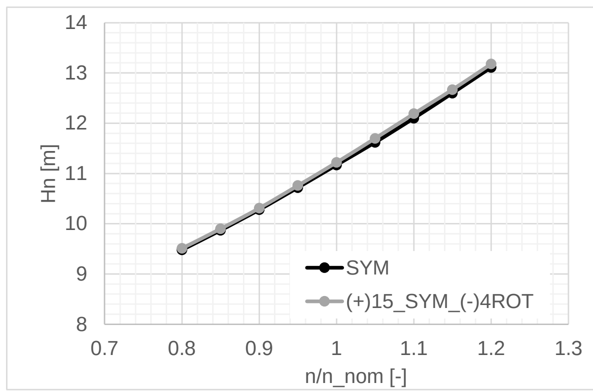

Fig.7.97 Turbine head comparison

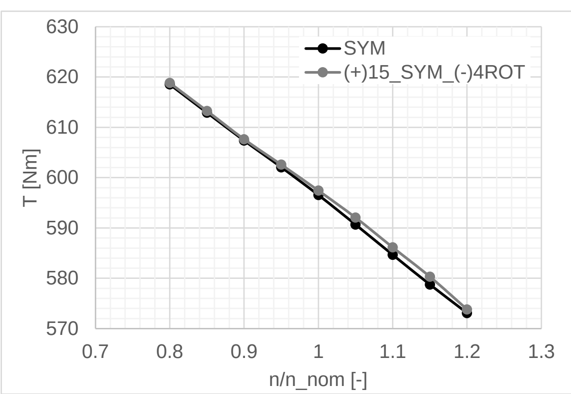

Fig.7.98 Comparison of torques

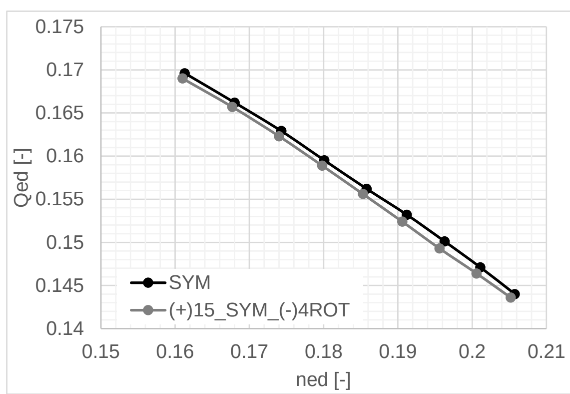

Fig.7.99 Comparison of reduced characteristics

The classical energy parameters presented in the charts make it obvious that the turbine as a system, and also the runner itself, behaves identically regardless of the type of the guide vanes. Therefore, the vectors at the runner inlet which form the velocity triangles are analysed, and the inflow loses at the runner are calculated.

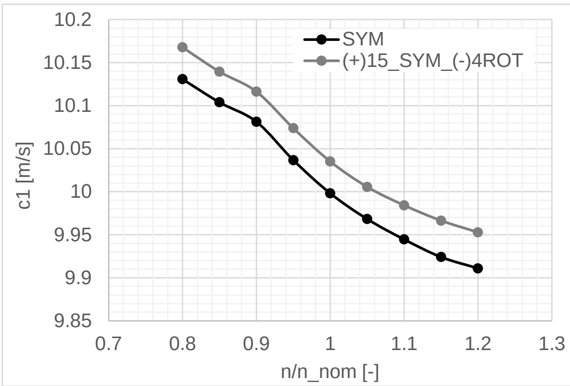

Fig.7.100 Absolute velocity vector comparison

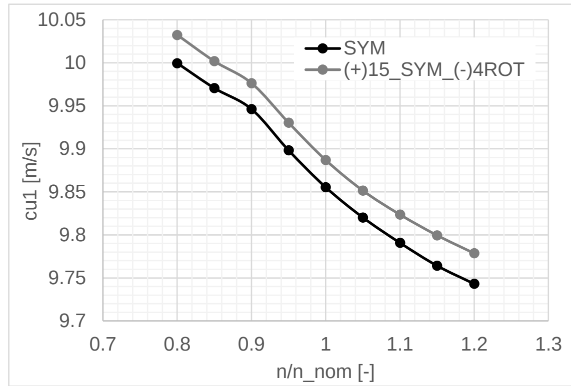

Fig.7.101 Circumferential velocity vector comparison

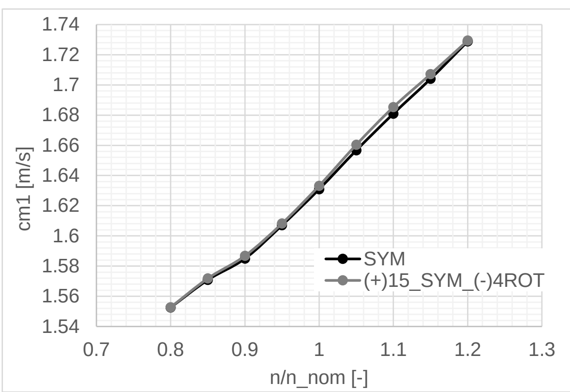

Fig.7.102 Meridian velocity vector comparison

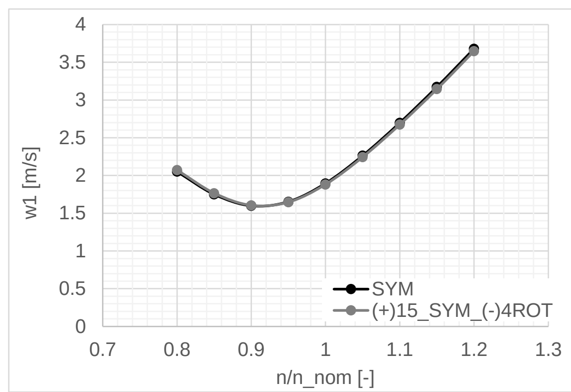

Fig.7.103 Relative velocity vector comparison

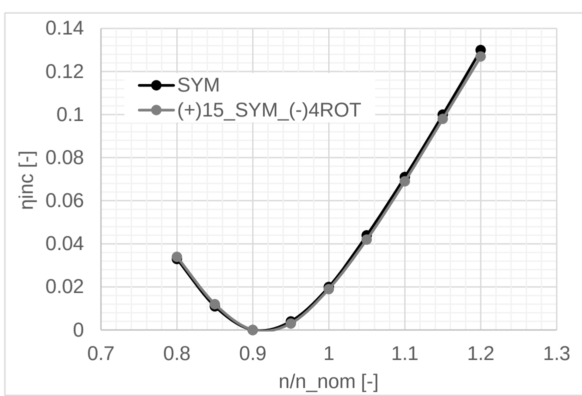

Fig.7.104 Runner inlet incidence losses

The only differences in the calculation of the velocity components at the runner inlet appear on the absolute and circumferential velocities, and the mutual differences are negligibly small. This leads to the conclusion that even with a non-uniform blade, all flow parameters can be adjusted in the same way as using a symmetrical blade. The difference in the efficiency and in the shape of the characteristics, as it can be noticed in this case, depends mainly on the drop of the total pressure through the cascades, but also on other flow phenomena that need to be investigated, such as the occurrence of rotational flow pattern due to the variety of profiles of the blade by height.

8. Conclusions and recommendations for further work

Variable speed turbine analysis is by no means a simple task because it is multidisciplinary and requires much more research, physical measurements, as well as real operating conditions of hydropower plants on that principle, to gain more practical experiences in this area. Although the electrical equipment allows this kind of turbine operation, the turbine itself and the created fluid flow under such conditions is a topic that continues to evolve, in the direction of the turbine runner, and the guide vanes and the other turbine parts as well.

In this doctoral dissertation a step forward is made towards defining the guide vanes' meaning in a variable speed operated hydraulic turbine. In this way, a contribution is made to insufficient body of literature in this field, especially on the topic of radial cascades used as guide vanes.

Several steps have been taken to reach the main goal, and that is the analysis of non-uniform guide vane blades and and their effect on the turbine characteristics at variable speed operation. At the beginning, the basic mathematical relations that describe the fluid flow are derived for the vaneless space, with a brief analysis of what variable speed means, from a kinematic and energy aspect.

In Chapter 3, using the basis of the derived physical laws, a parameterisation of the geometry and its mathematical description was realised in order to obtain various forms of guide vanes, which are used in the further analysis. This very approach for defining the geometry of the guide vanes is a novelty, same as defining the blade surface contours and their profiling which is influenced by the needed flow vector behind them, for a certain turbine operating point implemented in a program code.

The numerical model setup for the CFD simulations is based on a referent model of high-head Francis turbine (Francis 99) tested in the Waterpower Laboratory in NTNU, which represents a scaled model of the HPP Tokke turbine in Norway. This model is used in the analysis and the simulation guidance was defined by it in all the other performed analyses.

In this way, conditions are created for testing different geometries of guide vanes in order to define several limitations in the design itself. Influence of the pitch, clearance, or cascade density is examined through simulations to finally define a favourable blade geometry to which special geometric changes have been made to obtain non-uniformly profiled blades.

In Chapter 6, despite the mentioned analysis, a very important conclusion is reached regarding the blade placement in the cascade - that the blade chord lines should be collinear with the trailing edge angle, i.e. with the needed cascade outflow angle towards the runner for the given operating point. Any designed blade that deviates from this criterion can lead to off-design points and non-fulfilment of the fluid flow conditions. Introducing this criterion for the design of the guide vanes gives a direction for future designers on how to approach this part without searching through various blades positions.

Using all the conclusions from the previous chapters, an approach was made towards defining non-uniformly profiled blades. The starting geometry is a symmetrical blade profile, because of its simple geometry, and all the geometric changes on the trailing edge and on the blade chord line were made on the basis of it, as to achieve a collinearity with the flow angle.

The analyses show that small changes in the blade lead to a change – shift of the characteristics. So, the idea was developed to include all those partial changes as one, i.e. one blade made as combination of profiles which can cover the shifting to obtain group characteristics, with a lower efficiency in the best efficiency point, but with extended operating zone.

Changes in the profile geometry give unambiguous solutions, shifted characteristic in the direction of an increased or decreased rotational speed and appearance of local optimum in that zone. Thereby, a hydraulically favourable flow pattern is obtained in those operating zones which the base symmetrical blade cannot achieve.

Double geometry changes, i.e. a geometry composed of two profiles, give a characteristic that fits exactly between the partial characteristics of the two profiles separately. They also shift it somewhere between the two partial characteristics, at the same time hydraulically covering the entire range favourably, as for the flow pattern and in terms of efficiency, slightly reduced compared to the base model.

The goal achieved is covering both zones of increased and decreased rotational speeds. Theoretically, and intuitively, according to the results shown, the blade is formed of three profiles through its height to cover the operating range. Analyses of several models have shown that the characteristics extends, the efficiency increases for off-design rotational speeds, while the efficiency in the optimum slightly decreases. Configurations 3, 5 and 6, consisted of three profiles, show that there is an increase in operating efficiency for 20% reduced speed, from 0.3% to 1%. The optimal zone in these configurations decreases compared to the base model from 0.2% to 0.75%, and for increased speed of 20%, give an increase in efficiency of 0.5% to 2%.

Mainly, all the obtained characteristics are under the influence of the main blade formed by a symmetrical profile. This leads to a rough conclusion that a symmetrical profile is favourable for these operating conditions and covers all the rotational speed zones. Partial segments of the blades somewhere meet the flow conditions at a certain rotational speed. The overview that is obtained is that all three profiles by height influence on each other and form a weighted outflow conditions with one angle of flow distribution, but with lower performance at nominal speed and better at off-design speeds; similar to the conditions of placing a uniform blade, as well as for example increased losses in the guide vanes itself.

One of the conclusions in upgrading this research is related to the reference model, the high-head Francis 99 turbine. All the variable speed turbine analyses mentioned in the introductory chapters indicate that the low-head Francis turbines would benefit more from this technique. Also, from the aspect of turbine construction and type, Francis 99 is designed for very small blade openings and narrow manoeuvring spaces, where with only from $1 \div 2$ [°]change in the blade position, flow rate can change from 10 to 15%. It is concluded that the same analyses need to be performed for a low-head Francis turbine type with a known characteristic, so that the effect of the non-uniform blades of the guide vanes can be seen.

In general, for those turbines, from the aspect of turbine construction, the guide vane blade is characterised by an increased height, the flow created behind the guide vanes is a potential helical flow and there is a possibility for increased manipulation of the blade profiles by height and at the same time by the outflow angle, because these turbines operate at much larger opening angles.

The idea certainly turns out as justified. The effects are achieved for all non-uniform blades, where it can be seen that for a changed rotational speed, the individual zones make efficient flow filling of the runner, with less flow separations and with zone extension. It is concluded that the theory set forth in this study is that the variable speed, from a flow kinematic point of view, requires a different vector arrangement in the vaneless space, and it is possible to achieve this through the blades trailing edge. This defines the influence of the guide vanes on the turbine characteristics; it turns out that it can shift it and change it, a fact which so far in practice has not received significant attention.

Further research can take several directions. For example, to optimise the non-uniform blade, where each of its individual cross-sections in height gives the same hydraulic characteristic but different fluid flow direction. These include variations in the profile lengths for the cross-sections, as well as their percentage of participation in the blade, which is expected to give a flow energy balance in the guide vanes.

Another direction which arises from the obtained results is to analyse guide vanes with a possibility to change the trailing edge angle (wing flaps). The idea already exists in aircraft wings, where the trailing edge is retractable and rotates around a point; just in this case this effect can be used to direct the flow to the required flow angle for the assigned rotational speed.

The third possibility is to develop double-row (tandem) cascades. The first row should be composed of blades that will be designed for the nominal operating point, and the second row to make corrections of the flow direction when changing the rotational speed and achieving the necessary conditions.

And, finally, the fourth direction, more as an idea, comes from the research mentioned in the introductory part, and that is using blowing blade trailing edge water jets. The jet is supplied with pressure turbine penstock, so the same amount of water needed would be used to improve the flow in the vaneless space. Underwater jets have a much higher flow velocity compared to the speed between two blades to make a flow "curtain" (barrier) and additionally direct the flow with the required intensity and direction.

The above suggestions and guidelines for further work are still based on the main idea that a change of rotational speed leads to a change of the operating point, i.e. new hydraulic condition is obtained, an so a new vector arrangement with new intensities and directions, which need to be achieved in the vaneless space, for efficient turbine operation and coverage of that operating zone, no matter how it would be achieved. To define in which direction the further research can go, analyses of all these proposed solutions are needed, both energy and techno-economic, to examine which solution provides the best hydrodynamic conditions for a variable speed turbine, which solution covers the operating range best. The solution also depends on the operating conditions of the hydropower plant, how long and how it would work in such a mode, to see which solution satisfies, and at the same time to be economically viable for a longer period.

9. References

[1] Marius Siemonsmeier et. all - Three European Energy Scenarios (Hydropower Providing Flexibility for a Renewable Energy System – HydroFLEX Report, December 2018)

[2] Iliev I., Trivedi C., Dahlhaug O. G. (2019) Variable-speed operation of Francis turbines: A review of the perspectives and challenges. Renewable & Sustainable Energy Reviews. vol. 103.

[3] Farell C. et. all – Hydromechanics of variable speed turbines (Minnesota, 1983)

[4] Marija Lazarevikj, Filip Stojkovski, Valentino Stojkovski, Zoran Markov - Small scale variable speed Francis turbines: possibilities and challenges (Energetika 2020)

[5] Topazh G. I. – Lopastny gydromashini i gydrodynamichesky peredachi – Osnovi rabochego procesa i rascheta gydroturbin (St. Petersburg, Publishing House of the Polytechnic University, 2011)

[6] Krivchenko G. I. – Hydraulic Machines – Turbines and Pumps (Moscow, 1986)

[7] Barlit V. V. – Gidravlichesky turbini (Kiev, 1977)

[8] V.B. Andreev – Spravochink po gydroturbinam (Leningrad, 1984)

[9] N.N. Kovalev – Proektirovanie gydroturbin (Leningrad, 1974)

[10] J.R. Wilhelmi - Adjustable Speed Hydro Generation

[11] G. P. Heckelsmueller - Application of variable speed operation on Francis turbines (DOI: http://dx.doi.org/10.15446/ing.investig.v35n1.44995)

[12] A. Borghetti - Maximum Efficiency Point Tracking for Adjustable-Speed Small Hydro Power Plant

[13] Bortoni, E.; Souza, Z.d.; Viana, A.; Villa-Nova, H.; Rezek, Â.; Pinto, L.; Siniscalchi, R.; Bragança, R.; Bernardes, J., Jr. The Benefits of Variable Speed Operation in Hydropower Plants Driven by Francis Turbines. *Energies* 2019, *12*, 3719. https://doi.org/10.3390/en12193719

[14] Sh. I. Abubakirov - Performance Optimization Of Hydraulic Turbine By Use Of Variable Rotating Speed (Translated from Gidrotekhnicheskoe Stroitel’stvo, No. 2, February 2013, pp. 2 – 8.)

[15] E.H. Sundfør - Design and operation of a Francis Turbine with Variable Speed Capabilities (Master Thesis, NTNU 2017)

[16] A. Nordvik - Variable speed operations of Francis Turbines (Master Thesis, NTNU 2019)

[17] I. Iliev et. all - Optimization of Francis Turbines for Variable Speed Operation Using Surrogate Modeling Approach (ASME Journal of Fluid Engineering, 2020)

[18] Erik Tengs - Fully automated multidisciplinary design optimization of a variable speed turbine (doi:10.1088/1755-1315/774/1/012031)

[19] B.J Lewins - Wicket gate trailing-edge blowing: A method for improving off-design hydroturbine performance by adjusting the runner inlet swirl angle (27th IAHR Symposium on Hydraulic Machinery and Systems (IAHR 2014) doi:10.1088/1755-1315/22/1/012021

[20] Sailesh Chitrakar et al. - Numerical investigation of the flow phenomena around a low specific speed Francis turbines guide vane cascade (doi:10.1088/1755-1315/49/6/062016)

[21] Thapa BS, Trivedi C, Dahlhaug OG. Design and development of guide vane cascade for a low speed number Francis turbine. Journal of Hydrodynamics, Ser B. 2016;28(4):676-89. http://www.sciencedirect.com/science/article/pii/S1001605816606480

[22] Yu Chen et al. - Sediment Erosion Characteristics and Mechanism on Guide Vane End-Clearance of Hydro Turbine (Appl. Sci. 2019, 9, 4137; doi:10.3390/app9194137)

[23] Gnanasekaran KishorKumar et al - Influence of guide vane clearance on internal flow of medium specific speed Francis turbine (doi:10.1088/1755-1315/240/2/022056)

[25] K. Çelebioğlu – Numerical investigation of the effects of design parameters on hydraulic turbine guide vane design (doi: 10.5505/pajes.2019.70850)

[26] W W Zhang et al. - Influence of double-row guide vane cascade on performance of a Francis turbine (doi :10.1088/1755-1315/163/1/012093)

[27] C Devals et al. - CFD-based casing and distributor hydraulic design optimization (doi:10.1088/1755-1315/240/2/022033)

[28] I Iliev, C Trivedi and O G Dahlhaug - Simplified hydrodynamic analysis on the general shape of the hill charts of Francis turbines using shroud-streamline modeling (IOP Conf. Series: Journal of Physics: Conf. Series 1042 (2018) 012003 doi :10.1088/1742-6596/1042/1/012003)

[29] Stojkovski F., Markov Z., Kostikj Z. - Design of radial blade cascades using parametrization and correlation of geometry and flow parameters (International Conference COMETa, pp. 274-284)

[30] Stojkovski F., Markov Z., Stojkovski V. – CFD Study of Radial Guide Vane Cascade with Convex and Concave Blade Sets for Variable Speed Francis Turbines (The 5th international conference – Mechanical Engineering in XXI century – MASING 2020, pp. 109-114)

[31] Smirnov I. N. – Gydravlichesky turbini i nasosi (Moscow, 1969)

[32] Gerov, V. Vodni Turbini; State Publishing “Tehnika”: Sofia, Bulgaria, 1973.

[33] Lewis, R.I. Vortex Element Methods for Fluid Dynamic Analysis of Engineering Systems; Cambridge University Press: Cambridge, UK, 2005

[34] Miroslav Benišek – Hidraulične turbine (Mašinski Fakultet Beograd, 1998)

[35] Dr Zoran Stefanović – Aeroprofili (Mašinski Fakultet Beograd, 2005)

[36] T. Melin – Parametric Airfoil Catalog (Part 1&2, March 2013)

[37] Senay Baydas & Bulent Karakas (2019) Defining a curve as a Bezier curve, Journal of Taibah University for Science, 13:1, 522-528, DOI: 10.1080/16583655.2019.1601913

[38] BS 1042: Section 2.4. (1989) – Measurement of fluid flow in closed conduits (Part 2. Velocity-area method)

[39] IEC 60193 - Hydraulic turbines, storage pumps and pump-turbines – Model acceptance tests

[40] ANSYS FLUENT – Theory Guide (November, 2013)

[41] Tomislav Bundalevski – Mehanika na Fluidite (Skopje, 1992)

[42] Trivedi, C.; Dahlhaug, O.G.; Storli, P.T.S.; Nielsen, T.K. Francis-99 Workshop 3: Fluid structure interaction. J. Phys. Conf. Ser. 2019, 1296, 011001.

[43] Stojkovski, F.; Lazarevikj, M.; Markov, Z.; Iliev, I.; Dahlhaug, O.G. Constraints of Parametrically Defined Guide Vanes for a High-Head Francis Turbine. Energies 2021, 14, 2667. https://doi.org/ 10.3390/en14092667

[44] Filip Stojkovski, Zoran Markov - Influence of Particular Design Parameters of Radial Guide Vane Cascades on their Hydraulic Performance at Variable Speed Operated Francis Turbines (Energetika 2020)

[45] Filip Stojkovski, Marija Lazarevikj, Zoran Markov - Parametric Design Tool for Development of a Radial Guide Vane Cascade for a Variable Speed Francis Turbine (30th

IAHR Symposium on Hydraulic Machinery and Systems, doi:10.1088/1755-1315/774/1/012112)
[46] Francis 99 Turbine Model Test Program (NTNU, Ch.16)
[47] Hiroshi T. - Vibration Behavior and Dynamic Stress of Runners of Very High Head Reversible Pump-turbines (DOI: 10.5293/IJFMS.2011.4.2.289)
[48] Abbot I. H. – National Advisory Committee for Aeronautics - Summary of airfoil data (Report no. 824, 1945)
[49] Rouse H. – Elementary Mechanics of Fluids (Dover Publications Inc. New York, 1946)
[50] Lazarevikj, M., Stojkovski, F., Markov, Z., Iliev, I., Dahlhaug, O. G., Parameter based tool for Francis turbine guide vanes design using coupled MATLAB - ANSYS approach, J.sustain. dev. energy water environ. syst., 1090410, DOI: https://doi.org/10.13044/j.sdewes.d9.0410
[51] Koirala R. et al. - Effect of Guide Vane Clearance Gap on Francis Turbine Performance (Energies 2016, 9, 275; doi:10.3390/en9040275)
[52] Ujjwal Shrestha et al. - A CFD-Based Shape Design Optimization Process of Fixed Flow Passages in a Francis Hydro Turbine (Processes 2020, 8, 1392; doi:10.3390/pr8111392)
[53] Thapa BS, Dahlhaug OG, Thapa B., Flow measurements around guide vanes of Francis turbine: A PIV approach, J. Renewable Energy, 2018, vol 126, pp 177-188 https://www.sciencedirect.com/science/article/pii/S0960148118303537
[54] Tong Zheming et al. – Investigating the Performance of a Super High-head Francis turbine under Variable Discharge Conditions Using Numerical and Experimental Approach (Energies 2020, 13, 3868; doi:10.3390/en13153868)
[55] Trivedi C., Michel J. C., B. K. Gandhi – Investigation of a High Head Francis turbine at Runaway Operating Conditions (Energies 2016, 9, 149; doi:10.3390/en9030149)
[56] Milun B. & Svetislav S. – Osnove Turbomašina (Naučna knjiga Beograd, 1990)
[57] Alan J. Wadcock – Simple turbulence models and their application to boundary layer separation (NASA Contractor Report 3283, May 1980)
[58] Robert W. Kermeen - Water Tunnel Tests of NACA 4412 and WALCHNER profile 7 Hydrofoils in non - cavitating and cavitating flows (Hydrodynamics Laboratory, California Institute of technology, 1956)
[59] D.B.Sannes - Pressure Pulsation in a High Head Francis Turbine Operatingat Variable Speed (IOP Conf. Series: Journal of Physics: Conf. Series 1042 (2018) 012005 doi :10.1088/1742-6596/1042/1/012005)
[60] Zoran Markov, Filip Stojkovski, Marija Lazarevikj - Investigation Of The Possibilities For Development Of A Variable Speed Hydraulic Turbine (ZEMAK 2018)

APPENDIX

Selected papers published at referent conferences and journals

1. Stojkovski, F.; Lazarevikj, M.; Markov, Z.; Iliev, I.; Dahlhaug, O.G. Constraints of Parametrically Defined Guide Vanes for a High-Head Francis Turbine. Energies 2021, 14, 2667. https://doi.org/ 10.3390/en14092667

2. Filip Stojkovski, Marija Lazarevikj, Zoran Markov - Parametric Design Tool for Development of a Radial Guide Vane Cascade for a Variable Speed Francis Turbine (30th IAHR Symposium on Hydraulic Machinery and Systems, doi:10.1088/1755-1315/774/1/012112)

3. Filip Stojkovski, Zoran Markov - Influence of Particular Design Parameters of Radial Guide Vane Cascades on their Hydraulic Performance at Variable Speed Operated Francis Turbines (Energetika 2020)

energies

Article

Constraints of Parametrically Defined Guide Vanes for a High-Head Francis Turbine

Filip Stojkovski [1,*], Marija Lazarevikj [1], Zoran Markov [1], Igor Iliev [2] and Ole Gunnar Dahlhaug [2]

[1] Faculty of Mechanical Engineering, Ss. Cyril and Methodius University in Skopje, 1000 Skopje, North Macedonia; marija.lazarevikj@mf.edu.mk (M.L.); zoran.markov@mf.edu.mk (Z.M.)
[2] Waterpower Laboratory, Department of Energy and Process Engineering, Norwegian University of Science and Technology (NTNU), Alfred Getz' Vei 4, 7034 Trondheim, Norway; igor.iliev@ntnu.no (I.I.); ole.g.dahlhaug@ntnu.no (O.G.D.)
* Correspondence: filip_stojkovski@outlook.com; Tel.: +389-707-633-45

Abstract: This paper is focused on the guide vane cascade as one of the most crucial stationary sub-systems of the hydraulic turbine, which needs to provide efficient inflow hydraulic conditions to the runner. The guide vanes direct the flow from the spiral casing and the stay vanes towards the runner, regulating the desired discharge. A parametric design tool with normalized geometrical constraints was created in MATLAB, suitable for generating guide vane cascade geometries for Francis turbines. The goal is to determine the limits of these constraints, which will lead to future faster prediction of initial guide vane configurations in the turbine optimal operating region. Several geometries are developed using preliminary design data of the turbine and are investigated using CFD simulations close to the best efficiency point (BEP) of the turbine. This research is part of the Horizon-2020—HydroFlex project led by the Norwegian University of Science and Technology (NTNU), focusing on the development of a flexible hydropower generation.

Keywords: guide vanes; parametric design; Francis turbine; CFD

Citation: Stojkovski, F.; Lazarevikj, M.; Markov, Z.; Iliev, I.; Dahlhaug, O.G. Constraints of Parametrically Defined Guide Vanes for a High-Head Francis Turbine. *Energies* **2021**, *14*, 2667. https://doi.org/10.3390/en14092667

Academic Editor: Cécile Münch-Allигné

Received: 18 March 2021
Accepted: 28 April 2021
Published: 6 May 2021

1. Introduction

Hydropower, as a part of the family of renewable energy sources, is an active engineering and scientific field which focuses on optimization of the entire energy transformation process so as to attain more efficient, flexible, and reliable electricity generation. Increased electricity demands for balancing and, sometimes, temptingly high profit margins for off-design operation have pushed hydroturbines to their structural limits. The turbines are being operated at unfavorable loads, which has raised concerns and challenged the existing design philosophy. The critical requirements for modern turbines are high efficiency and stability over the wide operating range. Increasing flexibility in energy production from hydropower plants is a task demanded by the hydropower sector in Europe and worldwide, especially in off-design operation conditions of the turbines. The turbines need to operate with more start–stop cycles and high ramping rates. Variable-speed operation of Francis turbines is seen as an alternative solution to achieve high ramping rates and more efficient energy production in off-design operating conditions [1–3].

As a part of the HydroFlex project, the goal of this research is to develop a robust parametric tool for the generation of radial guide vane cascades for low specific speed Francis turbines. In this case, the open Francis-99 turbine geometry was used as a reference, and the tool was developed and further tested for this particular geometry [1]. However, the research shows that the applied methods can be generalized and used for various types of high-head Francis turbines as well.

Due to confidentiality, it is very hard to get to the turbine design approaches used by the manufacturers, which makes it difficult for researchers to engage their skills and knowledge in evaluating the turbine designs. Computational fluid dynamics (CFD) is generally used for the design of turbine passages and for evaluation of the hydrodynamic behavior of the entire machine. Combining CFD with parametrically defined guide vanes, numerical calculations for different cascade configurations are performed with the goal to identify the limits of the guide vane design procedure for high-head Francis turbines, in this case, the zone of best efficiency operation of the turbine, taken as a starting point for the design. The limits of the geometrical parameters are further used to propose an optimization objective in the narrow range, and to improve the tool in MATLAB for guide vane cascade configuration development.

2. Geometry Description

Figure 1 shows the main geometrical parameters that are considered for the development of the guide vane cascade [4–8]. Primarily, the goal is to estimate the ranges for these parameters under the design conditions of the turbine.

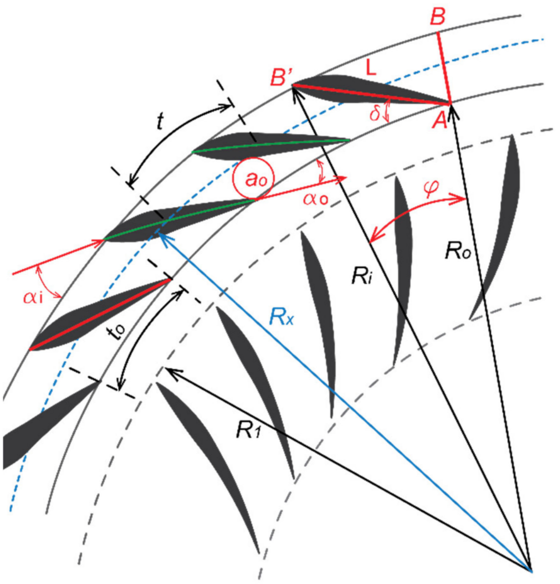

(a)

Symbol	Unit	Description
R_i	(m)	Cascade inlet design radius
R_o	(m)	Cascade outlet design radius
R_x	(m)	Cascade axis circumference radius
B_{gv}	(m)	Cascade height
R_1	(m)	Runner blades inlet radius
φ	(deg)	Blade chord wrap angle
point A	(-)	Starting point for chord placement
point B	(-)	Starting point for the end of chord
point B′	(-)	Rotated point B about the blade chord wrap angle
L	(m)	Blade chord length
t	(m)	Cascade pitch measured at axis circumference
t_o	(m)	Cascade pitch measured at blades outlet
L/t	(-)	Cascade density at axis circumference
α_i	(deg)	Cascade inlet flow angle
α_o	(deg)	Cascade outlet flow angle
δ	(deg)	Blade chord angle enclosed with outlet radius
a_o	(m)	Blades opening
a_o/L	(-)	Relative blade opening

(b)

Figure 1. Radial cascade geometry parameters: (**a**) Geometrical scheme representation; (**b**) description of geometrical parameter symbols.

As Figure 1 shows, all geometrical parameters are obtained in relation to the turbine's center of rotation. Their values are defined according to the turbine runner inlet diameter, inlet height, rotational speed, and design flow rate and head. All of these geometrical constraints are further generalized to obtain a "non-dimensional" guide vane cascade [9].

The main geometrical parameters of the guide vanes include the guide vane outlet circumference radius *Ro*. It represents the distance from the blades' trailing edges to the runner inlet edges in the turbine design conditions, which, in this case, is the best efficiency point. It is represented as a ratio from the runner inlet radius as:

$$\frac{R_o}{R_1} = C_{Ro}. \tag{1}$$

The guide vane inlet circumference radius *Ri* represents the cascade inlet circle. The vanes' hydraulic profiles are positioned between these radii. The inlet radius is represented as a ratio of the guide vane outlet radius as:

$$\frac{R_i}{R_o} = C_{Ri}\,. \tag{2}$$

A fixed point (starting point) of the chord line is selected on the guide vane outlet radius, indicated as Point A. The point where the chord line begins is on the top of the guide vane inlet radius, noted as Point B, as shown in Figure 2. A rotation of the chord line is introduced around the turbine rotation axis to place the chord line between the guide vane radii by rotating the top Point B positioned on the inlet radius. For an arbitrary number of blades in the cascade, noted as Zgv, the blades angular distribution will be:

$$\varphi_{gv} = \frac{360}{Z_{gv}}, \tag{3}$$

and the normalized (relative) wrap angle of the chord line will be the ratio of the actual wrap angle φ and the blades' angular distribution φgv:

$$\varphi_N = \frac{\varphi}{\varphi_{gv}}. \tag{4}$$

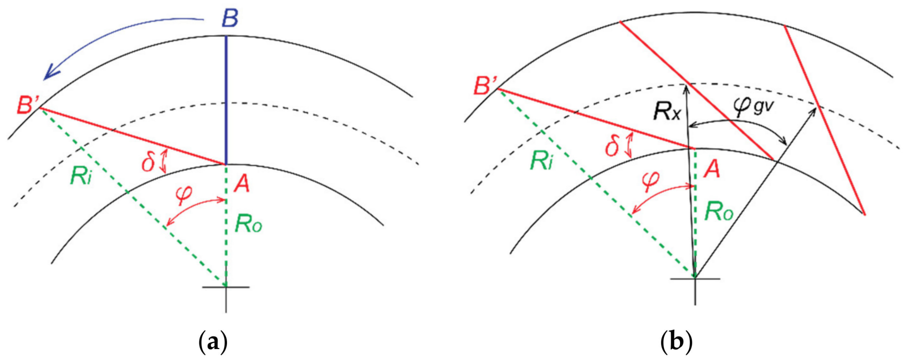

Figure 2. Radial cascade development: (**a**) Chord line positioning; (**b**) angular normalization.

The chord line forms an angle δ with the cascade outlet diameter; the angle shows the leaning of the chord line towards the outlet.

The chord length, indicated as L, represents the actual blade length, and according to the selected number of blades Zgv, a cascade pitch is formed, marked as t, to obtain the cascade density, as the ratio between the length and the pitch:

$$\frac{L}{t} = \frac{L}{\frac{2R_x\pi}{Z_{gv}}}, \tag{5}$$

where the pitch t is calculated according to the axis radius Rx where the blades are assumed to be pivoted. In this initial case, as the pivot point location is not observed, the axis radius is calculated as the average radius between the inlet and outlet circumference:

$$R_x = \frac{R_i + R_o}{2}. \tag{6}$$

For the obtained position of the chord line, a simplified calculation is made for the velocity triangles at the guide vane inlet and outlet. According to the free-vortex theory [9–12], where the circulation remains constant in the vaneless space, the flow velocity and its radial and tangential components are obtained, yielding the flow direction that the guide vanes need to achieve. Deriving from the Euler turbine equation, the needed inflow angle at the turbine design point is obtained as:

$$tg\alpha_1 = \frac{n_d}{60}\frac{Q_d}{B_{r1}gH_n}, \tag{7}$$

where n_d is the design rotational speed, Qd is the design flow rate, Hn is the design net head, Br_1 is the runner inlet height, and g is the gravitational acceleration. According to this, the runner inlet velocity triangle is obtained. The angle α_o in Figure 1 is the cascade outlet flow angle which needs to be developed, and it slightly differs from the absolute velocity angle α_1 at the runner inlet, due to the free-vortex effect in the vaneless space. The radial cascade outflow conditions are guided from the outlet velocity and its components in a radial (which represents the flow rate) and the tangential (which represents the circulation) manner. The free-vortex law which preserves in the vaneless space is transferred from the runner inlet to the guide vane outlet, with respect to the change of the radial distance as:

$$v_{ou} = c_{1u}\frac{R_1}{R_o} , \tag{8}$$

where v_{ou} represents the tangential velocity component of the guide vanes and c_{1u} is the tangential velocity at the runner inlet. The radial velocity component is directly influenced by the turbine flow rate at certain radial distance, with respect to the cascade height B_{gv} as:

$$v_{or} = \frac{Q_d}{2R_o\pi B_{gv}} . \tag{9}$$

The vector sum of these two components gives the outlet velocity of the cascade:

$$\vec{v_o} = \vec{v_{or}} + \vec{v_{ou}} , \tag{10}$$

and it has an angle α_o at the cascade outlet:

$$tg\alpha_o = \frac{v_{or}}{v_{ou}} . \tag{11}$$

The inflow angle to the guide vanes is pre-defined from the spiral casing and the stay vanes of the observed turbine. These calculated flow angular directions are enclosing angles with the chord line, shown in Figure 3, from which a polynomial equation is derived and the camber line yc of the blades can be calculated as follows [13]:

$$y_c = Ax^3 - Bx^2 + Cx , \tag{12}$$

where x represents the non-dimensional chord length. The following relations for the coefficients of the equation are obtained:

$$B = tg(\beta_o) + 2tg(\beta_i) \; ; \; A = B - tg(\beta_i) \; ; \; C = tg(\beta_i) , \tag{13}$$

where βo is the enclosed outflow angle and βi is the enclosed inflow angle with the chord line. This shows that the camber-line polynomial equation coefficients are strictly dependent from the flow angles which are enclosed with the chord line. This equation is developed to obtain hydrofoils with a reflexed camber-line, if needed [13]. After obtaining the camber-line, a Bezier curve is developed for the thickness distribution, where the curve weights are selected in the range of several recommended hydrofoil configurations. The idea was to enable changes in the location of maximal thickness of the blade and to include it into the optimization procedure. The Bezier parametrized points are calculated as [14]:

$$B(t) = \sum_{i=0}^{n} \binom{n}{i} (1-t)^{n-i} t^i P_i \; ; \; \binom{n}{i} = \frac{n!}{i!(n-i)!} \tag{14}$$

where n represents the number of parameters (weights) and P_i are the adopted parameters for thickness distribution development of the blade.

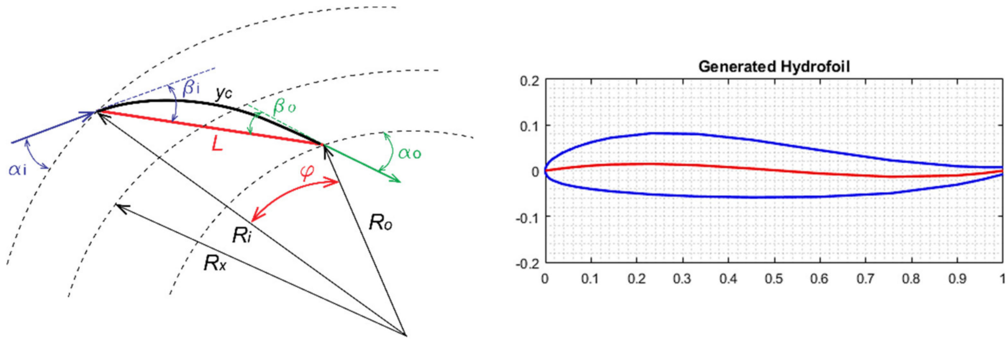

(**a**) (**b**)

Figure 3. Development of a hydrofoil blade: (**a**) Calculated velocity flow angles enclosed with the chord line (scheme); (**b**) Bezier thickness distribution and camber-line used for developing a hydrofoil.

The opening between two blades a_o, presented in Figure 1, shows particular difficulty for geometrical parametrization. In this case, the opening is observed afterwards as a relative parameter a_{oN} in a ratio to the chord length, and it is further investigated as an obtained result of:

$$a_{oN} = \frac{a_o}{L} \tag{15}$$

3. Turbine Inputs and Developed Guide Vane Configurations

The developed guide vane configurations correspond to the previous geometrical explanations and flow considerations. The turbine inputs, which are crucial for the initial design, are given in Table 1. The following parameters represents the Francis-99 turbine model installed at the Waterpower Laboratory at NTNU [15], for which, from the model hill chart, the following values have been adopted:

Table 1. Turbine input parameters.

Description	Symbol	Unit	Value
Net head	H_n	(m)	11.2
Design flow rate	Q_d	(m^3/s)	0.2
Design rotational speed	n_d	(rpm)	333.33
Runner inlet diameter	D_{r1}	(m)	0.62
Runner outlet diameter	D_{r2}	(m)	0.349
Guide vane height	B_{gv}	(m)	0.06
Speed factor (IEC60193)	n_{ed}	(–)	0.185
Discharge factor (IEC60193)	Q_{ed}	(–)	0.1567

According to the turbine inputs, several guide vane configurations were developed within the available space of the examined turbine. Changes were made in the guide vane geometries by analyzing the relative position of the guide vane outlet diameter from the runner *Cro*, their inlet diameter relative to the outlet diameter *Cri*, blade chord wrap angle φ, and number of blades *Zgv*. The hydrofoil profile thickness distribution function was fixed, but the overall shape changes as the camber-line changes, with the chord wrap angle φ and *Cri*. The thickness to length ratio is also kept constant. The following configurations are presented in Figure 4.

Combination (-)	Zgv (-)	fi_N (-)	L/t (-)	ao/L (-)
1	32	1.42	1.575	0.079
2	28	1.24	1.378	0.111
3	26	1.16	1.28	0.135
4	24	1.07	1.181	0.167
5	32	1.42	1.579	0.085
6	28	1.24	1.382	0.119
7	26	1.16	1.283	0.145
8	24	1.07	1.184	0.179
9	32	1.42	1.497	0.091
10	28	1.24	1.31	0.128
11	26	1.16	1.216	0.155
12	24	1.07	1.123	0.191
13	32	1.42	1.459	0.098
14	28	1.24	1.277	0.137
15	26	1.16	1.185	0.166
16	24	1.07	1.094	0.204
17	32	1.42	1.496	0.089
18	28	1.24	1.31	0.123
19	26	1.16	1.215	0.148
20	24	1.07	1.122	0.18
21	32	1.42	1.537	0.127
22	28	1.24	1.343	0.166
23	26	1.16	1.248	0.193
24	24	1.07	1.152	0.226
25	32	1.42	1.583	0.156
26	28	1.24	1.384	0.199
27	26	1.16	1.285	0.227
28	24	1.07	1.187	0.262
29	28	1.4	1.456	0.071
30	26	1.3	1.351	0.088
31	24	1.2	1.248	0.111
32	28	1.32	1.383	0.112
33	26	1.23	1.284	0.134
34	24	1.13	1.186	0.162
35	32	1.24	1.3	0.108
36	28	1.09	1.138	0.155
37	26	1.01	1.056	0.189

(**a**)

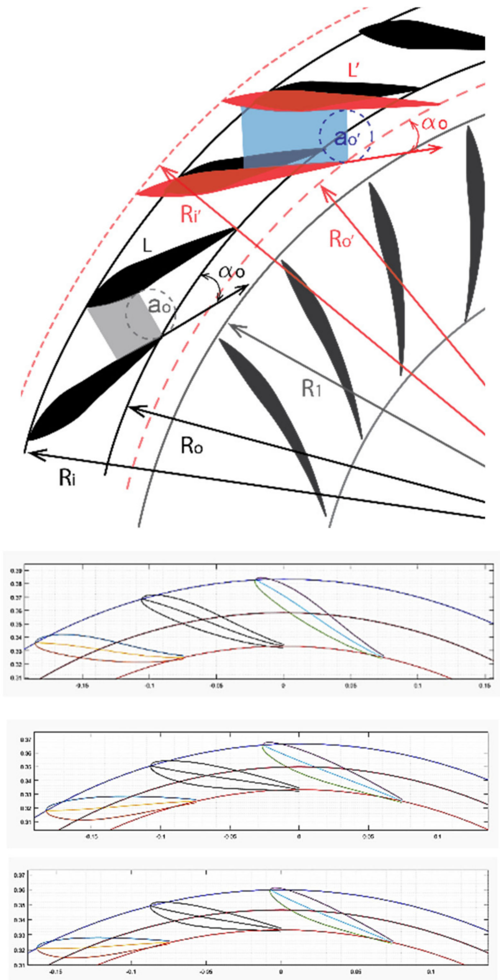

(**b**)

Figure 4. Developed guide vane configurations: (**a**) Developed configuration geometrical data; (**b**) schematic representation of the geometry changes and analysis of opening space and overlap section with examples of several developed configurations in MATLAB.

It is evident from Figure 4b that a change of the inlet/outlet radii leads to a change of the chord wrap angle of the blades, which causes the change of the blade length. That results in an increased or decreased opening between the blades, and it also influences their overlap, affecting the cascade density. All the configurations are developed for shock-free inflow conditions of the cascade, and the trailing edge bending angles are developed for shock-free flow entrance into the runner ($\alpha_o = \text{const.}$), for the given turbine inputs.

The configuration geometries were developed in MATLAB and transferred to ANSYS Workbench, where the flow domains were created. The mesh was built in ANSYS TurboGrid and assembled with a previously meshed runner of the Francis-99 turbine. The simulations were guided in ANSYS Fluent. The numerical model is simplified to the guide vanes, the runner, and the draft tube cone. The numerical mesh consists of ca. 1.5 million cells, where the runner and the draft tube cone consist of 810 k and 150 k cells, respectively. A zone mesh independence test for the guide vane domain was carried out, observing the total pressure drop through the cascade, for obtaining low deviations of the total pressure in front of the runner, i.e., the guide vane outlet, where a number of cells from 0.4 to 1 million gave a total pressure deviation of ±2%, so the meshes for the guide vanes were created within the range of 550 k to 650 k cells [–]. Sections of the numerical mesh and the zone mesh independence test are shown in Figure 5.

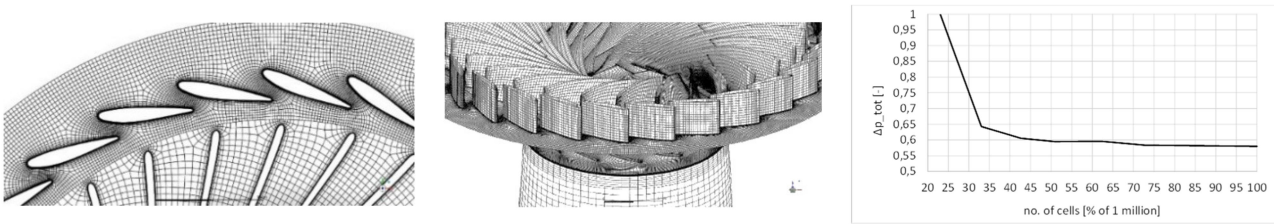

(**a**) (**b**) (**c**)

Figure 5. Numerical mesh: (**a**) Mesh at the hubs; (**b**) overall mesh preview; (**c**) guide vane zone mesh independence test.

In order to obtain the value of the turbine design head, the boundary conditions of the model are inlet and outlet total pressures, where a fixed flow direction is imposed at the inlet. Realizable *k-ε* is used as turbulence model, using standard wall functions. The *y*+ distance for the guide vane blades changes throughout the blades' height, having a growth rate of 1.2. For around 83.3% of the blades' height, the mesh has a *y*+ range from 3.5 to 30, giving an average value of ~16, so a larger portion of the blade is covered where the flow phenomena are predominant. The other 16.7%, which is near the ends of the blade (the top and low point near the hub and shroud), has a value of *y*+>30.

The runner of the Francis-99 turbine consists of 15 full blades and 15 splitter blades, which are assumed as "moving walls", along with the runner hub and shroud surfaces, with no slip conditions. The runner domain frame is given motion around the *z*-axis as a "frozen rotor". The guide vane models consist of 24 to 32 blades. The frames are connected to each other via moving reference frame interfaces. The simulations were guided as steady state.

4. CFD Results

As mentioned, the guide vane configurations are developed according to the turbine design point, i.e., the best efficiency point. Other operating points of the turbine are not observed in this analysis because the main goal is to determine the influence of some geometrical parameters towards the design point. The turbine efficiency are calculated according to the IEC 60193 [16] standard, by defining the total pressure differences at the guide vane inlet and the draft tube cone outlet. The variations of the head between the analyzed cases are in the range of ±3% of the design net head given in Table 1, so they are taken without any correction. The turbine efficiency is calculated as:

$$\eta = \frac{P_m}{P_h} = \frac{T_{num} \cdot \omega}{\rho \cdot g \cdot H_{num} \cdot Q_{num}} \, [-] \tag{16}$$

where *Pm* is the mechanical power of the turbine runner developed, calculated as the product of the numerically obtained runner torque *Tnum* and the angular velocity *ω*, divided by the hydraulic available power *Ph* in the system, which is product of the numerically obtained head *Hnum* and flow rate *Qnum*. The combination which results in the highest absolute value for the efficiency from the CFD analysis is normalized as $\eta = 1$ [–], and all other efficiencies are compared to this value in relative terms. The influences of particular geometrical constraints are represented by 2D contour plots, where the variable geometry parameters are set on the *x* and *y* axis, and the turbine efficiency is presented on the vertical *z* axis, to observe how certain changes of geometrical constraints influence the turbine efficiency. Primarily, a chart of all the combinations is plotted in Figure 6 against relative turbine efficiency to further determine which zones of interest shall be implemented in an optimization algorithm.

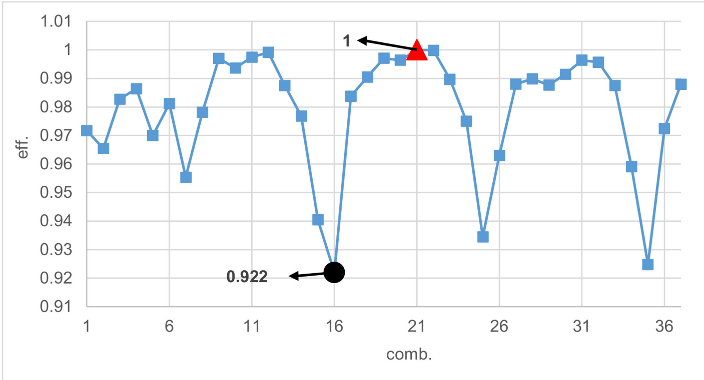

Figure 6. Relative turbine efficiency for each of the tested combinations described in Figure 4 and the highest and lowest efficiencies for the tested combinations.

Despite the applied theory for designing the guide vanes for all the configurations, some configurations show higher efficiencies and some of them show lower efficiencies. In this analyzed case, the lowest efficiency is obtained for combination 16 and the best for combination 21, both shown in the results of this analysis.

For a given constant number of guide vanes Zgv, the 2D charts presented in Figures 7–10 are obtained, from which it can be seen that a peak of the curve is formed, showing the potential optimization zone when the cascade consists of that number of blades.

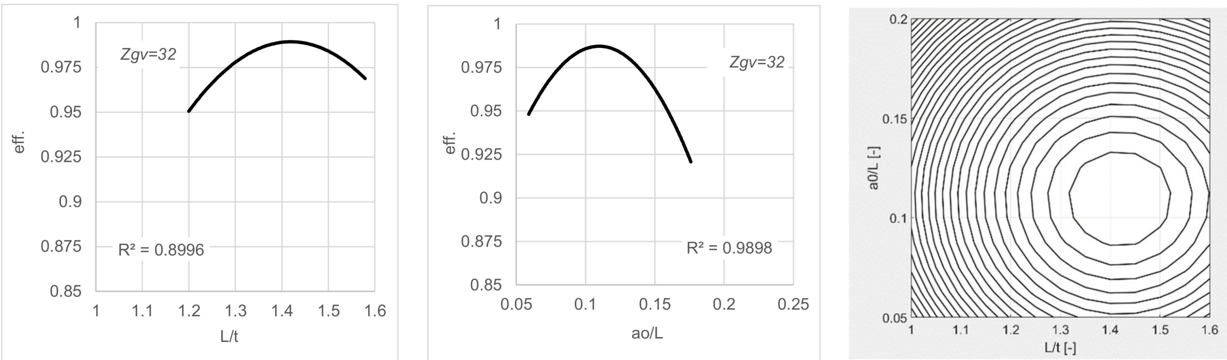

(**a**) (**b**) (**c**)

Figure 7. Results interpretation for Zgv = 32 blades: (**a**) Cascade density vs. relative turbine efficiency; (**b**) relative opening vs. relative turbine efficiency; (**c**) contour plot of (**a**,**b**).

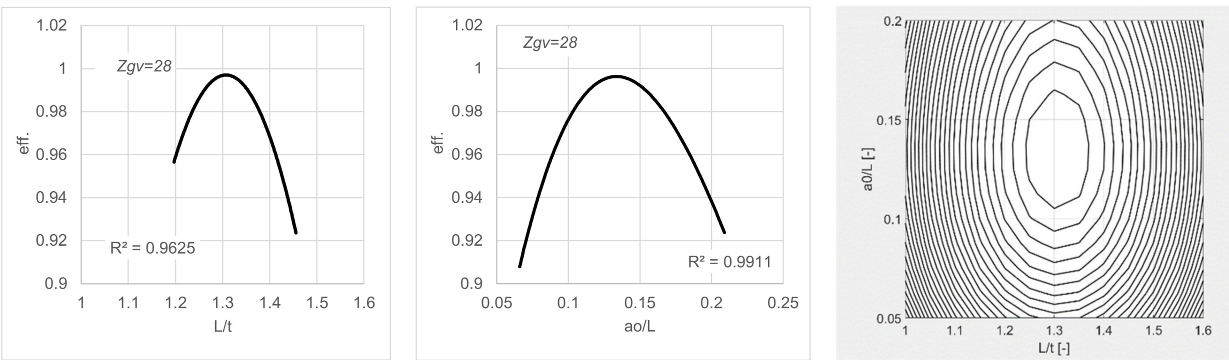

(**a**) (**b**) (**c**)

Figure 8. Results interpretation for Zgv = 28 blades: (**a**) Cascade density vs. relative turbine efficiency; (**b**) relative opening vs. relative turbine efficiency; (**c**) contour plot of (**a**,**b**).

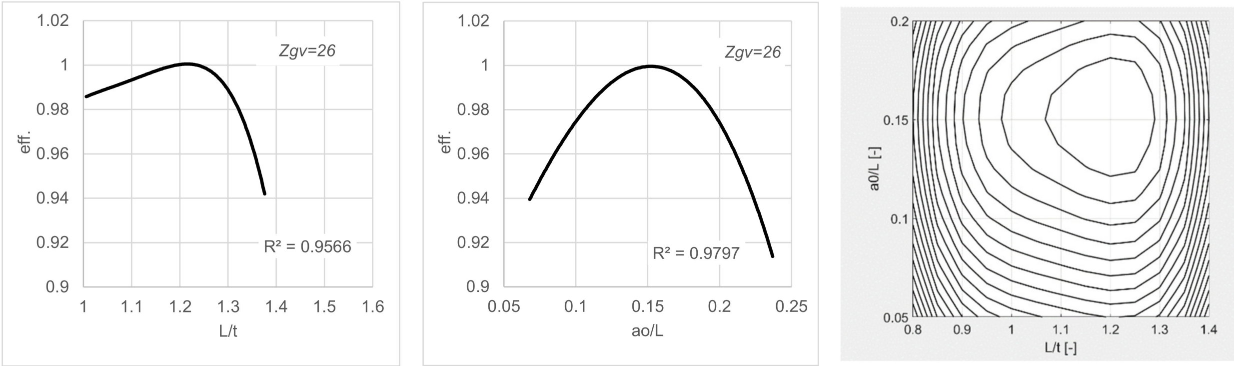

(**a**) (**b**) (**c**)

Figure 9. Results interpretation for *Zgv* = 26 blades: (**a**) Cascade density vs. relative turbine efficiency; (**b**) relative opening vs. relative turbine efficiency; (**c**) contour plot of (**a**,**b**).

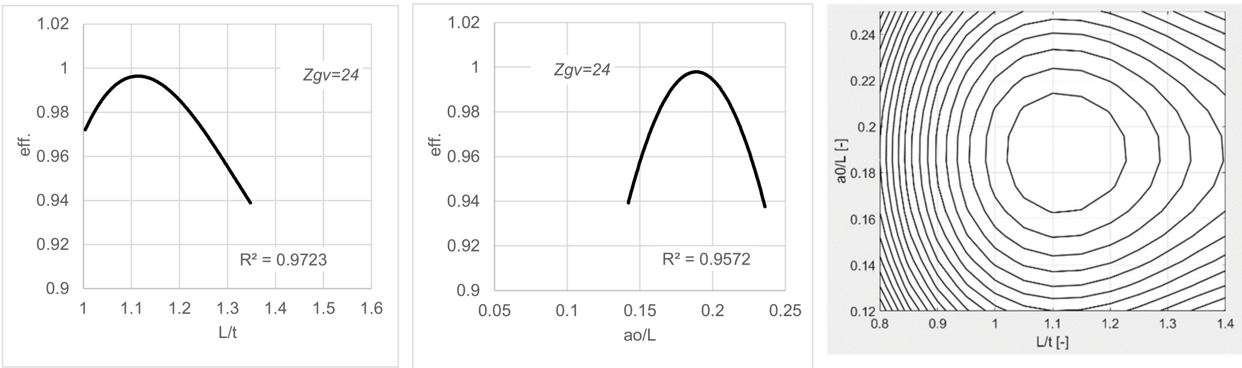

(**a**) (**b**) (**c**)

Figure 10. Results interpretation for *Zgv* = 24 blades: (**a**) Cascade density vs. relative turbine efficiency; (**b**) relative opening vs. relative turbine efficiency; (**c**) contour plot of (**a**,**b**).

It can be noted from Figures 7–10 that for a certain number of blades in the cascade, the analyzed density and the opening between the blades change. These geometrical parameters are results of the given cascade configuration. For cascades consisting of 32 blades, the zone of optimal operation lies between densities of 1.35–1.55 and a relative opening to length ratio from 0.075–0.125. For cascades consisting of 28 blades, the zone of optimal operation shifts and, regarding the density, skews in the range of 1.2–1.4 and the relative opening to length ratio ranges from 0.1–0.17. For cascades consisting of 26 blades, the zone shifts towards larger opening to length ratios from 0.125–0.175 and towards smaller cascade densities, in the range of 1.05–1.35. For cascades consisting of 24 blades, the zone shifts as in the previous case in the range of densities from 1.05–1.25 and opening to length ratios from 0.17–0.21.

These charts represent the geometrical constraints which are related to the future development of the guide vanes for high-head Francis turbines, which need to be taken into account. Additionally, a comparison between the ratios of the guide vanes' outlet diameter and inlet diameter is shown in the charts in Figure 11.

From the charts in Figure 11, it can be concluded that as the number of the blades decreases, the optimal zone of guide vane diameter ratios expands. The outlet diameter of the guide vanes, which is related to the runner inlet diameter, has the greatest influence. The guide vane inlet diameter, related to the outlet diameter, changes slightly in the range of 1.09–1.12 for all cases.

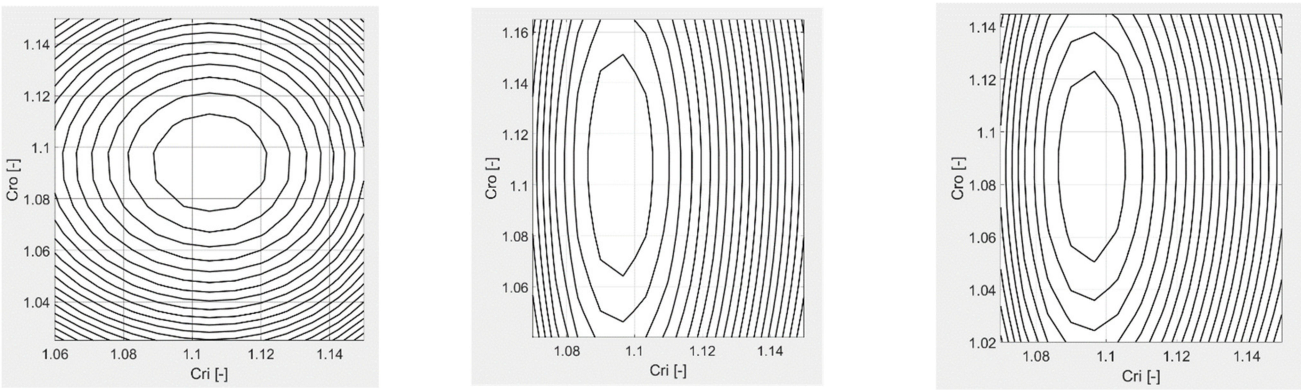

(**a**) (**b**) (**c**)

Figure 11. Results interpretation for guide vane diameters ratios: (**a**) For Zgv = 32; (**b**) for Zgv = 28; (**c**) for Zgv = 26.

An interesting behavior of the chord angle enclosed with the outlet diameter is noticed. Taking into account the outflow angle of the cascade, shown in Figures 1 and 3 as α_o and calculated in accordance with the Euler turbine equation, the relation can be presented as:

$$\delta_{rel} = \frac{\delta}{\alpha_o} \quad (17)$$

The chart in Figure 12 shows that if this angle varies around the calculated outflow angle, we exit from the optimal operation zone of the turbine. The fitting curve tends towards the calculated cascade outflow angle. This is crucial for further development of the guide vanes and the wrap angle of the blades related to the outflow angle of the cascade, to obtain a cascade which performs well in the design zone.

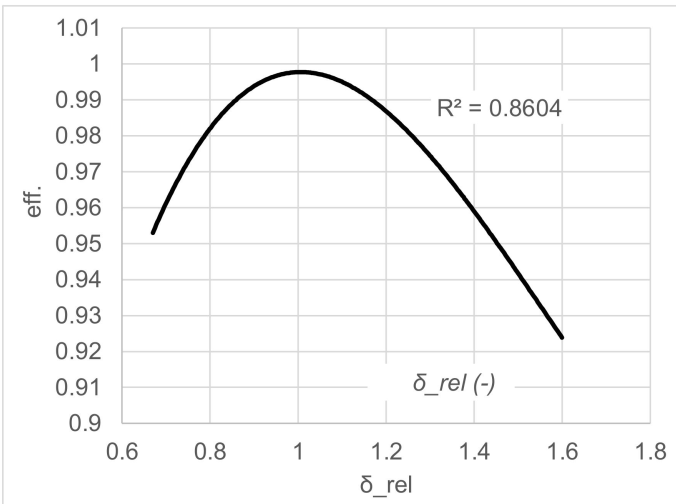

Figure 12. Relative chord angle to outlet diameter against relative turbine efficiency.

The current obtained ranges will be further implemented in an optimization algorithm, using the ANSYS Design Explorer, to test the design configurations in these limited ranges and to maximize turbine efficiency.

In Figure 13, a comparison between combinations 16 and 21 is made, as these two combinations showed the lowest and the highest efficiencies, shown in Figure 6. The geometrical and flow differences between them are shown throughout CFD post-processed images. The configurations were generated according to equal theory and initial turbine data. Their main differences are the inlet/outlet radius ratio, the number of guide vanes, and the chord wrap angle, which lead to different cascade densities and different opening spaces between the blades. The blades trailing edge angles in all the cases are constant and derived from the calculations in the MATLAB code, with an expected result of different magnitudes of the slip effects between the configurations. The blades' thickness to length ratio for all cases is constant, maintained at 16% of the blades' length, no matter how long the blades are.

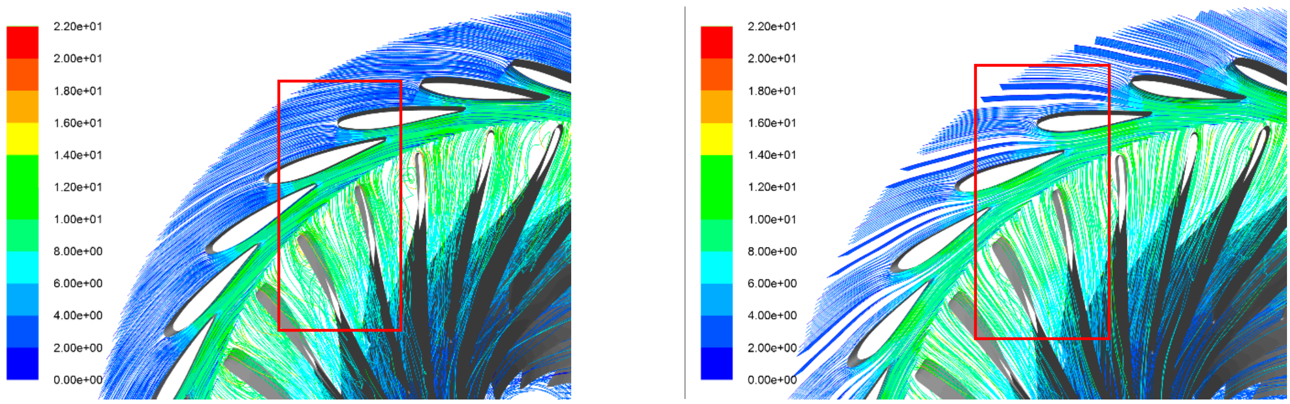

Figure 13. CFD post-process of velocity streamlines: (**a**) Combination 16—streamlines (*Cri* = 1.1; *Cro* = 1.075; *L/t* = 1.456; *a/L* = 0.071; *fi* = 1.4; *Zgv* = 28); (**b**) combination 21—streamlines (*Cri* = 1.1; *Cro* = 1.75; *L/t* = 1.138; *a/L* = 0.155; *fi* = 1.09; *Zgv* = 26).

From the velocity streamlines, it can be seen that combination 16 does not perform efficient filling of the runner blade inner channel, creating flow separations in the runner, compared to combination 21. For these two cases, a comparison between their velocity profiles was made. The velocity distribution was observed [17] at the guide vanes' outlet radius, between two blades. It can be seen in Figure 14b that the velocity profile of combination 21 is more symmetrical and uniform compared to combination 16 (Figure 14a), plotted against the guide vane relative outlet pitch *to*.

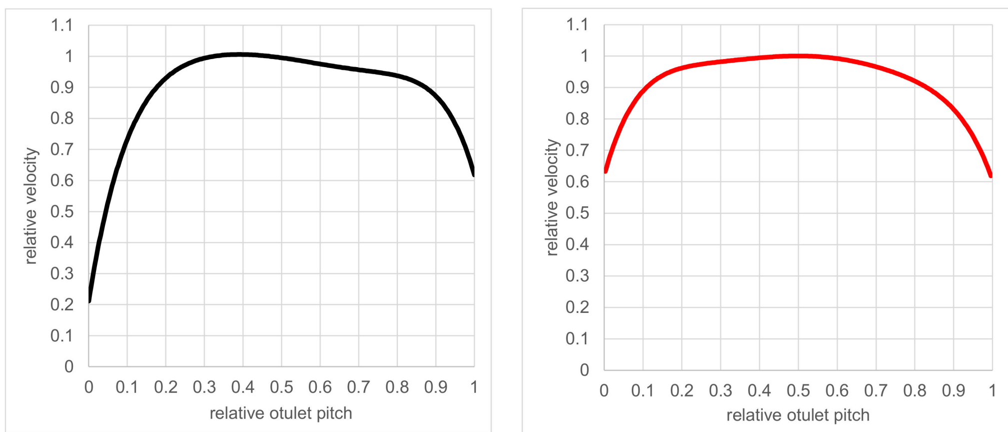

Figure 14. Velocity profile comparison: (**a**) Combination 16; (**b**) combination 21.

5. Conclusions

In this paper, an approach for further optimization of the guide vane design for high-head Francis turbines has been presented, by developing several geometries within a design space pre-described by the Francis-99 turbine model from the Waterpower Laboratory at NTNU. First, a MATLAB calculation tool for generating guide vane configurations suitable for Francis turbines was developed; the tool creates plausible cascade geometries according to turbine input data. The free geometry parameters for the final choice of the desired cascade are described and changed in a range which the design space dictates.

Several cascade geometries were developed and tested through CFD simulations for the turbine model in order to obtain the crucial geometrical parameters and their influence on the turbine efficiency, as a way of determining their limits of change which need to be implemented in an automated algorithm for further optimization. In order to obtain the relative values for the system efficiency, the CFD model was simplified and consisted of guide vanes, a runner, and a draft tube cone. All the geometries were developed according to the adopted turbine design point, which is the highest efficiency point, and the analysis was carried out to see how the guide vane configurations deviate from the efficiency around this point.

The results were obtained with curve fitting and surface fitting between two variable parameters and the turbine efficiency, while the third variable parameter was left uncontrolled. This showed how certain geometrical relations, such as inlet/outlet radius, cascade density, guide vanes' opening clearance, chord line wrap angle, etc., within their tight range, influence the turbine efficiency and design flow rate. According to the results, limits for the mentioned geometrical constraints were interpreted for their further development. One of the main conclusions which can be derived from this analysis is the chord leaning angle towards the guide vanes' outlet diameter, which has to be collinear with the cascade outflow angle. This conclusion for the chord leaning angle will be implemented, along with the blade thickness distribution law and the maximal blade thickness location, which were fixed geometrical constraints in this analysis, and they will be separately tested within the further developed optimization.

This approach offers a better understanding for the basic cascade geometrical relations and their influence, especially for high-head Francis turbines, whereas for low-head machines, it is expected that the region of the limits will change, as these machines are inclined towards greater guide vanes' opening angles. Additionally, two optimization objectives can be derived from this analysis, which can be further implemented—one is to maximize the turbine efficiency and the other is to maximize velocity profile uniformity. The second objective comes from the velocity profile comparison, where combination 21 obtained in this analysis shows a more uniform velocity profile towards the turbine runner. Further, an index of asymmetry can be introduced for the relative shape of the velocity profile [18] of the guide vanes, in a relation with some geometrical parameters, in order to obtain hydraulic/geometry parametrization for further optimization.

It is important to note that some other objectives, such as the static pressure losses or the energy losses through the cascade, turned out to be unnecessary as they can lead to misguidance towards the estimation of optimal turbine operation; however, they are crucial in cases when the guide vane cascade is developed separately from the turbine.

Author Contributions: Conceptualization, I.I. and Z.M.; methodology, F.S.; software, F.S. and M.L.; validation, F.S.; formal analysis, F.S. and M.L.; investigation, F.S. and M.L.; writing—original draft preparation, F.S.; writing—review and editing, I.I. and Z.M.; supervision, O.G.D.; project administration, I.I. and Z.M.; funding acquisition, O.G.D. All authors have read and agreed to the published version of the manuscript.

Funding: This project has received funding from the European Union's Horizon 2020 "Secure, Clean and Efficient Energy" Programme, H2020-LCE-07-2016-2017, under grant agreement no 764011. Project: Increasing the value of hydropower through increased flexibility—HydroFlex (www.h2020hydroflex.eu, accessed on 17 March 2021), 2018.

Institutional Review Board Statement: Not applicable.

Informed Consent Statement: Not applicable.

Data Availability Statement: Not applicable.

Conflicts of Interest: The authors declare no conflict of interest.

References

1. Trivedi, C.; Dahlhaug, O.G.; Storli, P.T.S.; Nielsen, T.K. Francis-99 Workshop 3: Fluid structure interaction. *J. Phys. Conf. Ser.* **2019**, *1296*, 011001. [CrossRef]
2. Trivedi, C.; Iliev, I.; Dahlhaug, O.G.; Markov, Z.; Engstrom, F.; Lysaker, H. Investigation of a Francis turbine during speed variation: Inception of Cavitation. *Renew. Energy* **2020**, *166*, 147–162. [CrossRef]
3. Iliev, I.; Trivedi, C.; Dahlhaug, O.G. Variable-speed operation of Francis turbines: A review of the perspectives and challenges. *Renew. Sustain. Energy Rev.* **2019**, *103*, 109–121. [CrossRef]
4. Stojkovski, F.; Markov, Z.; Kostikj, Z. Design of radial blade cascades using parametrization and correlation of geometry and flow parameters. In Proceedings of the International Conference COMETa, Jahorina, Bosnia and Herzegovina, 26–28 October 2020; pp. 274–284.
5. Stojkovski, F.; Markov, Z.; Stojkovski, V. CFD Study of Radial Guide Vane Cascade with Convex and Concave Blade Sets for Variable Speed Francis Turbines. In Proceedings of the 5th International Conference—Mechanical Engineering in XXI Century—MASING, Niš, Serbia, 9–10 December 2020; pp. 109–114.
6. Koirala, R.; Zhu, B.; Neopane, H.P. Effect of Guide Vane Clearance Gap on Francis Turbine Performance. *Energies* **2016**, *9*, 275. [CrossRef]
7. Thapa, B.S.; Trivedi, C.; Dahlhaug, O.G. Design and development of guide vane cascade for a low speed number Francis turbine. *J. Hydrodyn. Ser. B* **2016**, *28*, 676–689. [CrossRef]
8. Thapa, B.S.; Dahlhaug, O.G.; Thapa, B. Flow measurements around guide vanes of Francis turbine: A PIV approach. *J. Renew. Energy* **2018**, *126*, 177–188. [CrossRef]
9. Gerov, V. *Vodni Turbini*; State Publishing "Tehnika": Sofia, Bulgaria, 1973.
10. Krivchenko, G.I. *Hydraulic Machines: Turbines and Pumps*; Mir Publishers: Moscow, Russia, 1986.
11. Barlit, V.V. *Gidravlichesky Turbini*; Head Publishing House, Publishing Association "Vishta Shkola": Kiev, Ukraine, 1977.
12. Lewis, R.I. *Vortex Element Methods for Fluid Dynamic Analysis of Engineering Systems*; Cambridge University Press: Cambridge, UK, 2005.
13. Abbot, I.H. *National Advisory Committee for Aeronautics—Summary of Airfoil Data*; Langley Memorial Aeronautical Laboratory, Report no. 824; Langley Field: Hampton, VA, USA, 1945.
14. Baydas, S.; Karakas, B. Defining a curve as a Bezier curve. *J. Taibah Univ. Sci.* **2019**, *13*, 522–528. [CrossRef]
15. Nordvik, A.; Iliev, I.; Trivedi, C.; Dahlhaug, O.G. Numerical prediction of hill charts of Francis turbines. *J. Phys. Conf. Ser.* **2019**, *1266*, 012011. [CrossRef]
16. IEC 60193. In *Hydraulic Turbines, Storage Pumps and Pump-Turbines—Model Acceptance Tests*, 2nd ed.; International Electrotechnical Comission: Geneva, Switzerland, 1999.
17. Chitrakar, S.; Thapa, B.S.; Dahlhaug, O.G.; Neopane, H.P. Numerical investigation of the flow phenomena around a low specific speed Francis turbines guide vane cascade. *IOP Conf. Ser. Earth Environ. Sci.* **2016**, *49*, 062016. [CrossRef]
18. BS 1042. In *Measurement of Fluid Flow in Closed Conduits—Part 2: Velocity-Area Method*; Section 2.4; British Standard Institution: London, UK, 1989.

Parametric Design Tool for Development of a Radial Guide Vane Cascade for a Variable Speed Francis Turbine

Filip Stojkovski, Marija Lazarevikj, Zoran Markov
Ss."Cyril and Methodius" University in Skopje, Faculty of Mechanical Engineering Skopje, Rugjer Boshkovikj 18, 1000 Skopje, Republic of North Macedonia

Corresponding author: filip_stojkovski@outlook.com

Abstract. Hydropower as a part of the family of renewable energy sources represents an engineering and scientific field which inspires researchers to work on development of the systems and sub-systems in a way of optimizing the whole energy transformation process to obtain more efficient, flexible and reliable hydropower operation with the best possible water to energy ratio. This research is part of a Horizon 2020 HydroFlex project by the Norwegian University of Science and Technology (NTNU), where the main goal is development of a flexible hydropower generation. The guide vane cascade is one of the most crucial stationary sub-systems of the hydraulic turbine and is a subject of this study. Its re-design for obtaining a quality "flow-feeding" of a variable speed high head Francis turbine is developed. Having this goal in mind, a MATLAB code was generated, based on several key parameters, such as initial energy conditions as net head and turbine discharge at best efficiency point (BEP). Turbine runner geometrical constraints are taken into account during this process, while using recommendations for some initial guide vane calculations such as their number, inlet and outlet diameter, guide vane axis diameter, delivery angles etc. Using an inverse Euler turbine equation, the operating range of the turbine was calculated for a variable speed and discharge conditions, keeping the shock-free flow for all states at the runner's inlet, as it is the most favourable inflow condition. For those operating points, the flow streamlines angles were obtained at the guide vanes leading and trailing edges. With an interpolating mathematical functions between the angles of the leading and trailing edges, the camber lines of the hydrofoils were obtained for further guide vane cascade geometry development. This algorithm can be implemented on any given runner geometry. The guide vane design is then exported into ANSYS Workbench for further numerical tests, such as CFD simulations for verifying the hydrodynamic characteristics and FEM analysis for verifying the structural integrity of this sub-system for variable speed operating conditions.

Keywords: Guide Vanes, Parametric Design, Variable Speed, Francis Turbines

Acknowledgement/Funding: This project has received funding from the European Union's Horizon 2020 "Secure, Clean and Efficient Energy" programme, H2020-LCE-07-2016-2017, under grant agreement no 764011. Project: Increasing the value of hydropower through increased flexibility - HydroFlex (www.h2020hydroflex.eu).

1. Introduction

Increasing flexibility in energy production from hydropower plants is a task demanded by the hydropower sector in Europe and worldwide, especially at off-design operation conditions of the turbines. Using flexibility, variable speed operation (VSO) can be implemented to perform more efficient energy production at off-design operating conditions. As part of the HydroFlex project, the goal of this research is to develop a parameter based code for generating favourable designs of a radial guide vane cascade for low specific speed Francis turbines. In this case, the code was developed for the existing Francis 99 turbine runner from the open source web-site of the Waterpower Laboratory [11] at NTNU, but the research shows that it can be generalized for various high head Francis turbine runners.

To start with, the theoretical background was implemented and researched by using the classic turbine theory to obtain the one-dimensional mathematical relations which describe the flow conditions in the guide vanes, especially the flow conditions between the guide vanes and the runner. Secondly, the physics of variable speed turbine was studied and mathematically simplified as one dimensional models to obtain the relations and dominant parameters which need to be examined. Next, a matrix based calculation was performed to obtain the operating ranges of the turbine and the guide vanes openings for settled range of rotational speed and discharges, by keeping constant head as the situation is observed as steady state.

The geometry of the radial cascade blades was developed by using recommendations for developing a 4 digit NACA hydrofoils and by implementing the camber and thickness functions. As previously the operating ranges of the turbine were calculated, following the one dimensional mid-span streamline curvature at the inlet and outlet of the guide vanes, by interpolating the hydrofoil camber functions, the camber line of the blade was obtained, and the thickness was obtained from other static calculations. Later, the initially obtained geometry was tested with Computational Fluid Dynamics (CFD) simulations for the previously given operating conditions and it was compared with the numerically obtained results for the existing guide vanes of the Francis 99 turbine.

2. Theoretical Background

During turbine operation, flow to the runner is managed by the guide vanes and depending on the opening position, turbine torque varies. The guide vane is the stationary component, and the runner is the rotating component of a turbine. We can represent the flow conditions between the guide vanes and the runner inlet i.e. in the vaneless space, considering the equation of motion of an ideal fluid in the vector form Lamb – Gromeko [2,3]:

$$\frac{\partial \vec{V}}{\partial t} + \vec{\Omega} \times \vec{V} = -grad(gH) \tag{1}$$

where H is the specific energy of the fluid in absolute movement, $\vec{V} = (\vec{V_z}, \vec{V_r}, \vec{V_u})$ is the absolute velocity vector having components in a cylindrical coordinate system, and $\vec{\Omega} = rot\vec{V}$ is the vortex vector whose projections on the axis of the cylindrical coordinate system are equal to:

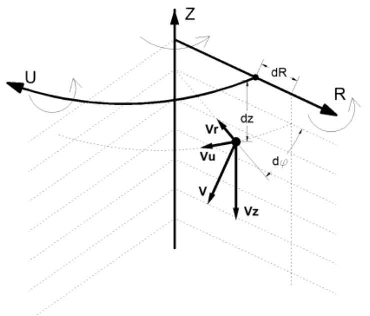

Fig.1. Absolute flow vector and its components in cylindrical coordinate system for the vaneless space

$$\begin{aligned} \Omega_r &= \frac{\partial v_z}{\partial \varphi} - \frac{\partial v_u}{\partial z} \\ \Omega_z &= -\frac{\partial v_u}{\partial r} + \frac{\partial v_r}{\partial \varphi} \\ \Omega_u &= -\frac{\partial v_r}{\partial z} + \frac{\partial v_z}{\partial r} \end{aligned} \tag{2}$$

Experimental studies show that in the area between the guide vanes and the runner, the fluid motion with sufficient accuracy can be considered steady and axisymmetric. With reasonable accuracy, we can also accept that in front of runner, the specific energy of the fluid is constant. In that case, for steady flow and for axisymmetric conditions:

$$\frac{\partial \vec{V}}{\partial t} = 0 \; ; \; \frac{\partial (v, H)}{\partial \varphi} = 0 \tag{3}$$

Two flow modules can be observed, i.e. the flow is **potential**, or the flow is **rotational (helical type)**. For potential flow it can be derived that there are no changes in the velocity in the radial direction:

$$\frac{\partial (v_u r)}{\partial z} dz + \frac{\partial (v_u r)}{\partial r} dr + \frac{\partial v_u}{r \partial \varphi} r d\varphi = d(v_u r) = 0 \tag{4}$$

and for helical flow, the vortex vector and the velocity vector are parallel to each other, i.e.:

$$d(v_u r) = \frac{\partial v_u}{\partial r} dr + \frac{\partial v_u}{\partial z} dz = 0 \tag{5}$$

From both cases the "free vortex" equation can be derived, which shows that the circulation created by the guide vanes in the vanelesss space preserves:

$$\Gamma = \oint v_u \, dl = 2r\pi \cdot v_u = const. \tag{6}$$

According to this, several conclusions can be derived:

- The guide vanes form a steady axisymmetric flow in front of the runner, which is either potential or rotational
- In the case of potential flow, the swirl is constant for all points of the liquid in the region between the guide vanes and the runner
- In the case of a rotational flow, the swirl of the flow maintains a constant value along the streamline and changes from one streamline to another

Let's consider in what cases behind the guide vanes potential or helical flow is formed. This is mainly determined by the outlines of the flowing part in the area between the guide apparatus and the runner, and also depends on the height of the guide apparatus. In the present case, a high-head Francis turbine runner is studied. The leading edge of the runner blade is located in the zone of radial movement of the liquid and represents a vertical line, i.e., $r_1 \approx const.$ along the leading edge of the runner blade.

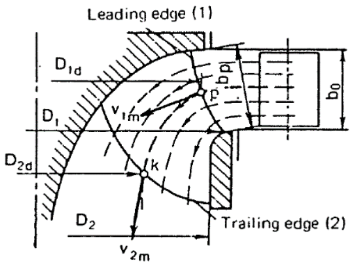

Fig.2. Flow path of Radial-axial hydraulic turbine [1]

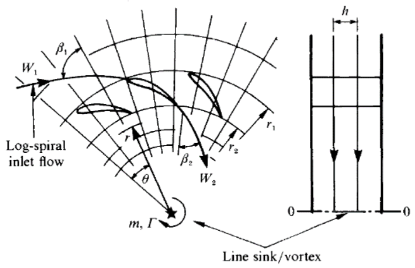

Fig.3. Radial cascades [5]

Following the classic turbine theory, a mean mid-span streamline method was used to develop the mathematical relations valid for the guide vanes outlet i.e. runner inlet conditions. The water flow in front of the runner is formed by the annular (radial) cascade of guide vanes, which is characterized by the form of the blade profiles and the chord spacing of the cascade [1]. The blade profile can be symmetric if the camber line of the profile is represented by straight line, or asymmetric if the camber line of the profile is curved. The cascade is defined by the pitch, which means the distance between two blades in the row, and the chord length of the blades. The ratio of the chord length and the pitch, i.e. L/t indicates the cascade density. As the guide vane must ensure complete closure of the turbine runner, the ratio L/t is greater than unity, which shows that the cascade is sufficiently dense, and by that, it can be assumed that the direction of water velocity is very close to the direction of the blades outlet edges. For radial-flow cascade, the vector of absolute water flow can be presented as a sum of two vector components: the radial (meridian) component and the peripheral (circulation) component:

$$\overrightarrow{v_0} = \overrightarrow{v_{0r}} + \overrightarrow{v_{0u}} \tag{7}$$

Knowing the flow rate through the turbine and the dimensions (height) of the guide vanes, the radial component can be specified as:

$$v_{0r} = \frac{Q}{D_{o2} \pi B_o} \tag{8}$$

The angle between the vector components is derived from the geometry relation of the guide vanes opening as:

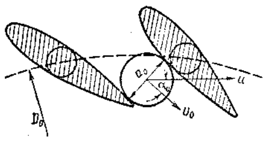

Fig.4. Guide vanes opening parameters [4]

$$v_0 = \frac{v_{0r}}{sin\alpha_0}\ ; v_{0u} = v_0 cos\alpha_0 \tag{9}$$

The flow conditions just in front of the runner, for high-head (low-speed) turbines, in a relation with the constant circulation created from the guide vanes (eq.6), the velocity parallelograms can be related as:

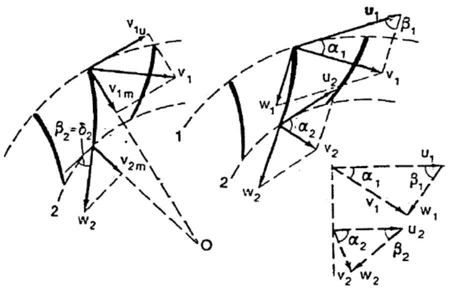

Fig.5. Velocity parallelograms [1]

$$\begin{aligned} v_{1m} &= \frac{Q}{D_{1d}\pi B_1} \\ v_{1u} &= v_{0u}\cdot\frac{D_{o2}}{D_{1d}} \\ v_1 &= v_{1m} + v_{1u} \\ u_1 &= \frac{D_{1d}\cdot\pi\cdot n}{60} \end{aligned} \tag{10}$$

Including the Euler turbine equation, the torque and the energy created in the runner can be written as:

$$\sum M_0 = \rho Q(r_1 c_{1u} - r_2 c_{2u}) = \frac{\rho Q}{2\pi}(\Gamma_1 - \Gamma_2) \tag{11}$$

$$gH\eta_h = u_1 c_{1u} - u_2 c_{2u} = \frac{\omega}{2\pi}(\Gamma_1 - \Gamma_2) \tag{12}$$

from which several essential conclusions can be considered:

- The principal importance is the structure of the flow in front and behind the runner.
- Most favourable operating condition regarding the efficiency is the outlet circulation $\Gamma_2 \approx 0$; where the front circulation is constant and can be estimated as $\Gamma_1 \approx \Gamma_0 \approx const.$ from the circulation created behind the guide vanes.
- Most favourable inflow conditions can be estimated when shock-free (zero-incidence) entry in the runner is provided, i.e. the leading edge angle remains constant $\beta_1 = const.$

Previous explanations are derived for constant rotational velocity of the runner. The variable speed operation assumptions regarding the guide vanes, can be derived from the Euler equation observing the possibility of flow regulation with the guide vanes. After several mathematical operations, the flow regulation can be expressed as [3]:

$$Q = \frac{\left(\frac{gH\eta_h}{\omega}\right) + (\omega r_2^2)}{\left(\frac{ctg\alpha_0}{2\pi B_{o1}}\right) + \left(\frac{r_2 ctg\beta_2}{A_2}\right)} \ \rightarrow \ ctg\alpha_0 = \left[\frac{\left(\frac{gH\eta_h}{\omega}\right) + (\omega r_2^2)}{Q} - \left(\frac{r_2 ctg\beta_2}{A_2}\right)\right]\cdot 2\pi B_{o1} \tag{13}$$

where Q is the flow rate, ω is the angular velocity of the runner, α_0 is the guide vanes outlet angle (fig.4), β_2 is the runner blades trailing edge angle (fig.5) and A_2 is the runner outlet surface. In the case that it is analysed, this equation was implemented in the previously tested operating region of the turbine, which is described later in this paper. The physical phenomenon of variable speed used at high-head (low-speed) turbines, keeping the head constant, at constant guide vanes opening, can be written as:

$$u_2 < \sqrt{gH\eta_h} \tag{14}$$

which shows that the flow rate decreases with the increasing of the rotational speed of the runner [4]. Physically this can be described as the near positioning of the runner blades and the guide vanes, when the rotational speed increases, the rotational “frames” created of the runner blades inner channels are more frequent and they are “repelling” the amount of flow, in other case when the rotational speed decreases, the rotational “frames” of the runner blades inner channels are less frequent and the runner is absorbing increased amount of flow, observing runner with fixed number of blades. This shows how the runners rotational speed influence on the flow rate, for constant head and constant guide vanes opening [4]:

$$A \cdot \frac{dQ}{d\omega} = \frac{u_2^2 - gH\eta_h}{\omega^2} + \frac{gH}{\omega} \cdot \frac{d\eta_h}{d\omega} \tag{15}$$

where A is positive number, and the change of the hydraulic efficiency with the rotational velocity can be neglected for further simplifications.

3. Hydrodynamic profile of a guide vane

Profiling the hydrofoil of the guide vanes by using the derived one-dimensional relations can be made with several easy steps. Observing the hydrofoil camber line, for the calculated velocities and streamlines angles for the BEP of the turbine, we can “interpolate” the camber line as a function between the streamlines angles, taking into account the previously assumptions for most favourable inflow conditions. Observing fig.3. we can conclude that the guide vane hydrofoil camber is positioned in a way that the leading edge of the hydrofoil is corresponding with the spiral case and stay vanes outlet angle of the absolute velocity vector. The trailing edge of the guide vane hydrofoil shall be in accordance with the guide vanes outlet angle (fig.4) i.e. $\alpha_0 \approx \alpha_1$, previously calculated for various runner inflow conditions. The NACA standards, are recommending equations for describing the geometry of their 4-digit MPXX hydrofoils, such as [10]:

$$y_{c1} = \frac{M}{P^2}(2Px - x^2)\,; for\ 0 < x < P \tag{16}$$

$$y_{c2} = \frac{M}{(1-P)^2}[(1-2P) + 2Px - x^2]\,; for\ P < x < c \tag{17}$$

where eq.16 describes the law of camber-line distribution from the beginning to the location of maximal camber deflection and eq.17 describes the camber-line distribution from the maximal camber location to the full length of the chord line ‘c’, M defines the maximal camber deflection and P is the location of maximal camber. The thickness distribution above and below of the hydrofoil is described as:

$$\pm y_t = \frac{t}{0{,}2}\left(a_0\sqrt{x} - a_1 x - a_2 x^2 + a_3 x^3 - a_4 x^4\right) \tag{18}$$

$$a_0 = 0{,}2969\,[-]; a_1 = 0{,}1260\,[-]; a_2 = 0{,}3516\,[-]; a_3 = 0{,}2843\,[-]; a_4 = 0{,}1015\,[-] \tag{19}$$

The coordinate points for the hydrofoil up/low contour lines are calculated as:

$$tan(\theta) = \frac{dy_{ci}}{dx} \tag{20}$$

$$x_U = x - y_t \cdot sin\theta\,;\ y_U = y_{ci} + y_t \cdot cos\theta \tag{21}$$

$$x_L = x + y_t \cdot sin\theta\,;\ y_L = y_{ci} - y_t \cdot cos\theta \tag{22}$$

where x_U, y_U, x_L and y_L are the coordinates of the upper/lower curves respectively, and θ is the angle of the camber increment. The equations for the camber line can be equalized for M and P as the camber is represented by two functions having the same camber criterions - parameters. Using the tangency rule for the leading and trailing edge angles of the foil, with the eq.20, we can simply represent that the first camber function is strictly dependent from the leading edge angle, and the second camber function from the trailing edge angle. Developing a system of two equations and representing M and P as two variables, for previously calculated angles of the leading edge (the angle of the stay vanes outflow) and trailing edge (delivery angle of the guide vanes), we can determine the M and P parameter of the hydrofoil for the calculated streamline angles:

$$P^2 \cdot [tg\alpha_0 - tg\alpha_{svo}] - P \cdot [2tg\alpha_0 + tg\alpha_{svo}] + tg\alpha_0 = 0 \quad (23)$$
$$P \cdot tg\alpha_{svo} - 2 \cdot M = 0 \quad (24)$$

Solving this system of equations gives the values of M and P, and then by implementing those values, by using the equations of the camber line, the hydrofoil geometry is determined.

4. Parametric Design Tool - Initial Calculations and Geometry Development

All of the above equations and calculation procedure is implemented into a MATLAB code which is performing calculations for deriving the initial geometry of the radial guide vane cascade, where all previously described assumptions and simplifications are respected. First, the theoretical velocity triangles for the given runner geometry are calculated for obtaining the location of the best efficiency point. After that, the code is developed for calculating the velocity parallelograms for the vaneless space between the guide vanes and the runner, and also at the guide vanes inlet (constraints from the spiral case and stay vanes distributors). The number, diameters and pivot diameter for the guide vanes are calculated acc. to recommendations from the literature, which gives us space for further optimization including these variables. As it was mentioned, the principle of variable speed was implemented. For the given runner and measured model data, a flow and speed range were determined in the working area of the runner. According to eq.13, as the runner speed and flow are changing, disregarding the changes in the head (eq.3), the resulting variable is the guide vane flow delivery angle. All results are represented in relative values.

Q [m3/s]	0,21
H [m]	12,38
n [rpm]	333,33
ned [-]	0,176
Qed [-]	0,156
Dgv1 [m]	0,8
Dgv2 [m]	0,65
Dgv_ax [-]	0,71
Bgv [m]	0,06
ngv [-]	28
alfa_gvo [deg]	10,103

Tab.1. Turbine and Guide Vanes Calculated Design Parameters

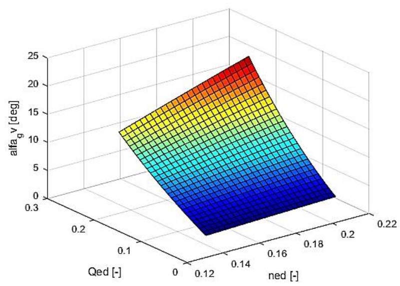

Fig.6. Guide vanes delivery angles H=const.;Q=var.; n=var

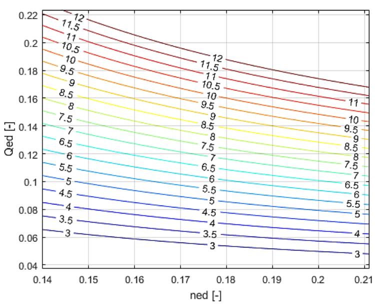

Fig.7. Guide vanes delivery angles H=const.;Q=var.; n=var

From the charts on fig.6 and 7, it can be concluded that the guide vanes flow delivery angle increases with the rate of increased flow and runner speed. The function curvature is concave instead of convex because the losses through the guide vanes are neglected. The range on the 3D surface plot shows the maximal opening the guide vanes can have in the defined range of calculation for the machine, and the range on the 2D contour plot is constrained within the range up to 12 [deg] where later CFD calculations are performed. Using simplified mathematical models for the hydraulic losses in the turbine and with the indirect method for determining the efficiency, the theoretical hill chart was calculated using the one-dimensional theory developed before for the mid-streamline, within the runners operating domain, and also the mechanical torque that the runner can produce for these conditions.

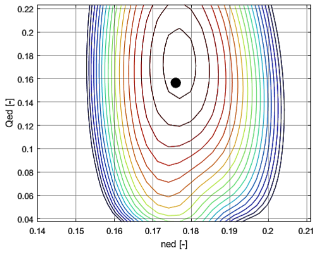

Fig.8. Predicted turbine hill (H=const.;Q=var.; n=var)

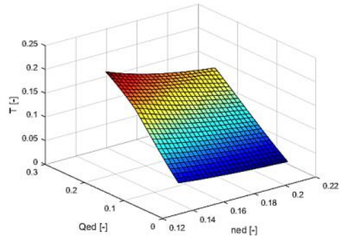

Fig.9. Runner Torque (H=const.;Q=var.; n=var)

From the predicted hill chart it can be concluded that the previously calculated BEP corresponds with the iso-lines for the zone of maximal predicted efficiency. From the chart on fig.9, it is evident that the torque increases with the increased amounts of discharge and reduced runner's speed. The point of variable speed in our case is to catch and connect the local best efficiency points of the turbine in different operating conditions. As expected, for keeping the head constant, and changing the guide vanes opening and runner rotational speed, we will obtain a similar behavior as double regulated turbine. Using the relations described in part 3, a guide vane hydrofoil is developed for the BEP and a radial guide vane cascade is plotted, which is later exported into ANSYS Workbench and ANSYS CFX for further CFD analysis.

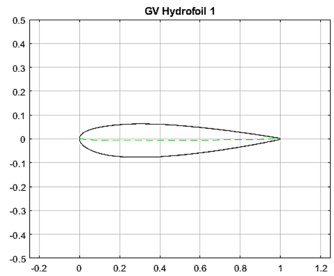

Fig.10. Developed guide vane hydrofoil
(M = -0,7265 ; P = 1,7738 ; XX=14%)

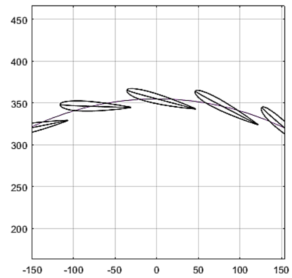

Fig.11. Guide vanes radial cascade plot

5. CFD Analysis

Two CFD models were built, tested and compared for similar mesh sizes and identical conditions, i.e. tested for constant head and $\pm 5\%$ off-design rotational speed. The first CFD model i.e. Model 0 is the original Francis 99 Turbine, where the guide vane cascade and runner performance ware examined and tested. Model 1 is represented with fig.10. from above, developed with the design tool. Comparison of the guide vanes hydrofoils is given on the figures 12 and 13.

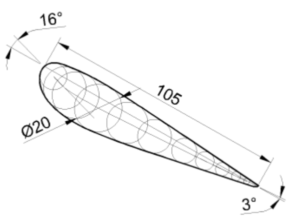

Fig.12. Francis 99 – Hydrofoil (Model 0)

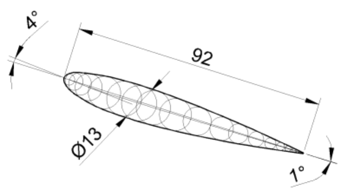

Fig.13. Developed Hydrofoil (Model 1)

According to the calculations in the design tool, the developed geometry of the blades in Model 1 is shorter. Also the thickness of the blade was calculated according to the maximal hydrostatic pressure for prototype pressure conditions, i.e. calculated as 14% of the blade chord length. The leading and trailing edge angles differs also as the NACA recommendations were implemented for 4 digit hydrofoils where the maximal camber and its location is strictly influenced from the calculated streamline angles, where in this case, it pulls behind the camber extension. The hydrofoil of Model 0 has a maximal thickness of 20% located at 20% chord length, compared to Model 1 where the maximal thickness is

14% located at 30% of the chord length. The pivot point of the blades in Model 1 is adopted to be at the gravity center of the blade. These calculations do not take into account the pivot point location, as the blade torque need to be examined via CFD simulation in some positions of partial opening to obtain a "zero torque". The numerical models are consisted of 3.3 - $3.4{\cdot}10^6$ cells. The number and size of the cells was selected according to previous performed CFD simulations of 3 operating points of the existing Francis 99 turbine model which showed good corresponding with the same points from the turbine hill chart. Zone mesh independence test for the guide vane domain was carried out, observing the total pressure drop through the cascade, for obtaining low deviations of the total pressure in front of the runner, i.e. the guide vanes outlet, where the number of cells from 0,4 to 1 million gave total pressure deviation of ±2%, so the meshes for the guide vanes were created within the range of $450\text{-}600{\cdot}10^3$ cells (fig.13.1.). The runner was consisted of $1.97{\cdot}10^6$ cells, the draft tube from $70{\cdot}10^3$ cells and the spiral casing with the stay vanes from $776{\cdot}10^3$ cells. The non-conformal meshes are connected with general grid interface. The boundary conditions of the models are set as constant inlet total pressure and outlet static pressure, i.e. the head is constant $H_n = 12{,}4\ [m]$ as it was calculated within the design tool. Multiple openings for the guide vanes were taken into account to obtain the operating range of turbine. The simulations were guided as steady using the "Frozen Rotor" interface model for the runner. The selected turbulence model is standard $k - \varepsilon$ as it was previously tested for giving best predictions for the hydraulic character of the guide vanes blades [7] and the efficiency of the turbine [8]. The number of iterations was set to 1000, and the convergence of the results was successful reaching a residuals for the continuity up to RMS to 10^{-8} (fig.13.2).

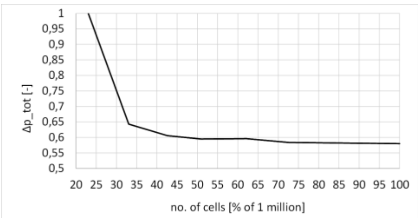

Fig.13.1. Mesh independence test for the guide vanes

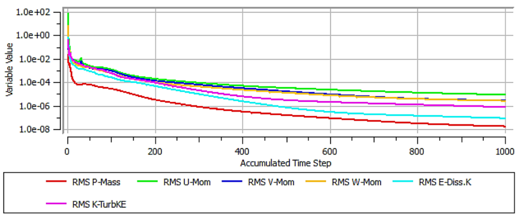

Fig.13.2. Convergence of residuals

The results obtained from the CFD simulations represented on a relative and non-dimensional scales for the discharge and the efficiency, where the calculated parameters for the Model 0 are the basis and the results from Model 1 are compared with them. The results for the head from the CFD calculations which are calculated according to IEC 60193 [13] varied cca. ±0,06% which is negligible. The efficiency is calculated as the ratio of mechanical power of the runner with the hydraulic power of the turbine, i.e.

$$\eta_t = \frac{P_m}{P_h} = \frac{T \cdot \omega}{\rho g H_n Q}\ [-] \tag{25}$$

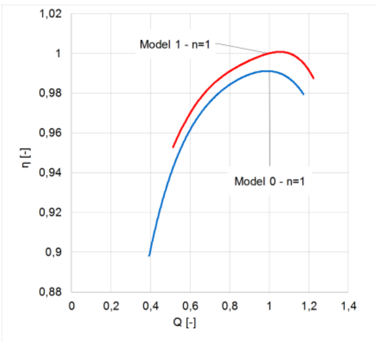

Fig.14. Turbine efficiency (n=1)

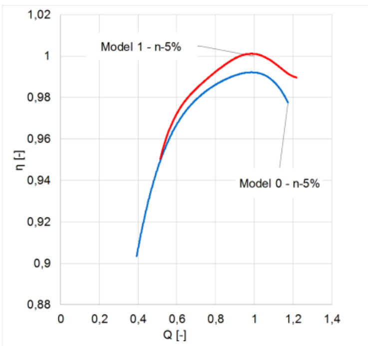

Fig.15. Turbine efficiency (n-5%)

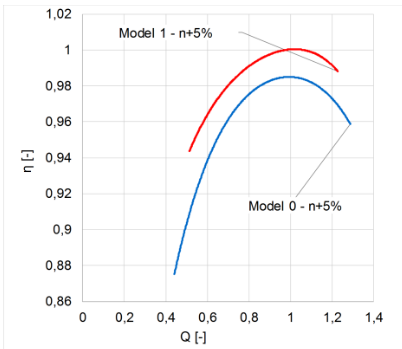

Fig.16. Turbine efficiency (n+5%)

According to the charts it can be concluded that the efficiency is increased with using the guide vanes in Model 1. For runner design rotational speed (n=333,33 [rpm], i.e. n=1 [-]) the BEP location is shifted

IOP Conf. Series: Earth and Environmental Science **774** (2021) 012112 doi:10.1088/1755-1315/774/1/012112

to increased discharge from the location of the design basis BEP and the trend of the curve is similar with the basis curve. For runner rotational speed decreased by -5%, the local BEP location corresponds with the basis local BEP location, where it can be seen that the trend of the efficiency curve is not similar with the trend of the basis curve. For runner rotational speed increased by +5%, the local BEP location corresponds with the basis local BEP location and the trend of the curve is wider than the basis curve. By capturing the local best efficiency points and connecting them, a non-dimensional graph (Q_{ed} $[-]$, n_{ed} $[-]$) was plotted for showing the trend of the connected BEPs.

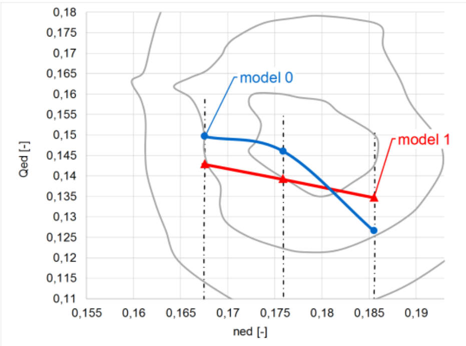

Fig.17. Connected local best efficiency points (hill efficiency zones are symbolic and generalized)

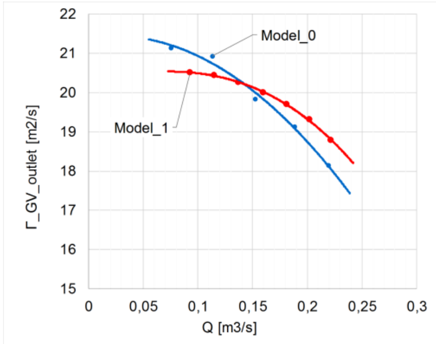

Fig.18. Guide Vanes outlet circulation v.s. flow rate

From the chart on fig.17. it can be concluded that the curve of the connected local BEP's for Model 1 is consistent showing how the runner's flow rate decreases with the increased rotational speed and vice versa. For Model 0 at n+5% it can be seen that the guide vanes are shifting the local BEP for a decreased flow rate. The guide vanes of Model 1 maintain higher outlet circulation which is one of the primary criteria for the efficiency of the guide vanes and the efficient "flow feeding" of high head turbines.

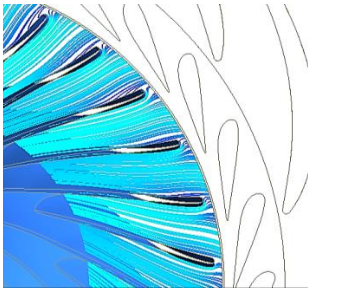

Fig.19. Mid-span streamlines in runner (Model 0, n=1, Local BEP)

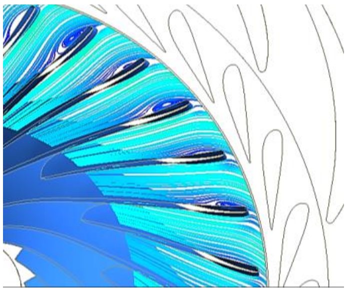

Fig.20.Mid-span streamlines in runner (Model 0, n=+5%, Local BEP)

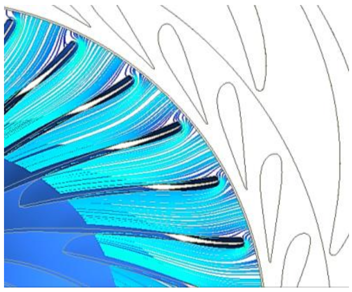

Fig.21. Mid-span streamlines in runner (Model 0, n=-5%, Local BEP)

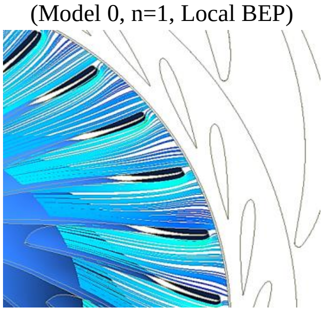

Fig.22. Mid-span streamlines in runner (Model 1, n=1, Local BEP)

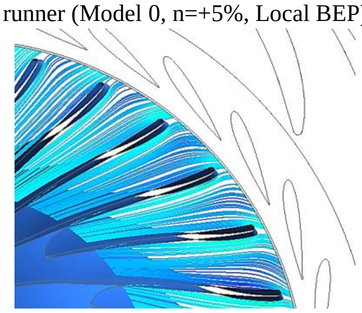

Fig.23.Mid-span streamlines in runner (Model 1, n=+5%, Local BEP)

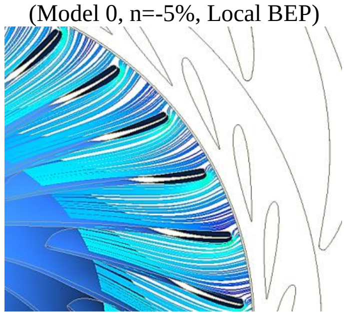

Fig.24. Mid-span streamlines in runner (Model 1, n=-5%, Local BEP)

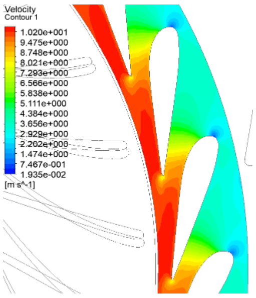

Fig.25. Model 0 – Velocity

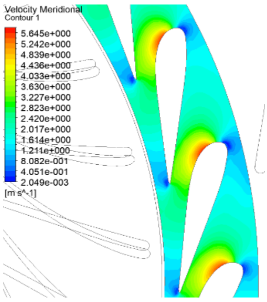

Fig.26. Model 0 – Meridian velocity

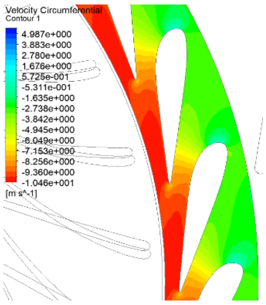

Fig.27. Model 0 – Circumferential Velocity

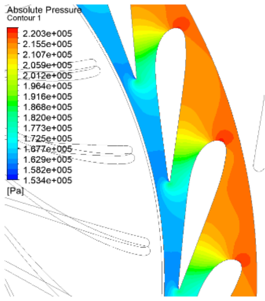

Fig.28. Model 0 – Local Static pressure

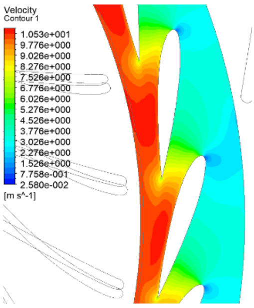

Fig.29. Model 1 –Velocity

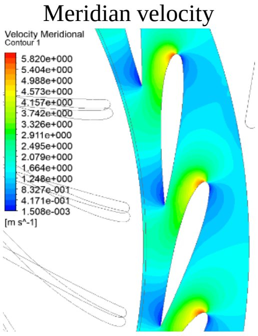

Fig.30. Model 1 – Meridian velocity

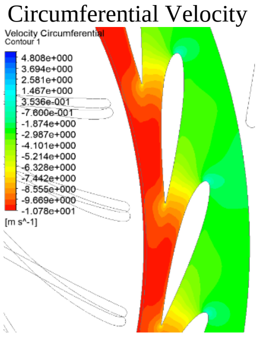

Fig.31. Model 1 – Circumferential Velocity

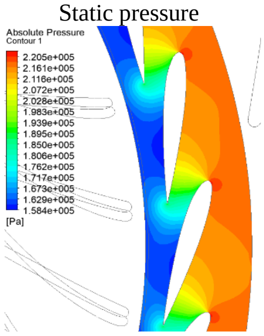

Fig.32. Model 1 – Local Static pressure

The differences between the local BEP's is represented by the velocity profiles developed behind the guide vanes for both models, where a sc. "index of asymmetry" of the velocity profile is pointed out. It shows the ratio of the standard deviation of the mean velocities calculated along each point with the mean axial fluid velocity of the channel (in our case the meridian velocity on the pitch between 2 guide vane blades) [6]. The surface between the 2 blades is represented as a rectangular cross section with the blades pitch length and the blade height.

$$Y = \frac{\sigma_{Ui}}{U} = \frac{1}{U}\sqrt{\left[\frac{\sum_{i=1}^{n}(U_i - U)^2}{n-1}\right]} \tag{26}$$

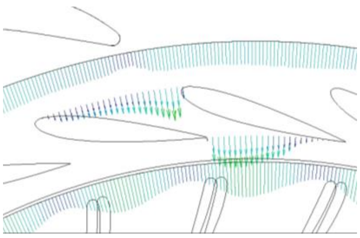

Fig.33. Meridian velocity profiles

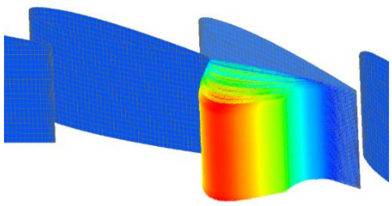

Fig.34. 3D Meridian velocity profile

On fig.33 it can be seen that the meridian (radial) velocities are not constant despite the assumption of simplification presented in eq.3. The guide vanes are creating crests which disrupt the velocity vector field in the vaneless space. Also because the angular change at constant radius, a localization of the maximal meridian vector was obtained near the first (left) blade. The velocity profile is disturbed along the guide vanes height because the skin friction between the top and low guide vanes rings. All of all, a 3D deformed meridian velocity vector profile is obtained which needs to be examined. If we neglect the deformity of the velocity profile along the guide vanes height, we can extract the angular change of the meridian velocity which is dominant in cases like this.

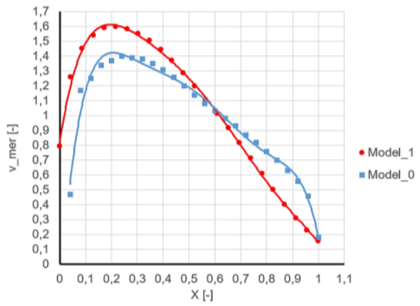

Fig.35. Comparison of the meridian velocity profiles for Model 0 and Model 1 at n=1 [-]; BEP

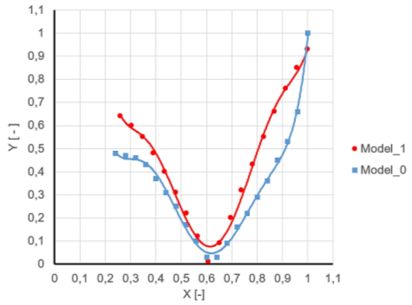

Fig.36. Relative deviation of the partial velocity vectors from the average velocity vector

At first sight, the primary difference between the velocity profiles for the both models occur at the location near the second (right) blade where for Model 1 the velocity vectors are more intense than the Model 0, resulting in reduced maximal meridian velocity. Using eq.26, the index of asymmetry is calculated for the observed profiles. Using the individual average velocity, the asymmetry is plotted and compared (fig.36.), where it can be concluded that deviation differences occur between the two observed velocity profiles from their average value, but the velocity profile of Model 0 shows slightly better than the Model 1 (35% vs. 50%) cca. difference of 15% which means that the velocity profile is more symmetric. Theoretically, obtaining more symmetric meridian velocity profile should produce more efficient inflow conditions for the runner. This situation preserves for all other cases and the asymmetry is produced mainly from the shape of the guide vanes. The asymmetry of the profile mostly changes with the guide vanes opening position and flow rate, where for constant guide vane opening and for variable speed conditions, the asymmetry remains almost constant and changes the intensity of the average meridian velocity vector because the changes in the flow rate. This shows that the one dimensional theory of velocity parallelograms is insufficient for describing all the phenomena occurring in the vaneless space.

6. Conclusions and Further Work

In this paper, a one-dimensional mathematical model was presented and implemented for development a radial guide vane cascade for the purposes of variable speed high head Francis turbine. For the guide vane hydrofoil geometry, the recommendations for 4 digit NACA hydrofoils were considered and the geometry was obtained by interpolating the camber functions between the guide vanes previously calculated inflow and outflow angles. The obtained geometry is represented as a slightly non-symmetrical concave hydrofoil (Model 1) and it was tested via CFD simulations and compared with the original guide vane hydrofoil (Model 0) from the turbine model Francis 99.

Primarily, the results are interpreted regarding the turbine efficiency, where the developed Model 1 showed better efficiency throughout the operating range of the turbine, for variable speed observed at ±5% change from nominal rotational speed, where at the best efficiency points, the efficiency increased up to 1%. This was obtained because the guide vanes of Model 1 keep higher values of the circulation in front of the runner, which is crucial for high head reaction turbines. Also, Model 1 has minor pressure and energy losses than Model 0 about 1%, which shows that it is hydraulically more efficient. One step further was taken and the meridian velocity profile was examined behind the guide vanes where a 3D deformed velocity field was obtained. By its simplifications, two averaged by height meridian velocity profiles were compared for both models and were statistically examined for deviations of the partial vectors from the average velocity vector, showing the rate of asymmetry in circumferential direction. Model 0 showed 15% more symmetry than Model 1, mainly because the shape of the trailing edge of the guide vanes, and because Model 0 produces lower circulation intensity.

The main conclusions include determination of the crucial parameters which are dominant for developing guide vanes for variable speed high head turbines, such as the intensity of the developed circulation and potentially more symmetrical meridian velocity profile behind the guide vanes for all variable speed operating points, to obtain some kind of law of similarity between the velocity profiles for various rotational speeds, because the laws of velocity parallelograms are insufficient for describing

IOP Conf. Series: Earth and Environmental Science **774** (2021) 012112 doi:10.1088/1755-1315/774/1/012112

these effects. Further work should include the pressure distribution at the trailing edges of the guide vanes, to prevent occurring of blade tip vortices [12].

The conclusions can be summarized as follows. First, the flow conditions in the vaneless space are far from axisymmetric, but they are repetitive for each guide vane section, which shows that the velocity profiles need to be examined to obtain theoretically close symmetrical meridian velocity profile. Also the average meridian velocity by theory shall be kept constant, which shows that this will influence the flow space between the guide vane blades. After that, the cascade shall be examined if it is accelerating or decelerating the fluid and how does it influence on the efficiency. Second, for high head turbines, the crucial parameter here is shown to be the circulation created by the guide vanes, which need to be increased or decreased for variable speed operations. Finally, the pivot point location and even eccentricity of the guide vanes shall be determined for obtaining "zero torque" on the blade. This condition will change the kinematical point of rotation of the blades, which can lead to reforming the shape of the flow path between two guide vanes, and by that, to change all flow conditions.

7. References

[1] Krivchenko G. I. – Hydraulic Machines - Turbines and Pumps (Mir publishers Moscow, 1986)
[2] Barlit V. V. – Gidravlichesky turbini (Kiev, 1977)
[3] Topazh G. I. – Lopastny gydromashini i dydrodynamichesky peredachi – Osnovi rabochego procesa i rascheta gydroturbin (St. Petersburg, Publishing House of the Polytechnic University, 2011)
[4] Smirnov I. N. – Gydravlichesky turbini i nasosi (Moscow, 1969)
[5] Lewis R. I. – Vortex element methods for fluid dynamic analysis of engineering systems (Cambridge University Press, 1991)
[6] BS 1042: Section 2.4. (1989) – Measurement of fluid flow in closed conduits (Part 2. Velocity-area method)
[7] Stojkovski F., Noshpal A. – Influence of the selected turbulence model on the lift and drag coefficients of parametric developed geometry of 4 digit NACA hydrofoil (19th International Conference On Thermal Science and Engineering of Serbia - Simterm 2019)
[8] Nordvik A.; Iliev I.; Trivedi C.; Dahlhaug, O. G. (2019) Numerical prediction of hill charts of Francis turbines. Journal of Physics: Conference Series. vol. 1266 (1)
[9] Iliev I., Trivedi C., Dahlhaug O. G. (2019) Variable-speed operation of Francis turbines: A review of the perspectives and challenges. Renewable & Sustainable Energy Reviews. vol. 103.
[10] Abbot I. H. – National Advisory Committee for Aeronautics - Summary of airfoil data (Report no. 824, 1945)
[11] https://www.ntnu.edu/nvks/francis-99
[12] Rouse H. – Elementary Mechanics of Fluids (Dover Publications Inc. New York, 1946)
[13] IEC 60193 - Hydraulic turbines, storage pumps and pump-turbines – Model acceptance tests
[14] Iliev I., Markov Z. - Grid dependency and relaxation of an iteration procedure for flow calculations in stationary hydraulic turbine parts (Mechanical Engineering Scientific Journal (Skopje); Journal Volume: 32; Journal Issue: 2)

Influence of Particular Design Parameters of Radial Guide Vane Cascades on their Hydraulic Performance at Variable Speed Operated Francis Turbines

Filip STOJKOVSKI, Zoran MARKOV

"Ss. Cyril and Methodius" University in Skopje, Faculty of Mechanical Engineering Skopje

Abstract- Design of radial blade cascades, with the intend to become turbine guide vanes, lies in the basis of satisfying turbine runner needs for particular turbine design point of interest. More or less, for conventional turbine operation, the hydrodynamic parameters in the pre-runner space can be easily estimated. For variable speed turbine operation at constant head, these parameters change in a way that cannot be easily predicted using conventional techniques. In this paper, the guide vanes, as crucial turbine sub-system which needs to perform efficient runner flow feeding for these operating ranges, are numerically tested in various geometrical shapes and configurations, to observe the cascades behavior, in a way of estimating which cascade configuration satisfies certain hydrodynamic and efficiency considerations of the operating points of interest. The criteria which the guide vanes need to meet are based on hydrodynamic parameters and expansion of the turbine operating range.

Index Terms- Guide Vanes, CFD, Francis Turbines, Variable Speed Operation (VSO)

I. INTRODUCTION

The design of guide vanes, more or less, so far has been developed for constant synchronous turbine runners, to meet some hydraulic criteria considering the turbine power output at given head/discharge conditions. For variable speed operating conditions, things changes drastically when the guide vanes design is considered, where multiple points of interest shall be met. The variable speed operating physics has been previously explained [6, 7] and this research represents a statistical upgrade towards definition of the influential geometrical constraints that the guide vane cascade has to the hydrodynamic and efficiency characteristics of the turbine.

The variable speed operated (VSO) Francis turbine is developed under the circumstances of constant head. Several methods of operation can be examined, and by those, the developing procedure of designs can be established and further optimized. First method is that the VSO of a turbine is strictly depending from the turbine universal characteristic chart (hill chart), by tracking local most efficient zones in a certain range of rotational speed. In that way, variable-speed operation gives the opportunity to adjust and optimize the rotational speed of the runner according to the available head for each guide vane opening.

Second method, which is observed, is focused on the result obtained from VS operation, i.e. expanding the operating range of the turbine, overall, and what hydrodynamic conditions has to be present in the pre-runner space to obtain operating range expansion. The definition of the hydrodynamic conditions for different rotational speed of the turbine runner directly influence the design of the guide vane cascade and the blades in the cascade.

The VS operation, the hydrodynamic conditions and the blades design are interacting between each other, so strict correlation from one to another cannot be made easily, and that is why, several partial analysis have been made: how the geometry influences the hydrodynamic conditions and how the changes of hydrodynamic conditions, due to VS operation, influences the geometry. In this paper, the first approach has been analyzed, defining which cascade configuration gives shrinkage or expanding of the turbine operating range.

II. VARIABLE SPEED OPERATION INTERPRETATION

The VSO turbine, as it was mentioned, can be examined in two ways. First, according to the universal hill chart of the turbine, where tracking of the local most efficient zones is done.

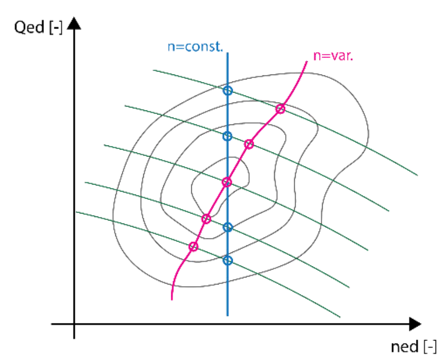

Fig.1. Variable speed operated turbine – example [5]

From fig.1, it can be seen that the guide vanes design is not influencing the turbine operation, as the variable speed method taken here can be achieved with ordinary guide vane cascade.

Thus, the hill chart shape also is obtained for a selected guide vanes configuration, and the situation looks like this.

If we observe the guide vanes, how they influence on the general shape of the hill chart, the main goal is to expand the turbine operating region, i.e. how the guide vanes configurations and influence on the hill chart shape. The following scheme is expected (fig.2).

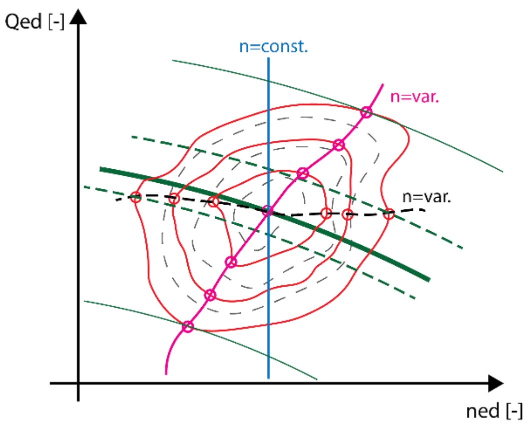

Fig.2. Guide vane reconfiguration and VSO

From the chart on fig.2 it can be seen that the guide vane curve characteristics are wider and it is expected to expand the operating region of the turbine (red iso-lines). Obtaining a guide vane configuration which will expand the operating region, than, by variable speed operation as in fig.1, the benefits are evident and the VSO effect is more dominant (magenta curve or black dashed curve).

This interpretation of the VSO turbine by operating schemes and regions, thus is only sufficient for observing the expected overall turbine behavior. The hydrodynamic parameters which leads to obtaining such expansions, are mainly defined from the turbine runner inlet flow conditions when VSO is present, and how they can be achieved with the guide vanes, which means that they influence the guide vanes design and vice versa. The velocity parallelograms in front of the turbine runner for VSO are presented on fig.3.

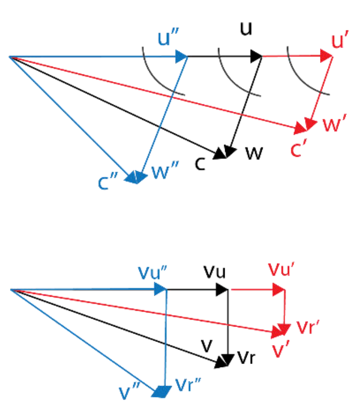

Fig.3. Runner inlet velocity triangles and guide vanes outlet velocity parallelograms

From the schematic charts from fig.1 and 2, it is evident that for constant head and change of rotational speed, the discharge of the turbine changes, either it increases or decreases. On basis of that, the velocity triangles were developed (fig.3) and the velocity parallelograms at the guide vanes outlet. The following velocity vector configurations shows that the guide vanes shall meet these velocity ratios for VSO turbine. It can be noticed that the runner inflow angle is kept constant, as the inflow conditions is desired to remain as more efficient as possible, by providing a shock-free (zero incidence) inflow conditions to the runner [1].

III. Guide Vanes Cascades Numerical Tests

As the last statement was to ensure shock-free inflow conditions to the runner, taking into account this criteria, several geometries were developed and tested through CFD analysis, to obtain how particular geometrical parameters influence on the overall turbine characteristics, when operation region expansion is demanded by VSO. The tested geometrical parameters of the cascades are the density *L/t [-]*, the relative opening of the guide vanes *a/L [-]*, the inlet cascade radius relative to the outlet C_{RI} *[-]* and the relative angular positioning of the blade chord length regarding the turbine center of rotation φ_N *[-]*. These geometry parameters are general for description a various types of radial cascades, where some detailed parameters such as blade thickness distribution or maximal thickness location etc. are neglected for further analysis.

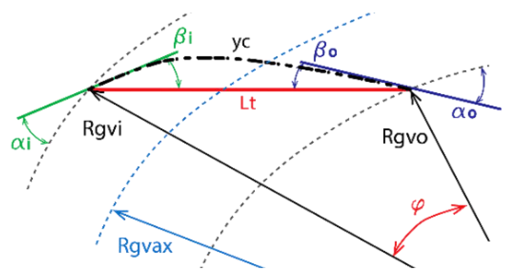

Fig. Blade in the cascade description

All the configurations are developed for shock-free inflow conditions to the cascade, and the trailing edge bending angles are developed for shock-free flow entrance into the runner, for the given turbine inputs (tab.1).

Table 1: Turbine input parameters

Net head	Hn [m]	11,2
Design flow rate	Qd [m3/s]	0,2
Design rotational speed	nd [rpm]	333,33
Runner inlet diameter	Dr1 [m]	0,62
Runner outlet diameter	Dr2 [m]	0,349
Guide vanes height	Bgv [m]	0,06
Speed Factor (IEC60193)	ned [-]	0,185
Discharge factor (IEC60193)	Qed [-]	0,1567

The configurations geometries were developed in MATLAB and transferred to ANSYS Workbench, where the flow domains were created. The mesh was built in ANSYS TurboGRID and assembled with previously meshed runner of the Francis 99 turbine. The numerical model is reduced, consisted only from the guide vanes, the runner and the draft tube cone. The numerical mesh is consisted of cca. 1.5 million cells, where approximately 550 to 650k cells were used in the guide vanes, the runner is consisted of 810k cells and the draft tube cone from 150k cells.

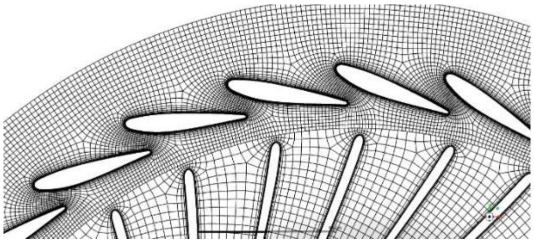

Fig.4. Mesh preview – example of the simulated models

The boundary conditions of the model are inlet and outlet total pressures, to obtain the value of the turbine design head, where at the inlet, a cylindrical components of the vector were adjusted. The turbulence model used is standard *k-ε*. The runner of the Francis 99 turbine is consisted of 15 full blades and 15 splitter blades, which are assumed as "moving walls" along with the runner hub and shroud surfaces, with no slip conditions. The runner domain frame is given motion around the vertical 'z' axis. The guide vanes models are consisted from 24 up to 32 blades. The frames are connected between each other via interfaces, which allows further easiness of transient simulations using the sliding-mesh technique. The simulations were guided as steady, changing the runner rotational speed in the range of ±15% of the nominal speed.

IV. Results

The guide vanes configurations are developed in one position, according to the turbine design point i.e. the best efficiency point. The same configurations are tested for off-design point of ±15% of the nominal speed.

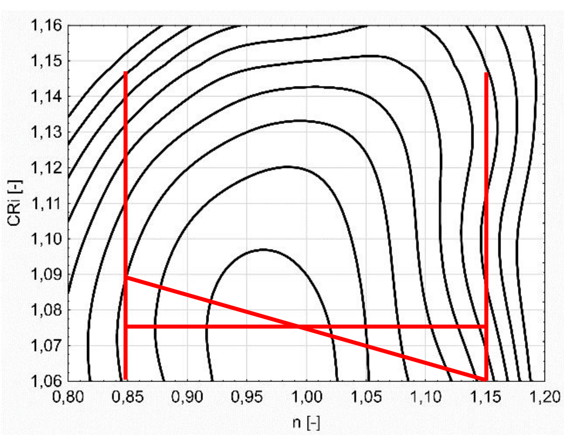

Fig.5. Influence of cascade inlet radius on operating range expansion at different rotational speeds

From fig.5. it can be concluded that the zone of optimal operation lies at the turbine design rotational speed n=1 [-], and with a cascade inlet radius from 5% to 10% larger than the outlet radius. Regarding the expansion of the operating range, it can be concluded that the iso-lines are most stretched at 7.5% of inlet radius ratio, which can be a guidance for further development of the "optimal" cascade.

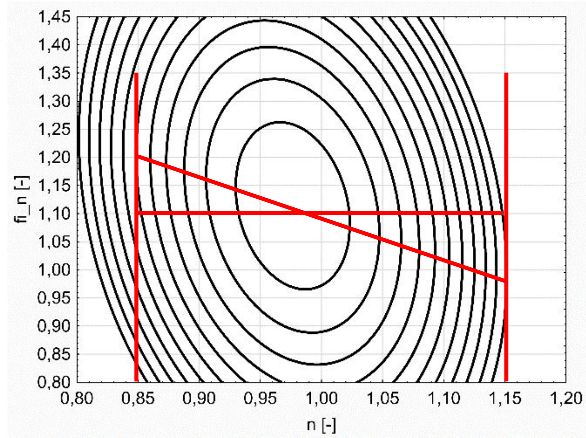

Fig.6. Influence of cascade blades chord line angular position on operating range expansion at different rotational speeds

From fig.6 it can be seen that the biggest extension of the range is when a variable angular position of the chord is given. As this, technically is plausible if the blades are "profiled" and have a changeable angular shape, will be analyzed further. For standard radial cascades of fixed blade geometry, the weighted angular position of the chord shall be around 1.11 [-].

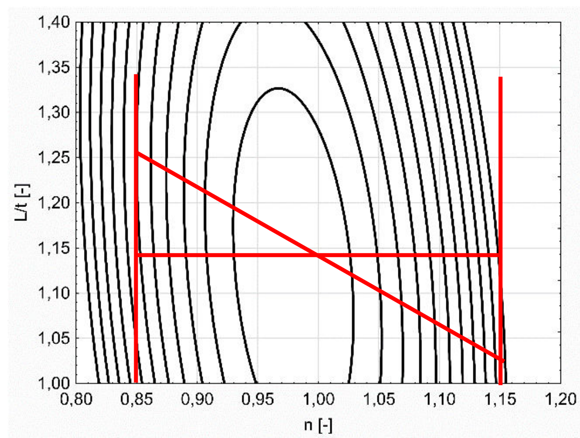

Fig.7. Influence of cascade density on operating range expansion at different rotational speeds

On this chart, it can be easily concluded that the cascade density i.e. the overlap between the blades influences on the expansion of the operating range. Most expand region is obtained between 10%-25% of blades overlap, i.e. cascade density of *L/t=1.1 - 1.25* [-].

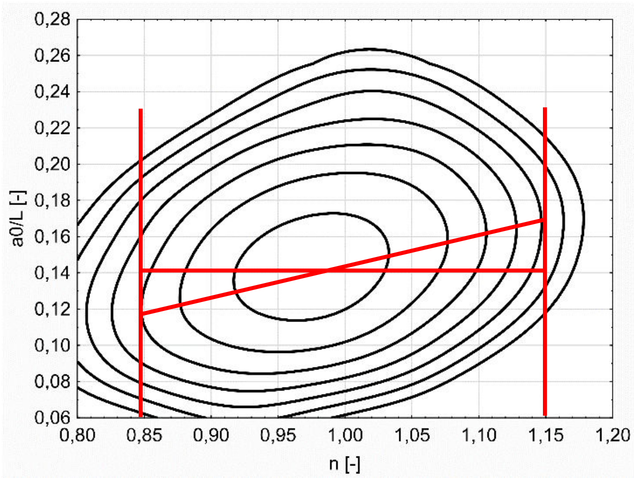

Fig.8. Influence of blades relative opening to their length on operating range expansion at different rotational speeds

The blades relative opening shows that maximal operating range expansion is obtained when there is a change of the opening from 12% to 17%. If the cascade is built from constant blade configurations, the weighted value of the relative opening shall be in the range around 14%-16% of the blade length.

V. Models Comparison

By taking the previous assumptions and calculations, how the cascade types behaves when variable speed is needed, for obtaining an expanded hill chart, previous analysis were guided to test and prove this approach for further development.

A strict comparison was made with the existing guide vanes on the observed turbine model Francis 99 which is in the Waterpower Laboratory at NTNU. The guide vanes are consisted of 28 blades, and the cascade has the following geometry parameters (tab.2). The developed model is geometrically very close to the existing guide vanes, as the turbine model has very tight geometrical constraints where the guide vanes can be positioned and examined. The following analysis was carried out for further development of this cascade and to further perform model tests.

Table 2: Model configurations compared

	CRi [-]	L/t [-]	a0/L [-]	fi_n [-]
FR99	1,126	1,324	0,166	1,23
MODEL1	1,127	1,3	0,148	1,25

The main difference between the cascades is the relative angular position of the chord lines of the blades, and the relative opening of the blades, which can be seen that the developed Model 1 has slightly smaller opening, related with the conclusions from the chart on fig.8. The other geometry parameters are selected to ensure that the developed cascade can be fitted in the turbine model test rig.

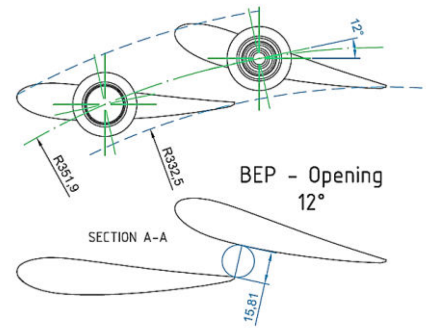

Fig.9. Developed guide vanes model

For several guide vanes openings and rotational speeds of the runner, for equal operating conditions, the turbine hill charts were obtained and plotted on relative efficiency scale from 0.9-1 [-].

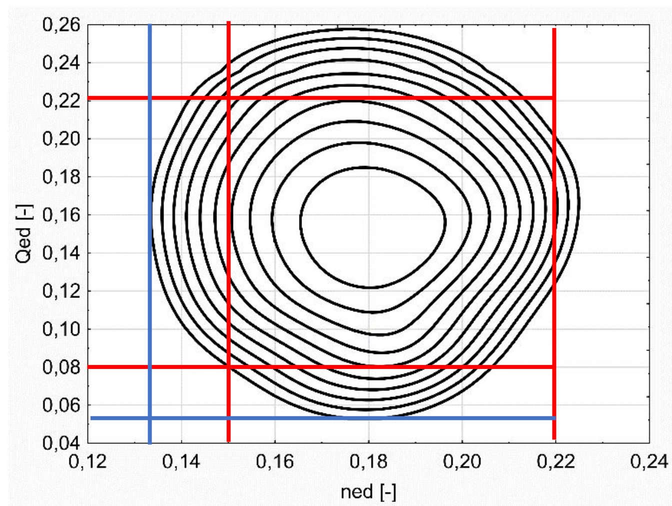

Fig.10. Developed guide vanes (Model 1) – turbine hill chart (pre-described operating limits and extensions)

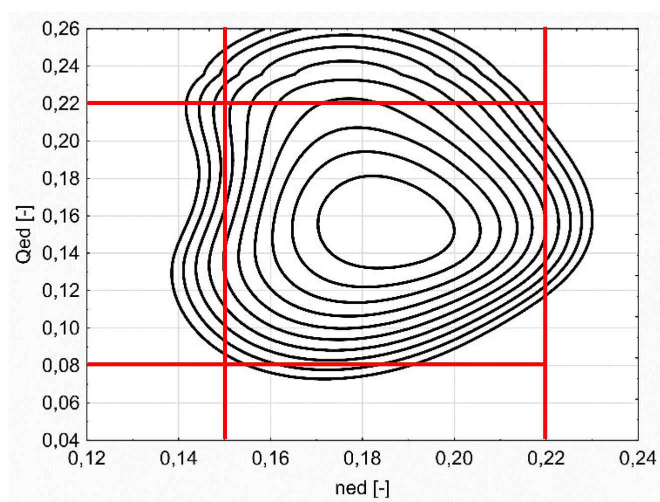

Fig.11. Francis 99 guide vanes model – turbine hill chart (pre-described operating limits)

From the results obtained in the hill charts, it can be easily concluded that, by respecting only one of the previous derived criteria (in this example the relative guide vane opening), an expansion of the turbine operating range is obtained, especially in the range of reduced rotational speed and reduced flow rates. This is significant increase of the operating range which intuitively shows that this turbine can operate with good efficiency out of the previous described operating limits.

According to fig.10 and 11 it can be concluded that the turbine characteristics compared for the 2 models, extends. Model 1 gives better performance compared to FR99 guide vanes. Extended characteristics is obtained for reduced rotational speed, compared as the ratio between the limitations:

$$\frac{n_{edFR99}}{n_{edM1}} = \frac{0.15}{0.132} = 1.364\ [-]$$

For reduced flow rates, the characteristics extends compared with the previous limitation:

$$\frac{Q_{edFR99}}{Q_{edM1}} = \frac{0.076}{0.052} = 1.462\ [-]$$

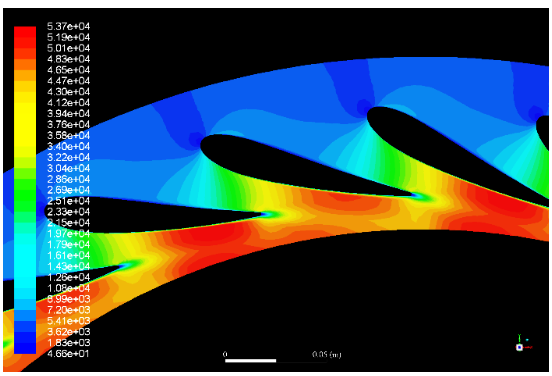

Fig.12.1. Dynamic pressure contours (Developed Model 1)

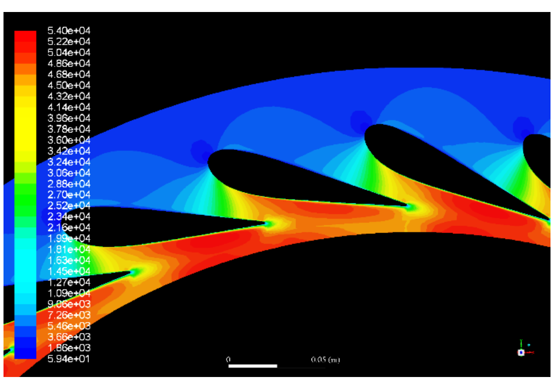

Fig.12.2. Dynamic pressure contours (Francis 99 Guide vanes)

The velocity profiles at the outlet pitch of the blades is compared to show the plausible hydrodynamic reason for extension of the operating range. The velocity profiles are analyzed also in relative manner, to obtain not the intensity, but the uniformity (asymmetry) of the profile, given on equal blade pitch.

From the chart on fig.13.1 it can be concluded that the velocity profile obtained for the developed model 1 remains almost equal for off-design rotational speeds, compared to the existing guide vanes, which for increases rotational speed of the runner, the velocity profile deforms and losses its symmetry.

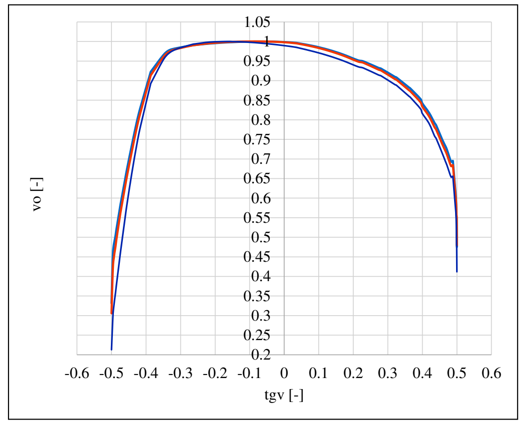

Fig.13.1. Velocity profile – Model 1

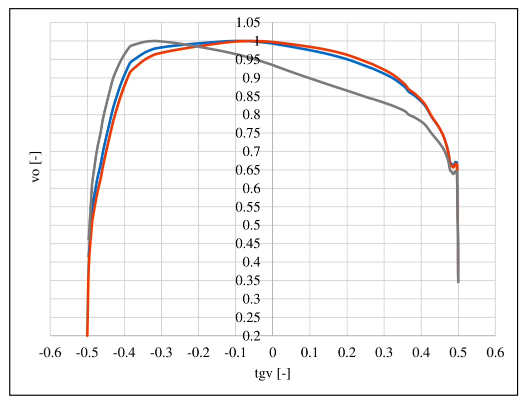

Fig.13.2. Velocity profile – Francis 99 Guide Vanes

According to this results, a decision was made to further develop a model of the guide vanes, to perform further measurements and mode tests, to prove these characteristics of operating range expansion and how does the guide vanes, overall, can re-shape the operating hill chart of the turbine.

VI. CONCLUSION

In this paper, a brief analysis was carried out for determining some of the influential geometry parameters of guide vanes, when variable speed operation is expected of the turbine runner, to cover more operating zones. Primarily, the guide vanes cascade is multiple times described and geometrically parametrized in the previous researches done, so a continuing to those researches was made here to the next step.

Several cascade configurations (particularly 21 configurations) were examined, with various geometry parameters differences, from different cascade inlet radius, different angular position of the blades chord line, different cascade density, opening etc. All these geometry parameters were tested with CFD simulations on a reduced numerical model of the Francis 99 turbine model from the NTNU Waterpower laboratory. All the cascades were developed for the best efficiency operating point of the turbine. The tests were carried out at constant head and opening, for variable rotational speeds of the runner. The results were plotted as contours (iso-lines) of 3 variables, the geometry parameter observed, the rotational speed and the turbine efficiency, to observe how the operating range extends and the optimal zone shifts with the change of rotational speed or with the change of the particular geometry parameter.

According to the primary results, it was obtained how certain geometry parameters influence the extension of operating range of the turbine. A comparison was made for a developed guide vane cascade (Model 1) with the existing guide vane cascade of the Francis 99 turbine model, to observe how the blades opening change influence the range extension. The results showed extension of the range, so a decision was made to further build a model of the guide vanes to prove these operational extensions, by performing model test at the laboratory.

From this analysis, generally, it can be concluded simply that the design of the guide vanes cascade is not unambiguous, but quite opposite. They represent a matter which needs to be evolved iteratively by certain combinations, which can give reasonable and favorable hydrodynamic conditions in the pre-runner space, and on the overall turbine efficiency.

ACKNOWLEDGMENT

This project has received funding from the European Union's Horizon 2020 "Secure, Clean and Efficient Energy" programme, H2020-LCE-07-2016-2017, under grant agreement no 764011. Project: Increasing the value of hydropower through increased flexibility - HydroFlex (www.h2020hydroflex.eu).

REFERENCES

[1] Krivchenko G. I. – Hydraulic Machines - Turbines and Pumps (Mir publishers Moscow, 1986)

[2] Barlit V. V. – Gidravlichesky turbini (Kiev, 1977)

[3] Lewis R. I. – Vortex element methods for fluid dynamic analysis of engineering systems (Cambridge University Press, 1991)

[4] Nordvik A.; Iliev I.; Trivedi C.; Dahlhaug, O. G. (2019) Numerical prediction of hill charts of Francis turbines. Journal of Physics: Conference Series. vol. 1266 (1)

[5] Iliev I., Trivedi C., Dahlhaug O. G. (2019) Variable-speed operation of Francis turbines: A review of the perspectives and challenges. Renewable & Sustainable Energy Reviews. vol. 103.

[6] Stojkovski F. , Markov Z., Kostikj Z. - Design of radial blade cascades using parametrization and correlation of geometry and flow parameters (International Conference COMETa, pp. 274-284)

[7] Stojkovski F., Markov Z., Stojkovski V. –CFD Study of Radial Guide Vane Cascade with Convex and Concave Blade Sets for Variable Speed Francis Turbines (The 5th international conference – Mechanical Engineering in XXI century – MASING 2020, pp. 109-114)

[8] IEC 60193 - Hydraulic turbines, storage pumps and pump-turbines – Model acceptance tests

AUTHORS

First Author – Filip Stojkovski, M.Sc.
"Ss. Cyril and Methodius" University in Skopje
Faculty of Mechanical Engineering Skopje
filip_stojkovski@outlook.com
Second Author – Zoran Markov, Ph.D.
"Ss. Cyril and Methodius" University in Skopje
Faculty of Mechanical Engineering Skopje
zoran.markov@mf.edu.mk

Correspondence Author – Filip Stojkovski, M.Sc.
"Ss. Cyril and Methodius" University in Skopje
Faculty of Mechanical Engineering Skopje
filip_stojkovski@outlook.com